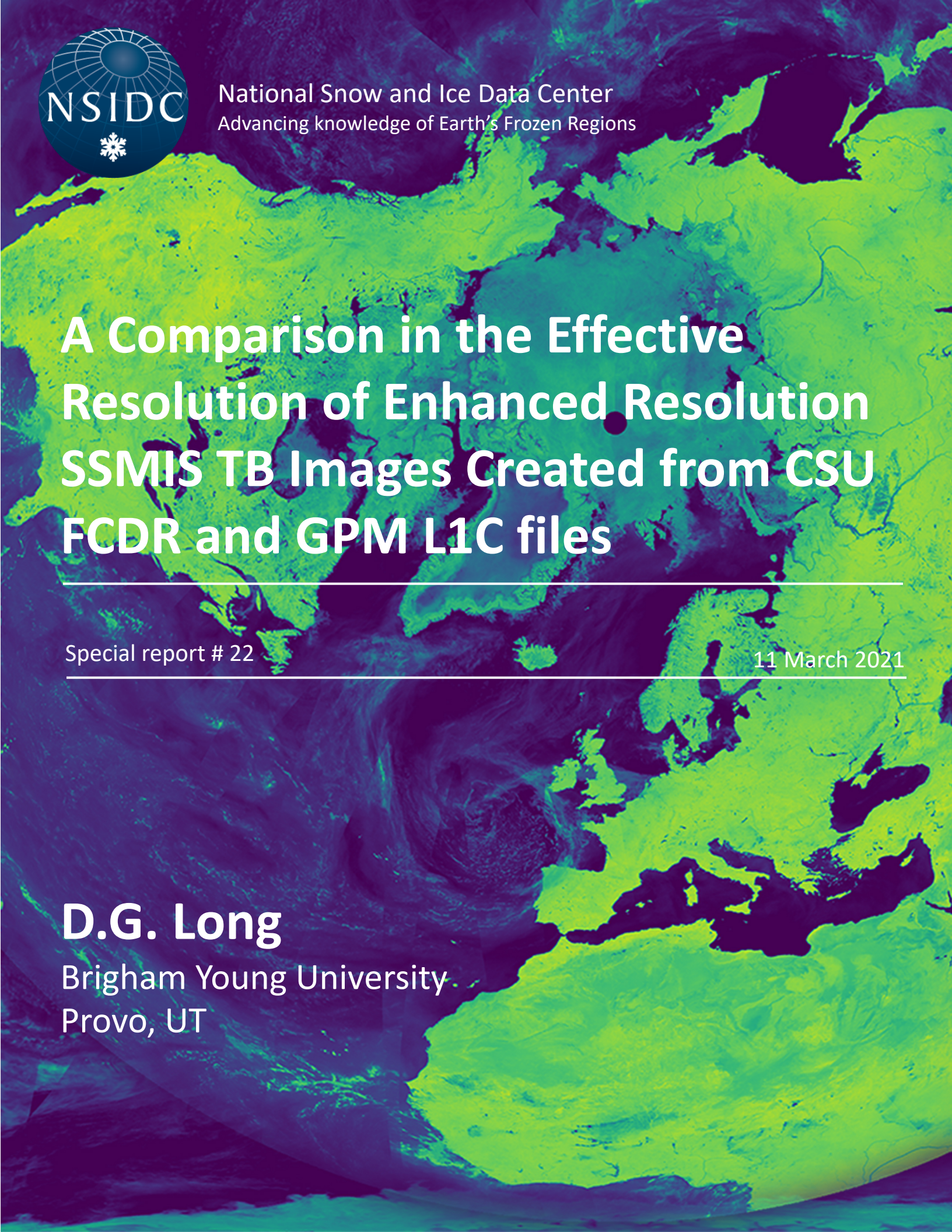

National Snow and Ice Data Center
Advancing knowledge of Earth's Frozen Regions

A Comparison in the Effective Resolution of Enhanced Resolution SSMIS TB Images Created from CSU FCDR and GPM L1C files

Special report # 22

11 March 2021

D.G. Long
Brigham Young University
Provo, UT

Citation

Long, David G. 2021. A Comparison in the Effective Resoluton of Enhanced Resolution SSMIS TB Images Created from CSU FCDR and GPM L1C Files. NSIDC Special Report 22. Boulder CO, USA: National Snow and Ice Data Center. https://nsidc.org/sites/nsidc.org/files/technical-references/NSIDC-Special-Report-22.pdf.

A Comparison in the Effective Resolution of Enhanced Resolution SSMIS T_B Images Created from CSU FCDR and GPM L1C Files

David G. Long
Brigham Young University, Provo, UT

March 11, 2021

Abstract

The Calibrated Passive Microwave Daily Equal-Area Scalable Earth (EASE) Grid 2.0 Brightness Temperature (CETB) Earth System Data Record (ESDR) project team has developed algorithms for creating Earth-based enhanced resolution brightness temperature (T_B) images from swath-based CSU FCDR files. In this report, these algorithms are applied to CSU FCDR and GPM L1C files and the effective resolution of the results compared for both conventional (low resolution) drop-in-the-bucket imaging and enhanced resolution using the radiometer form of the Scatterometer Image Reconstruction (rSIR) algorithm on a finer grid. The effective resolution of the CETB products using actual sensor data collected over coastline and island crossings is derived using the technique of [1]. We find that (1) the *effective* resolution of the rSIR images is 30–60% finer than conventionally processed gridded data and (2) both data sources provide essentially the same spatial resolution. Given the similarity of the two input sources, this last observation is expected.

1 Introduction

The NASA MEaSUREs Calibrated Passive Microwave Daily EASE-Grid 2.0 Brightness Temperature ESDR (CETB) Earth System Data Record (ESDR) project team has created a single, consistently processed, multi-sensor ESDR of Earth-gridded microwave brightness temperature (T_B) images spanning from 1978 to the present based on new fundamental climate data records (FCDRs) for passive microwave observations from a wide array of sensors [2, 4, 5]. The CETB dataset includes both conventional and enhanced resolution T_B images on standard map projections and is designed to serve the land surface and polar snow/ice communities in studies of climate and climate change [6].

The CETB image data set is produced from the Colorado State University (CSU) Fundamental Climate Data Record (CSU FCDR). The data producers used the same software system to produce an interim version of the data, produced and distributed in near real-time

(CSU ICDR). The CSU production team employed the SSM/I aboard DMSP-F13 as the calibration reference, as the best available choice prior to the launch of the GPM Microwave Imager (GMI). Specifically designed as a calibration reference standard, the GMI (launched in February 2014) provides unsurpassed accuracy and stability. Funded by the Precipitation Measurement Missions (PMM) science team, the intercalibration working group known as XCAL, which includes members of the CSU FCDR production team, has developed a separate processing stream, known as L1C, that uses GMI as the calibration reference [3].

The purpose of this report is to compare the effective resolutions of conventional and enhanced resolution T_B images generated from the two different data sources (CSU FCDR and GPM L1C). After providing background, the approach used for estimating the effective resolution is briefly summarized, and the results for both data sets are compared for both conventional and enhanced resolution processing.

2 Background

The conventional resolution T_B images are created using standard drop-in-the-bucket (DIB), also known as gridding (GRD), techniques. To create finer resolution images, reconstruction techniques are employed [6, 4]. The effective image resolution is defined by the 3 dB width of the pixel spatial response function (PSRF). Simulation was first used to validate the resolution enhancement [6, 7]. This was followed by analysis based on actual data.

The theory of radiometer reconstruction and resolution enhancement is provided in [6] and [7]. Brightness temperature (T_B) image products are created by mapping individual T_B measurements onto an Earth-based grid using standard EASE-Grid 2.0 map projections [9, 10]. In the conventional-resolution gridded images (GRD), the center of each measurement location is mapped to an output projected grid cell or pixel. All measurements within the specified time period whose center fall within the bounds of a particular grid cell are averaged together. The unweighted average becomes the reported pixel T_B value for that grid cell. Since measurement footprints can extend outside of the pixel, the effective resolution of GRD images is coarser than the pixel size. We call the spacing of pixels the "pixel posting" or the "posting resolution", see Fig. 1a.

To generate fine resolution T_B products by reconstruction we use the rSIR algorithm [6, 14]. The iterative rSIR algorithm employs regularization to tradeoff noise and resolution by limiting the number of iterations and thereby producing partial reconstruction [7]. The rSIR products are posted on fine resolution grids with an effective resolution that is coarser than the posting resolution, i.e., they are oversampled, see Fig. 1b.

3 Pixel Spatial Response Function

The *measurement* response function (MRF) describes the spatial characteristics of an *individual measurement*, i.e., how much the brightness temperature at each spatial location contributes

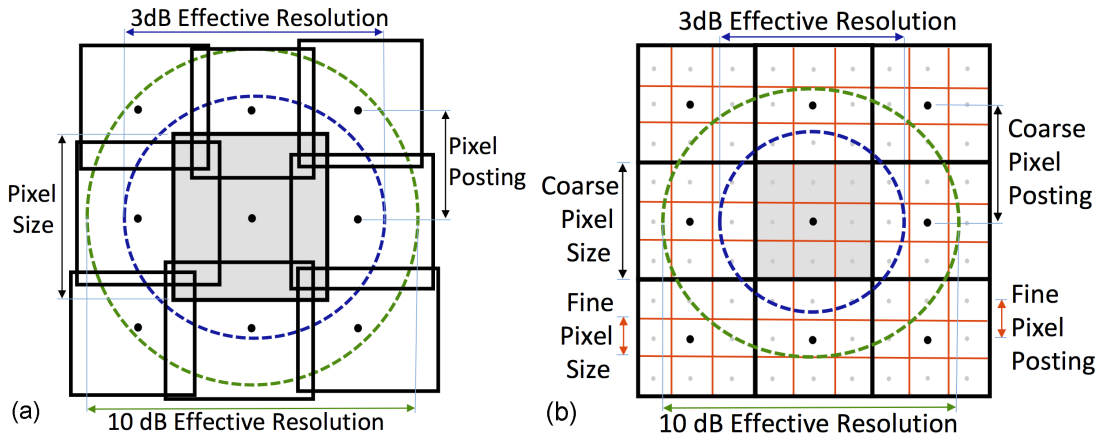

Figure 1: Pixel size versus posting illustrations. (a) Diagram showing irregularly sized and overlapping pixels posted on a uniform grid (discussed later). Due to the processing used to compute the pixel value, the −3-dB contour of the pixel spatial response function (PSRF) is larger than the pixel area. A −10-dB contour of PSRF is shown for comparison. (b) Diagram of uniform grids showing both fine and coarse pixels. The effective resolution solution of the PSRF of both coarse and fine pixels is the same, with the fine pixels posted at finer spacing (resolution).

to the measurement. Essentially, this is the antenna pattern[1], i.e., the temporally integrated antenna pattern of an individual measurement. When individual measurements are mapped onto a grid to create a T_B pixel *image*, the original measurements are combined (averaged), interpolated, resampled, or processed in another way (e.g., with a reconstruction algorithm). We are interested in the *pixel* spatial response function (PSRF) that describes the spatial characteristics of the estimated *pixel*, i.e., how much the brightness temperature at a particular spatial location contributes to the reported brightness temperature of the pixel. In effect, the PSRF is the impulse response of the measurement and image formation system, which includes the image formation from possibly multiple measurements of the same pixel, while the MRF is the spatial response of a single measurement. Analysis of the PSRF validates the effective resolution of the image formation.

Computation of the PSRF can be done with the MRFs of the individual measurements combined into the pixel values. The PSRF varies from pixel to pixel due to the differences in location of the measurement within the pixel area and variations in the MRFs for the measurements [7]. We note that the variation in the MRFs preclude the use of classic deconvolution algorithms because they require a fixed response function. Typically, the PSRF is normalized to a peak value of 1.

Note that the pixel values of simple image formation algorithms such as DIB are the mean of the measurements included in the pixel [6]. Thus, the PSRF is proportional to the measurements' MRF included in the pixel value. Similarly, for resampling or interpolation, the PSRF is proportional to the weighted linear sum of the measurement MRFs included in

[1]The MRF is really a "smeared" version of the antenna pattern which is the result of the movement of the antenna pattern on the surface over the measurement integration period, see [6].

the pixel value and combines the effects of the offset of the measurements from the pixel center and from each other [6, 18]. For rSIR, the PSRF linear summation approach cannot be used due to the non-linearity in the algorithm.

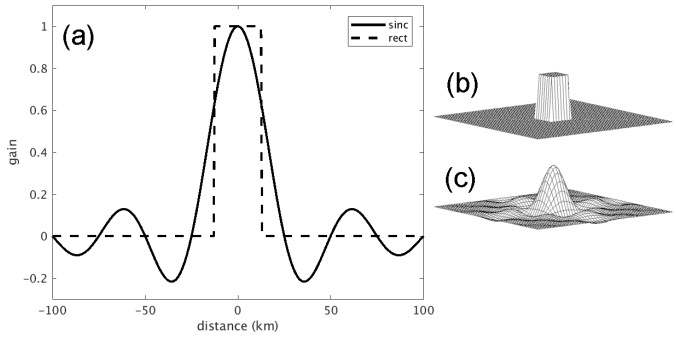

Figure 2: (a) One-dimensional sinc function compared to a rect function. Illustration of two-dimensional (b) rect and (c) sinc functions.

3.1 Relationship of the PSRF and the Effective Resolution

Given the PSRF, the effective resolution of the pixel corresponds to the area of the PSRF greater than a particular threshold, typically -3 dB [16, 7], though other values are sometimes used. We often express the resolution in terms of the square root of the area, which we call the "linear resolution" in this paper. For example, the ideal PSRF for a rectilinear image is a two-dimensional "rect" or "box-car" function that is valued at one over the pixel area and zero elsewhere, see Fig. 2. To build intutition on this, consider a 25 km image grid, i.e., a grid of square pixels that are each 25 km on a side. The ideal "pixel resolution" of this pixel is 625 km^2, which is a linear resolution of 25 km. Note, however, that according to the Nyquist criterion the finest spatial frequency that can be represented with pixel values spaced 25 km apart is 1/50 km^{-1}, that is, the wavelength of the finest representable spatial frequency is 50 km.

Since only a finite number of discrete measurements are available, we *must* assume that the signal and the PSRF are bandlimited in a way that is consistent with the sample spacing [17]. A bandlimited version of such an ideal boxcar PSRF is a two-dimensional sinc function, as seen in Fig. 2. For ideal 25 km sampling, this bandlimited PSRF is the best achievable PSRF that is consistent with the sampling. By the Nyquist criterion, signals with frequency higher than one half the sampling rate (posting) cannot be represented without aliasing.

The spacing of the pixels is called the "posting resolution". In general, the pixels can be larger than their spacing (the posting resolution) so that the pixels overlap, as illustrated in Fig. 1a. In this case, the pixel size is larger than the posting resolution. The resulting linear resolution of the PSRF is thus larger that the posting resolution, which means that the *effective resolution* is coarser than the posting resolution. When the posting resolution is finer than the effective resolution the signal is sometimes termed "oversampled" as illustrated in Fig. 1b.

One way to determine the effective resolution of actual images is based on first estimating the step response of the imaging process. Assuming the PSRF is essentially symmetric, the

PSRF can be derived from the observed step response by linear deconvolution. Recall that the step response is the convolution of the PSRF with a step function. The PSRF can thus be computed from the step response by deconvolution with a step function. The effective linear resolution is the dimension of the PSRF above the -3 dB threshold.

4 Effective Versus Posting Resolution

Regardless of the posting resolution (image pixel spacing), the effective resolution of the reconstructed T_B image is defined by the PSRF. To avoid aliasing, the posting resolution must be smaller (finer) than the effective resolution. We note that as long as this requirement is met, the posting resolution can be arbitrarily set. Thus, the pixel size can be arbitrarily determined based on the the pixel size of a standard map projection such as the EASE Grid 2.0 system [5, 9].

There are advantages of a finer posting resolution. For example, since the effective resolution can vary over the image due to the measurement geometry[2], the PSRF is not spatially constant. As a result, because the image has uniform pixel sizes, the image may be over or under sampled in some areas. Fine posting ensures all information is preserved and that Nyquist sampling criterion is met. Furthermore, finer posting provides optimum (in the bandlimited sense) interpolation of the effective information in the image. This interpolation can be better than bi-linear or bi-cubic schemes often used for interpolation. We also note that fine posting resolution is required by the signal processing in reconstruction to properly represent the sample locations and measurement response functions. On the other hand, oversampled images produce larger files and there is potential confusion among users in understanding the effective resolution and correlation between adjacent pixels. Of course, oversampled images can be low pass filtered and resampled to a coarser resolution to reduce data size.

As previously noted, the "ideal" PSRF is 1 over the pixel and 0 elsewhere, i.e. a small box car function. However, since the signal is on a discrete grid, we must assume that the signal is bandlimited so that the samples can represent the signal without aliasing. Thus, the band limited ideal PSRF is a low-pass filtered rect function, i.e., a two-dimensional sinc function (Fig. 2), though in practice the PSRF has a wider main lobe and smaller side lobes. Because the PSRF is non-zero outside of the pixel area, the signal from outside of the pixel area "leaks" into the observed pixel value. For example, if we have an open ocean pixel where the ocean at 160 K is adjacent to a land pixel where the land is 250 K, a PSRF that is down 10 dB at the next pixel will contribute approximately 9 K to the observed ocean value, essentially raising the observed value to 169 K from its ideal value of 160 K.

The fact that the PSRF is non-zero outside of the pixel area also means that nearby pixels are statistically correlated with each other – they are not independent even in the ideal case. The correlation is even stronger when the effective resolution is coarser than the posting

[2]In creating daily images, multiple orbit passes are combined. The overlapping coverage of the orbits is much greater in the polar regions than at lower latitudes. Further, due to the antenna rotation the measurement 3-dB footprint is elliptical whose aspect (rotation) angle varies over the swath. In addition, the effective density of the measurements is higher near the swath edge. As a a result the PSRF varies with location on the Earth even though the antenna pattern is fixed.

resolution. Choosing the posting resolution to be the same as the effective resolution can minimize the apparent statistical correlation between adjacent pixels.

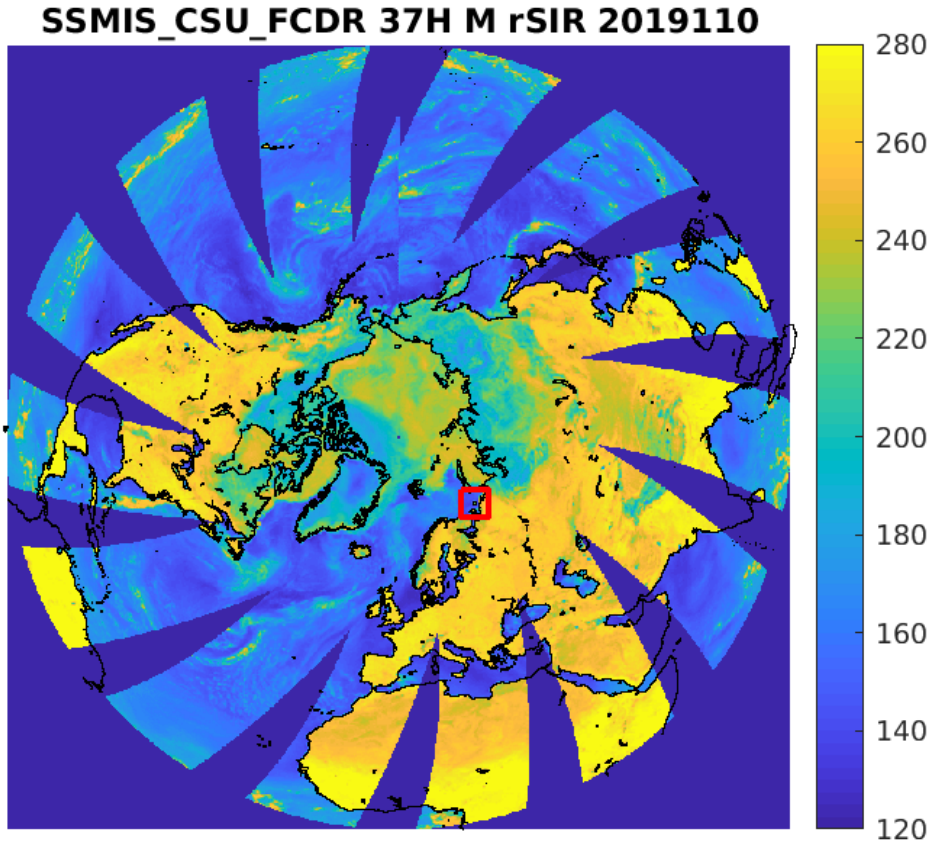

Figure 3: rSIR Northern Hemisphere SSMIS Radiometer T_B EASE-Grid 2.0 37 GHz, horizontall-polarized (H pol), brightness temperature image, morning, on day of year 108, 2019. Open ocean appears cold (low T_B) compared to land and sea-ice ice. The thick red box (right of and below the image center) outlines the study area.

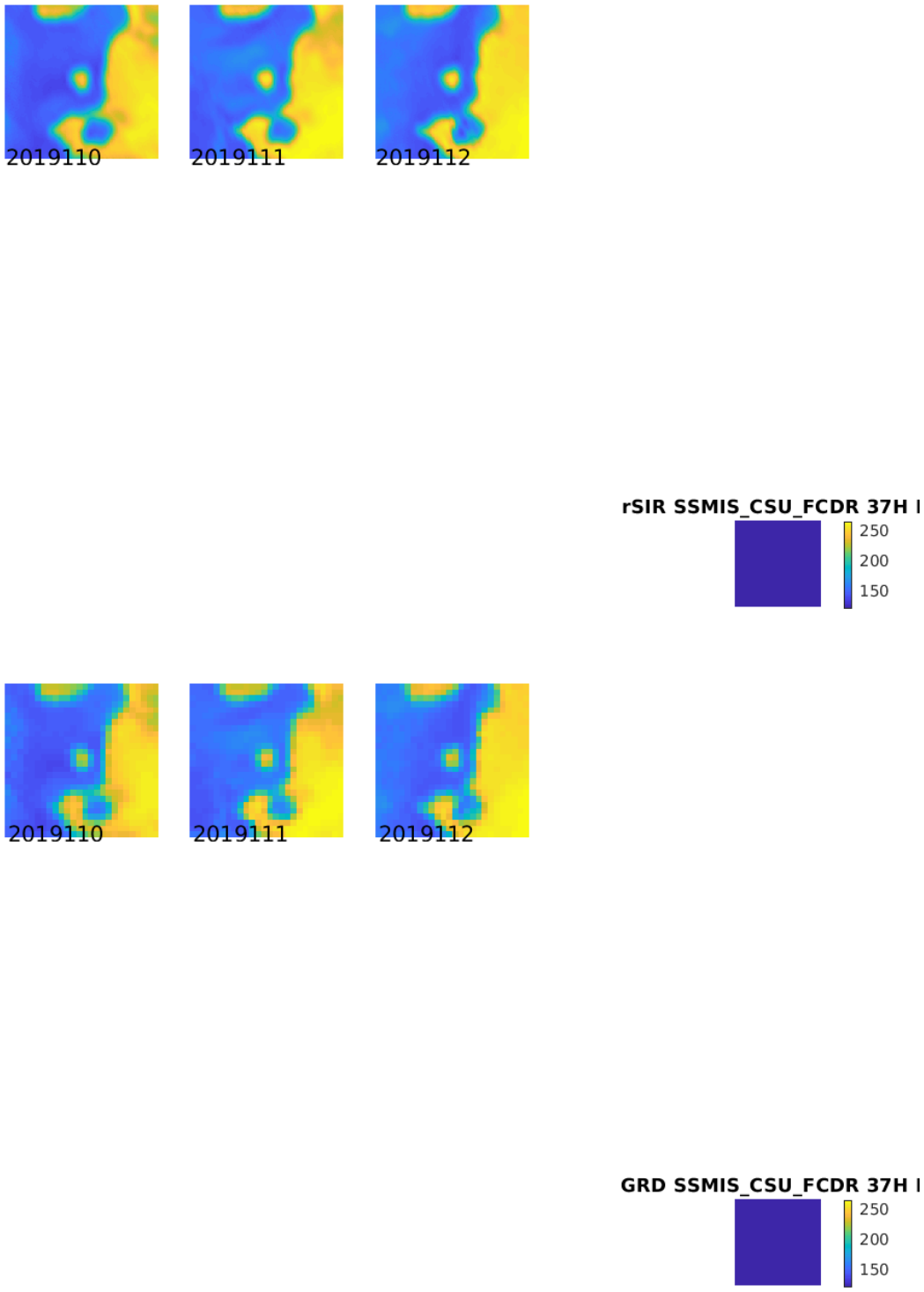

Figure 4: Time series of SSMIS 37VHMorning (top) rSIR (3.125 km) and (bottom) GRD (25 km) T_B images drived from CSU ICDR inputs over the study area. Image dates are labeled on the image. The box in the lower right corner next to the color bar is a plot routine artifact and should be ignored.

5 Resolution Estimation of Actual Data

To illustrate the estimation of the PSRF and the effective resolution, SSMIS F18 data is used. The same approach is applied to the other CETB sensors and data sources to compare the effective resolution enhancement of the CSU FCDR and GPM L1C data files later. We note that the CSU system that produces the FCDR swath data is used to produce the ICDR products in real time. While the FCDR reserve the option to correct potential problems in the final FCDR processing, this is rarely happens in practice. Thus, we expect the results of the two inputs to be very similar.

In this section we evaluate the effective linear resolution of SMMIS F18 CSU ICDR image data from CETB daily images at both conventional and enhanced resolution via estimation of the pixel step response. To do this, we arbitrarily select a small 200 km by 200 km region centered at approximately 69N and 49E in the Arctic Ocean to do the analysis, see Fig. 3. The cold ocean/warm land transitions provide sharp discontinuities that can be simply modeled. *Ostrov Kolguyev* is a nominally-flat, tundra-covered island that is approximately 81 km in diameter with a maximum elevation of ∼120 m. The island is nearly circular. Since there is variability (noise) from pass to pass, average results over a 20-day time period are considered. Figure 4 shows individual CETB subimages over the study period. The data time period was arbitrarily selected using CETB T_B images so that the T_B values vary only minimally, i.e., are essentially constant, over the time period with high contrast between land and ocean.

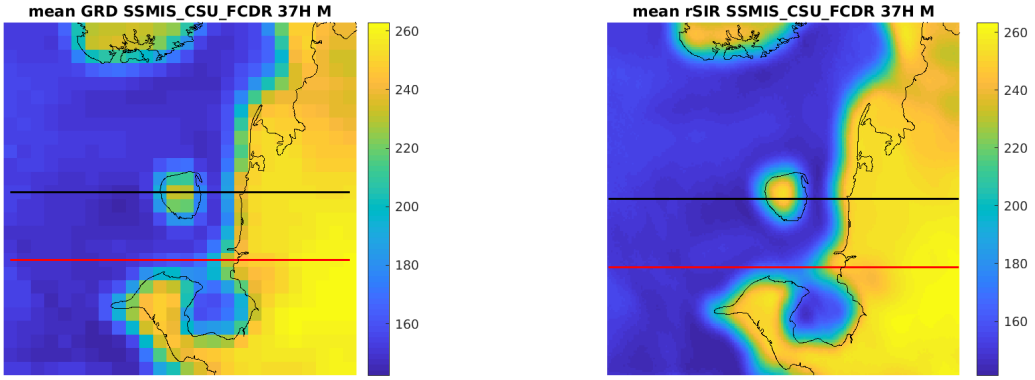

Figure 5: Average of daily SSMIS 37H T_B images over the study area spanning day-of-year 110-112, 2019 with a coastline overlay. (left) 25-km GRD. (right) 3-km rSIR. Note the apparent offset of the island in the GRD, which results from the coarse pixels. The thick horizontal lines show the data transect locations where data is extracted from the image for analysis. The black line is the "island-crossing" case while the red line is the "coastline-crossing" case.

Two horizontal transects of the study region are considered in separate cases. One crosses the island and the coast, while the second crosses a patch of sea ice and the coast, see Fig. 5. Due to the dynamics of the sea ice that is further from the shore, only the near-coast region is considered in the analysis. We model the surface brightness temperature as essentially constant with different values over land and water.

Fig. 5 compares the averaged daily GRD and rSIR images of the study region. In these images, the cooler (darker) areas are open ocean. Land areas have high temperatures, with sea-ice covered areas exhibiting a somewhat lower T_B. The GRD images are blocky, while the high-resolution images exhibit finer resolution and more accurately match the coastline. These images were created by averaging 20 days of daily T_B images in order to minimize noise-like effects due to (1) T_B measurement noise and (2) the effects of the variation in measurement locations and footprint orientation within each pass and from pass-to-pass. The derived PSRF and linear resolution thus represent temporal averages. The derived PSRFs are representative of single-pass PSRFs in other areas.

Examining Fig. 5 we observe that the ocean and land values are reasonably modeled by different constants, with a transition zone at the coastline. It is evident that the GRD images are much blockier than the rSIR images. This is due to the finer grid the rSIR images are computed on and their better effective resolution. Due to the coarse quantization of the GRD image the island looks somewhat offset downward whereas the rSIR image better corresponds to the superimposed coastline map.

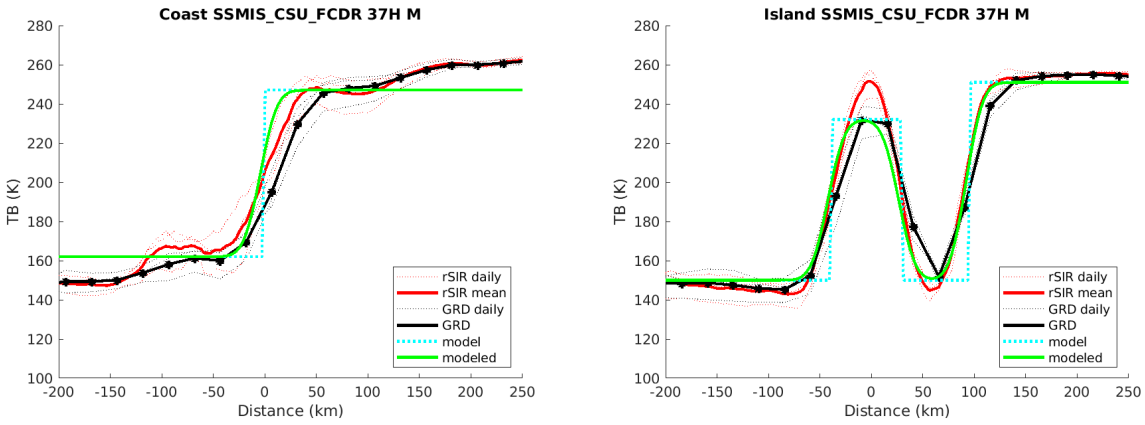

Figure 6: Plots of T_B along the two analysis case transect lines shown in Fig. 5 for the (left) coast-crossing and (right) island-crossing cases. Daily values over the study period are shown for rSIR and GRD as thin blue and yellow lines, respectively. The averages of these lines are shown in red and black. The discrete step and convolved Gaussian step models are also shown. The x axis is centered on the rSIR-derived coastline or island center for the particular case.

Fig. 6 plots the image T_B value along the two study transects. Note that rSIR T_B values have sharper transitions from land to ocean than the GRD images and that the GRD image underestimates the island T_B. The GRD values also have longer ocean-side transitions than rSIR and overestimate T_B in the *proliv Pomorskiy* strait separating the island and coastline south (right) of the island. On the other hand, the rSIR curves appear to exhibit a small under- and over-shoot near the transitions. The over-shoot is sometimes described as the "ringing" that observed near a sharp edge in an image. Its occurance is a consequence of Gibbs phenomena resulting from bandlimited reconstruction of a discontinuity and is evidence of the improved resolution of the reconstruction[3].

[3] "Ringing" occurs in conventional processing as well, but is often not as pronounced as in high resolution

Lacking high resolution maps of the true T_B, it is difficult to precisely analyze the accuracy and resolution of the images. However, we employ signal processing considerations to infer the expected behavior of the values. For analyzing the expected data behavior along these transects we introduce a simple step model for the underlying T_B. Noting that the T_B variation over land near the coast for the coastline case is a nearly constant 260 K with a variation no more than a few K, we model the land as a constant 260 K. Similarly, the ocean T_B is modeled as a constant 120 K. The modeled T_B is plotted in Fig. 5 for comparison with the observed and reconstructed values. The modeled T_B is filtered with a 25 km Gaussian response filter, shown in green, for comparison. The 25 km window represents the nominal antenna pattern on the surface [6]. The window-filtered model T_B thus represents the "ideal" result, i.e., the best than can be achieved from the model.

Examining Fig. 6, we note that the ripple artifacts in the rSIR T_B transition from ocean to land in both examples are the result of the implicit low pass filtering in the reconstruction. The pass-to-pass variability in the T_B observations is approximately the same for both GRD and rSIR in most places, suggesting that there is not a significant noise penalty when employing rSIR reconstruction.

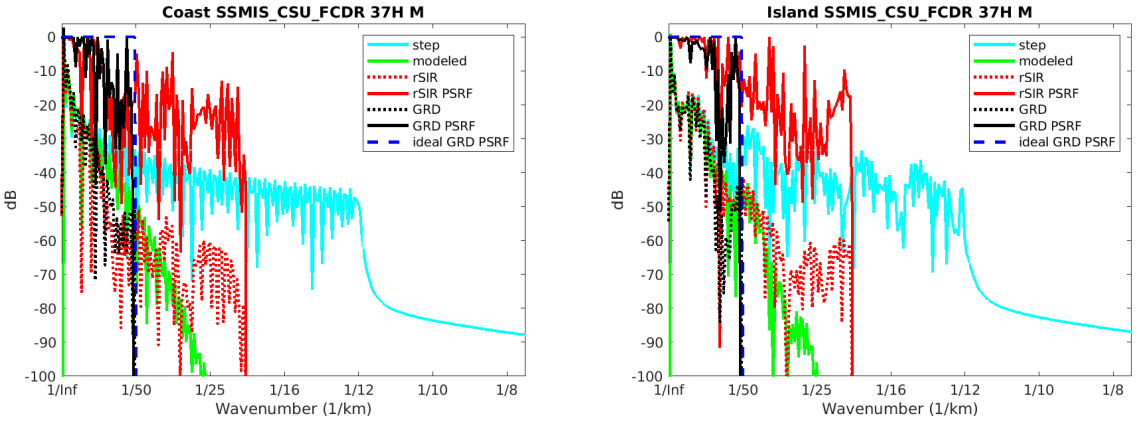

Figure 7: Wavenumber spectra of the T_B slices, the model, and the PSRF. (left) Coast-crossing case. (right) Island-crossing case. See text.

Insight can be gained by examining the spectra of the signal. Fig. 7 presents the wavenumber spectra of the key signals in Fig. 6. The spectra were computed by zero padding the data. For simplicity, only the Fourier transforms of the average curves are shown. The spectra of the modeled signal is shown in in blue. Peaking at 0 wavenumber, the modelled signal spectrum tapers off at higher wavenumbers. The filtered model signal, shown in red, represents the best signal that can be recovered. The GRD signal closely follows the ideal until it reaches the cut-off frequency permitted by the grid, beyond which it cannot represent the signal further. rSIR nicely follows this signal out to the limit of the graph and thus has higher effective resolution than GRD, even though the total energy in the signal is small at this level. Details of high wavenumber responses differ between the coast-crossing and island-crossing case, but the same conclusions apply.

images.

Deconvolution of the step response is accomplished in the frequency domain by dividing the step response by the spectra of the modeled step function, with care for how zeros and near-zeros in the modeled step function are handled in the inverse operation. The ideal GRD PRSF (blue dashed line) is a rect. The estimated GRD PSRF spectrum closely matches the ideal. The rSIR PSRF spectrum also matches the ideal in the low frequency region, but also contains additional information at higher wavenumbers, which gradually rolls off. This additional spectral content provides the finer resolution of rSIR compared to the GRD result.

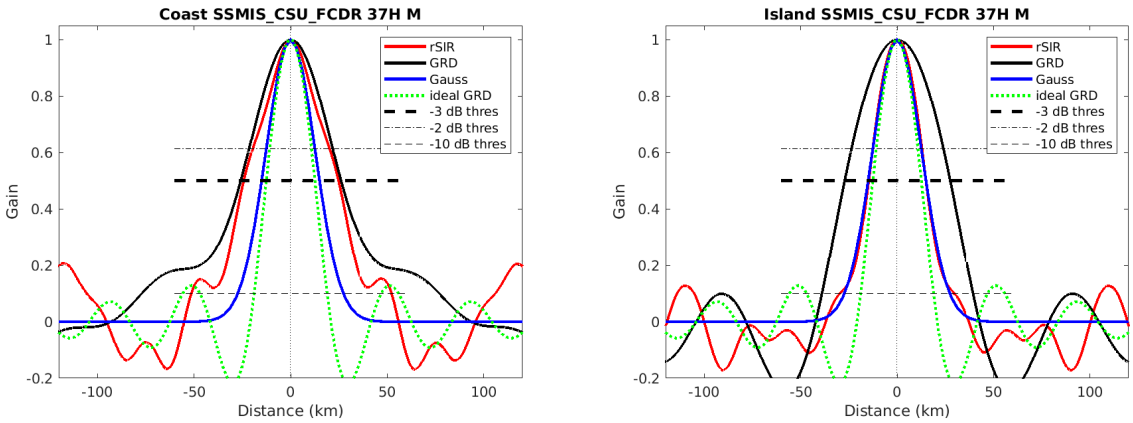

Figure 8: Derived single-pass rSIR and GRD PSRFs from the (left) coast-crossing and (right) island-crossing cases. Shown for comparison are a 25-km wide Gaussian window and a 25-km wide sinc function, which represents the ideal GRD pixel PSRF. The horizontal dashed line corresponds to the -3 dB line. The effective 3-dB linear resolution is the width of the PSRF at this line.

Finally, the estimated one-dimensional PSRFs are computed as the inverse Fourier transform of the PSRF spectra in Fig. 7 as shown in Fig. 8. Table 1 shows the linear resolution for each, computed as the width of the PSRF at the -3 dB point. For comparison, the linear resolution using both -2 dB and -10 dB thresholds is shown. In all cases the resolution of rSIR is better than the observed GRD resolution.

A key observation is that the effective resolution, as defined by the −3-dB width of the derived PSRFs, is very similar for both analysis cases. As expected, the observed GRD PSRFs results are coarser than the ideal GRD PSRFs due to the extension of the MRFs outside of the pixel area. The rSIR curve has a small shoulder on the right side which makes it asymmetric and wider in the coastal case than the island case, but otherwise the rSIR PSRF nearly matches the Gaussian-filtered model over the main lobe. The island crossing rSIR result has finer linear resolution than both the ideal GRD and actual GRD results. The island rSIR resolution represents an improvement of nearly 30% from the observed GRD resolution and 10% from the ideal GRD resolution. We conclude that rSIR does, in fact, provide finer effective resolution than GRD products, with an improvement of nearly 30% for this sensor.

The appendix provides an analysis that compares the estimated resolution of images derived from F18 SSMIS measurements from two different sources: FNMOC and CSU_ICDR L1C files. The analysis is by sensor, sensor channel (frequency and polarization), and local-time-of-day

Table 1: Inferred linear resolutions from Fig. 8 for various thresholds.

	-3 dB Thres		-2 dB Thres		-10 dB Thres	
Algorithm	Coast	Island	Coast	Island	Coast	Island
Gauss	30.0	30.0	24.5	24.5	54.8	54.8
rSIR	49.0	29.8	38.0	24.9	103.6	59.6
ideal GRD	36.2	36.2	30.3	30.3	54.5	54.5
GRD	51.1	54.7	42.0	46.5	154.0	78.2

(LTOD). For single day images, the improvement in resolution for rSIR versus GRD varies from approximately 30% to 60%, depending on sensor and channel. The results are similar for different image LTODs. The results are essentially identical for both signal sources.

6 Conclusion

This white paper considers the effective resolution of conventional and enhanced resolution T_B image products produced from two different processing streams of F18 SSMIS data. We find that the resolution enhancement results for both streams are essentially identical. As expected, the effective resolution of the images is coarser than the posting (pixel spacing) resolution for both conventionally processed (GRD) data and enhanced resolution rSIR images. The rSIR pixel spatial response function exhibits significantly finer spatial resolution than GRD, with a 30–60% improvement in effective resolution for rSIR compared to GRD regardless of the input data. Analysis of the precise resolution improvement of rSIR is channel dependent.

References

[1] D.G. Long, M.J. Brodzik, and M. Hardman, Evaluating the Effective Resolution of Enhanced Resolution SMAP Brightness Temperature Image Products, in review, *IEEE J. Sel. Topics Remote Sensing*, 2020.

[2] M.J. Brodzik, D.G. Long, M.A. Hardman, A. Paget, and R.L. Armstrong, MEaSUREs Calibrated Enhanced-Resolution Passive Microwave Daily EASE-Grid 2.0 Brightness Temperature ESDR, Version 1. National Snow and Ice Data Center, Boulder, CO USA, 2016, updated 2019. Digital Media http://nsidc.org/data/nsidc-0630.

[3] W. Berg, R. Kroodsma, C.D. Kummerow, and D.S. McKague, Fundamental Climate Data Records of Microwave Brightness Temperatures, *Remote Sensing*, vol. 10, no. 8, 2018.

[4] M.J. Brodzik, D.G. Long and M.A. Hardman. 2019. SMAP Radiometer Twice-Daily rSIR-Enhanced EASE-Grid 2.0 Brightness Temperatures, Version 1.0. Boulder, CO: National Snow and Ice Data Center. Digital media. doi:10.5067/QZ3WJNOUZLFK., 2019.

[5] M.J. Brodzik and D.G. Long, Calibrated passive microwave daily EASE-Grid 2.0 brightness temperature ESDR (CETB): Algorithm theoretical basis document, National Snow

and Ice Data Center (NSIDC) publication [Online] Available at: http://nsidc.org/pmesdr/files/MEaSUREs_CETB_ATBD_v1.0.pdf, 2018.

[6] D.G. Long and M.J. Brodzik, Optimum image formation for spaceborne microwave radiometer products, *IEEE Trans. Geosci. Remote Sensing*, vol. 54, no. 5, pp. 2763–2779, doi:10.1109/TGARS.2015.2505677, 2016.

[7] D.G. Long, M.J. Brodzik, and M. Hardman, Enhanced Resolution SMAP Brightness Temperature Image Products, *IEEE Trans. Geosci. Remote Sensing*, vol. 57, no. 7, pp. 4151–4163, doi:10.1109/TGRS.2018.2889427, 2019.

[8] J. Piepmeier, P. Mohammed, G. De Amici, E. Kim, J. Pen and C. Ruff, Algorithm Theoretical Basis Document: SMAP Calibrated, Time-ordered Brightness Temperatures L1B_TB Data Product, SMAP Project, Rev. A, 10 Dec 2014, available online at URL https://smap.jpl.nasa.gov/system/internal_resources/details/original/278_L1B_TB_RevA_web.pdf.

[9] M.J. Brodzik, B. Billingsley, T. Haran, B. Raup, M. H. Savoie, EASE-Grid 2.0: Incremental but significant improvements for Earth-Gridded data sets, *ISPRS Int. J. Geo-Information*, vol. 1, no. 1, pp. 32–45, 2012.

[10] M.J. Brodzik, B. Billingsley, T. Haran, B. Raup, M. H. Savoie, Correction: M.J. Brodzik, et al., EASE-Grid 2.0: Incremental but significant improvements for Earth-Gridded data sets, *ISPRS Int. J. Geo-Information*, vol. 1, no. 1, pp. 32–45, 2012, *ISPRS Int. J. Geo-Information*, vol. 3, no. 3, pp. 1154–1156, 2014.

[11] G.E. Backus and J.F. Gilbert, Numerical applications of a formalism for geophysical inverse problems, *Geophys. J. R. Astron. Soc.*, vol. 13, pp. 247–276, 1967.

[12] G.E. Backus and J.F. Gilbert, Resolving power of gross Earth data, *Geophys. J. R. Astron. Soc.*, vol. 16, pp. 169–205, 1968.

[13] A. Stogryn, Estimates of brightness temperatures from scanning radiometer data, *IEEE Trans. Antennas Propagat.*, vol. AP-26, pp. 720–726, 1978.

[14] D.G. Long and D.L. Daum, Spatial resolution enhancement of SSM/I data, *IEEE Trans. Geosci. Remote Sensing*, vol. 36, no. 2, pp. 407–417, 1998.

[15] D.S. Early and D.G. Long, Image reconstruction and enhanced resolution imaging from irregular samples, *IEEE Trans. Geosci. Remote Sensing*, vol. 39, no. 2, pp. 291–302, 2001.

[16] F. Ulaby and D.G. Long, *Microwave Radar and Radiometric Remote Sensing*, University of Michigan Press, Ann Arbor, Michigan, 2014.

[17] D.G. Long and R. Franz, Band-limited signal reconstruction from irregular samples with variable apertures, *IEEE Trans. Geosci. Remote Sensing*, vol. 54, no. 4, pp. 2424–2436, 2016.

[18] D.G. Long, Comparison of SeaWinds Backscatter Imaging Algorithms, *IEEE J. Sel. Topics in Applied Earth Observations*, vol. 10, no. 3, pp. 2214–2231, doi:10.1109/JSTARS.2016.2626966, 2017.

Appendix: Detailed Comparison by Channel and Data Source

In this appendix, the methodology described in the main report for analyzing the effective resolution of T_B images is applied to images created for two different SSMIS near real-time sources, CSU ICDR and GPM L1C. A separate analysis is provided for each channel for both "morning" (M) and "evening" (E) local-time-of-day (LTOD) images. Some tables and figures are repeated for convenience.

We note that some channels (notably the high frequency channels) include strong atmospheric interference and/or may have very little land/ocean/ice contrast. Channel 91V is notable for this where there is no discernable surface response over the time period considered. In these cases, the analysis cannot be expected to work, so no resolution estimates can be generated. The number of useful days also varies by channel and can be a small as two. Channels 37H and 37V are affected to a lesser extent by atmospheric noise, but the atmospheric effects degrade the resolution enhancement in the cases shown.

Some time-of-day variations in the average positions of the reported measurement locations cause the created images to be shifted relative to the fixed coastline map. (An example of this is Fig. 101 for SSMIS 22V Morning.) This causes some anomolies in the reported results. The reasons for the location shifts are not clear, but are not related to the reconstruction processing — the shifts are in the source measurement locations. Unfortunately, the shift seems to vary from day to day. The current processing does not adjust the reported positions. But correcting these would improve the results. To help compensate for the effect of the shifts, the island and coastline boundaries are individually choosen for each case rather than merely using fixed coastline map locations.

7 Resolution Difference Summary

The following tables the rSIR and GRD resolution estimates for the CSU data set followed by the difference in the estimated resolution differences between the CSU and L1C for each F18 channel and LTOD. The next section provides the detailed differences in tabular and graphical form for each case. Note that the Gaussian and Ideal results are the same for both data sets and so are not included in the difference tables. Not all cases have exactly the same number of comparison days due to noisy conditions.

Examining the results, the estimated GRD resolutions for the datasets are essentially numerically equivalent. Due to the non-linearity in the rSIR algorithm there are small (typically much less than 1%) differences in estimated resolutions. Given that the differences are small, we conclude that the effective resolutions of two datasets are essentially equivalent. A separate report considers the statististical differences in the datasets.

Table 2: rSIR resolution estimates for channel 19H LTOD E for sensor SSMIS_CSU_FCDR

	-3 dB Thres		-2 dB Thres		-10 dB Thres	
Algorithm	Coast	Island	Coast	Island	Coast	Island
Gauss	30.0	30.0	24.4	24.4	54.8	54.8
rSIR	53.3	53.3	41.5	35.0	103.0	91.5
ideal GRD	36.2	36.2	30.3	30.3	54.5	54.5
GRD	77.4	77.4	65.7	48.2	181.9	89.6

Table 3: Difference in resolution estimates for channel 19H LTOD E for SSMIS_CSU_FCDR and SSMIS_GPM_L1C

	-3 dB Thres		-2 dB Thres		-10 dB Thres	
Algorithm	Coast	Island	Coast	Island	Coast	Island
rSIR	-0.087	-0.087	-0.242	-1.233	-1.493	0.833
GRD	-0.814	-0.814	-1.261	0.020	-1.773	0.175

Table 4: rSIR resolution estimates for channel 19H LTOD M for sensor SSMIS_CSU_FCDR

	-3 dB Thres		-2 dB Thres		-10 dB Thres	
Algorithm	Coast	Island	Coast	Island	Coast	Island
Gauss	30.0	30.0	24.4	24.4	54.8	54.8
rSIR	48.4	48.4	35.9	36.5	99.2	77.6
ideal GRD	36.2	36.2	30.3	30.3	54.5	54.5
GRD	84.6	84.6	77.5	54.6	109.3	93.5

Table 5: Difference in resolution estimates for channel 19H LTOD M for SSMIS_CSU_FCDR and SSMIS_GPM_L1C

	-3 dB Thres		-2 dB Thres		-10 dB Thres	
Algorithm	Coast	Island	Coast	Island	Coast	Island
rSIR	0.492	0.492	-0.814	1.093	-1.047	-0.298
GRD	0.476	0.476	0.545	0.858	1.411	0.752

Table 6: rSIR resolution estimates for channel 19V LTOD E for sensor SSMIS_CSU_FCDR

	-3 dB Thres		-2 dB Thres		-10 dB Thres	
Algorithm	Coast	Island	Coast	Island	Coast	Island
Gauss	30.0	30.0	24.4	24.4	54.8	54.8
rSIR	57.7	57.7	47.1	35.8	88.0	78.6
ideal GRD	36.2	36.2	30.3	30.3	54.5	54.5
GRD	60.7	60.7	47.4	56.1	137.7	128.2

Table 7: Difference in resolution estimates for channel 19V LTOD E for SSMIS_CSU_FCDR and SSMIS_GPM_L1C

	-3 dB Thres		-2 dB Thres		-10 dB Thres	
Algorithm	Coast	Island	Coast	Island	Coast	Island
rSIR	1.236	1.236	2.170	-1.130	0.562	-0.350
GRD	-2.484	-2.484	-2.140	0.316	0.657	-0.045

Table 8: rSIR resolution estimates for channel 19V LTOD M for sensor SSMIS_CSU_FCDR

	-3 dB Thres		-2 dB Thres		-10 dB Thres	
Algorithm	Coast	Island	Coast	Island	Coast	Island
Gauss	30.0	30.0	24.4	24.4	54.8	54.8
rSIR	49.4	49.4	38.1	41.4	85.6	86.9
ideal GRD	36.2	36.2	30.3	30.3	54.5	54.5
GRD	83.2	83.2	76.6	55.1	105.0	99.2

Table 9: Difference in resolution estimates for channel 19V LTOD M for SSMIS_CSU_FCDR and SSMIS_GPM_L1C

	-3 dB Thres		-2 dB Thres		-10 dB Thres	
Algorithm	Coast	Island	Coast	Island	Coast	Island
rSIR	0.137	0.137	-1.019	1.642	-1.562	-6.570
GRD	0.431	0.431	0.522	-0.626	0.888	-2.513

Table 10: rSIR resolution estimates for channel 22V LTOD E for sensor SSMIS_CSU_FCDR

	-3 dB Thres		-2 dB Thres		-10 dB Thres	
Algorithm	Coast	Island	Coast	Island	Coast	Island
Gauss	30.0	30.0	24.4	24.4	54.8	54.8
rSIR	58.9	58.9	49.1	36.5	86.4	75.6
ideal GRD	36.2	36.2	30.3	30.3	54.5	54.5
GRD	64.9	64.9	53.0	50.7	121.7	95.2

Table 11: Difference in resolution estimates for channel 22V LTOD E for SSMIS_CSU_FCDR and SSMIS_GPM_L1C

	-3 dB Thres		-2 dB Thres		-10 dB Thres	
Algorithm	Coast	Island	Coast	Island	Coast	Island
rSIR	1.057	1.057	2.380	-1.373	0.399	-0.319
GRD	-1.192	-1.192	-1.234	-0.098	0.855	-0.199

Table 12: rSIR resolution estimates for channel 22V LTOD M for sensor SSMIS_CSU_FCDR

	-3 dB Thres		-2 dB Thres		-10 dB Thres	
Algorithm	Coast	Island	Coast	Island	Coast	Island
Gauss	30.0	30.0	24.4	24.4	54.8	54.8
rSIR	50.2	50.2	39.9	42.4	83.2	101.1
ideal GRD	36.2	36.2	30.3	30.3	54.5	54.5
GRD	82.4	82.4	75.7	68.3	103.5	114.5

Table 13: Difference in resolution estimates for channel 22V LTOD M for SSMIS_CSU_FCDR and SSMIS_GPM_L1C

	-3 dB Thres		-2 dB Thres		-10 dB Thres	
Algorithm	Coast	Island	Coast	Island	Coast	Island
rSIR	0.339	0.339	-0.742	2.151	-1.366	-3.685
GRD	-0.678	-0.678	-0.766	1.604	0.396	0.041

Table 14: rSIR resolution estimates for channel 37H LTOD E for sensor SSMIS_CSU_FCDR

	-3 dB Thres		-2 dB Thres		-10 dB Thres	
Algorithm	Coast	Island	Coast	Island	Coast	Island
Gauss	30.0	30.0	24.4	24.4	54.8	54.8
rSIR	41.6	41.6	34.9	33.8	71.0	66.5
ideal GRD	36.2	36.2	30.3	30.3	54.5	54.5
GRD	58.1	58.1	48.9	47.7	88.9	80.1

Table 15: Difference in resolution estimates for channel 37H LTOD E for SSMIS_CSU_FCDR and SSMIS_GPM_L1C

	-3 dB Thres		-2 dB Thres		-10 dB Thres	
Algorithm	Coast	Island	Coast	Island	Coast	Island
rSIR	1.320	1.320	1.537	0.716	2.280	3.754
GRD	-0.027	-0.027	-0.027	-0.541	-0.011	-0.318

Table 16: rSIR resolution estimates for channel 37H LTOD M for sensor SSMIS_CSU_FCDR

	-3 dB Thres		-2 dB Thres		-10 dB Thres	
Algorithm	Coast	Island	Coast	Island	Coast	Island
Gauss	30.0	30.0	24.4	24.4	54.8	54.8
rSIR	40.4	40.4	30.0	32.4	62.3	70.6
ideal GRD	36.2	36.2	30.3	30.3	54.5	54.5
GRD	39.9	39.9	33.0	46.7	65.9	76.2

Table 17: Difference in resolution estimates for channel 37H LTOD M for SSMIS_CSU_FCDR and SSMIS_GPM_L1C

	-3 dB Thres		-2 dB Thres		-10 dB Thres	
Algorithm	Coast	Island	Coast	Island	Coast	Island
rSIR	0.170	0.170	0.234	0.618	-0.692	-0.288
GRD	0.022	0.022	0.104	-11.916	-2.195	-13.079

Table 18: rSIR resolution estimates for channel 37V LTOD E for sensor SSMIS_CSU_FCDR

	-3 dB Thres		-2 dB Thres		-10 dB Thres	
Algorithm	Coast	Island	Coast	Island	Coast	Island
Gauss	30.0	30.0	24.4	24.4	54.8	54.8
rSIR	42.3	42.3	35.4	36.2	73.8	74.1
ideal GRD	36.2	36.2	30.3	30.3	54.5	54.5
GRD	46.7	46.7	38.0	52.9	139.7	84.7

Table 19: Difference in resolution estimates for channel 37V LTOD E for SSMIS_CSU_FCDR and SSMIS_GPM_L1C

	-3 dB Thres		-2 dB Thres		-10 dB Thres	
Algorithm	Coast	Island	Coast	Island	Coast	Island
rSIR	0.670	0.670	0.769	0.077	0.929	3.602
GRD	-0.421	-0.421	-0.339	-0.428	-0.531	-0.208

Table 20: rSIR resolution estimates for channel 37V LTOD M for sensor SSMIS_CSU_FCDR

	-3 dB Thres		-2 dB Thres		-10 dB Thres	
Algorithm	Coast	Island	Coast	Island	Coast	Island
Gauss	30.0	30.0	24.4	24.4	54.8	54.8
rSIR	35.3	35.3	24.8	26.7	88.3	68.2
ideal GRD	36.2	36.2	30.3	30.3	54.5	54.5
GRD	50.7	50.7	42.6	38.0	76.9	67.1

Table 21: Difference in resolution estimates for channel 37V LTOD M for SSMIS_CSU_FCDR and SSMIS_GPM_L1C

	-3 dB Thres		-2 dB Thres		-10 dB Thres	
Algorithm	Coast	Island	Coast	Island	Coast	Island
rSIR	-0.820	-0.820	-0.371	-5.531	-1.754	3.276
GRD	-3.607	-3.607	-3.542	1.163	-2.577	0.046

Table 22: rSIR resolution estimates for channel 91H LTOD E for sensor SSMIS_CSU_FCDR

	-3 dB Thres		-2 dB Thres		-10 dB Thres	
Algorithm	Coast	Island	Coast	Island	Coast	Island
Gauss	30.0	30.0	24.4	24.4	54.8	54.8
rSIR	20.6	20.6	17.0	14.1	34.5	28.5
ideal GRD	36.2	36.2	30.3	30.3	54.5	54.5
GRD	31.0	31.0	25.9	31.7	47.6	52.9

Table 23: Difference in resolution estimates for channel 91H LTOD E for SSMIS_CSU_FCDR and SSMIS_GPM_L1C

	-3 dB Thres		-2 dB Thres		-10 dB Thres	
Algorithm	Coast	Island	Coast	Island	Coast	Island
rSIR	2.075	2.075	1.759	1.023	2.585	1.924
GRD	0.019	0.019	0.020	1.410	-0.037	2.150

Table 24: rSIR resolution estimates for channel 91H LTOD M for sensor SSMIS_CSU_FCDR

	-3 dB Thres		-2 dB Thres		-10 dB Thres	
Algorithm	Coast	Island	Coast	Island	Coast	Island
Gauss	30.0	30.0	24.4	24.4	54.8	54.8
rSIR	29.4	29.4	26.1	14.0	40.0	28.2
ideal GRD	36.2	36.2	30.3	30.3	54.5	54.5
GRD	36.4	36.4	30.0	19.0	61.6	31.8

Table 25: Difference in resolution estimates for channel 91H LTOD M for SSMIS_CSU_FCDR and SSMIS_GPM_L1C

	-3 dB Thres		-2 dB Thres		-10 dB Thres	
Algorithm	Coast	Island	Coast	Island	Coast	Island
rSIR	0.975	0.975	1.796	0.635	-4.560	1.711
GRD	-1.420	-1.420	-1.184	0.131	-1.910	0.280

Table 26: rSIR resolution estimates for channel 91V LTOD E for sensor SSMIS_CSU_FCDR

	-3 dB Thres		-2 dB Thres		-10 dB Thres	
Algorithm	Coast	Island	Coast	Island	Coast	Island
Gauss	30.0	30.0	24.4	24.4	54.8	54.8
rSIR	12.0	12.0	10.0	8.5	18.9	14.7
ideal GRD	36.2	36.2	30.3	30.3	54.5	54.5
GRD	27.3	27.3	22.9	33.1	40.3	57.8

Table 27: Difference in resolution estimates for channel 91V LTOD E for SSMIS_CSU_FCDR and SSMIS_GPM_L1C

	-3 dB Thres		-2 dB Thres		-10 dB Thres	
Algorithm	Coast	Island	Coast	Island	Coast	Island
rSIR	2.843	2.843	2.262	-0.091	5.553	-0.312
GRD	-0.941	-0.941	-0.777	0.700	-1.572	1.082

Table 28: rSIR resolution estimates for channel 91V LTOD M for sensor SSMIS_CSU_FCDR

	-3 dB Thres		-2 dB Thres		-10 dB Thres	
Algorithm	Coast	Island	Coast	Island	Coast	Island
Gauss	30.0	30.0	24.4	24.4	54.8	54.8
rSIR	11.5	11.5	9.7	14.0	17.1	58.6
ideal GRD	36.2	36.2	30.3	30.3	54.5	54.5
GRD	25.5	25.5	21.5	36.0	36.7	65.5

Table 29: Difference in resolution estimates for channel 91V LTOD M for SSMIS_CSU_FCDR and SSMIS_GPM_L1C

	-3 dB Thres		-2 dB Thres		-10 dB Thres	
Algorithm	Coast	Island	Coast	Island	Coast	Island
rSIR	-0.640	-0.640	-0.511	0.857	-1.104	30.848
GRD	-0.527	-0.527	-0.415	1.039	-0.990	1.619

8 Detailed Analysis for Each Case

8.1 Channel 19H E Figures

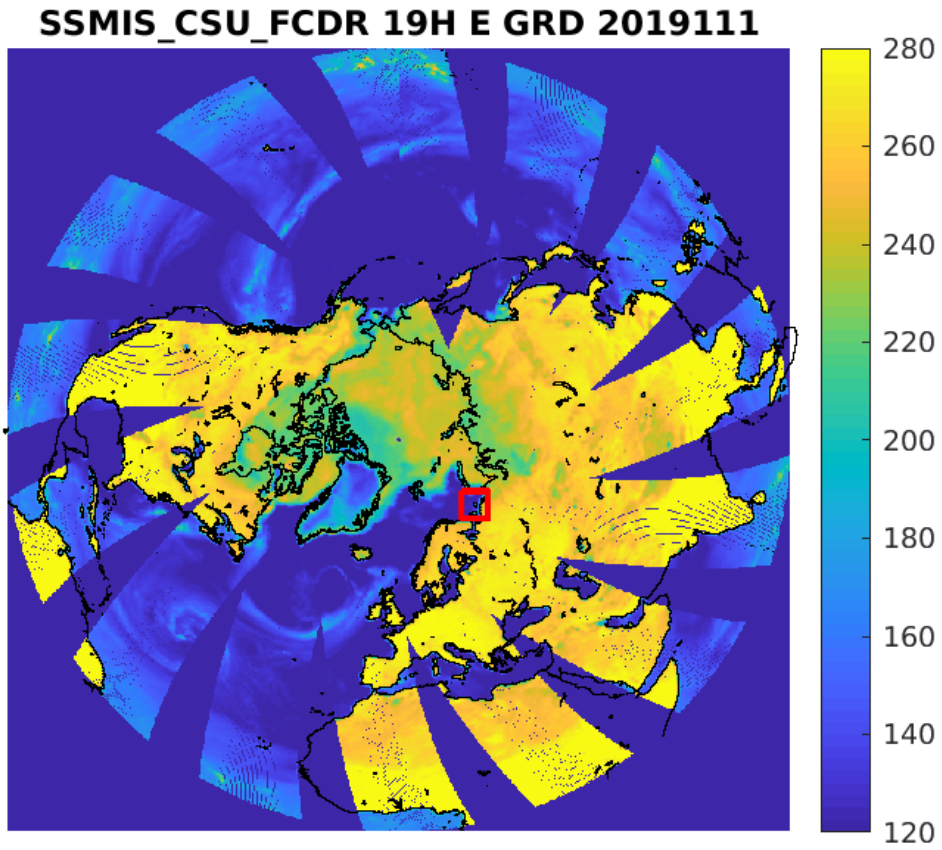

Figure 9: rSIR Northern Hemisphere view.

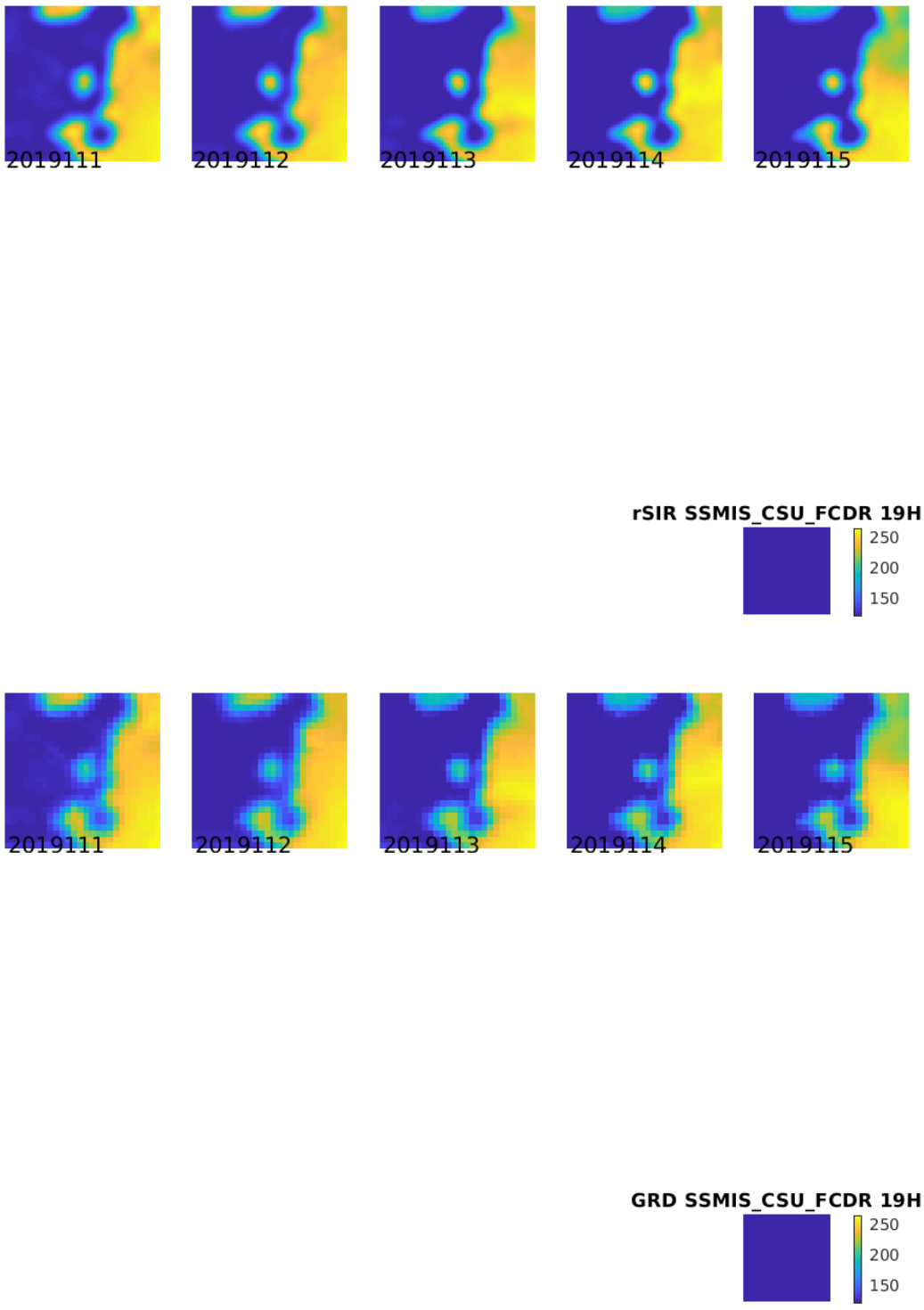

Figure 10: Time series of (top) rSIR and (bottom) GRD T_B images over the study area. Image dates are labeled on the image.

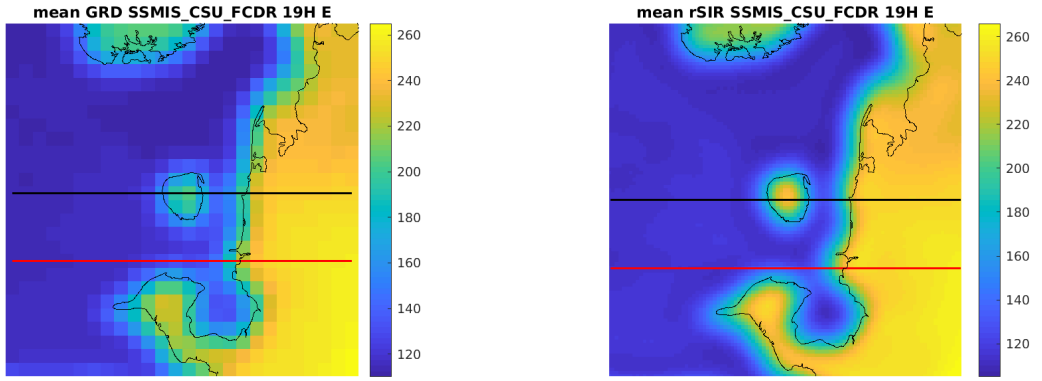

Figure 11: Average of daily T_B images over the study area. (left) 25-km GRD. (right) 3.125-km rSIR. The thick horizontal lines show the data transect locations where data is extracted from the image for analysis.

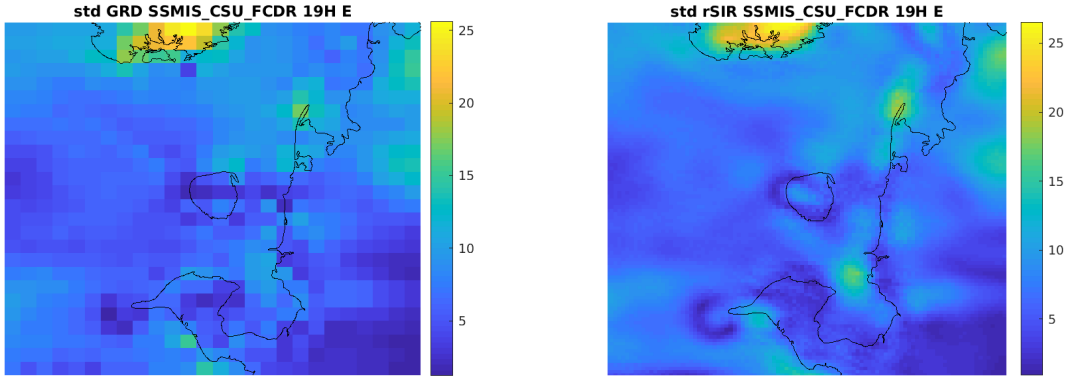

Figure 12: Standard deviation of daily T_B images over the study area. (left) 25-km GRD. (right) 3.125-km rSIR.

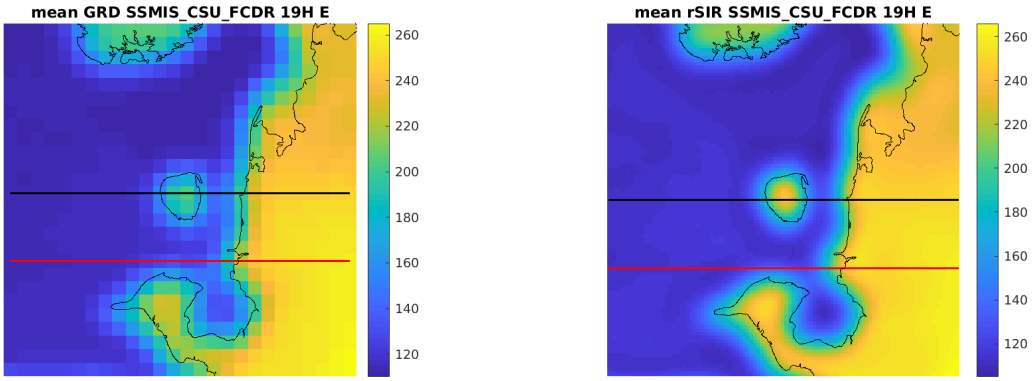

Figure 13: [Repeated] Average of daily T_B images over the study area. (left) 25-km GRD. (right) 3.125-km rSIR. The thick horizontal lines show the data transect locations where data is extracted from the image for analysis.

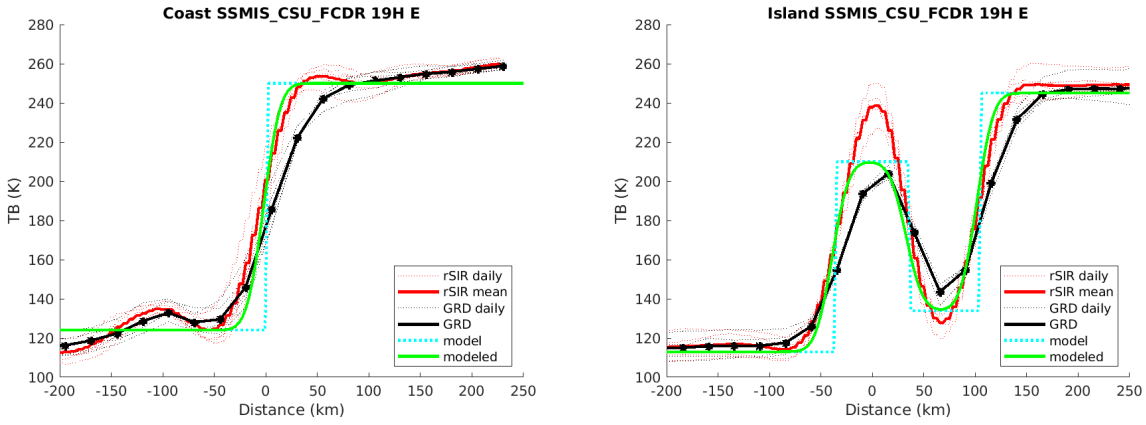

Figure 14: Plots of T_B along the two analysis case transect lines for the (left) coast-crossing and (right) island-crossing cases.

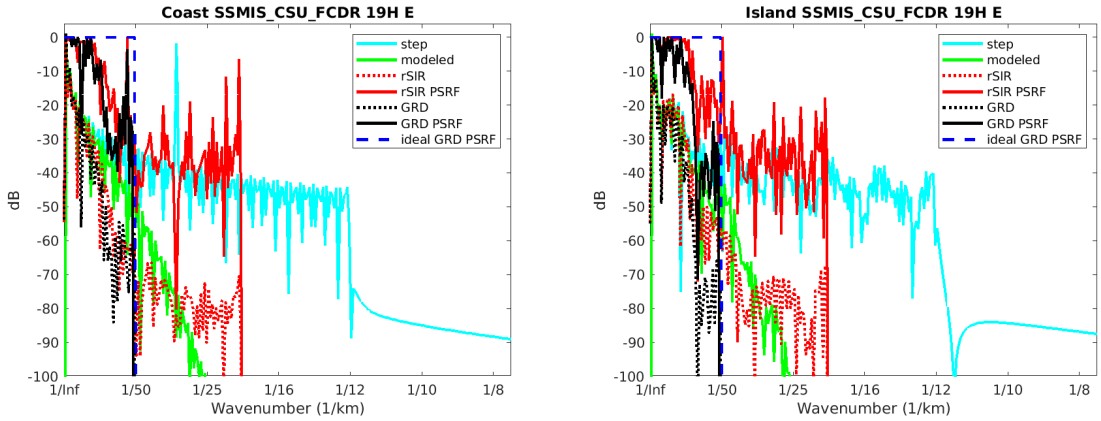

Figure 15: Wavenumber spectra of the T_B slices, the model, and the PSRF. (left) Coast-crossing case. (right) Island-crossing case.

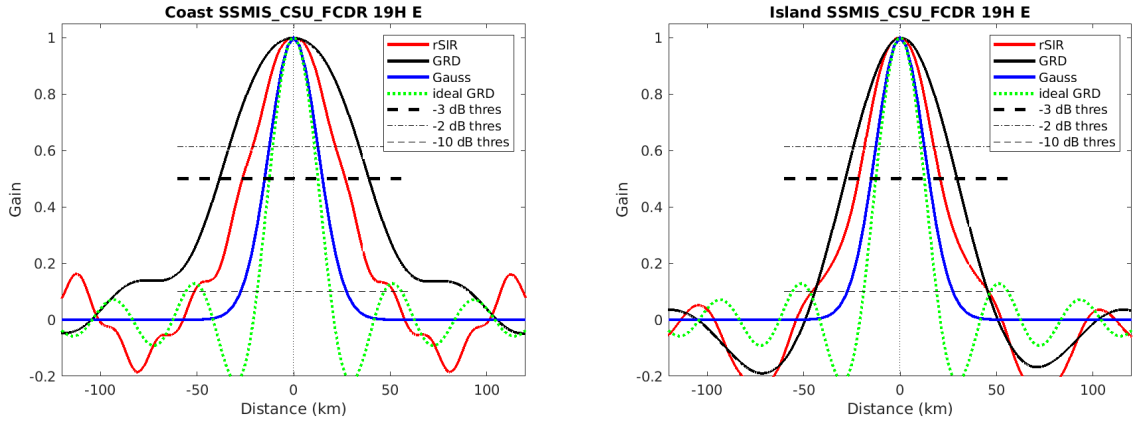

Figure 16: Derived single-pass rSIR and GRD PSRFs from the (left) coast-crossing and (right) island-crossing cases.

Table 30: Resolution estimates for SSMIS_CSU_FCDR channel 19H LTOD E

	-3 dB Thres		-2 dB Thres		-10 dB Thres	
Algorithm	Coast	Island	Coast	Island	Coast	Island
Gauss	30.0	30.0	24.4	24.4	54.8	54.8
rSIR	53.3	42.3	41.5	35.0	103.0	91.5
ideal GRD	36.2	36.2	30.3	30.3	54.5	54.5
GRD	77.4	58.0	65.7	48.2	181.9	89.6

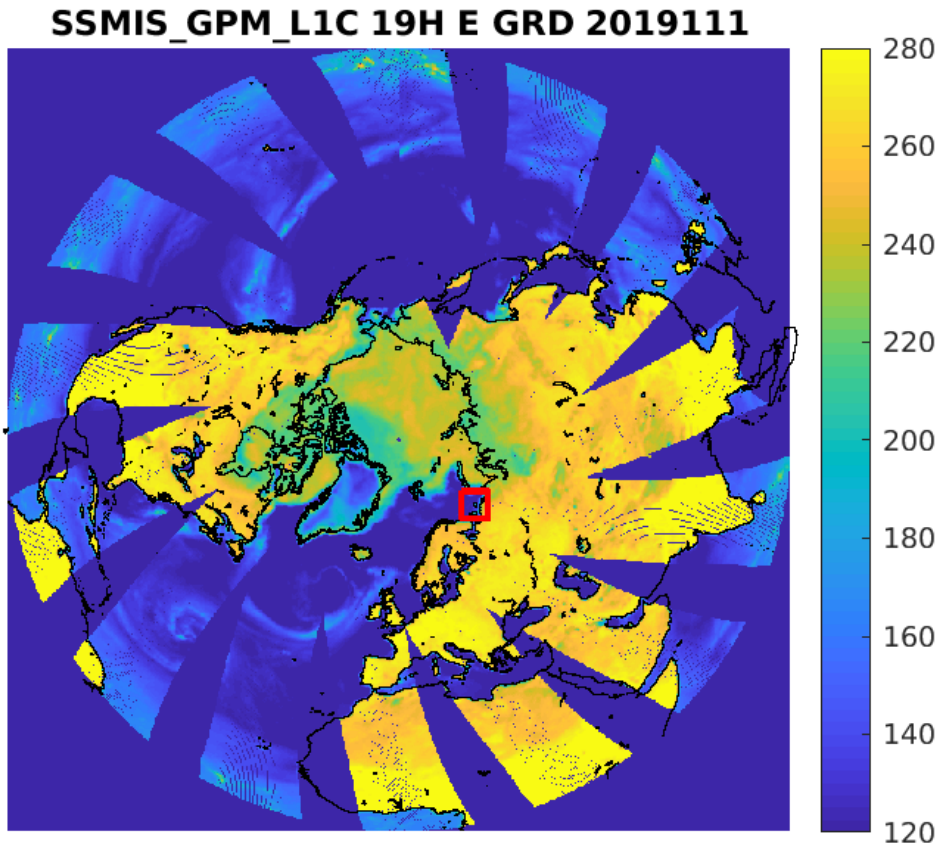

Figure 17: rSIR Northern Hemisphere view.

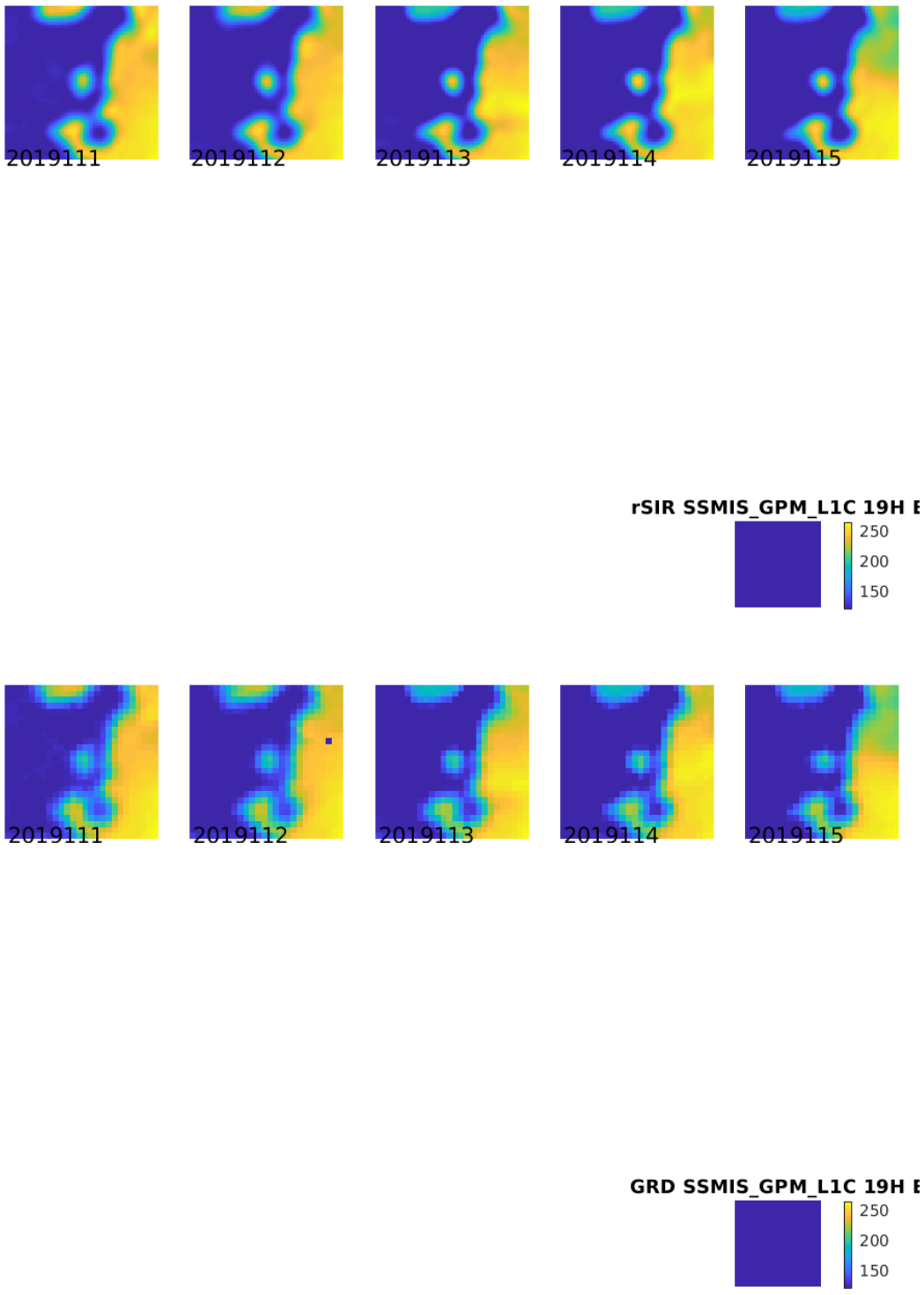

Figure 18: Time series of (top) rSIR and (bottom) GRD T_B images over the study area. Image dates are labeled on the image.

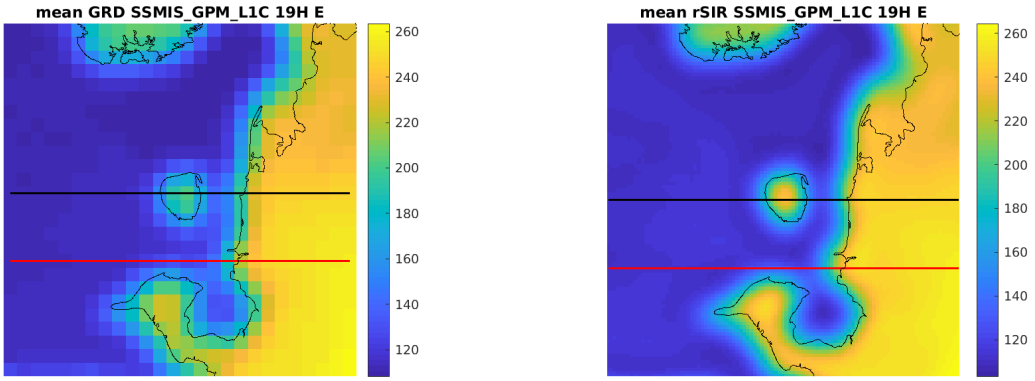

Figure 19: Average of daily T_B images over the study area. (left) 25-km GRD. (right) 3.125-km rSIR. The thick horizontal lines show the data transect locations where data is extracted from the image for analysis.

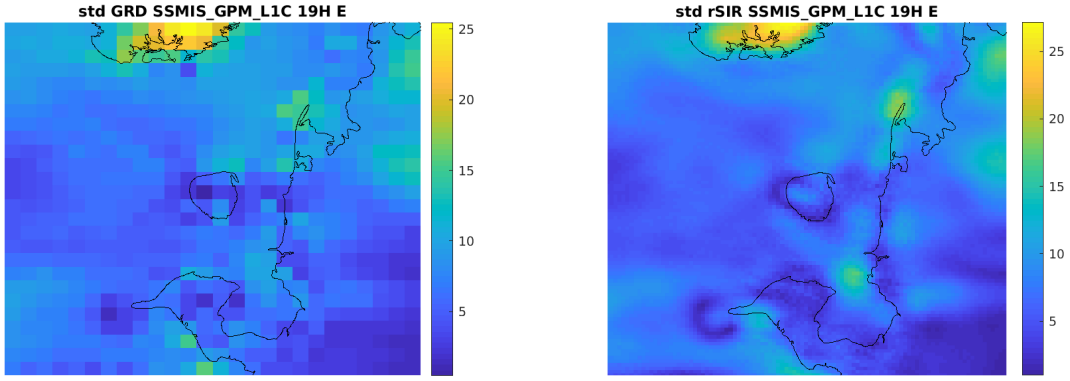

Figure 20: Standard deviation of daily T_B images over the study area. (left) 25-km GRD. (right) 3.125-km rSIR.

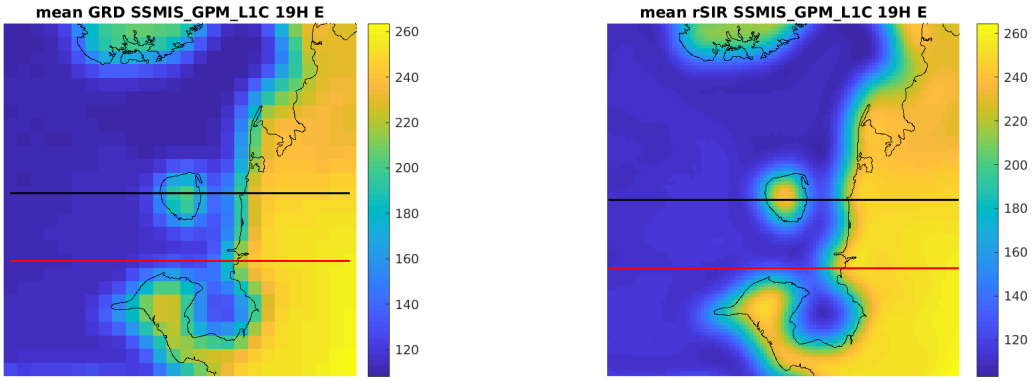

Figure 21: [Repeated] Average of daily T_B images over the study area. (left) 25-km GRD. (right) 3.125-km rSIR. The thick horizontal lines show the data transect locations where data is extracted from the image for analysis.

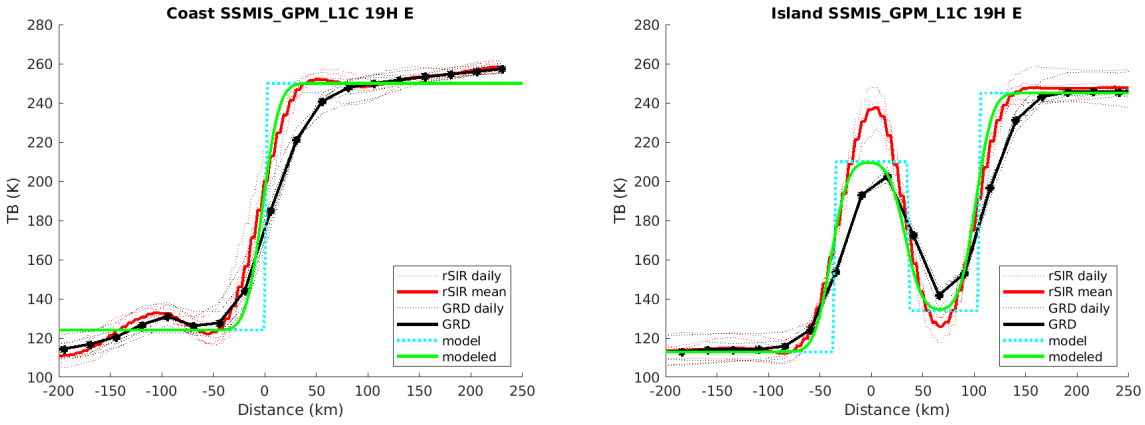

Figure 22: Plots of T_B along the two analysis case transect lines for the (left) coast-crossing and (right) island-crossing cases.

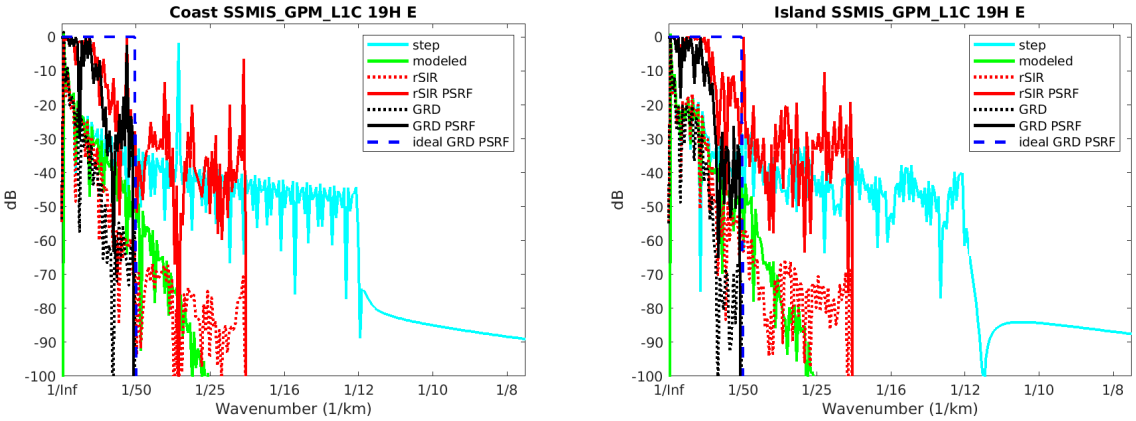

Figure 23: Wavenumber spectra of the T_B slices, the model, and the PSRF. (left) Coast-crossing case. (right) Island-crossing case.

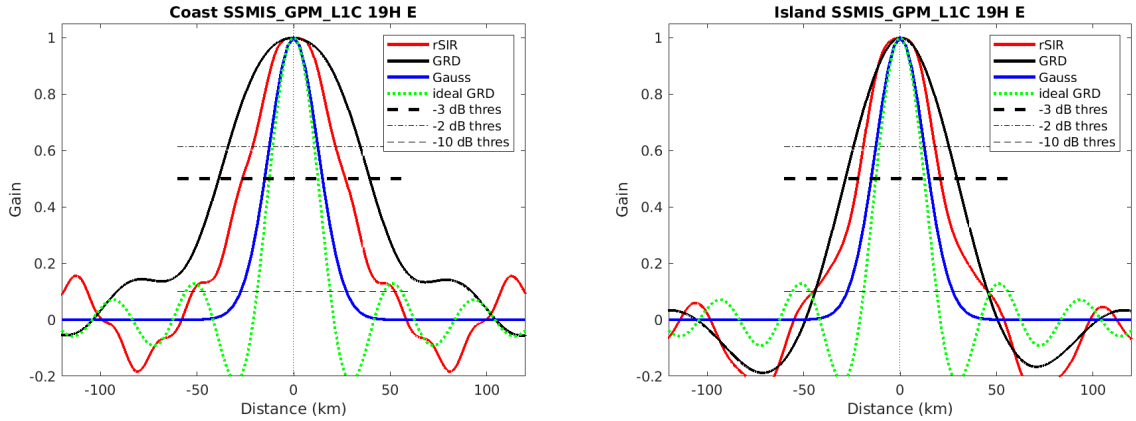

Figure 24: Derived single-pass rSIR and GRD PSRFs from the (left) coast-crossing and (right) island-crossing cases.

Table 31: Resolution estimates for SSMIS_GPM_L1C channel 19H LTOD E

	-3 dB Thres		-2 dB Thres		-10 dB Thres	
Algorithm	Coast	Island	Coast	Island	Coast	Island
Gauss	30.0	30.0	24.4	24.4	54.8	54.8
rSIR	53.3	42.5	41.7	36.2	104.5	90.7
ideal GRD	36.2	36.2	30.3	30.3	54.5	54.5
GRD	78.2	57.9	67.0	48.1	183.7	89.4

8.2 Channel 19H M Figures

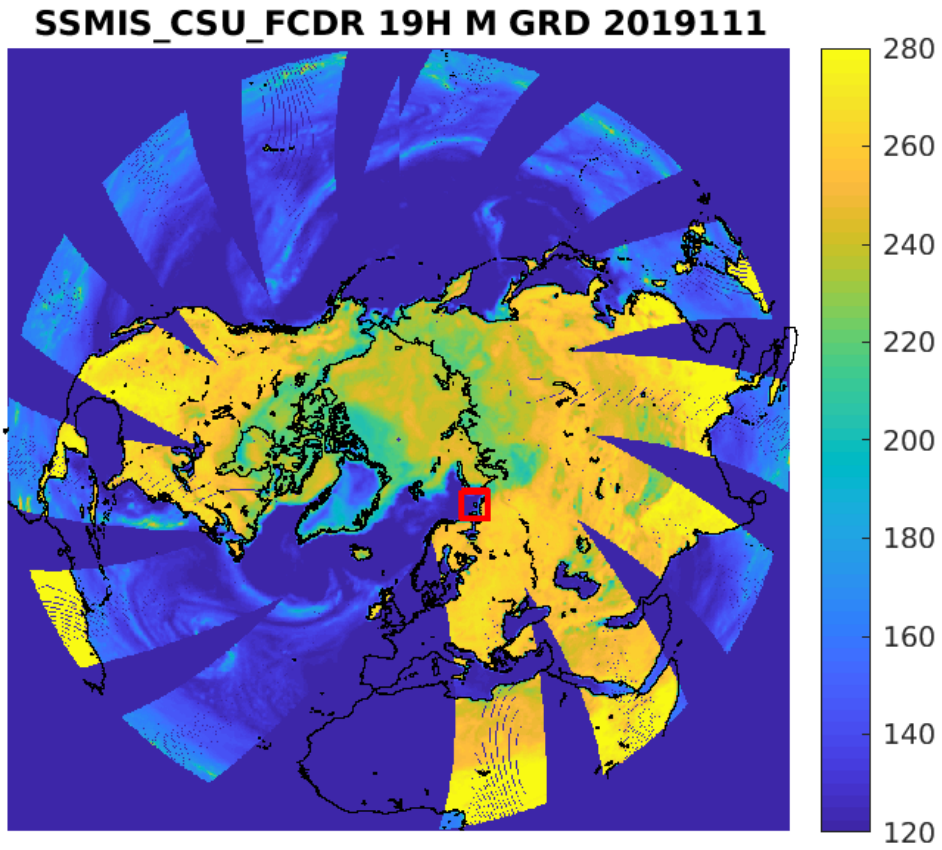

Figure 25: rSIR Northern Hemisphere view.

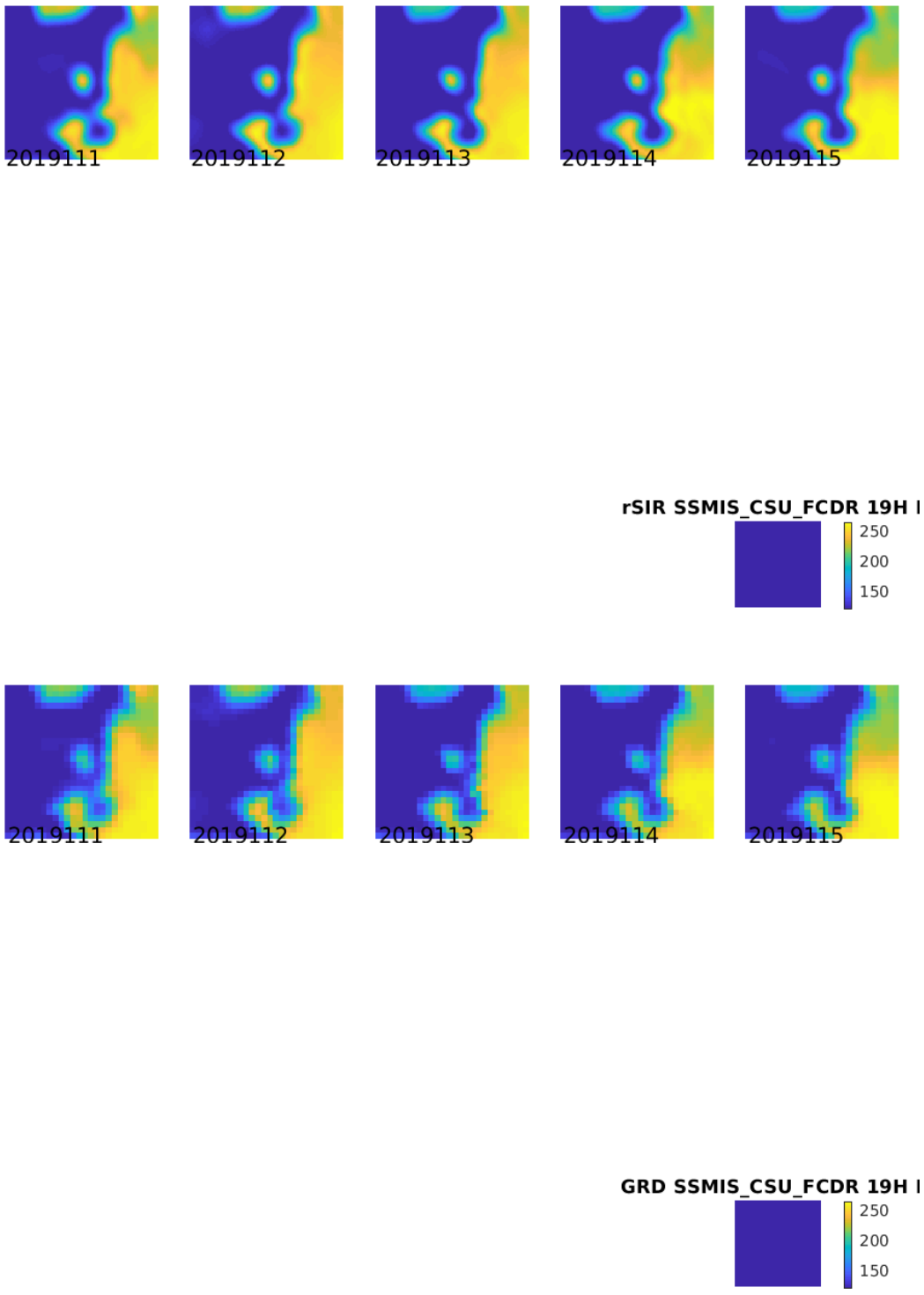

Figure 26: Time series of (top) rSIR and (bottom) GRD T_B images over the study area. Image dates are labeled on the image.

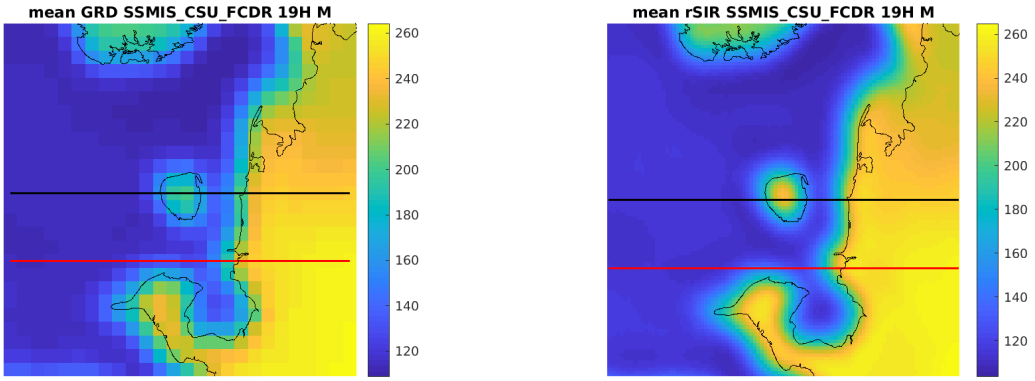

Figure 27: Average of daily T_B images over the study area. (left) 25-km GRD. (right) 3.125-km rSIR. The thick horizontal lines show the data transect locations where data is extracted from the image for analysis.

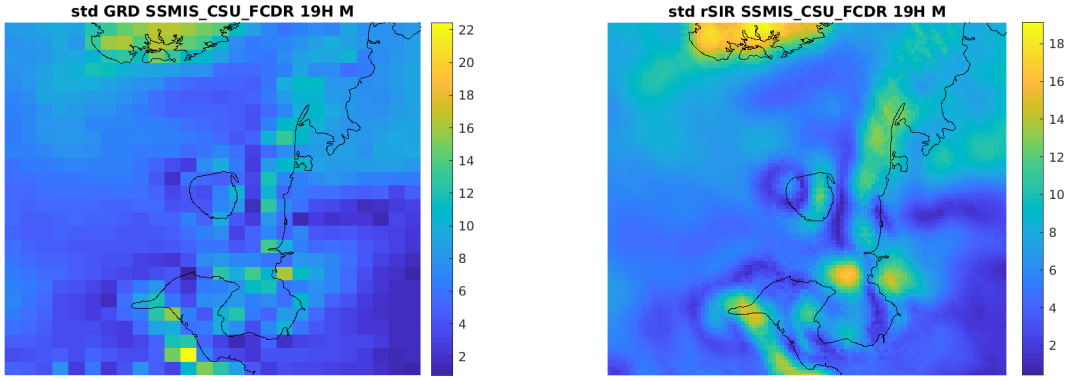

Figure 28: Standard deviation of daily T_B images over the study area. (left) 25-km GRD. (right) 3.125-km rSIR.

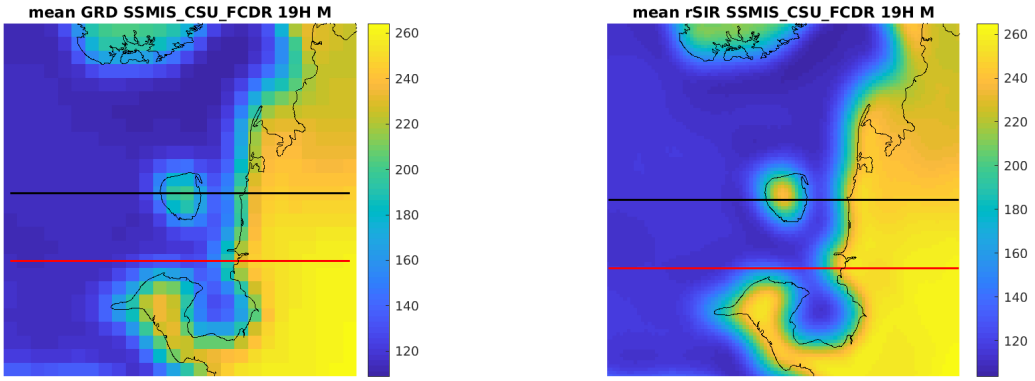

Figure 29: [Repeated] Average of daily T_B images over the study area. (left) 25-km GRD. (right) 3.125-km rSIR. The thick horizontal lines show the data transect locations where data is extracted from the image for analysis.

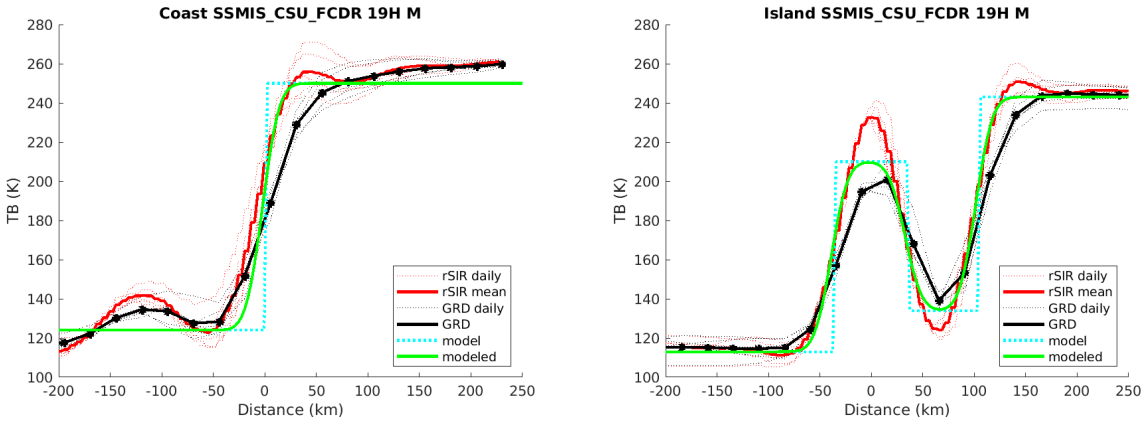

Figure 30: Plots of T_B along the two analysis case transect lines for the (left) coast-crossing and (right) island-crossing cases.

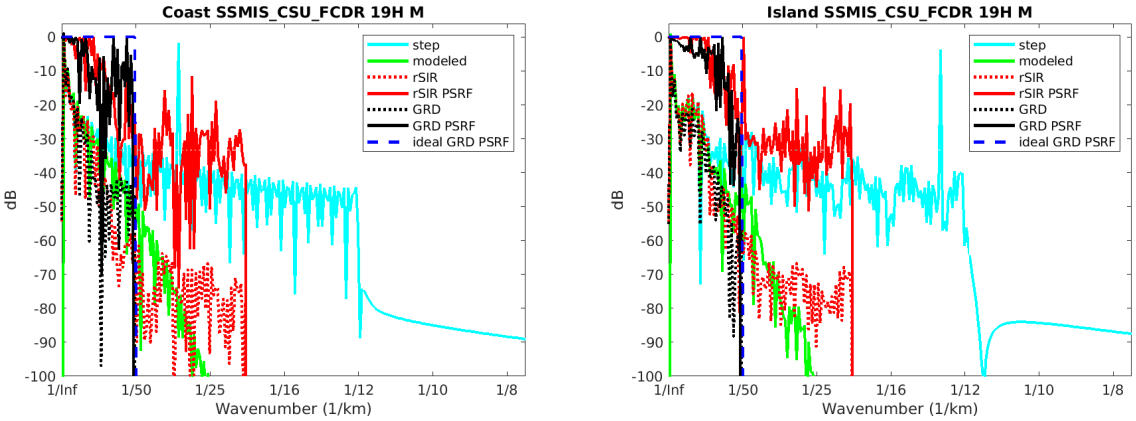

Figure 31: Wavenumber spectra of the T_B slices, the model, and the PSRF. (left) Coast-crossing case. (right) Island-crossing case.

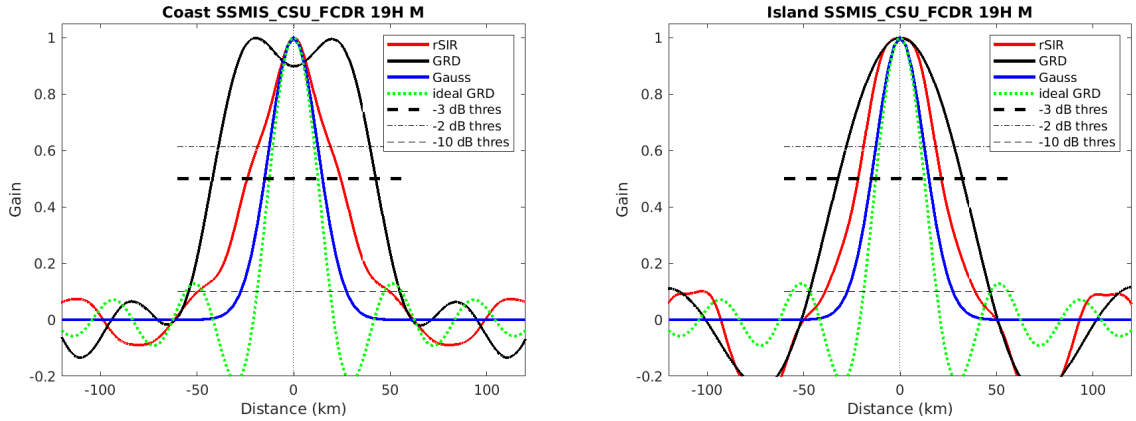

Figure 32: Derived single-pass rSIR and GRD PSRFs from the (left) coast-crossing and (right) island-crossing cases.

Table 32: Resolution estimates for SSMIS_CSU_FCDR channel 19H LTOD M

	-3 dB Thres		-2 dB Thres		-10 dB Thres	
Algorithm	Coast	Island	Coast	Island	Coast	Island
Gauss	30.0	30.0	24.4	24.4	54.8	54.8
rSIR	48.4	43.0	35.9	36.5	99.2	77.6
ideal GRD	36.2	36.2	30.3	30.3	54.5	54.5
GRD	84.6	64.5	77.5	54.6	109.3	93.5

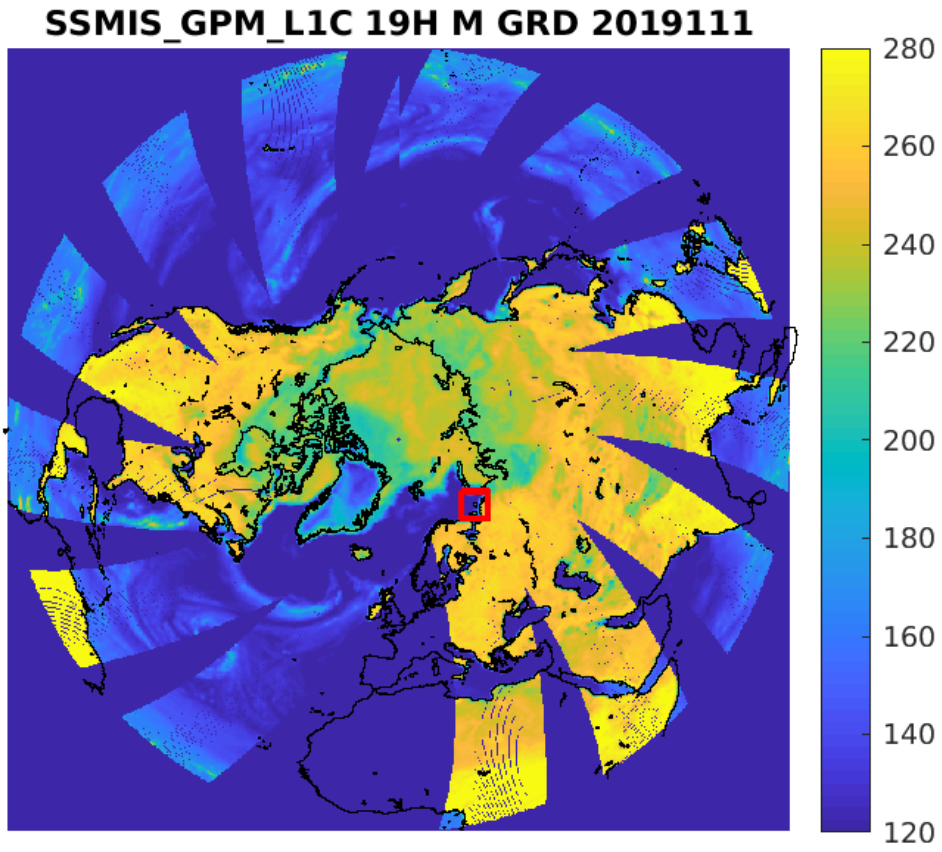

Figure 33: rSIR Northern Hemisphere view.

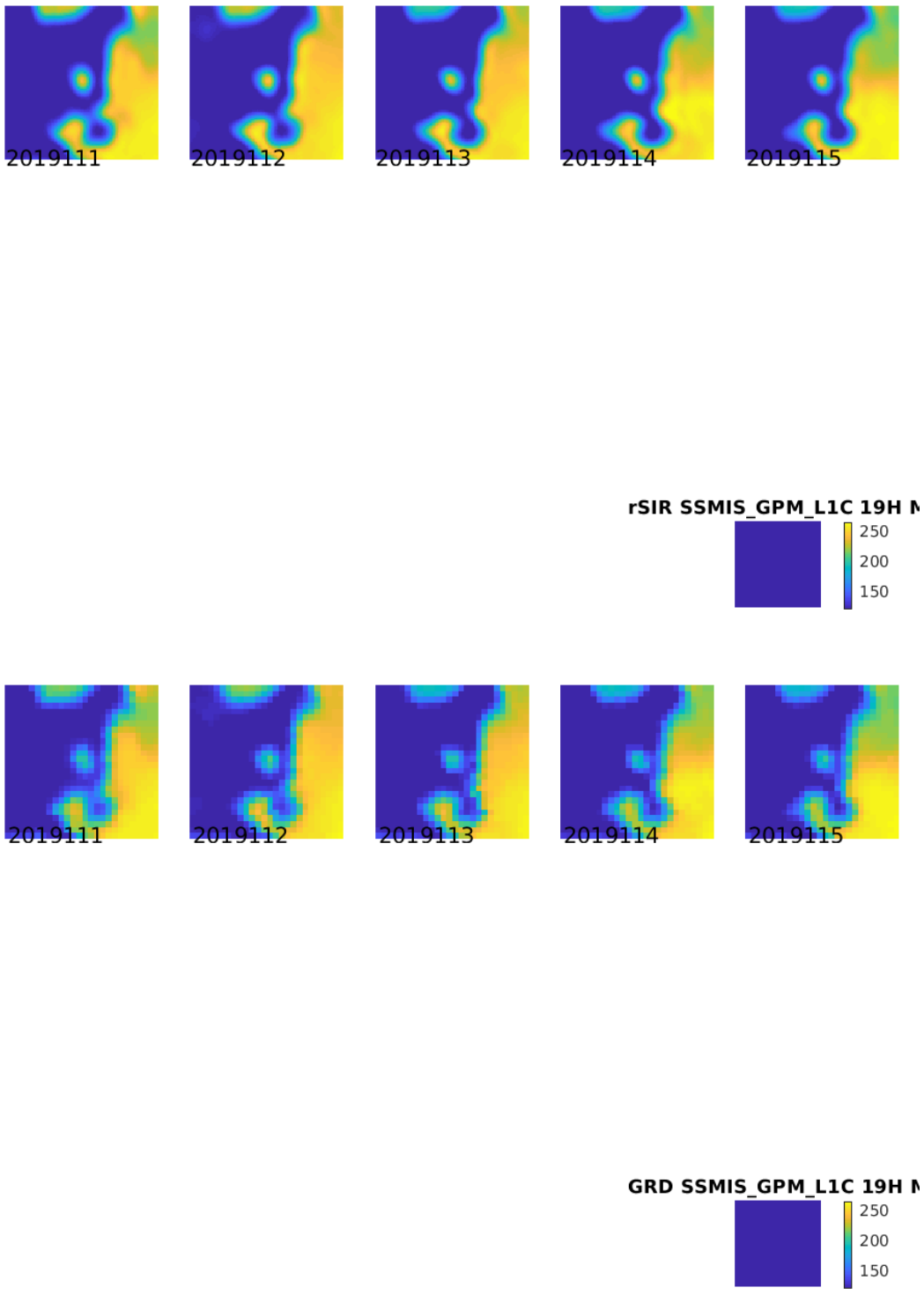

Figure 34: Time series of (top) rSIR and (bottom) GRD T_B images over the study area. Image dates are labeled on the image.

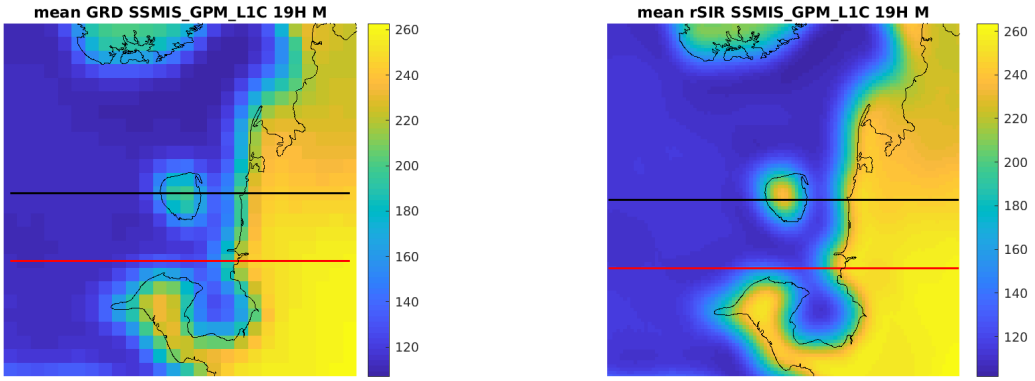

Figure 35: Average of daily T_B images over the study area. (left) 25-km GRD. (right) 3.125-km rSIR. The thick horizontal lines show the data transect locations where data is extracted from the image for analysis.

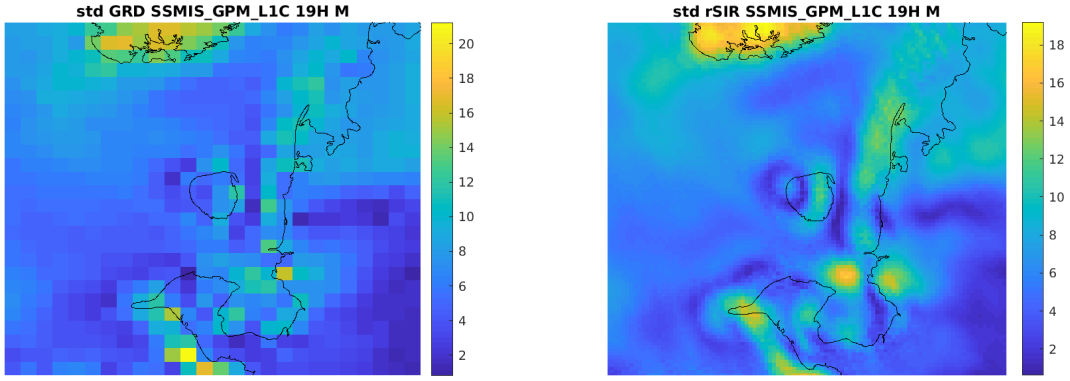

Figure 36: Standard deviation of daily T_B images over the study area. (left) 25-km GRD. (right) 3.125-km rSIR.

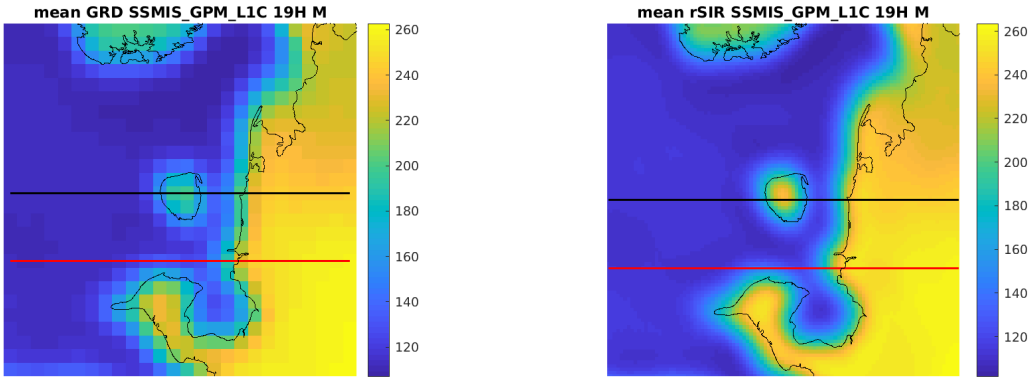

Figure 37: [Repeated] Average of daily T_B images over the study area. (left) 25-km GRD. (right) 3.125-km rSIR. The thick horizontal lines show the data transect locations where data is extracted from the image for analysis.

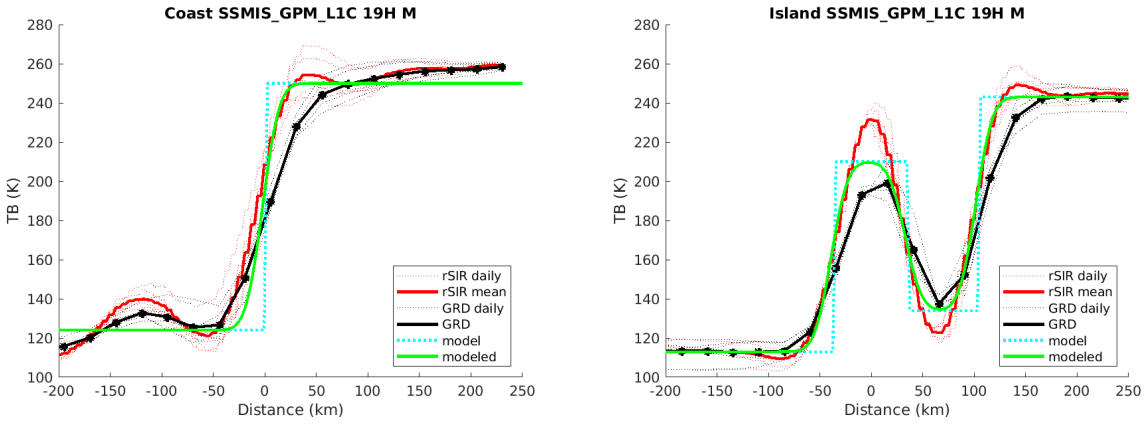

Figure 38: Plots of T_B along the two analysis case transect lines for the (left) coast-crossing and (right) island-crossing cases.

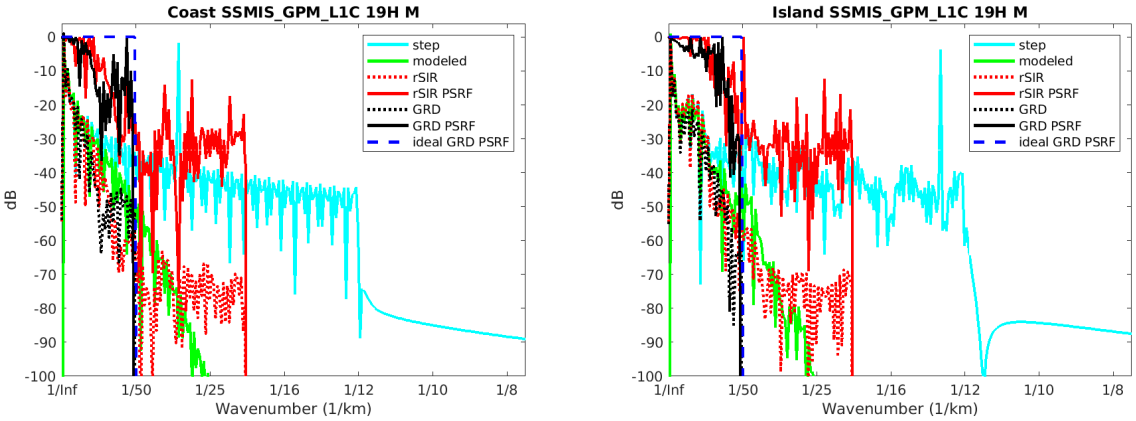

Figure 39: Wavenumber spectra of the T_B slices, the model, and the PSRF. (left) Coast-crossing case. (right) Island-crossing case.

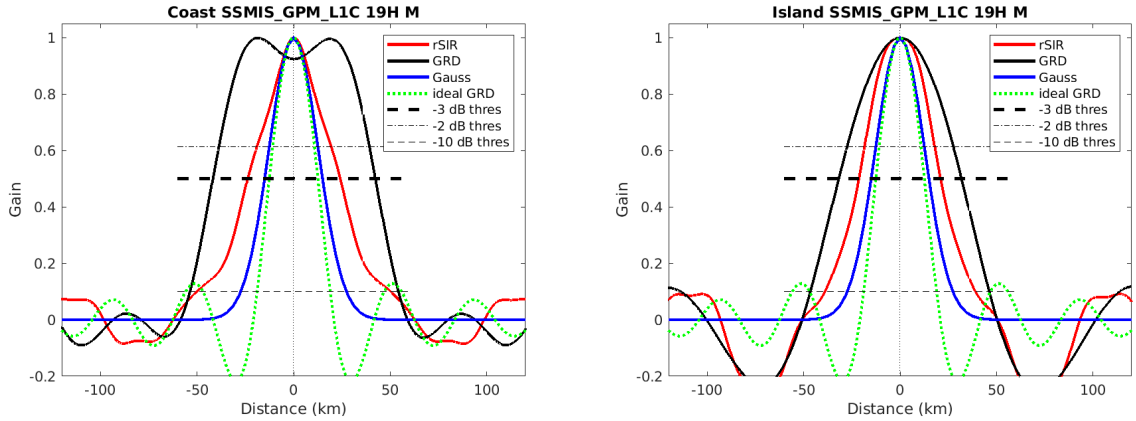

Figure 40: Derived single-pass rSIR and GRD PSRFs from the (left) coast-crossing and (right) island-crossing cases.

Table 33: Resolution estimates for SSMIS_GPM_L1C channel 19H LTOD M

	-3 dB Thres		-2 dB Thres		-10 dB Thres	
Algorithm	Coast	Island	Coast	Island	Coast	Island
Gauss	30.0	30.0	24.4	24.4	54.8	54.8
rSIR	48.0	42.2	36.7	35.4	100.3	77.9
ideal GRD	36.2	36.2	30.3	30.3	54.5	54.5
GRD	84.1	63.7	77.0	53.8	107.9	92.8

8.3 Channel 19V E Figures

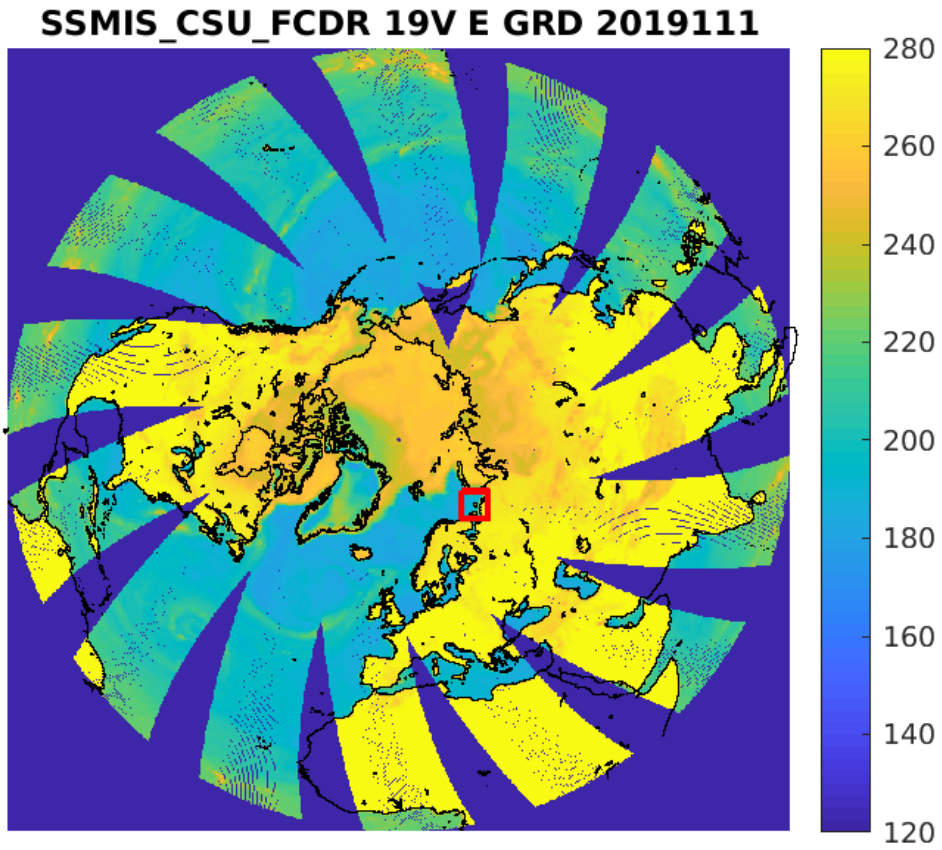

Figure 41: rSIR Northern Hemisphere view.

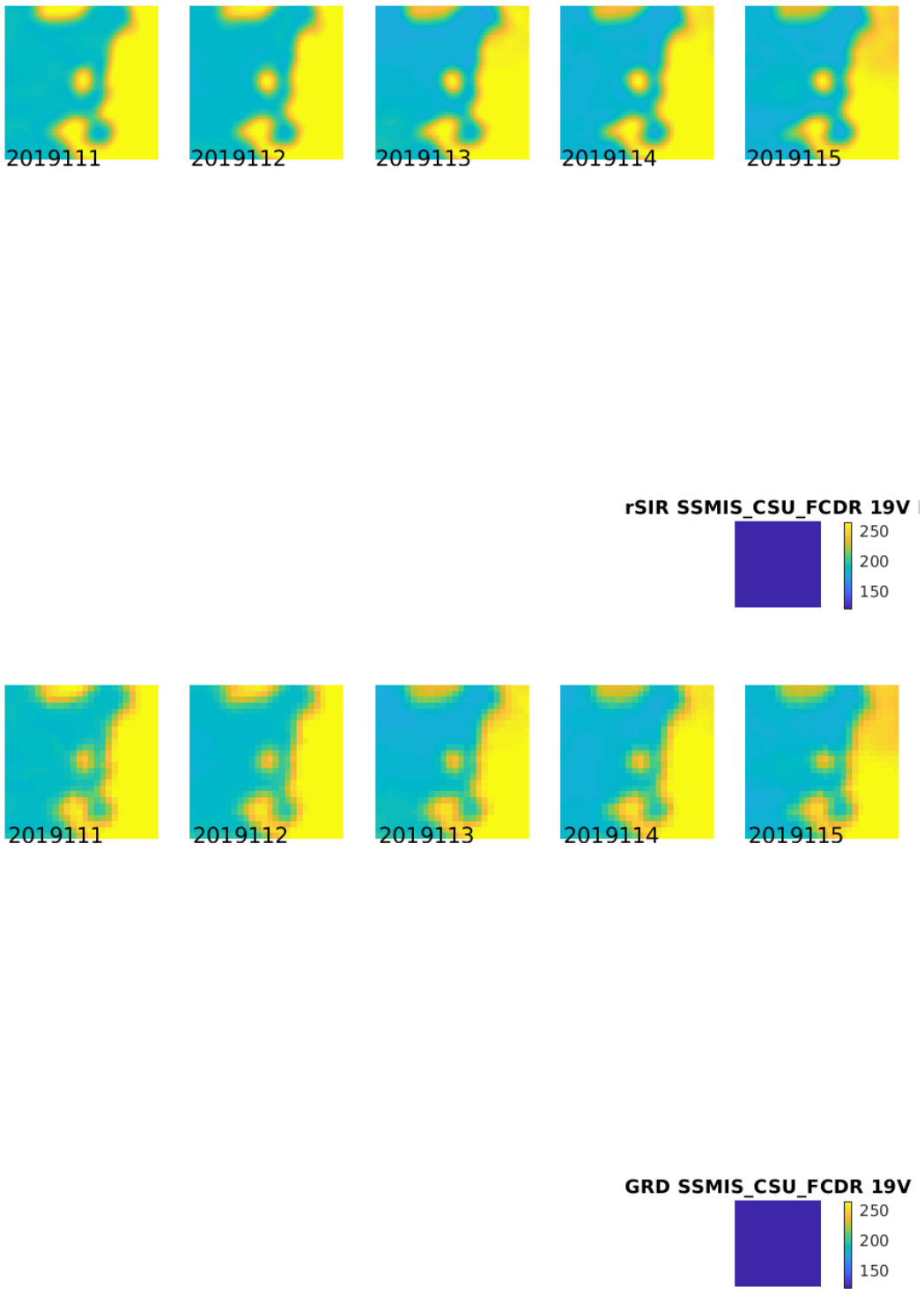

Figure 42: Time series of (top) rSIR and (bottom) GRD T_B images over the study area. Image dates are labeled on the image.

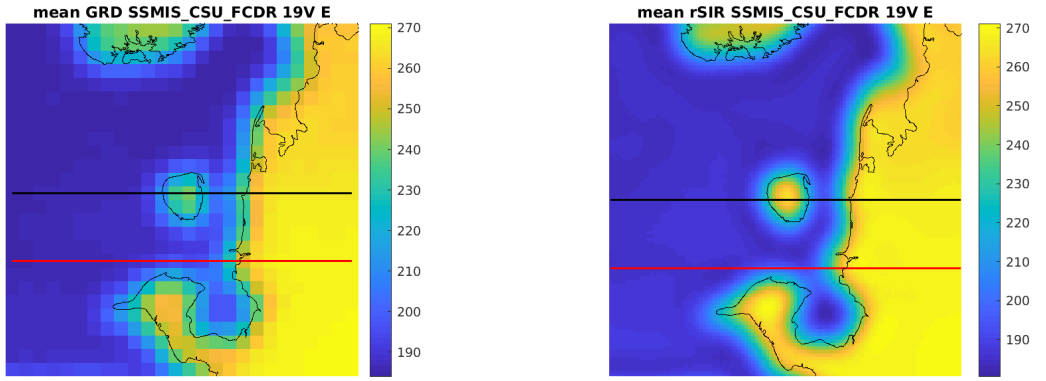

Figure 43: Average of daily T_B images over the study area. (left) 25-km GRD. (right) 3.125-km rSIR. The thick horizontal lines show the data transect locations where data is extracted from the image for analysis.

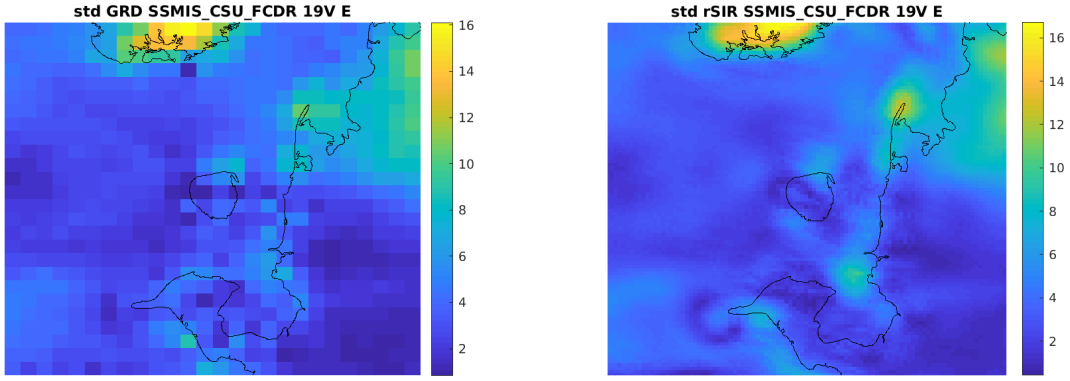

Figure 44: Standard deviation of daily T_B images over the study area. (left) 25-km GRD. (right) 3.125-km rSIR.

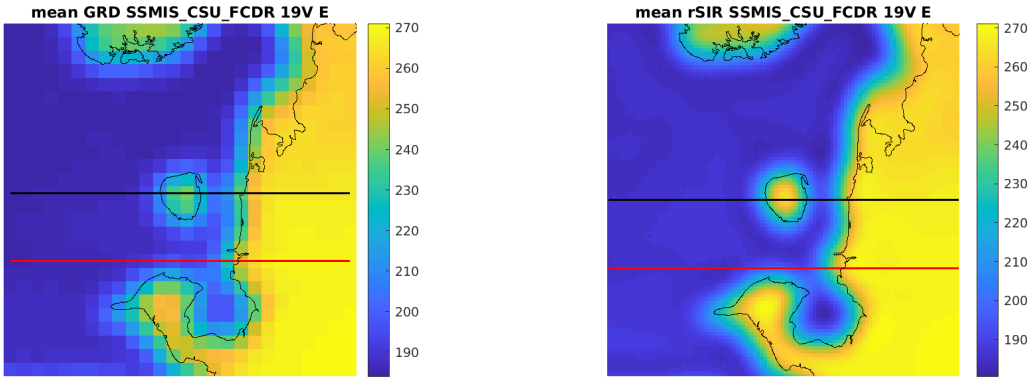

Figure 45: [Repeated] Average of daily T_B images over the study area. (left) 25-km GRD. (right) 3.125-km rSIR. The thick horizontal lines show the data transect locations where data is extracted from the image for analysis.

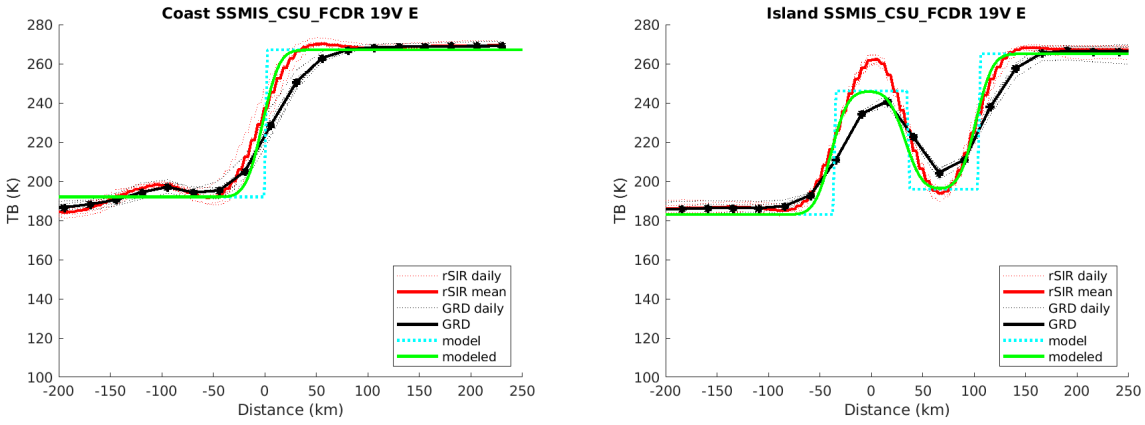

Figure 46: Plots of T_B along the two analysis case transect lines for the (left) coast-crossing and (right) island-crossing cases.

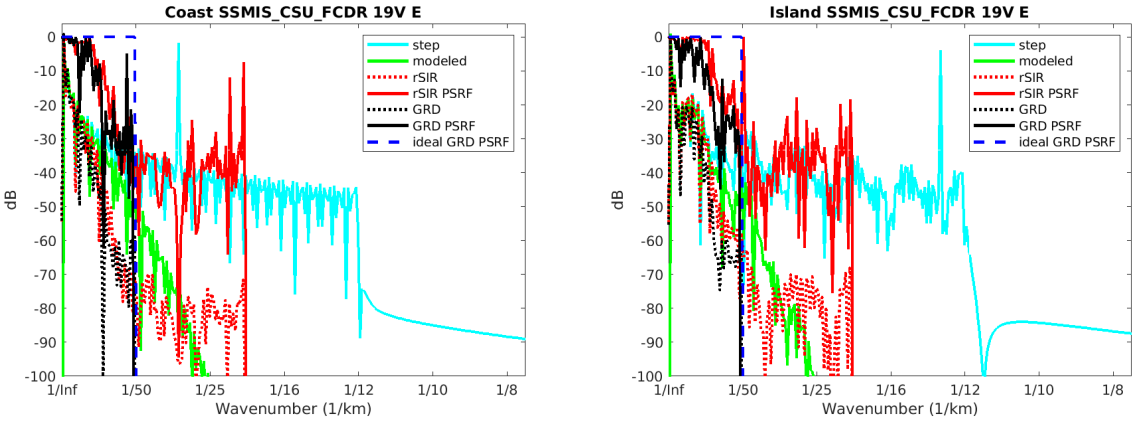

Figure 47: Wavenumber spectra of the T_B slices, the model, and the PSRF. (left) Coast-crossing case. (right) Island-crossing case.

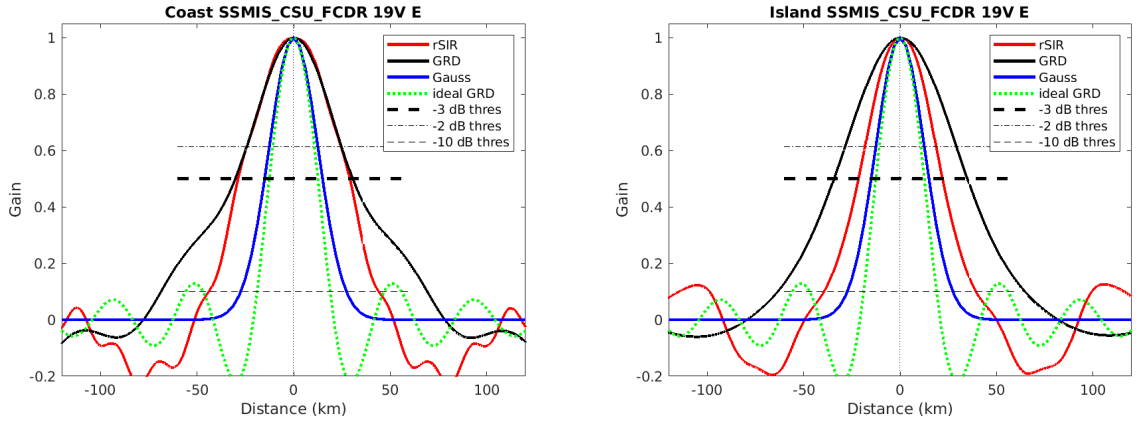

Figure 48: Derived single-pass rSIR and GRD PSRFs from the (left) coast-crossing and (right) island-crossing cases.

Table 34: Resolution estimates for SSMIS_CSU_FCDR channel 19V LTOD E

	-3 dB Thres		-2 dB Thres		-10 dB Thres	
Algorithm	Coast	Island	Coast	Island	Coast	Island
Gauss	30.0	30.0	24.4	24.4	54.8	54.8
rSIR	57.7	43.4	47.1	35.8	88.0	78.6
ideal GRD	36.2	36.2	30.3	30.3	54.5	54.5
GRD	60.7	69.2	47.4	56.1	137.7	128.2

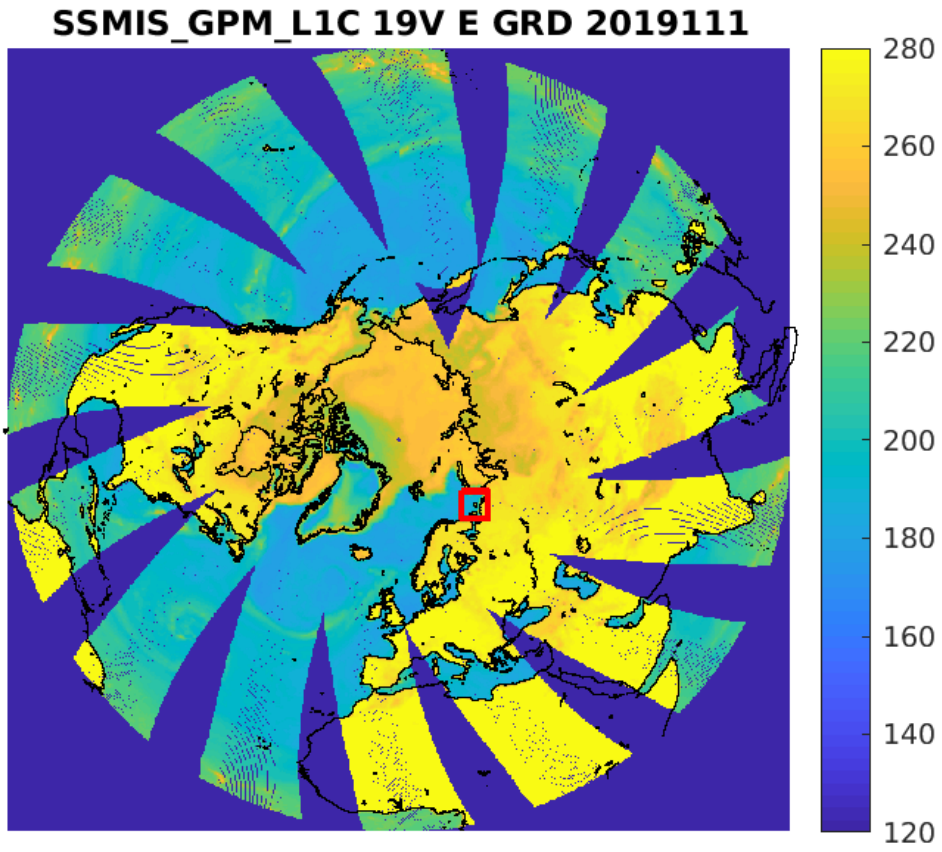

Figure 49: rSIR Northern Hemisphere view.

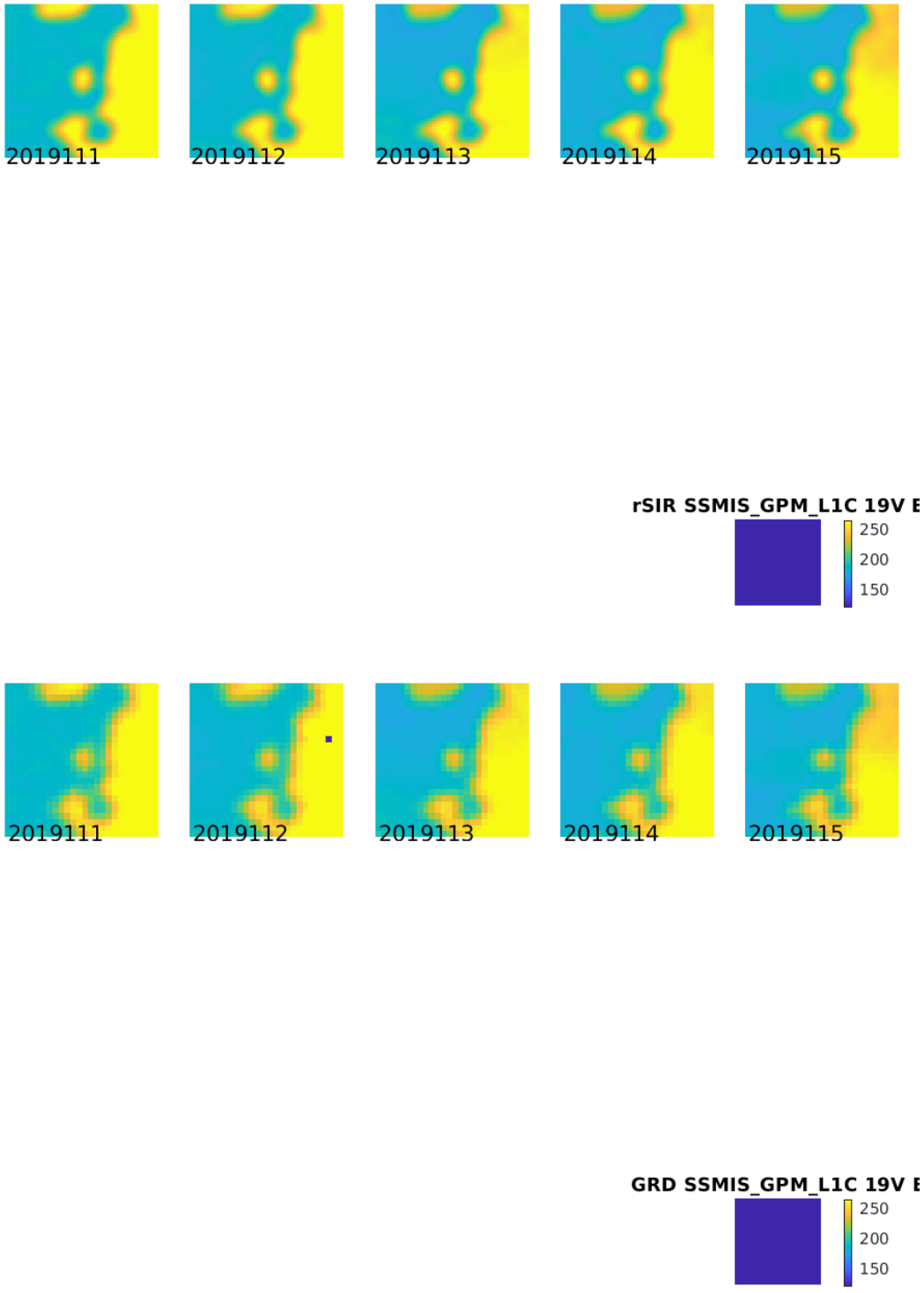

Figure 50: Time series of (top) rSIR and (bottom) GRD T_B images over the study area. Image dates are labeled on the image.

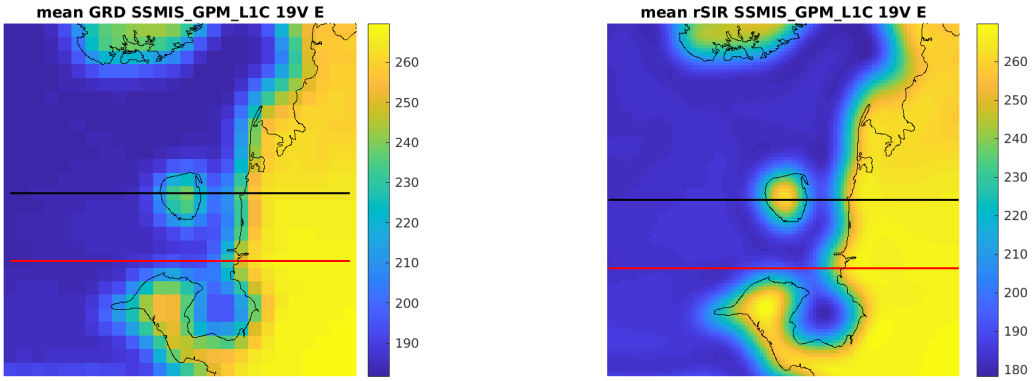

Figure 51: Average of daily T_B images over the study area. (left) 25-km GRD. (right) 3.125-km rSIR. The thick horizontal lines show the data transect locations where data is extracted from the image for analysis.

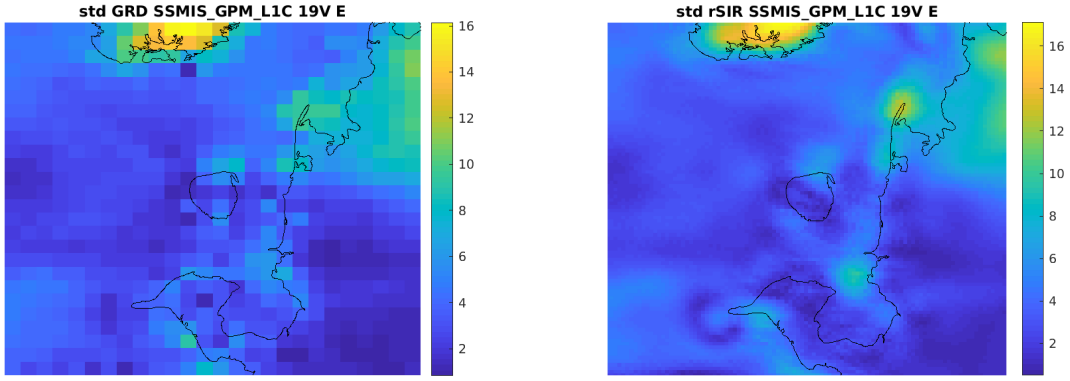

Figure 52: Standard deviation of daily T_B images over the study area. (left) 25-km GRD. (right) 3.125-km rSIR.

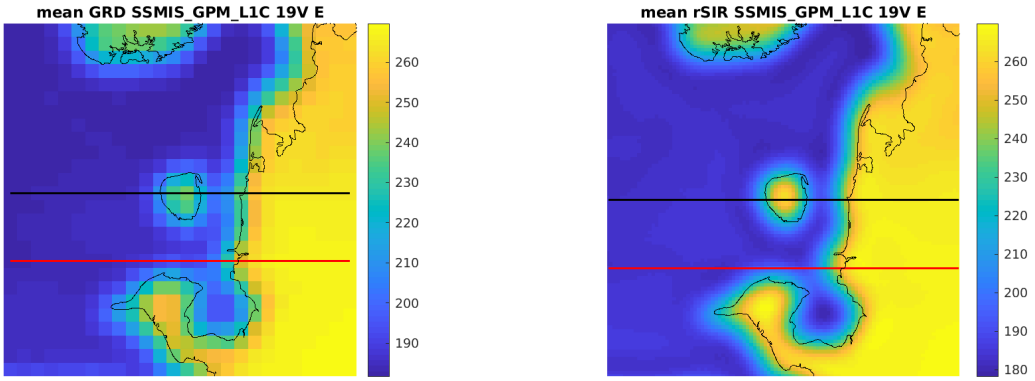

Figure 53: [Repeated] Average of daily T_B images over the study area. (left) 25-km GRD. (right) 3.125-km rSIR. The thick horizontal lines show the data transect locations where data is extracted from the image for analysis.

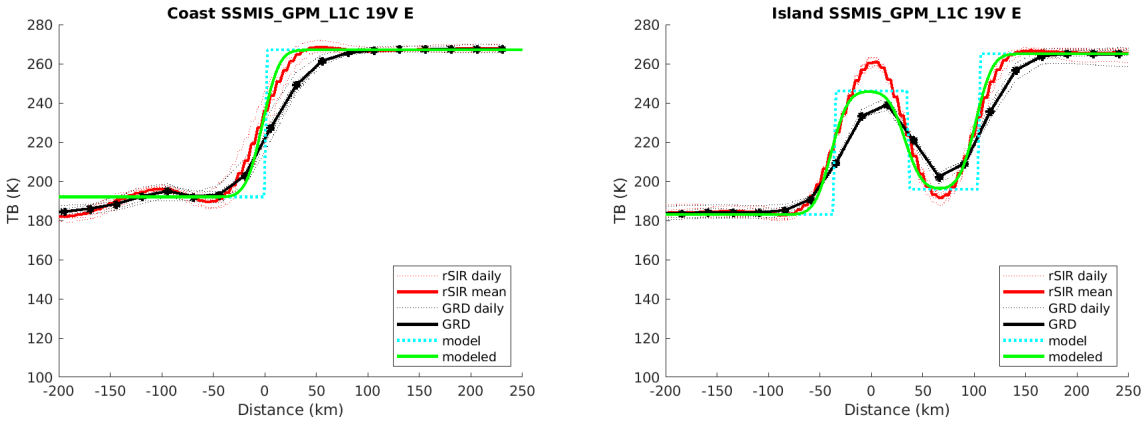

Figure 54: Plots of T_B along the two analysis case transect lines for the (left) coast-crossing and (right) island-crossing cases.

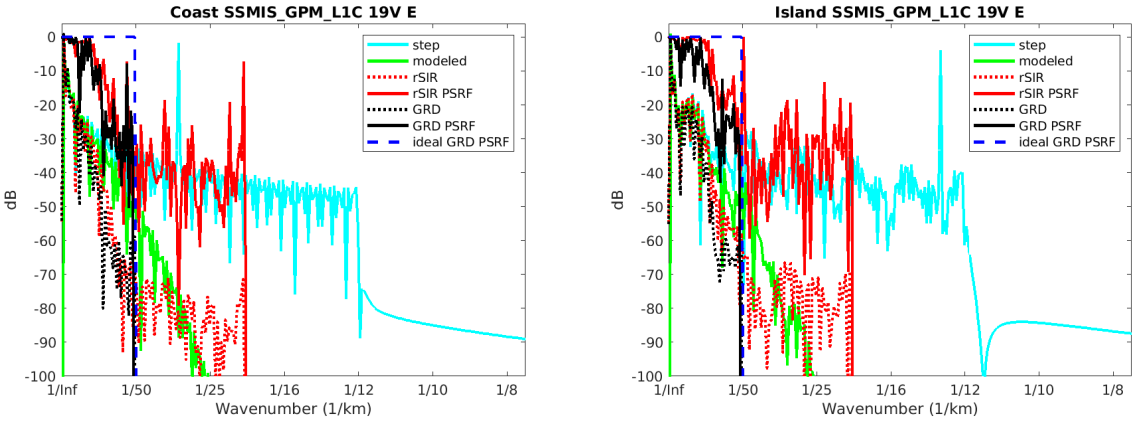

Figure 55: Wavenumber spectra of the T_B slices, the model, and the PSRF. (left) Coast-crossing case. (right) Island-crossing case.

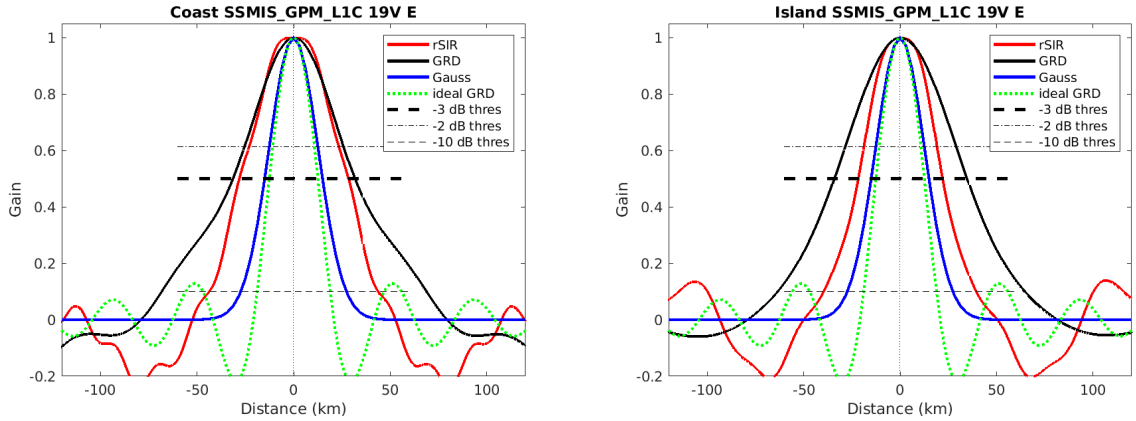

Figure 56: Derived single-pass rSIR and GRD PSRFs from the (left) coast-crossing and (right) island-crossing cases.

Table 35: Resolution estimates for SSMIS_GPM_L1C channel 19V LTOD E

	-3 dB Thres		-2 dB Thres		-10 dB Thres	
Algorithm	Coast	Island	Coast	Island	Coast	Island
Gauss	30.0	30.0	24.4	24.4	54.8	54.8
rSIR	56.5	43.6	45.0	37.0	87.4	79.0
ideal GRD	36.2	36.2	30.3	30.3	54.5	54.5
GRD	63.2	68.9	49.6	55.8	137.1	128.2

8.4 Channel 19V M Figures

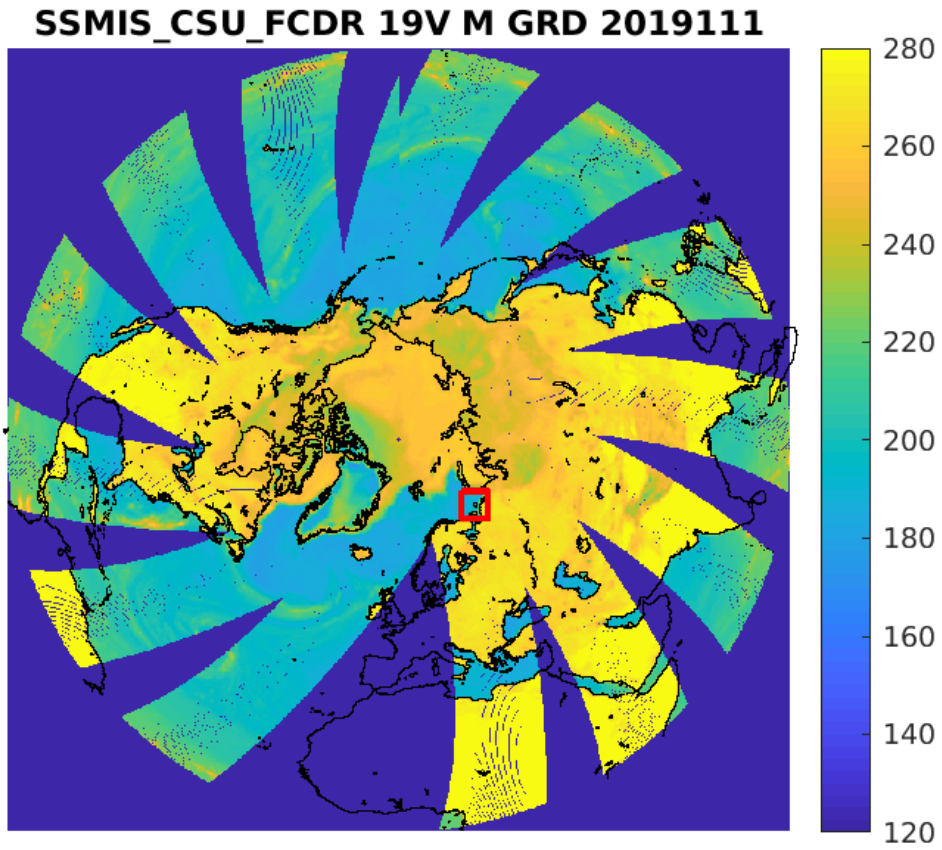

Figure 57: rSIR Northern Hemisphere view.

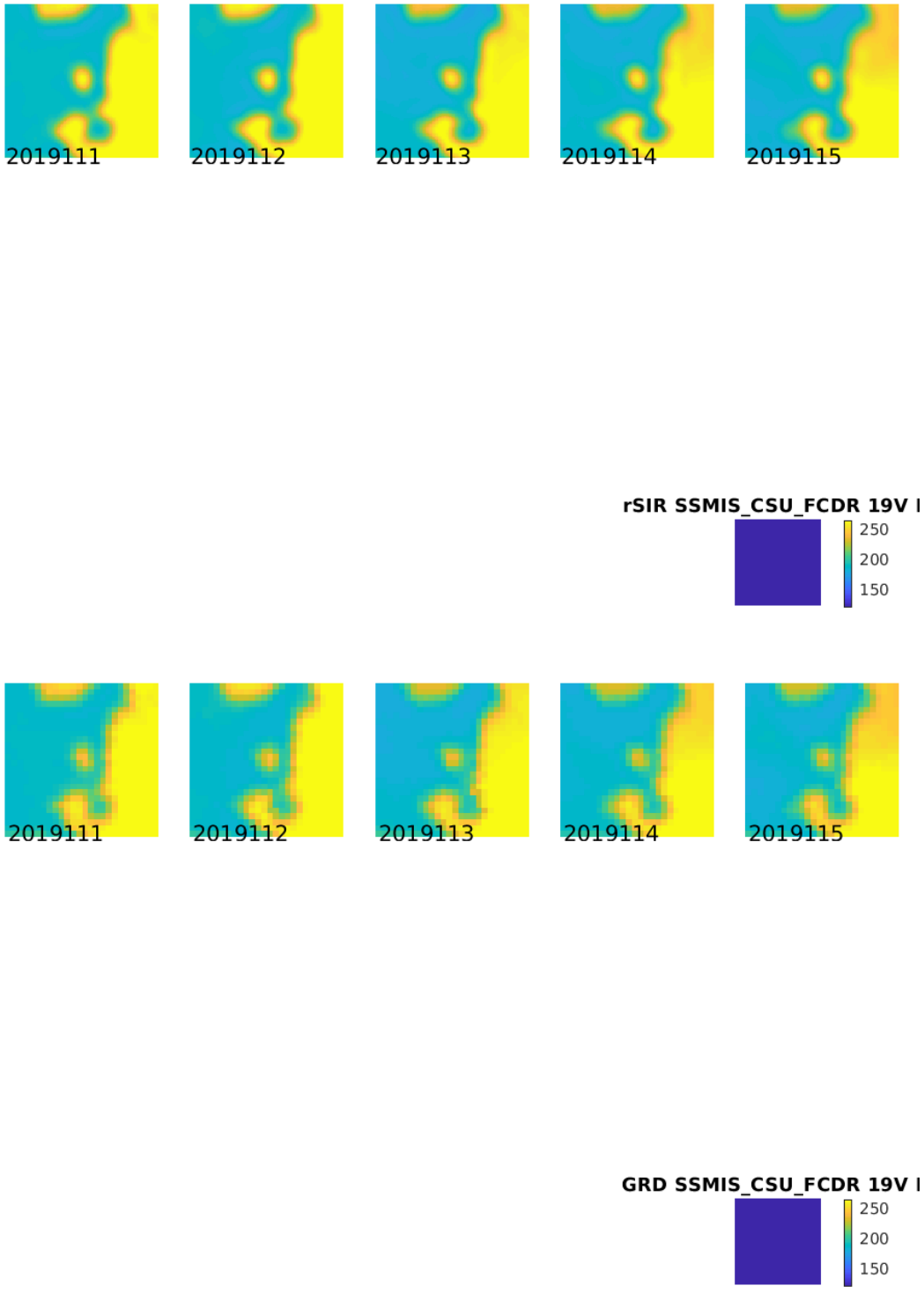

Figure 58: Time series of (top) rSIR and (bottom) GRD T_B images over the study area. Image dates are labeled on the image.

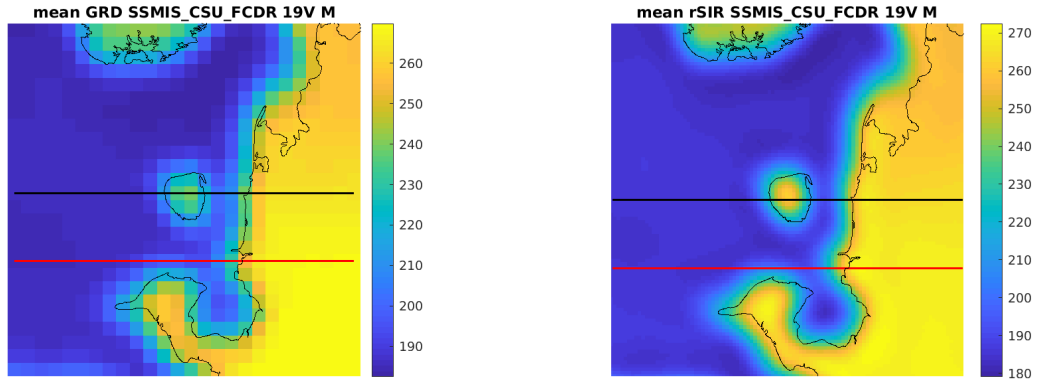

Figure 59: Average of daily T_B images over the study area. (left) 25-km GRD. (right) 3.125-km rSIR. The thick horizontal lines show the data transect locations where data is extracted from the image for analysis.

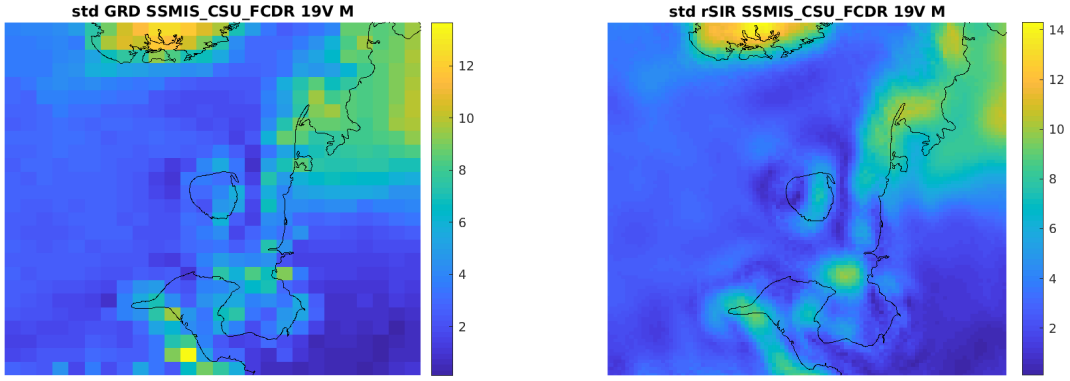

Figure 60: Standard deviation of daily T_B images over the study area. (left) 25-km GRD. (right) 3.125-km rSIR.

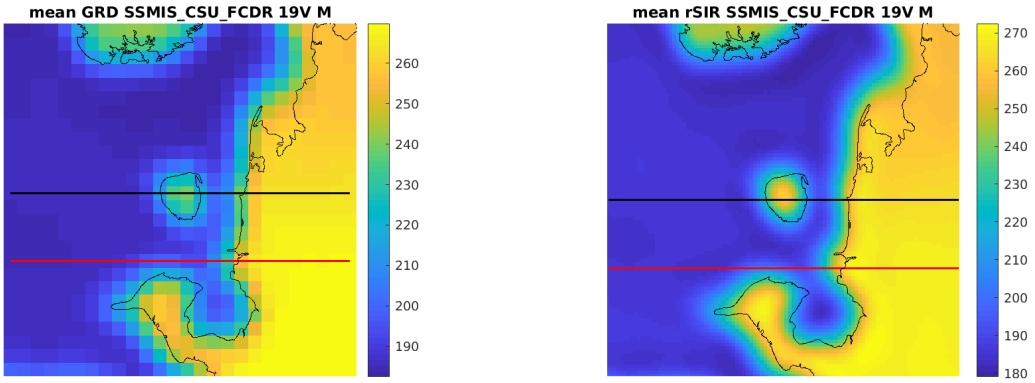

Figure 61: [Repeated] Average of daily T_B images over the study area. (left) 25-km GRD. (right) 3.125-km rSIR. The thick horizontal lines show the data transect locations where data is extracted from the image for analysis.

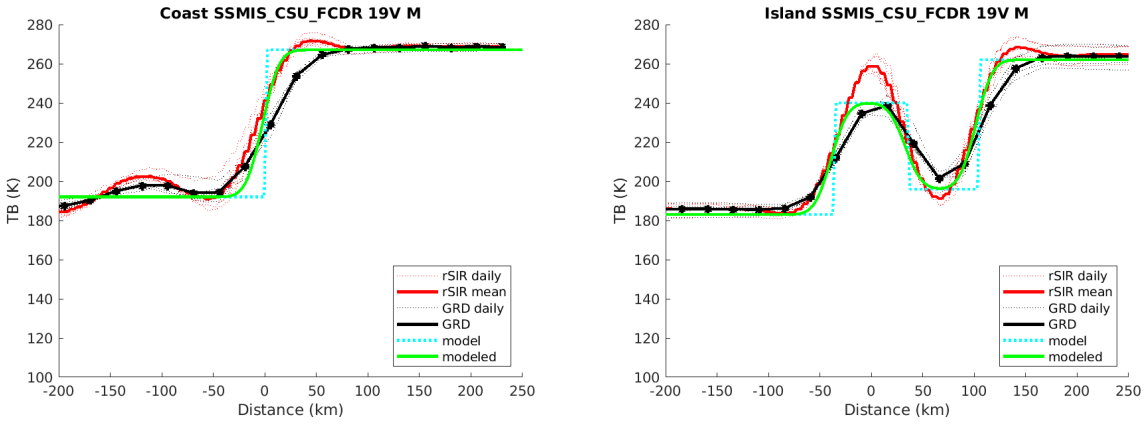

Figure 62: Plots of T_B along the two analysis case transect lines for the (left) coast-crossing and (right) island-crossing cases.

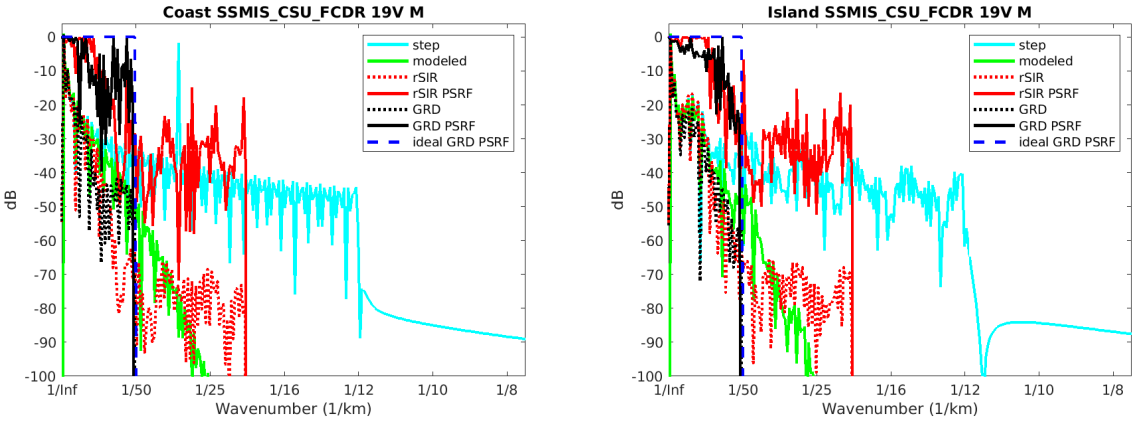

Figure 63: Wavenumber spectra of the T_B slices, the model, and the PSRF. (left) Coast-crossing case. (right) Island-crossing case.

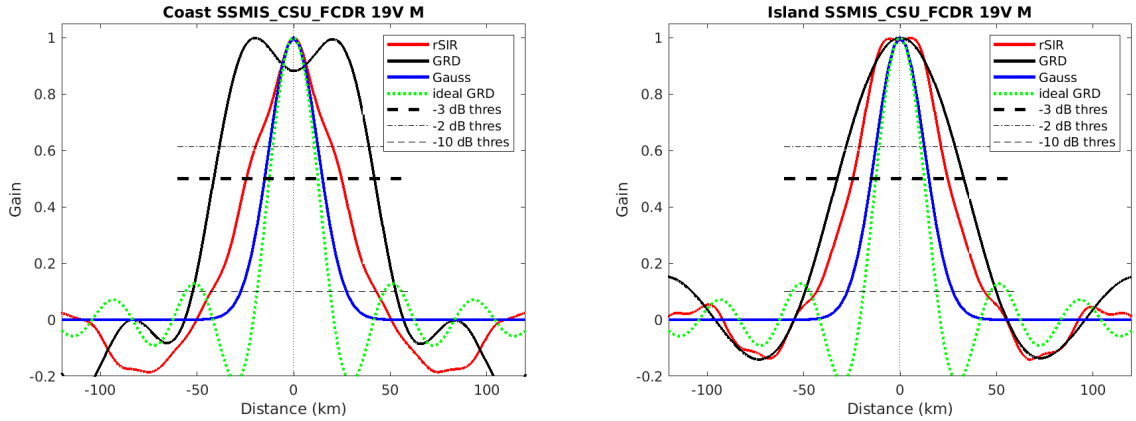

Figure 64: Derived single-pass rSIR and GRD PSRFs from the (left) coast-crossing and (right) island-crossing cases.

Table 36: Resolution estimates for SSMIS_CSU_FCDR channel 19V LTOD M

	-3 dB Thres		-2 dB Thres		-10 dB Thres	
Algorithm	Coast	Island	Coast	Island	Coast	Island
Gauss	30.0	30.0	24.4	24.4	54.8	54.8
rSIR	49.4	49.2	38.1	41.4	85.6	86.9
ideal GRD	36.2	36.2	30.3	30.3	54.5	54.5
GRD	83.2	65.7	76.6	55.1	105.0	99.2

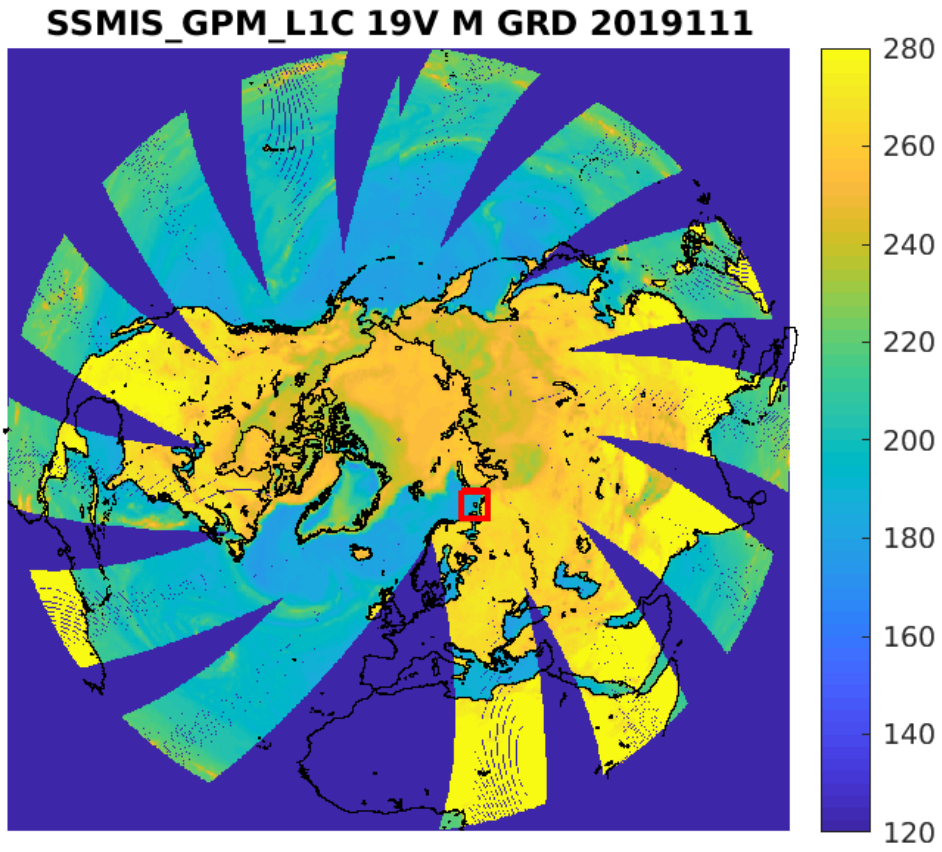

Figure 65: rSIR Northern Hemisphere view.

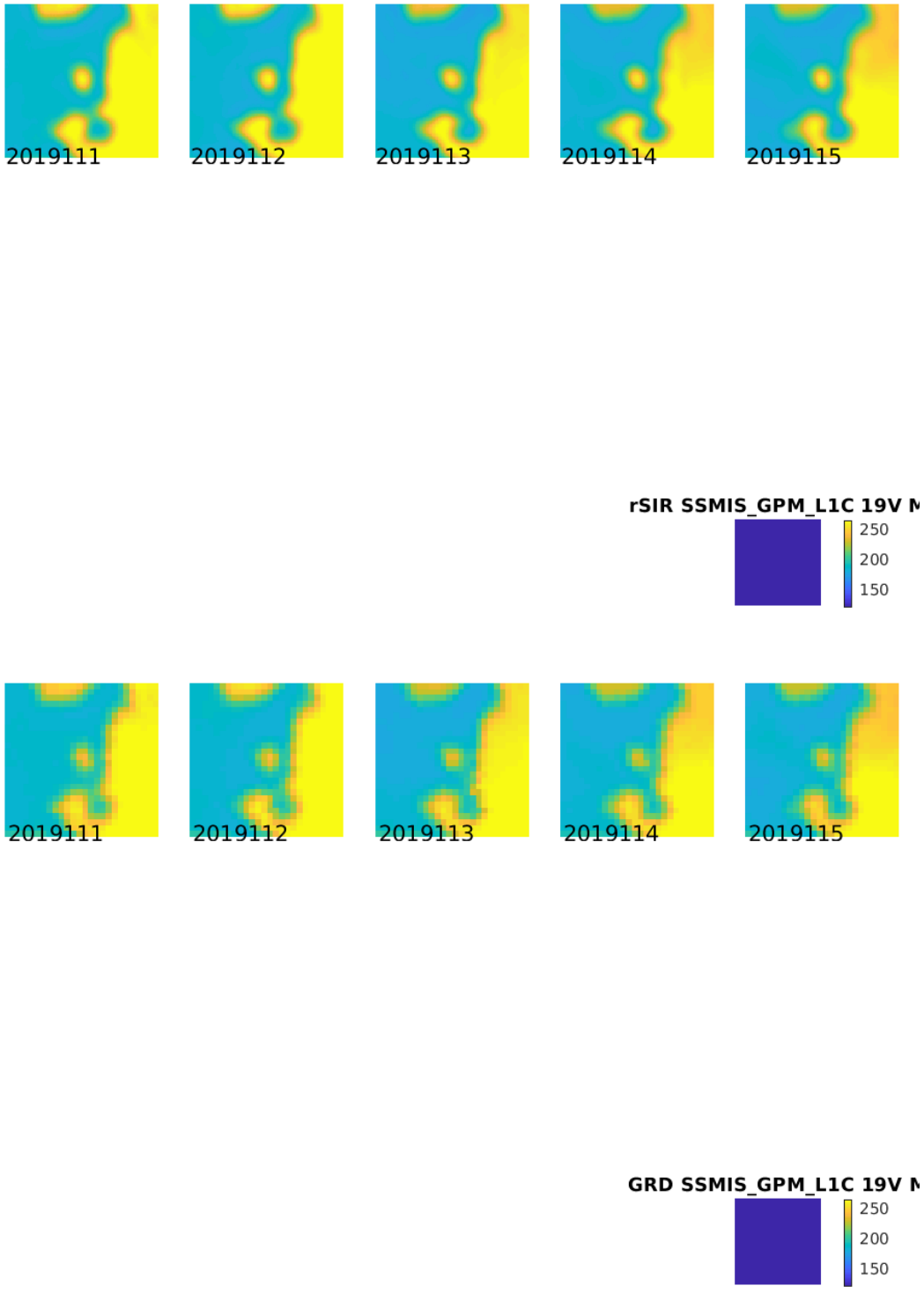

Figure 66: Time series of (top) rSIR and (bottom) GRD T_B images over the study area. Image dates are labeled on the image.

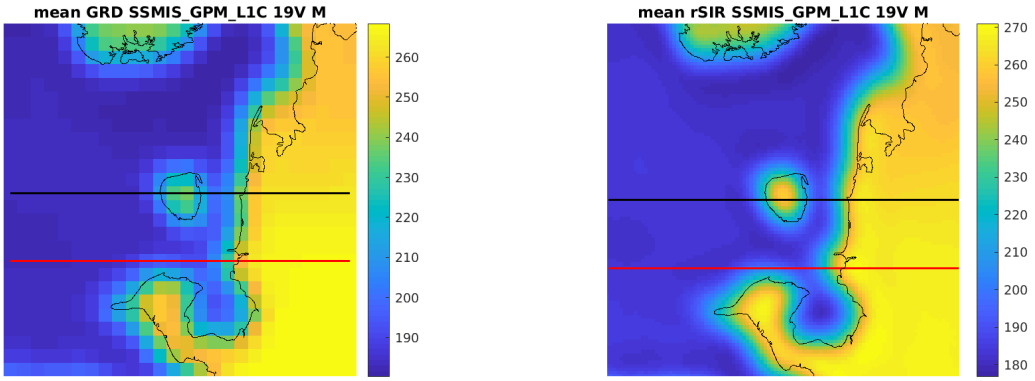

Figure 67: Average of daily T_B images over the study area. (left) 25-km GRD. (right) 3.125-km rSIR. The thick horizontal lines show the data transect locations where data is extracted from the image for analysis.

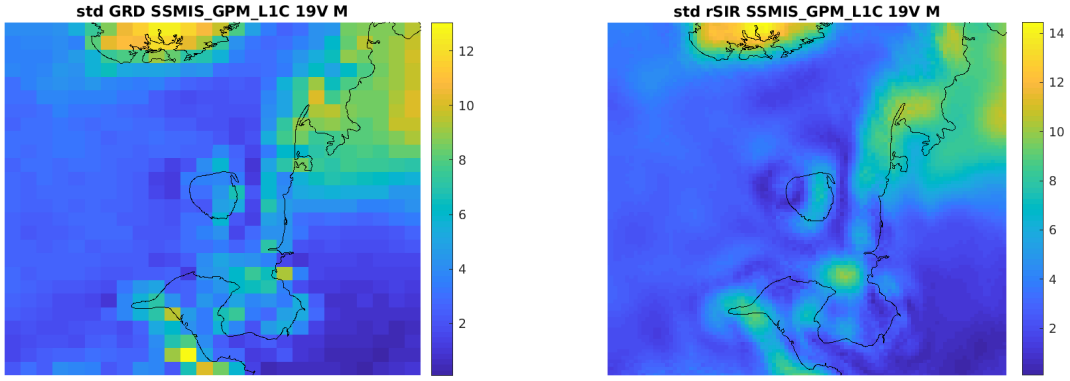

Figure 68: Standard deviation of daily T_B images over the study area. (left) 25-km GRD. (right) 3.125-km rSIR.

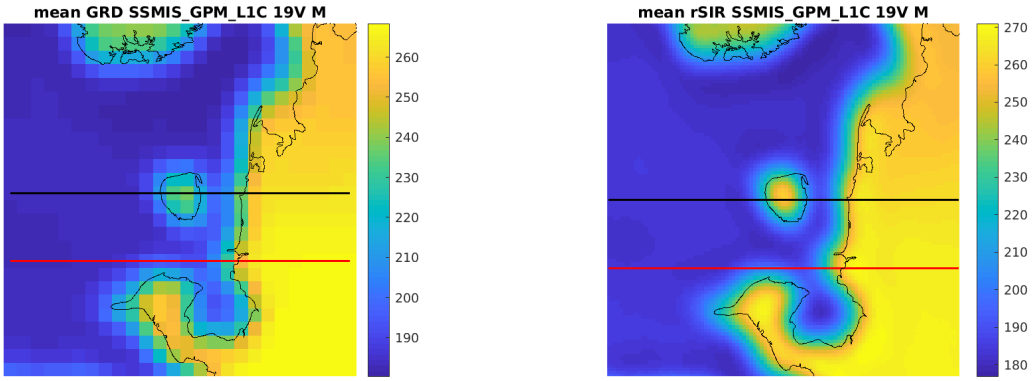

Figure 69: [Repeated] Average of daily T_B images over the study area. (left) 25-km GRD. (right) 3.125-km rSIR. The thick horizontal lines show the data transect locations where data is extracted from the image for analysis.

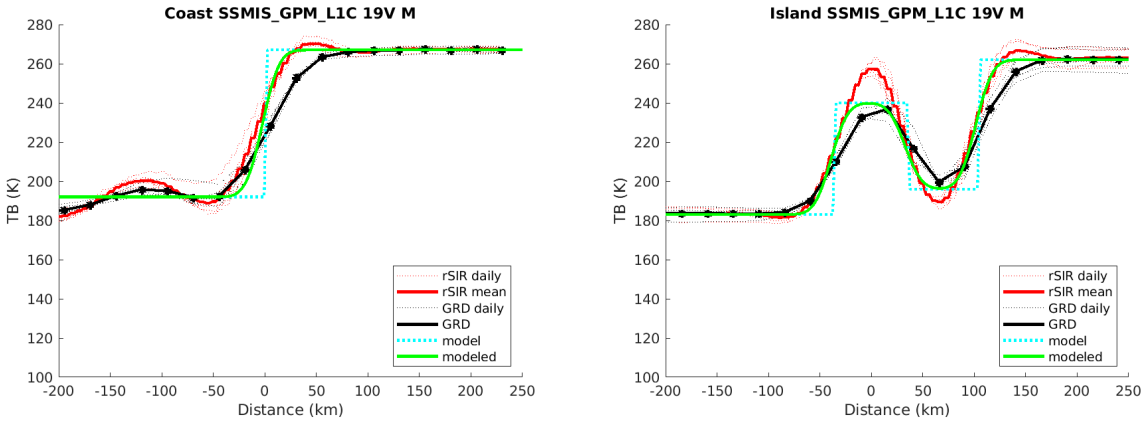

Figure 70: Plots of T_B along the two analysis case transect lines for the (left) coast-crossing and (right) island-crossing cases.

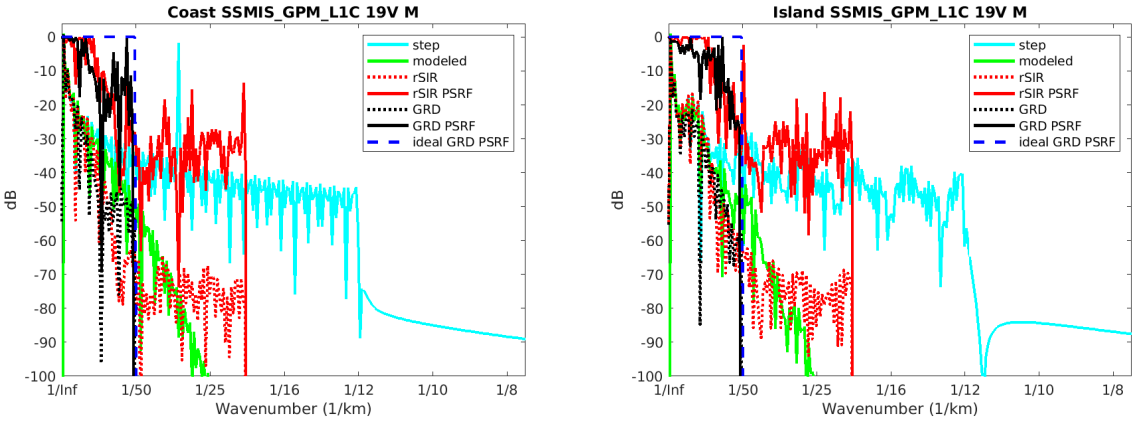

Figure 71: Wavenumber spectra of the T_B slices, the model, and the PSRF. (left) Coast-crossing case. (right) Island-crossing case.

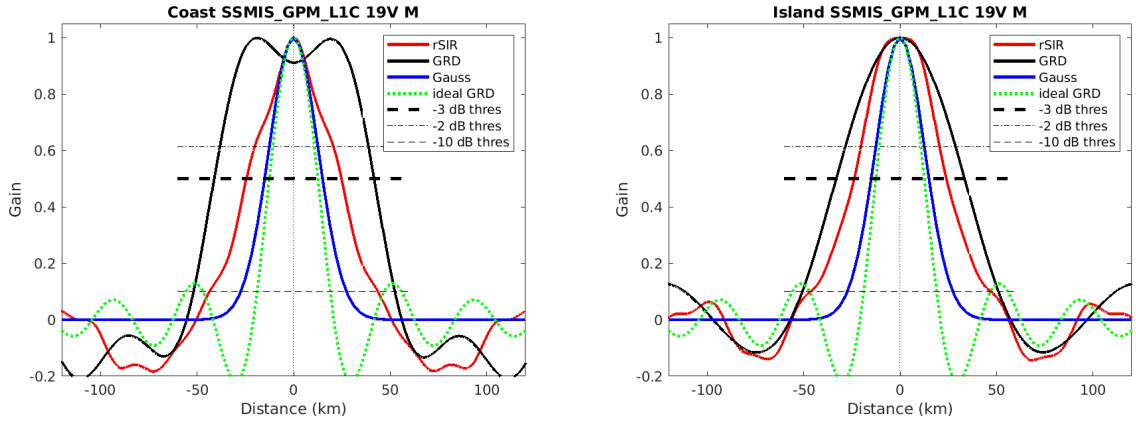

Figure 72: Derived single-pass rSIR and GRD PSRFs from the (left) coast-crossing and (right) island-crossing cases.

Table 37: Resolution estimates for SSMIS_GPM_L1C channel 19V LTOD M

	-3 dB Thres		-2 dB Thres		-10 dB Thres	
Algorithm	Coast	Island	Coast	Island	Coast	Island
Gauss	30.0	30.0	24.4	24.4	54.8	54.8
rSIR	49.3	47.7	39.1	39.7	87.1	93.5
ideal GRD	36.2	36.2	30.3	30.3	54.5	54.5
GRD	82.8	66.6	76.0	55.7	104.2	101.7

8.5 Channel 22V E Figures

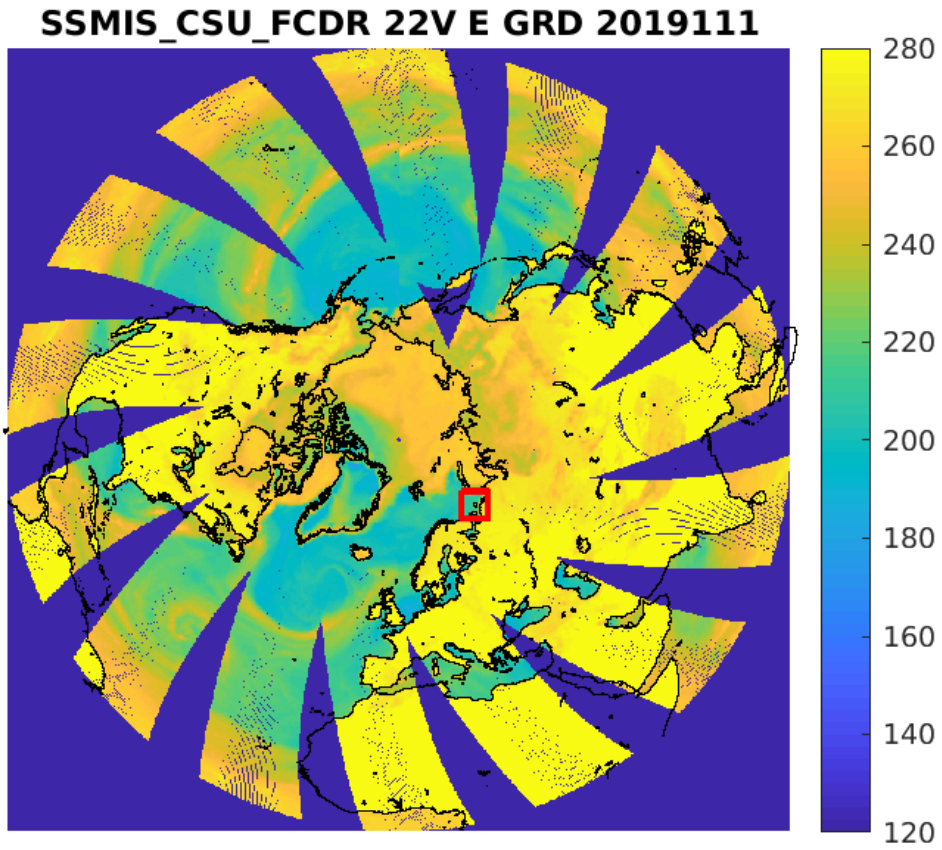

Figure 73: rSIR Northern Hemisphere view.

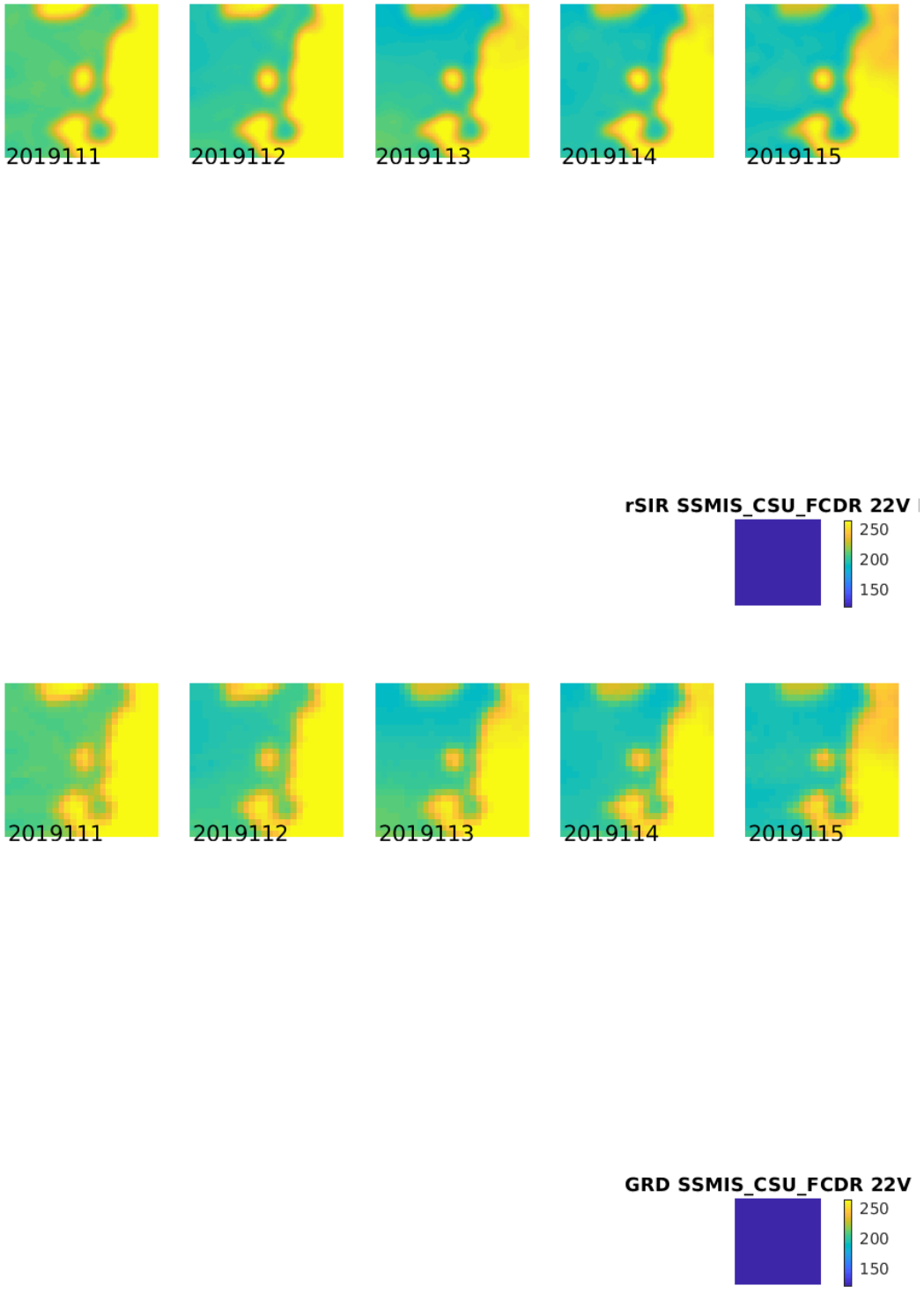

Figure 74: Time series of (top) rSIR and (bottom) GRD T_B images over the study area. Image dates are labeled on the image.

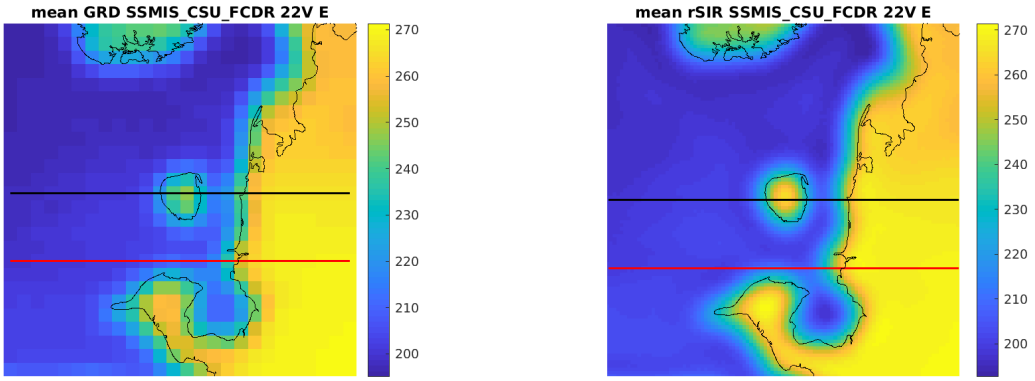

Figure 75: Average of daily T_B images over the study area. (left) 25-km GRD. (right) 3.125-km rSIR. The thick horizontal lines show the data transect locations where data is extracted from the image for analysis.

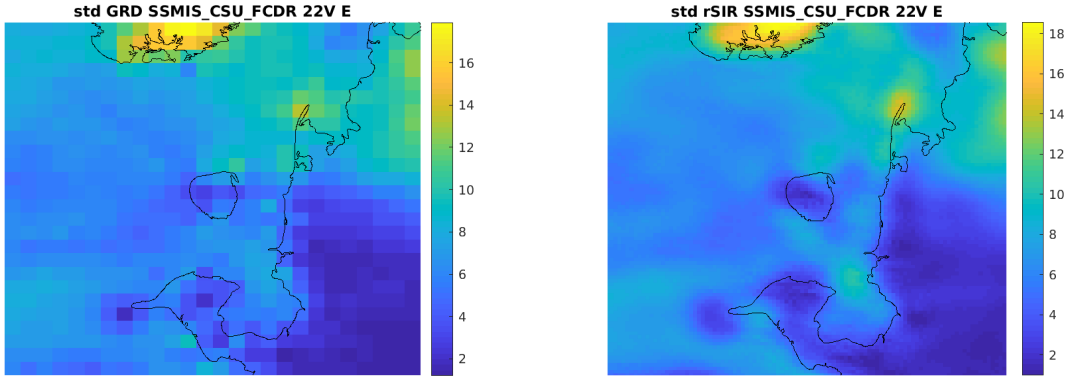

Figure 76: Standard deviation of daily T_B images over the study area. (left) 25-km GRD. (right) 3.125-km rSIR.

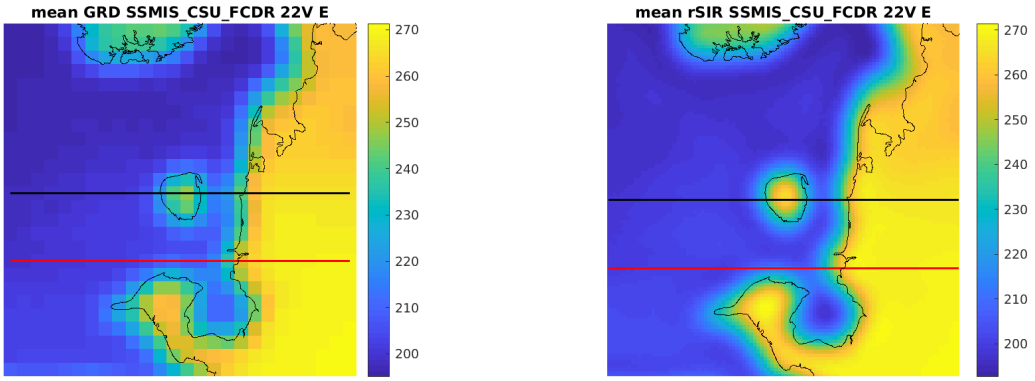

Figure 77: [Repeated] Average of daily T_B images over the study area. (left) 25-km GRD. (right) 3.125-km rSIR. The thick horizontal lines show the data transect locations where data is extracted from the image for analysis.

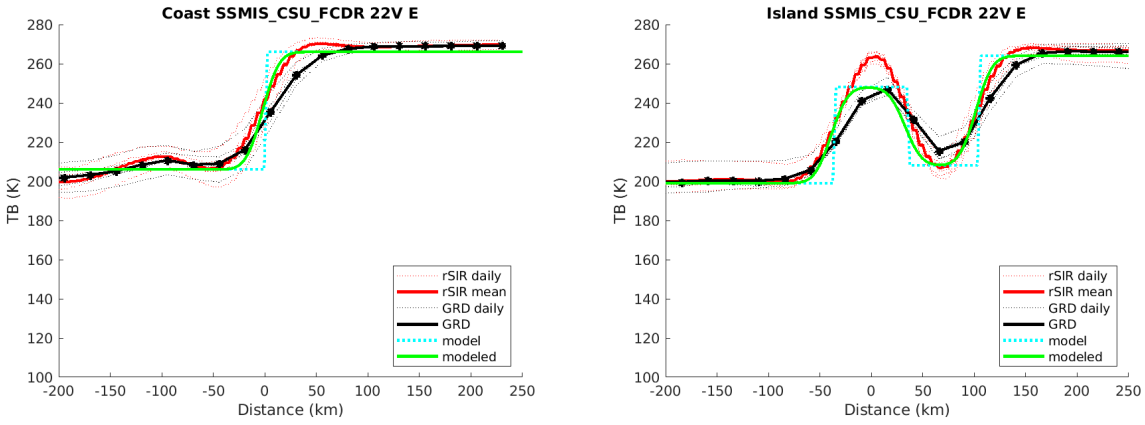

Figure 78: Plots of T_B along the two analysis case transect lines for the (left) coast-crossing and (right) island-crossing cases.

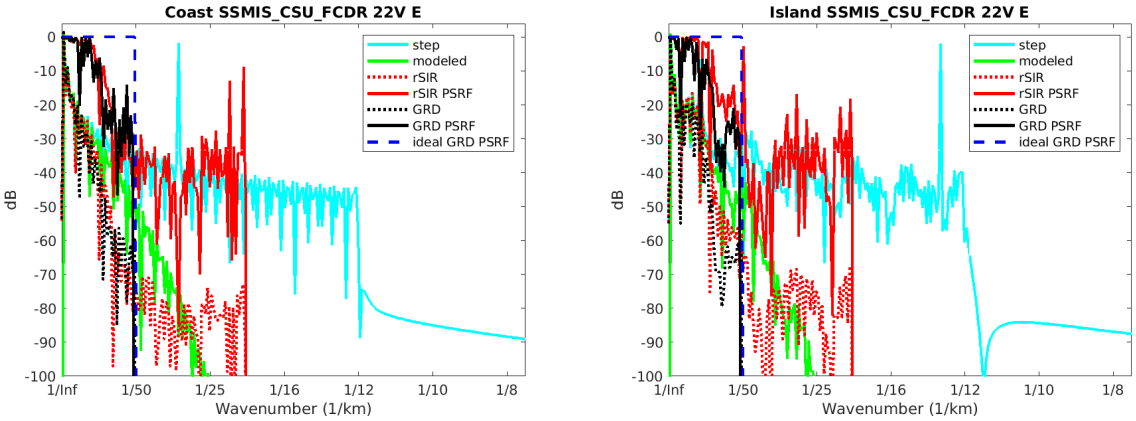

Figure 79: Wavenumber spectra of the T_B slices, the model, and the PSRF. (left) Coast-crossing case. (right) Island-crossing case.

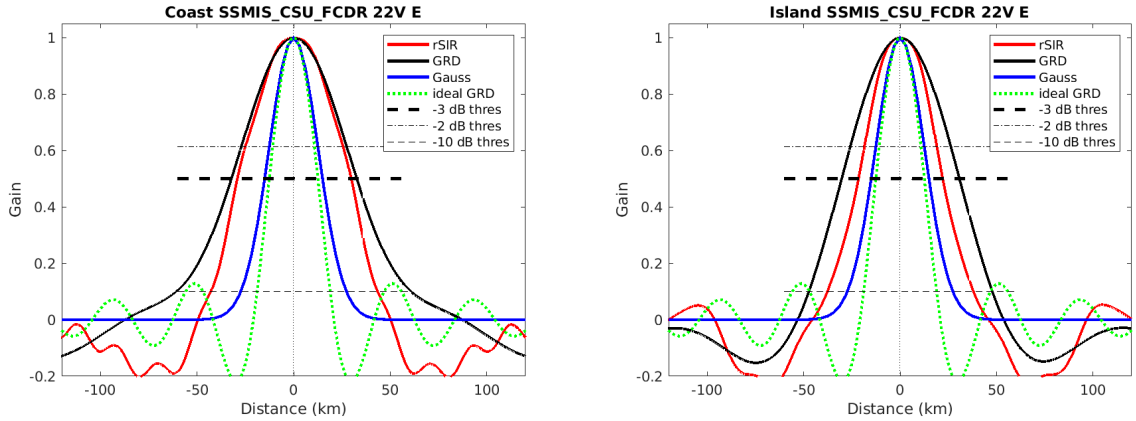

Figure 80: Derived single-pass rSIR and GRD PSRFs from the (left) coast-crossing and (right) island-crossing cases.

Table 38: Resolution estimates for SSMIS_CSU_FCDR channel 22V LTOD E

	-3 dB Thres		-2 dB Thres		-10 dB Thres	
Algorithm	Coast	Island	Coast	Island	Coast	Island
Gauss	30.0	30.0	24.4	24.4	54.8	54.8
rSIR	58.9	43.6	49.1	36.5	86.4	75.6
ideal GRD	36.2	36.2	30.3	30.3	54.5	54.5
GRD	64.9	61.1	53.0	50.7	121.7	95.2

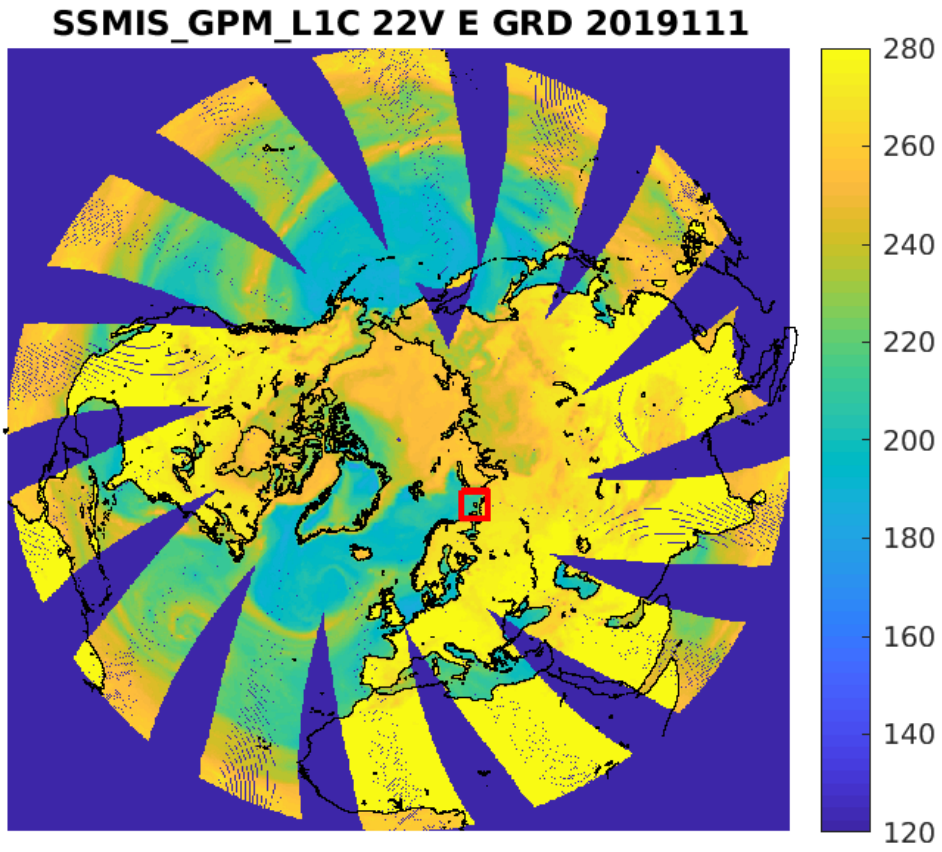

Figure 81: rSIR Northern Hemisphere view.

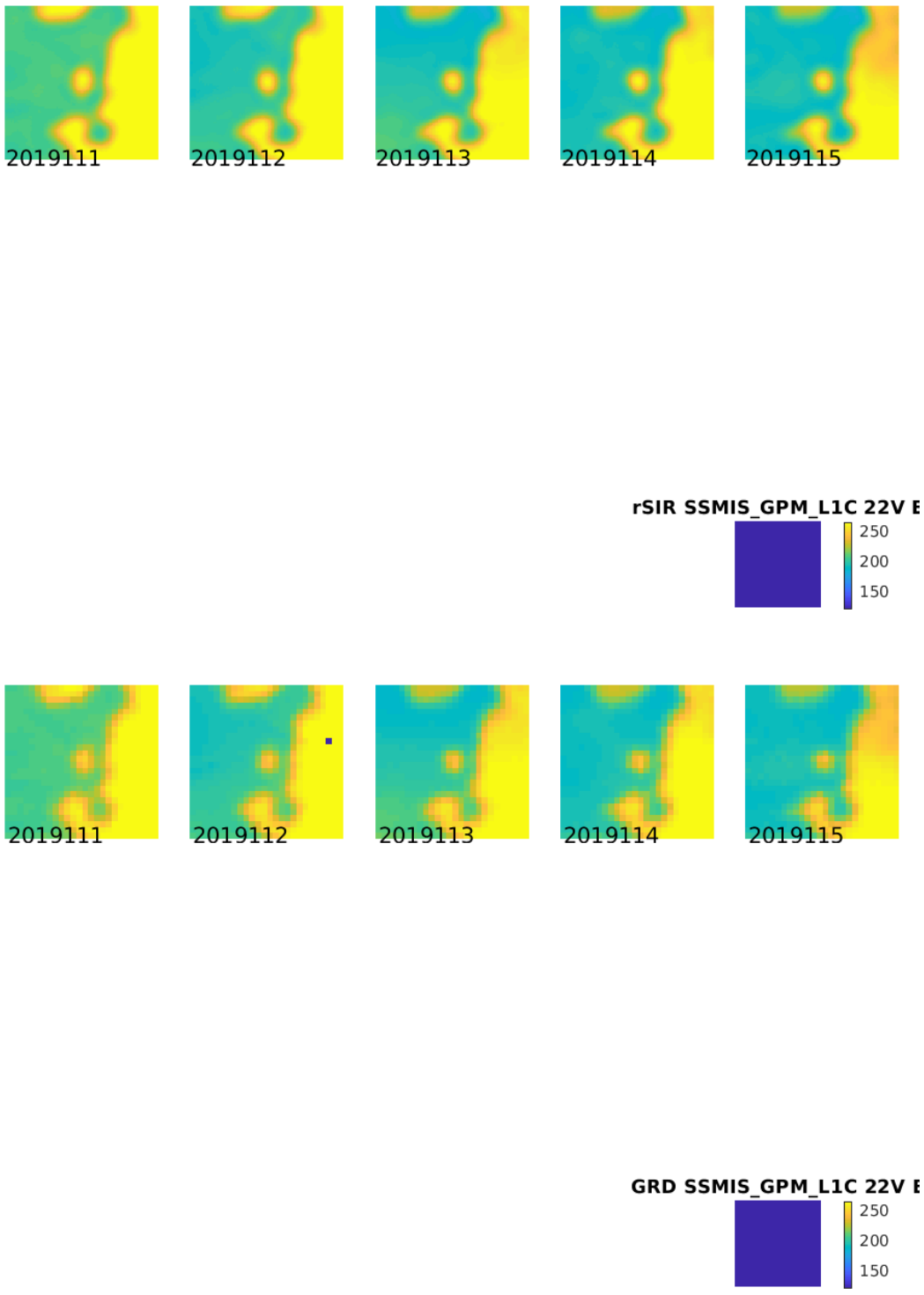

Figure 82: Time series of (top) rSIR and (bottom) GRD T_B images over the study area. Image dates are labeled on the image.

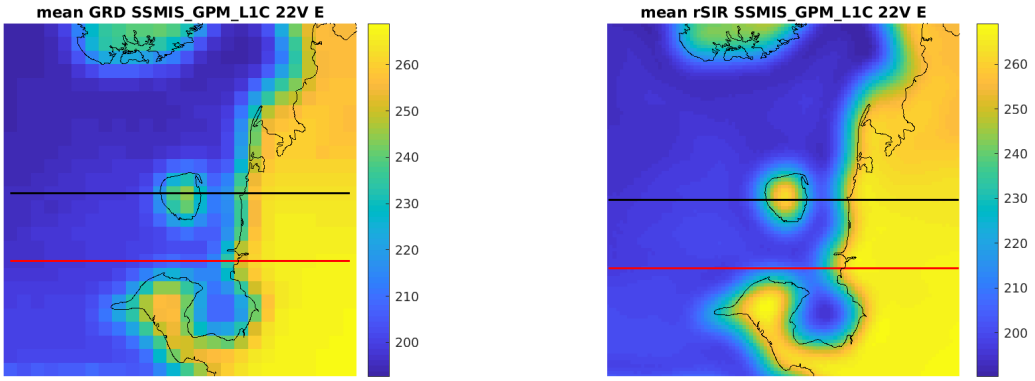

Figure 83: Average of daily T_B images over the study area. (left) 25-km GRD. (right) 3.125-km rSIR. The thick horizontal lines show the data transect locations where data is extracted from the image for analysis.

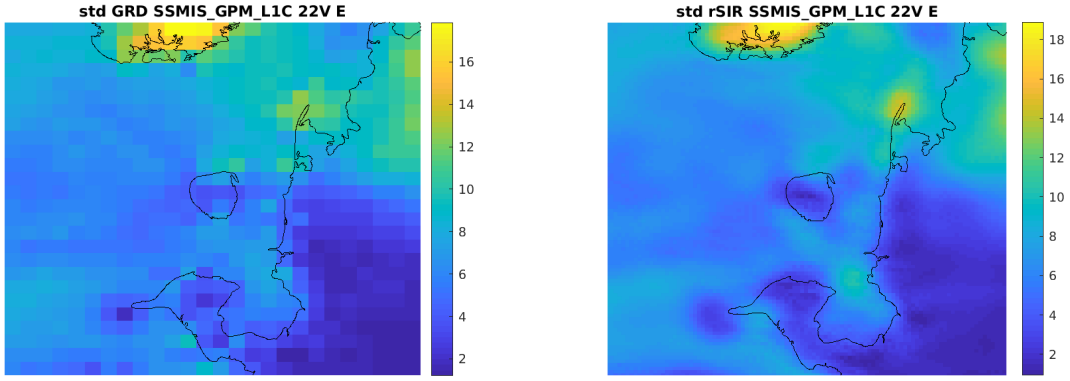

Figure 84: Standard deviation of daily T_B images over the study area. (left) 25-km GRD. (right) 3.125-km rSIR.

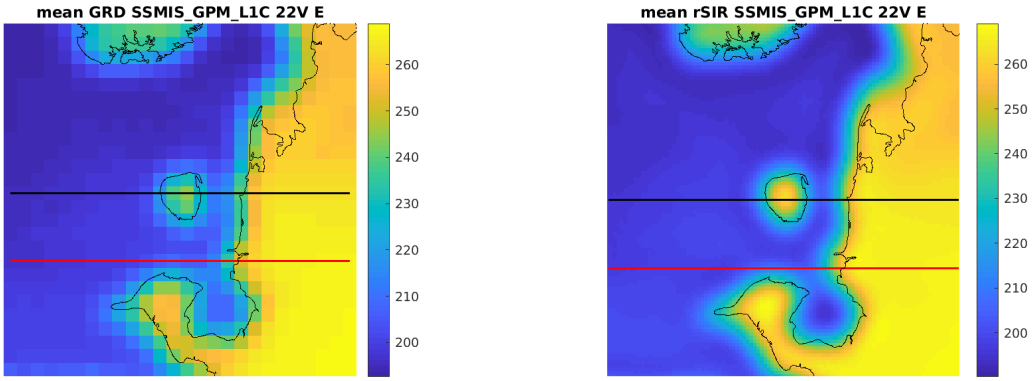

Figure 85: [Repeated] Average of daily T_B images over the study area. (left) 25-km GRD. (right) 3.125-km rSIR. The thick horizontal lines show the data transect locations where data is extracted from the image for analysis.

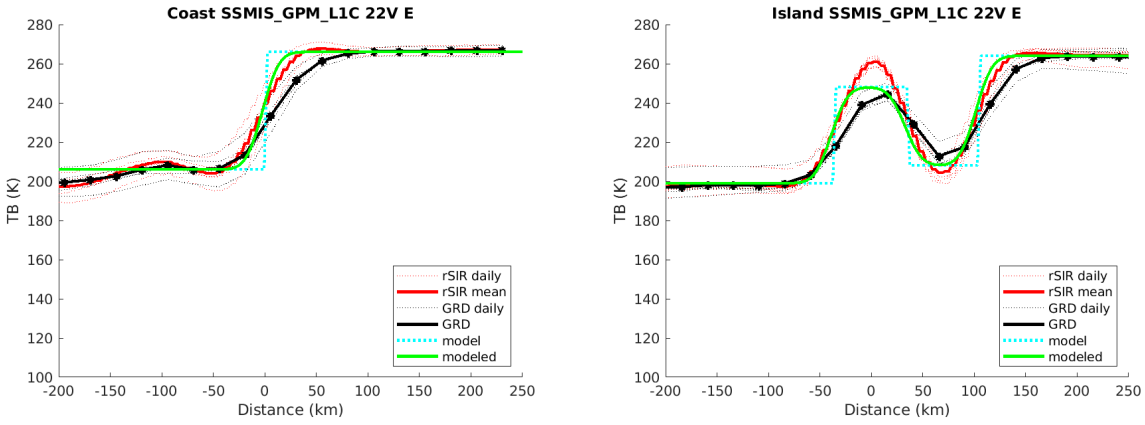

Figure 86: Plots of T_B along the two analysis case transect lines for the (left) coast-crossing and (right) island-crossing cases.

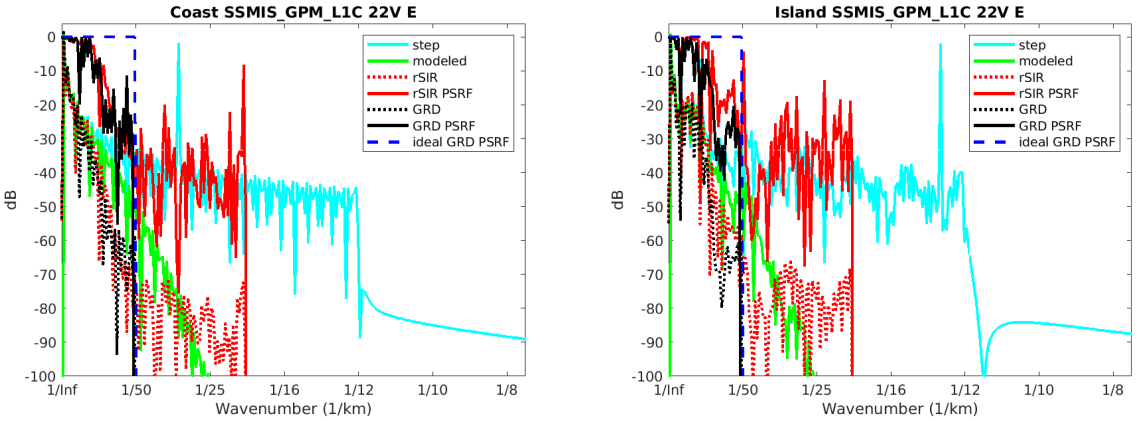

Figure 87: Wavenumber spectra of the T_B slices, the model, and the PSRF. (left) Coast-crossing case. (right) Island-crossing case.

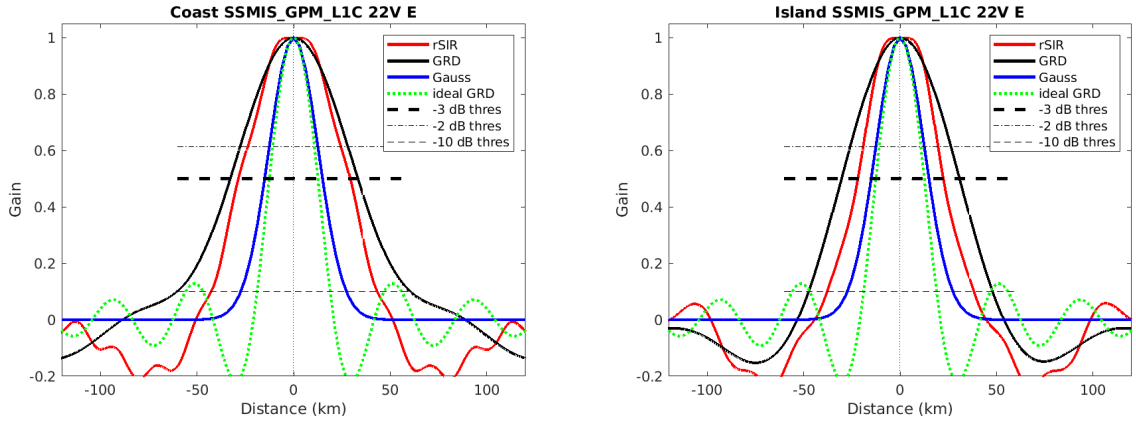

Figure 88: Derived single-pass rSIR and GRD PSRFs from the (left) coast-crossing and (right) island-crossing cases.

Table 39: Resolution estimates for SSMIS_GPM_L1C channel 22V LTOD E

	-3 dB Thres		-2 dB Thres		-10 dB Thres	
Algorithm	Coast	Island	Coast	Island	Coast	Island
Gauss	30.0	30.0	24.4	24.4	54.8	54.8
rSIR	57.8	44.2	46.7	37.9	86.0	75.9
ideal GRD	36.2	36.2	30.3	30.3	54.5	54.5
GRD	66.0	61.2	54.2	50.8	120.9	95.4

8.6 Channel 22V M Figures

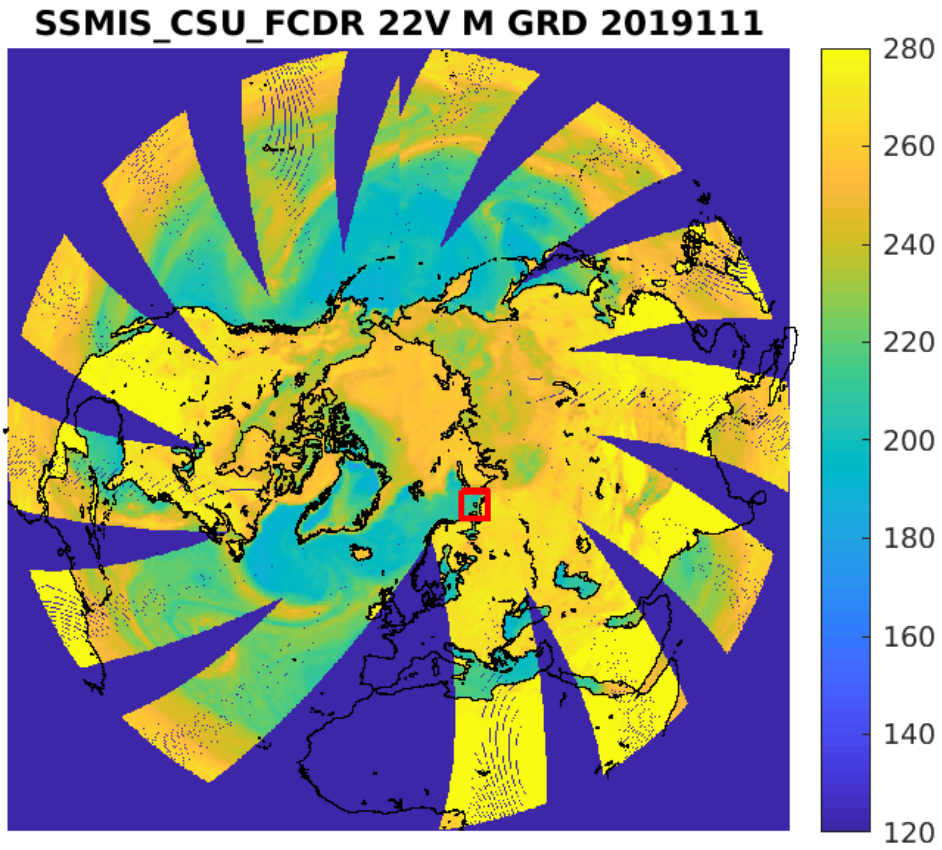

Figure 89: rSIR Northern Hemisphere view.

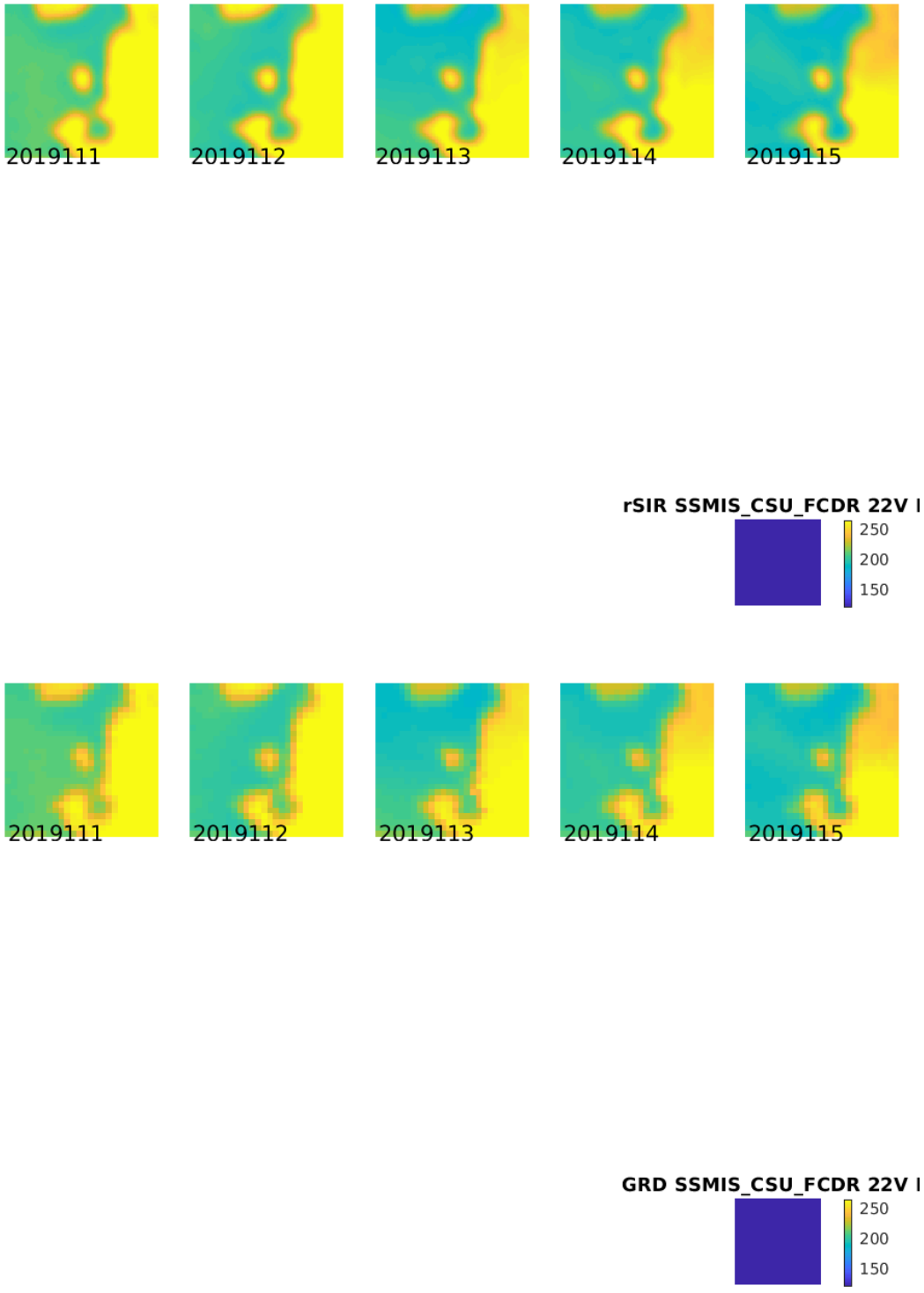

Figure 90: Time series of (top) rSIR and (bottom) GRD T_B images over the study area. Image dates are labeled on the image.

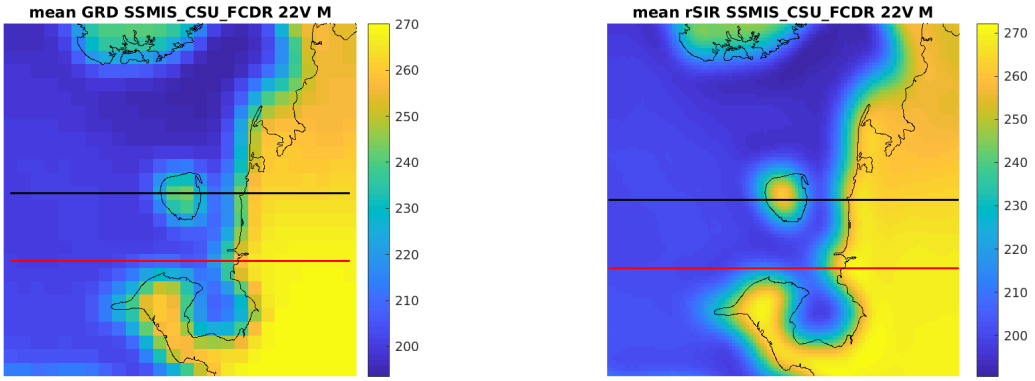

Figure 91: Average of daily T_B images over the study area. (left) 25-km GRD. (right) 3.125-km rSIR. The thick horizontal lines show the data transect locations where data is extracted from the image for analysis.

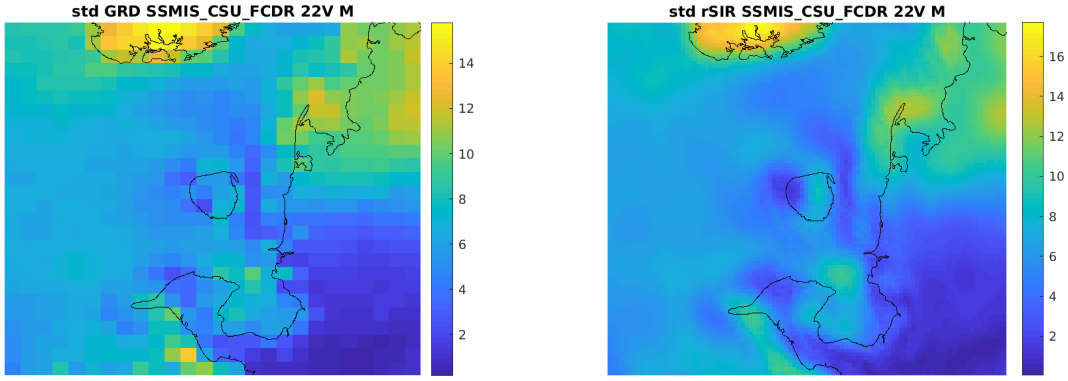

Figure 92: Standard deviation of daily T_B images over the study area. (left) 25-km GRD. (right) 3.125-km rSIR.

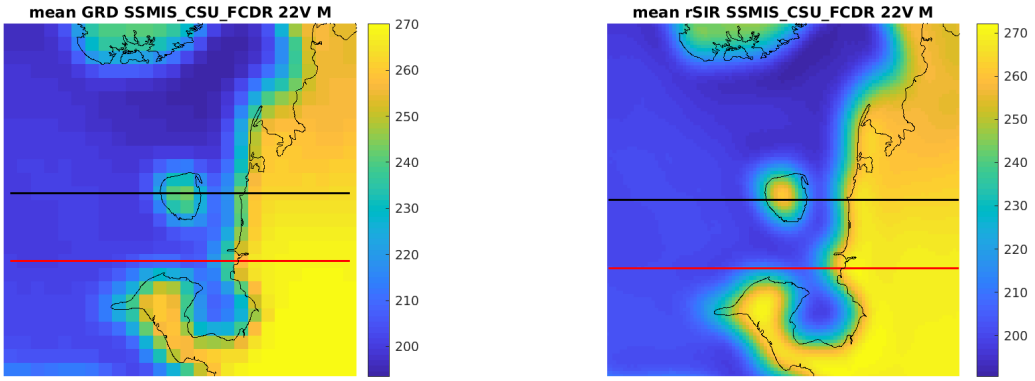

Figure 93: [Repeated] Average of daily T_B images over the study area. (left) 25-km GRD. (right) 3.125-km rSIR. The thick horizontal lines show the data transect locations where data is extracted from the image for analysis.

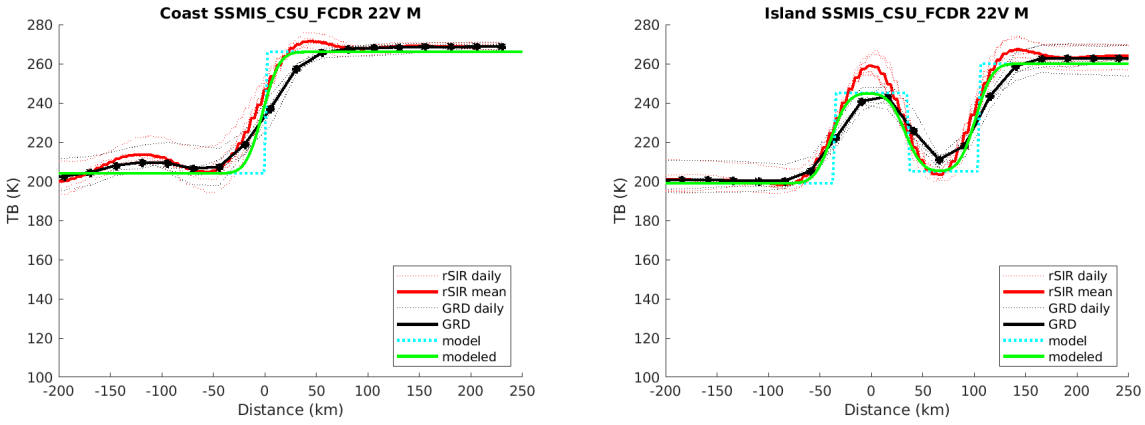

Figure 94: Plots of T_B along the two analysis case transect lines for the (left) coast-crossing and (right) island-crossing cases.

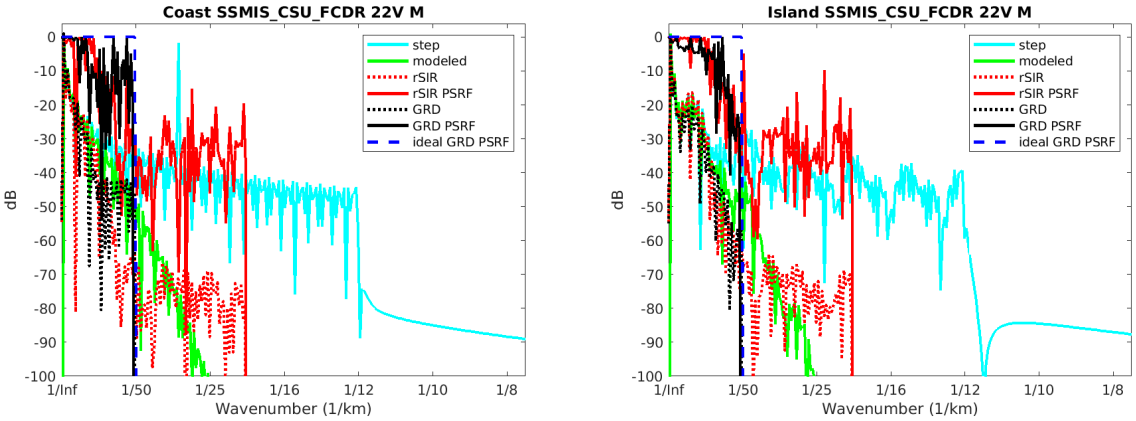

Figure 95: Wavenumber spectra of the T_B slices, the model, and the PSRF. (left) Coast-crossing case. (right) Island-crossing case.

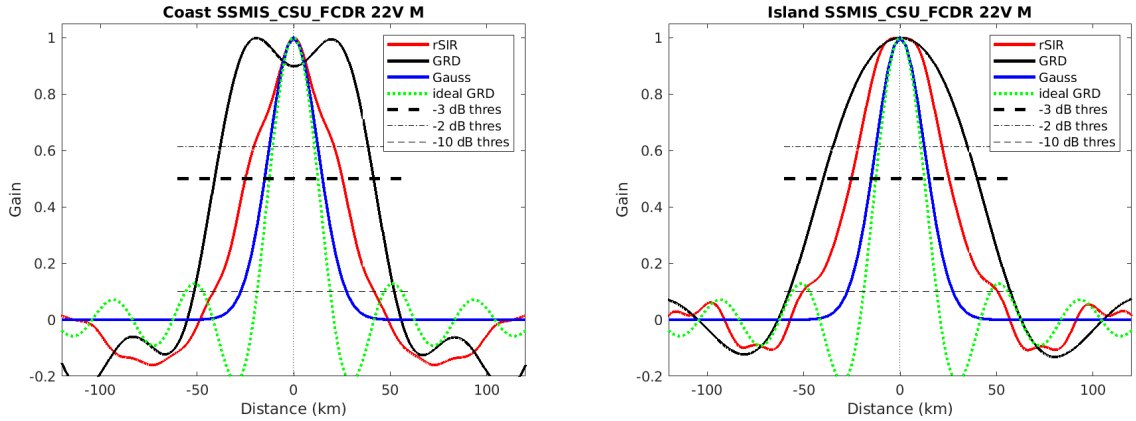

Figure 96: Derived single-pass rSIR and GRD PSRFs from the (left) coast-crossing and (right) island-crossing cases.

Table 40: Resolution estimates for SSMIS_CSU_FCDR channel 22V LTOD M

	-3 dB Thres		-2 dB Thres		-10 dB Thres	
Algorithm	Coast	Island	Coast	Island	Coast	Island
Gauss	30.0	30.0	24.4	24.4	54.8	54.8
rSIR	50.2	50.6	39.9	42.4	83.2	101.1
ideal GRD	36.2	36.2	30.3	30.3	54.5	54.5
GRD	82.4	79.7	75.7	68.3	103.5	114.5

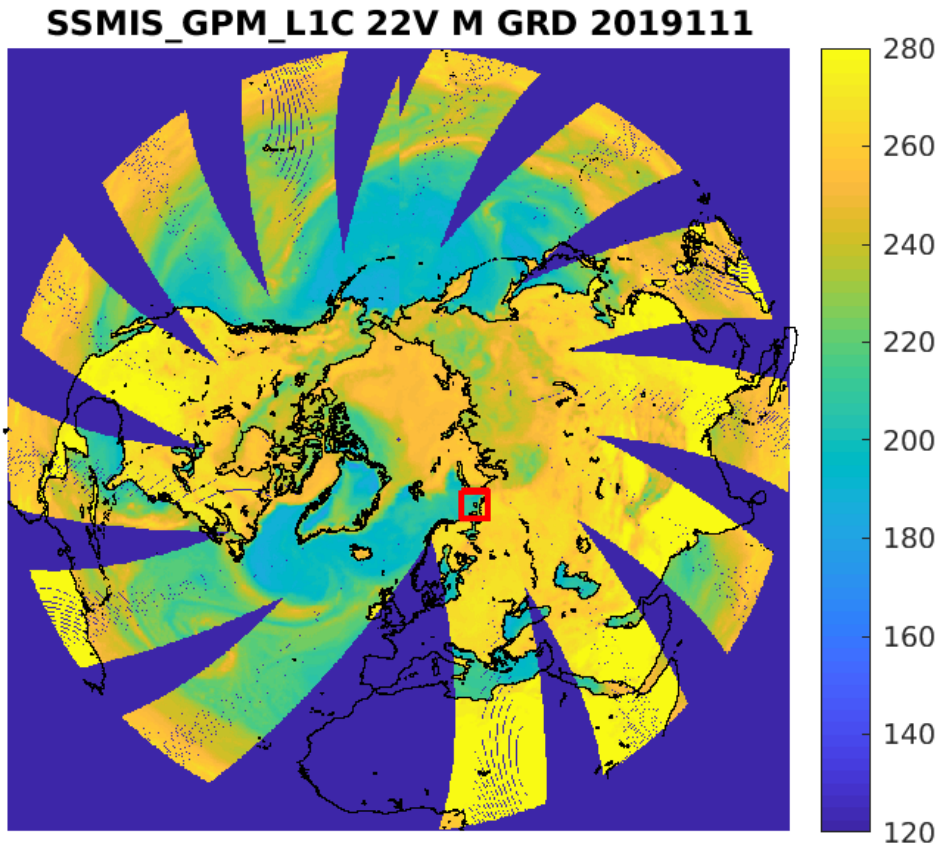

Figure 97: rSIR Northern Hemisphere view.

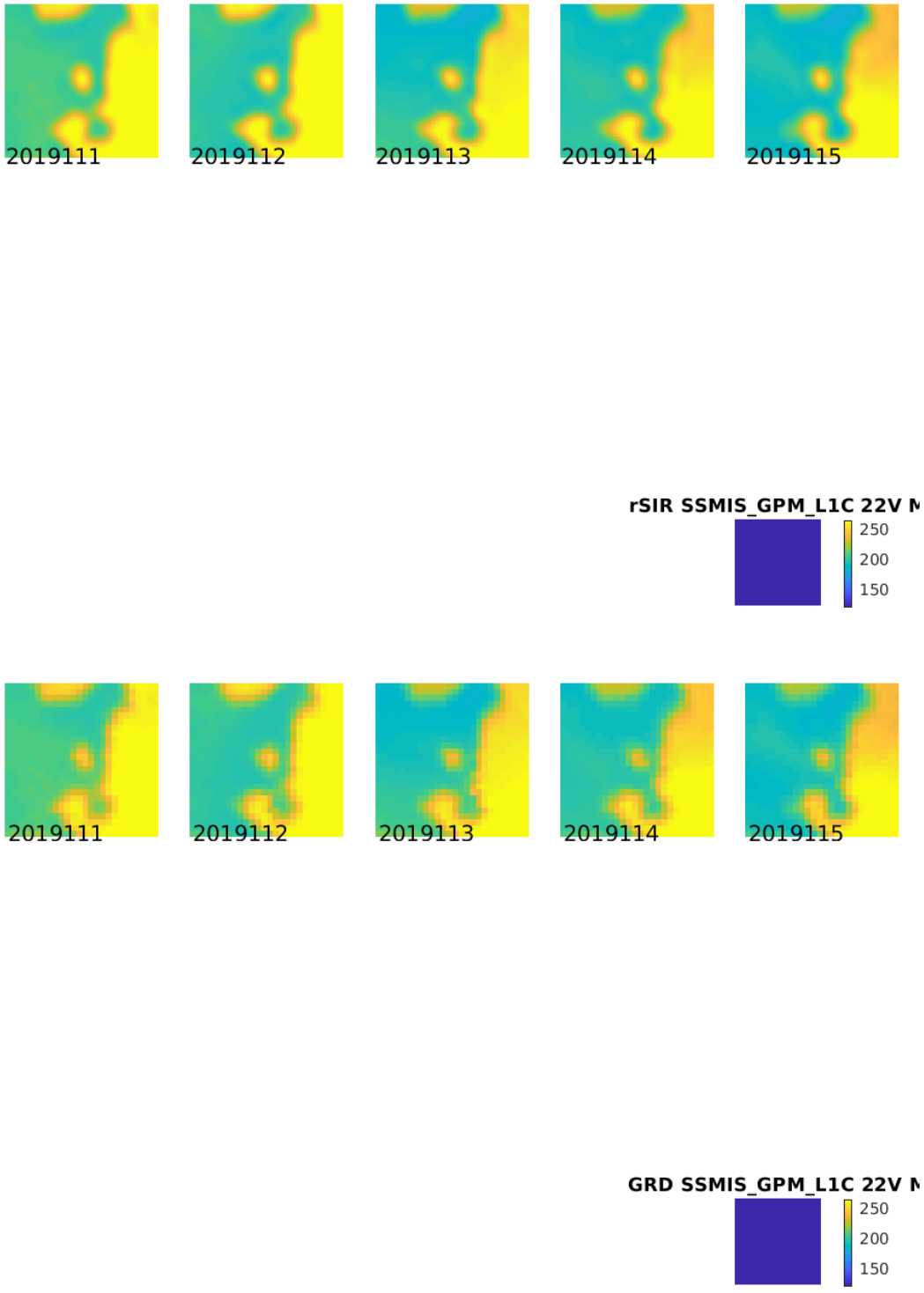

Figure 98: Time series of (top) rSIR and (bottom) GRD T_B images over the study area. Image dates are labeled on the image.

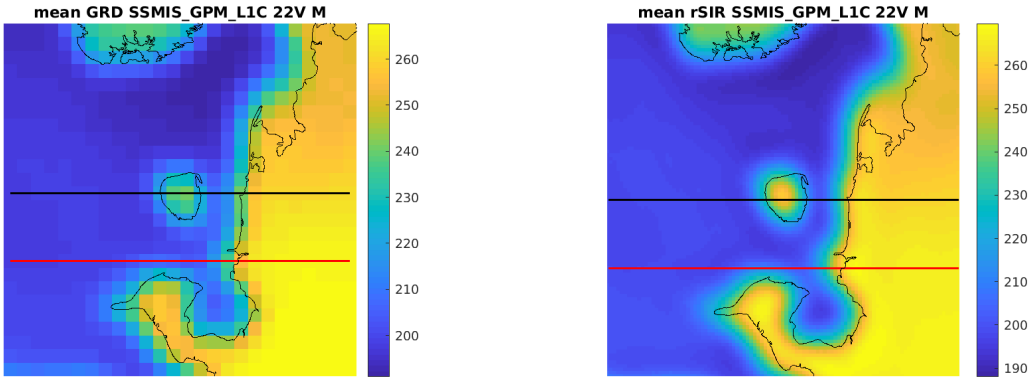

Figure 99: Average of daily T_B images over the study area. (left) 25-km GRD. (right) 3.125-km rSIR. The thick horizontal lines show the data transect locations where data is extracted from the image for analysis.

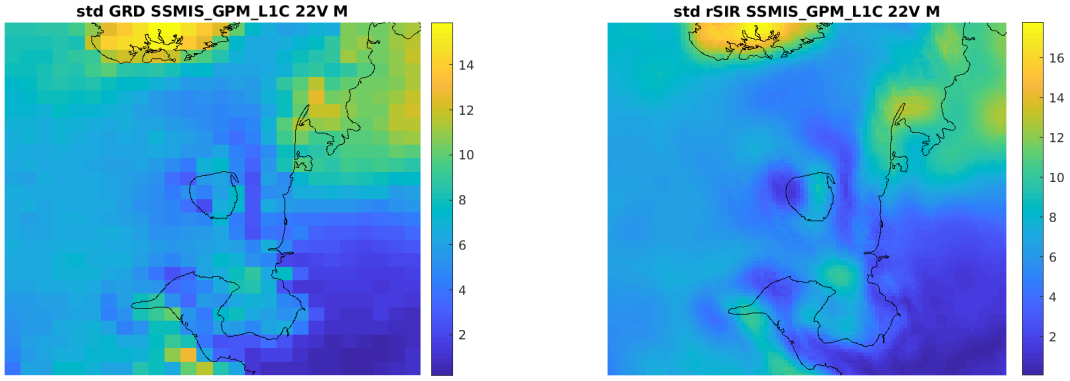

Figure 100: Standard deviation of daily T_B images over the study area. (left) 25-km GRD. (right) 3.125-km rSIR.

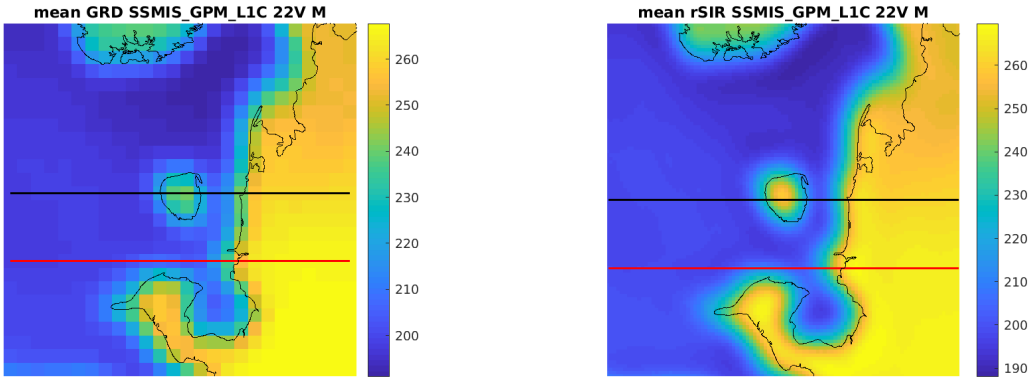

Figure 101: [Repeated] Average of daily T_B images over the study area. (left) 25-km GRD. (right) 3.125-km rSIR. The thick horizontal lines show the data transect locations where data is extracted from the image for analysis.

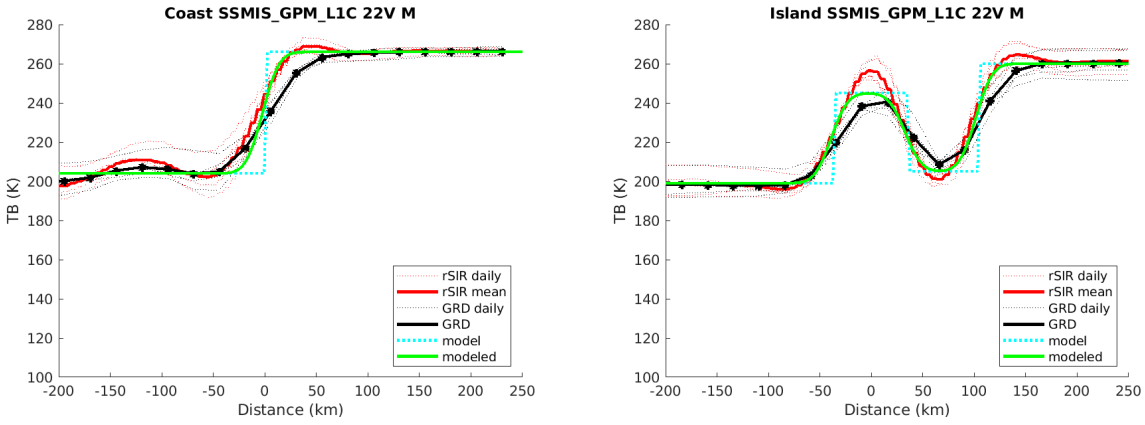

Figure 102: Plots of T_B along the two analysis case transect lines for the (left) coast-crossing and (right) island-crossing cases.

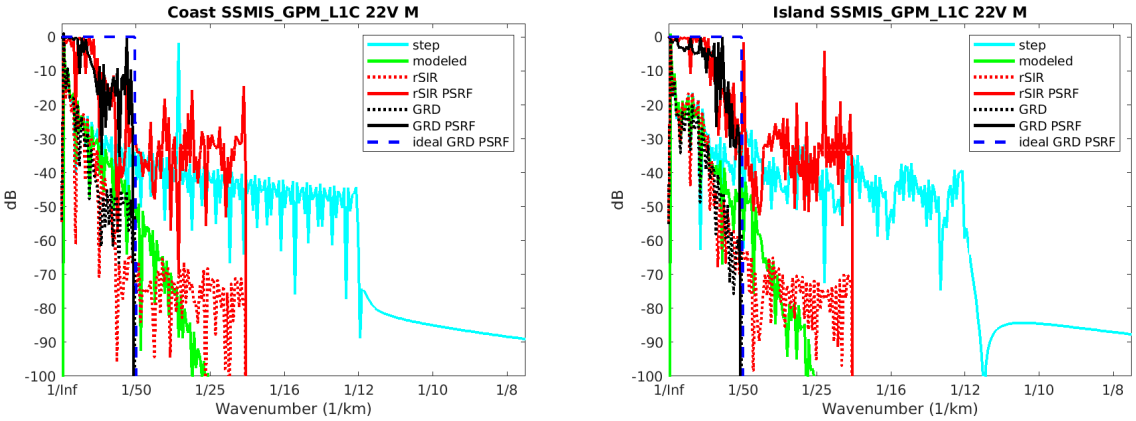

Figure 103: Wavenumber spectra of the T_B slices, the model, and the PSRF. (left) Coast-crossing case. (right) Island-crossing case.

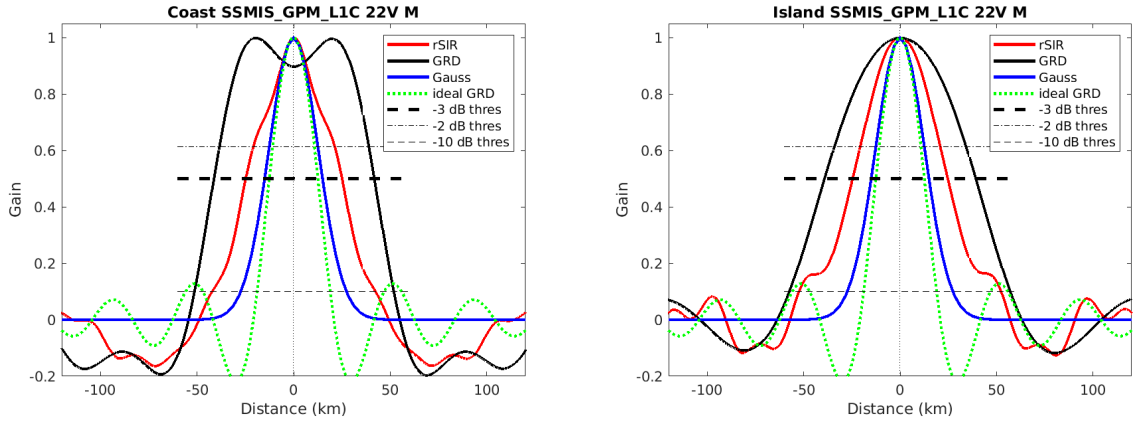

Figure 104: Derived single-pass rSIR and GRD PSRFs from the (left) coast-crossing and (right) island-crossing cases.

Table 41: Resolution estimates for SSMIS_GPM_L1C channel 22V LTOD M

	-3 dB Thres		-2 dB Thres		-10 dB Thres	
Algorithm	Coast	Island	Coast	Island	Coast	Island
Gauss	30.0	30.0	24.4	24.4	54.8	54.8
rSIR	49.9	49.3	40.7	40.2	84.6	104.8
ideal GRD	36.2	36.2	30.3	30.3	54.5	54.5
GRD	83.0	78.4	76.5	66.7	103.1	114.5

8.7 Channel 37H E Figures

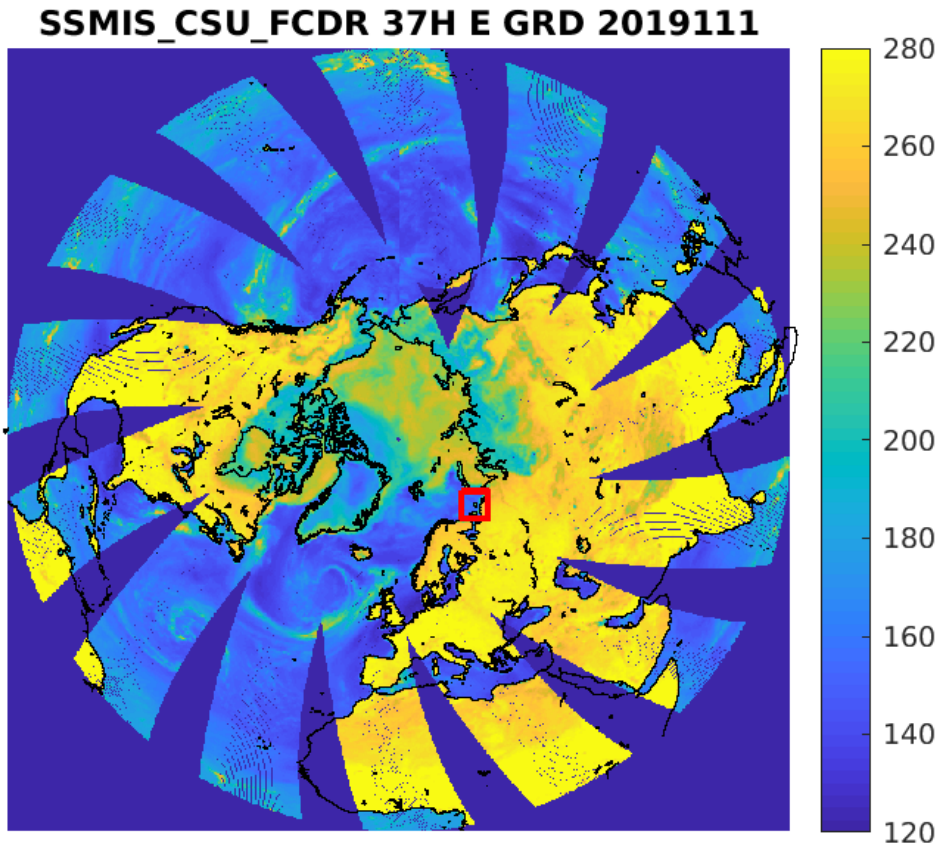

Figure 105: rSIR Northern Hemisphere view.

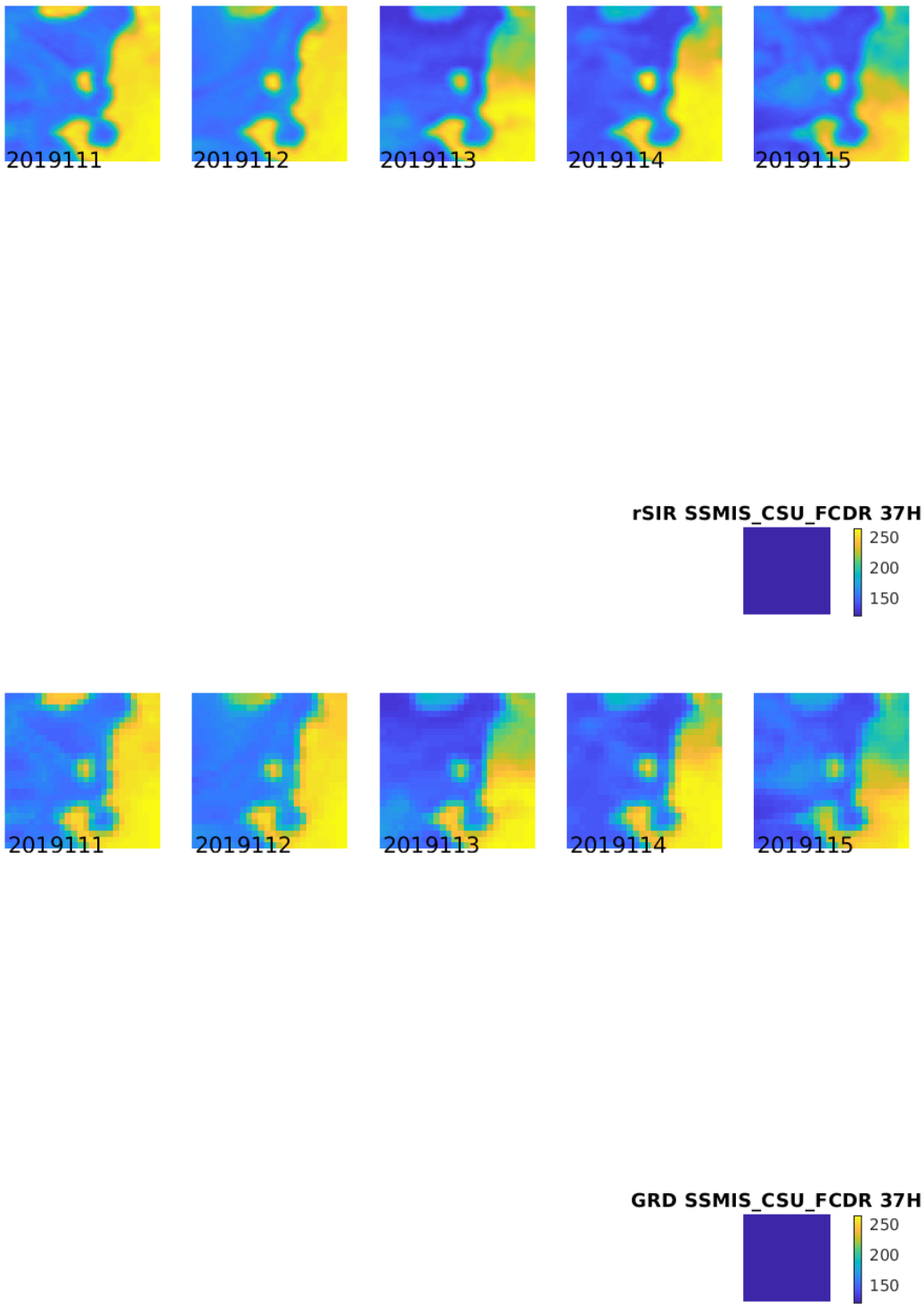

Figure 106: Time series of (top) rSIR and (bottom) GRD T_B images over the study area. Image dates are labeled on the image.

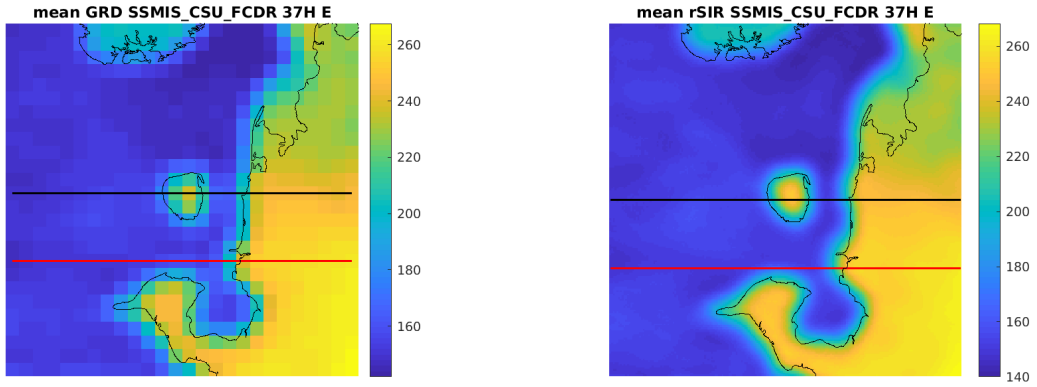

Figure 107: Average of daily T_B images over the study area. (left) 25-km GRD. (right) 3.125-km rSIR. The thick horizontal lines show the data transect locations where data is extracted from the image for analysis.

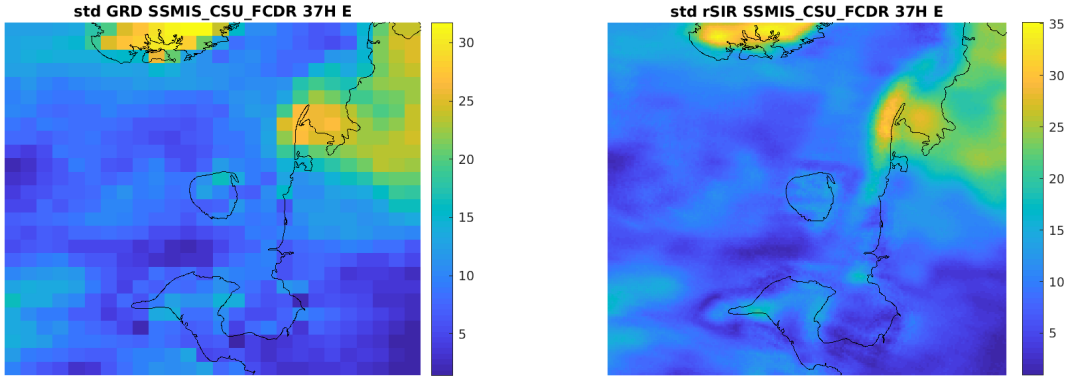

Figure 108: Standard deviation of daily T_B images over the study area. (left) 25-km GRD. (right) 3.125-km rSIR.

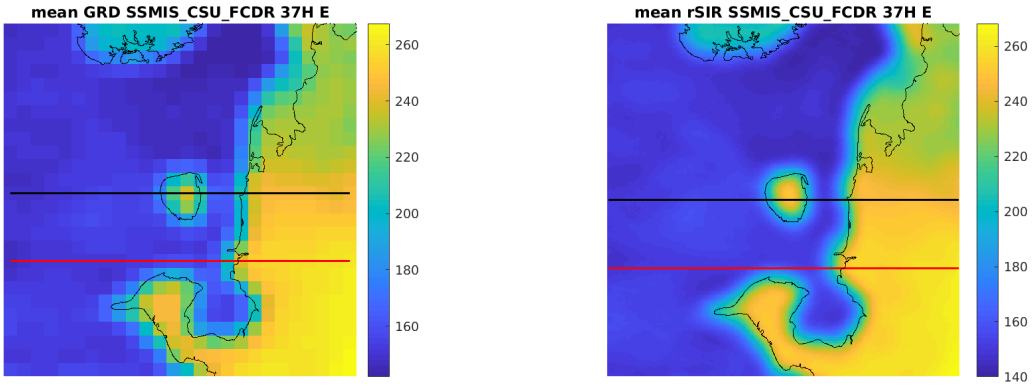

Figure 109: [Repeated] Average of daily T_B images over the study area. (left) 25-km GRD. (right) 3.125-km rSIR. The thick horizontal lines show the data transect locations where data is extracted from the image for analysis.

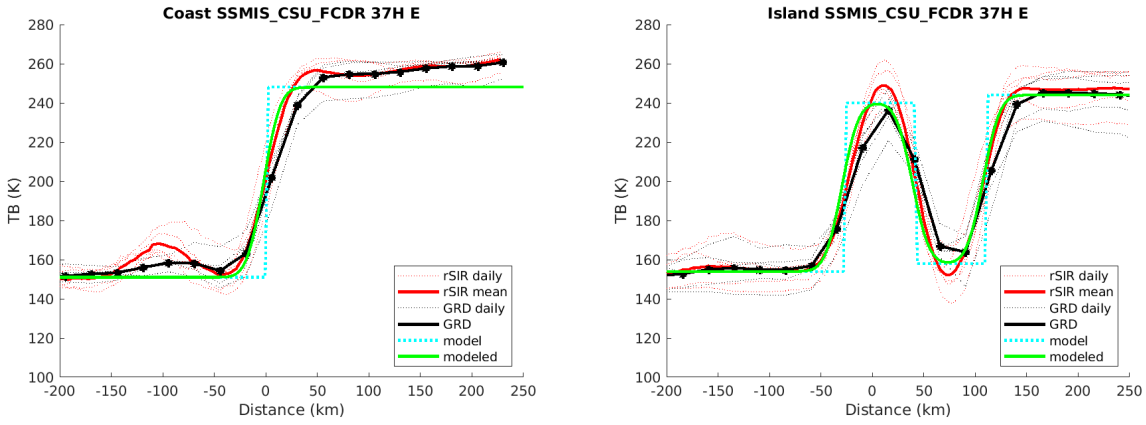

Figure 110: Plots of T_B along the two analysis case transect lines for the (left) coast-crossing and (right) island-crossing cases.

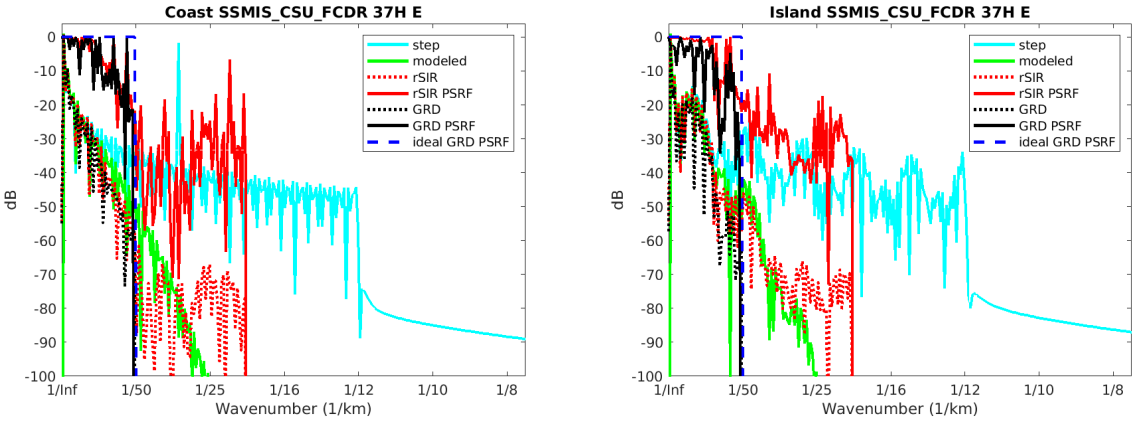

Figure 111: Wavenumber spectra of the T_B slices, the model, and the PSRF. (left) Coast-crossing case. (right) Island-crossing case.

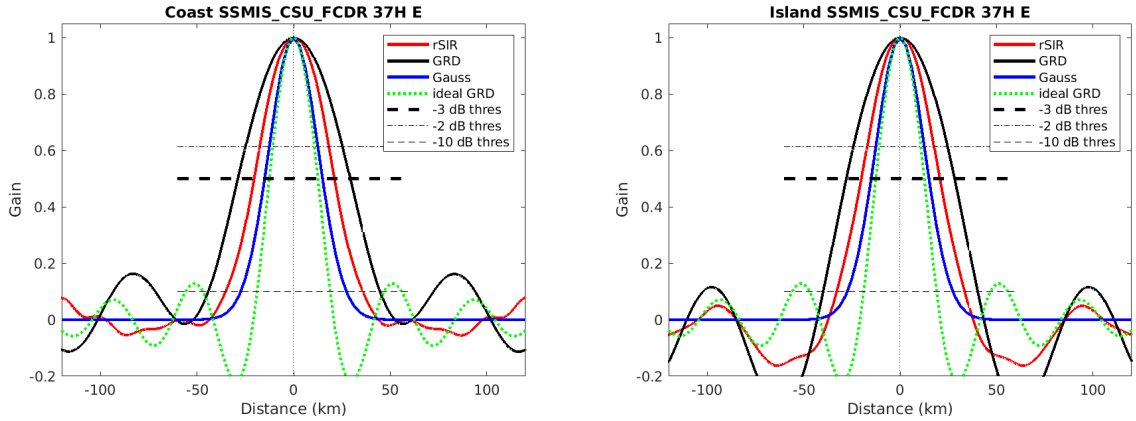

Figure 112: Derived single-pass rSIR and GRD PSRFs from the (left) coast-crossing and (right) island-crossing cases.

Table 42: Resolution estimates for SSMIS_CSU_FCDR channel 37H LTOD E

	-3 dB Thres		-2 dB Thres		-10 dB Thres	
Algorithm	Coast	Island	Coast	Island	Coast	Island
Gauss	30.0	30.0	24.4	24.4	54.8	54.8
rSIR	41.6	40.6	34.9	33.8	71.0	66.5
ideal GRD	36.2	36.2	30.3	30.3	54.5	54.5
GRD	58.1	56.2	48.9	47.7	88.9	80.1

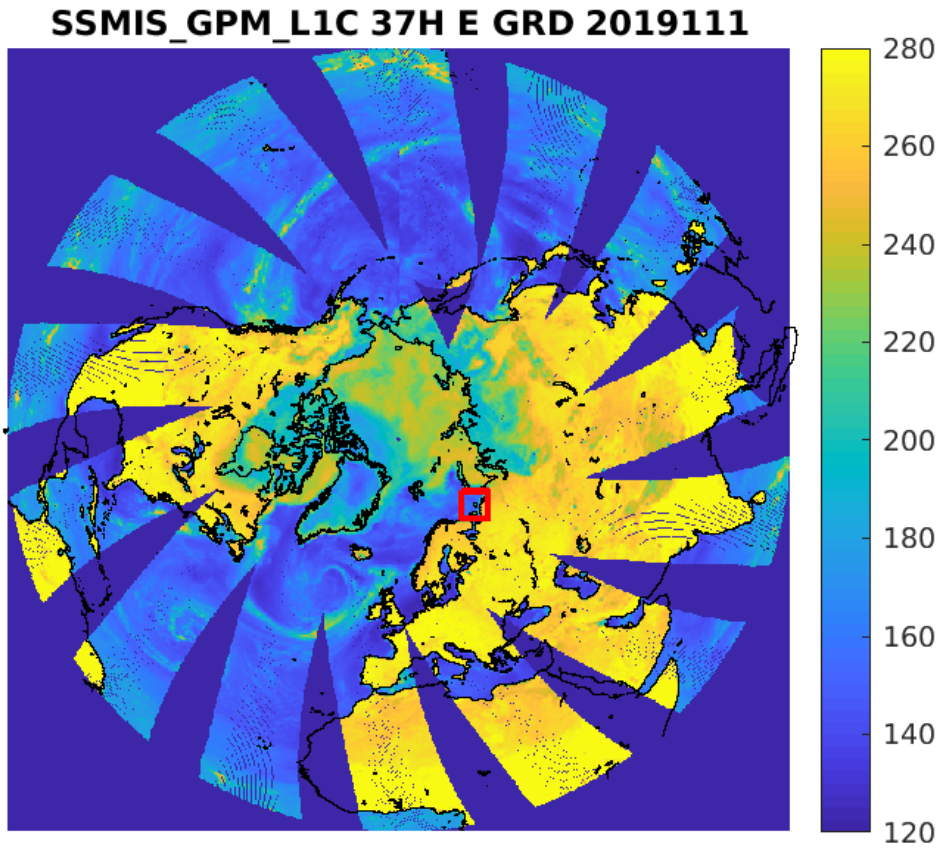

Figure 113: rSIR Northern Hemisphere view.

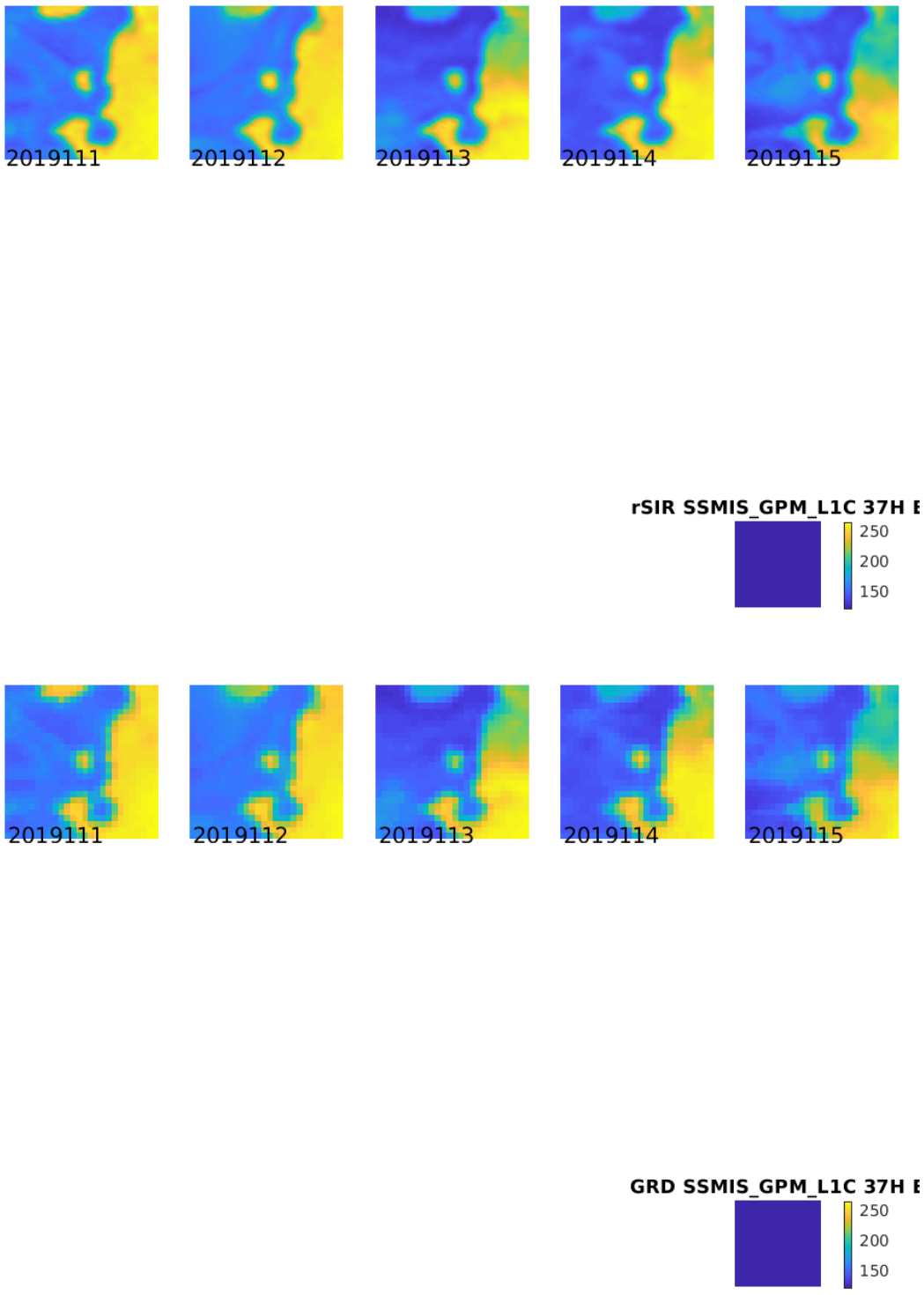

Figure 114: Time series of (top) rSIR and (bottom) GRD T_B images over the study area. Image dates are labeled on the image.

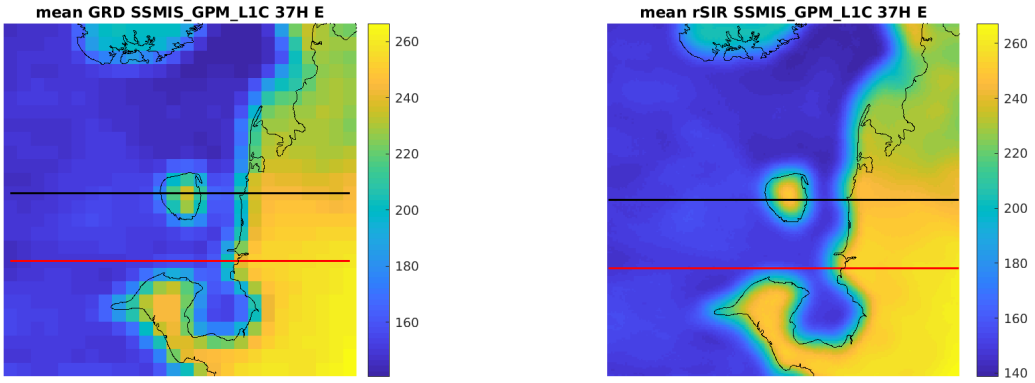

Figure 115: Average of daily T_B images over the study area. (left) 25-km GRD. (right) 3.125-km rSIR. The thick horizontal lines show the data transect locations where data is extracted from the image for analysis.

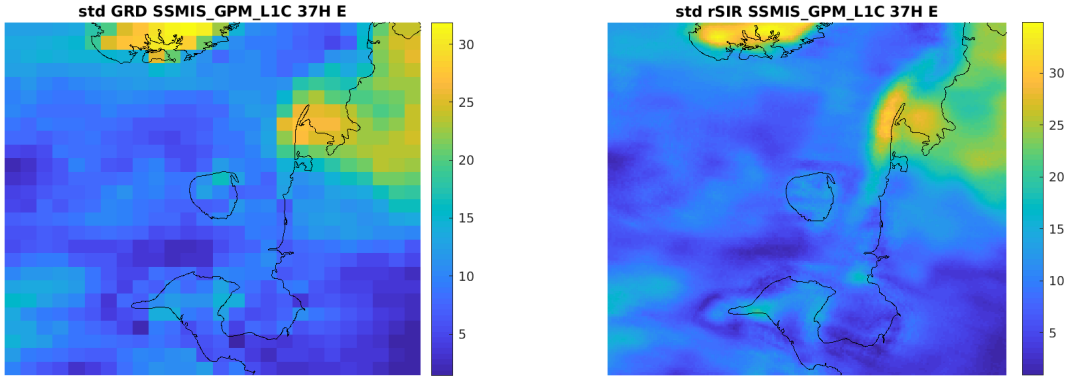

Figure 116: Standard deviation of daily T_B images over the study area. (left) 25-km GRD. (right) 3.125-km rSIR.

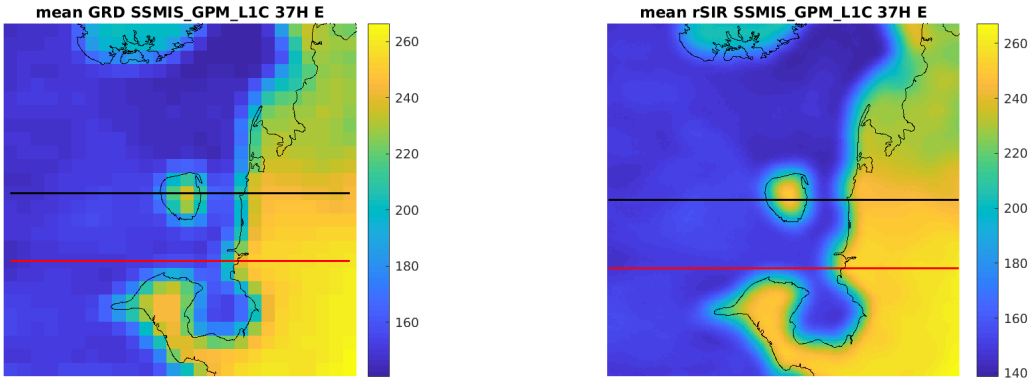

Figure 117: [Repeated] Average of daily T_B images over the study area. (left) 25-km GRD. (right) 3.125-km rSIR. The thick horizontal lines show the data transect locations where data is extracted from the image for analysis.

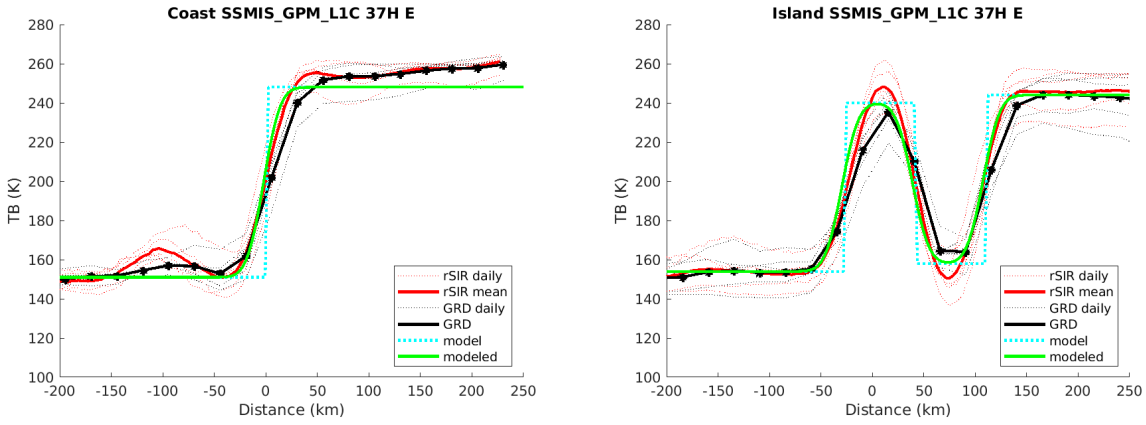

Figure 118: Plots of T_B along the two analysis case transect lines for the (left) coast-crossing and (right) island-crossing cases.

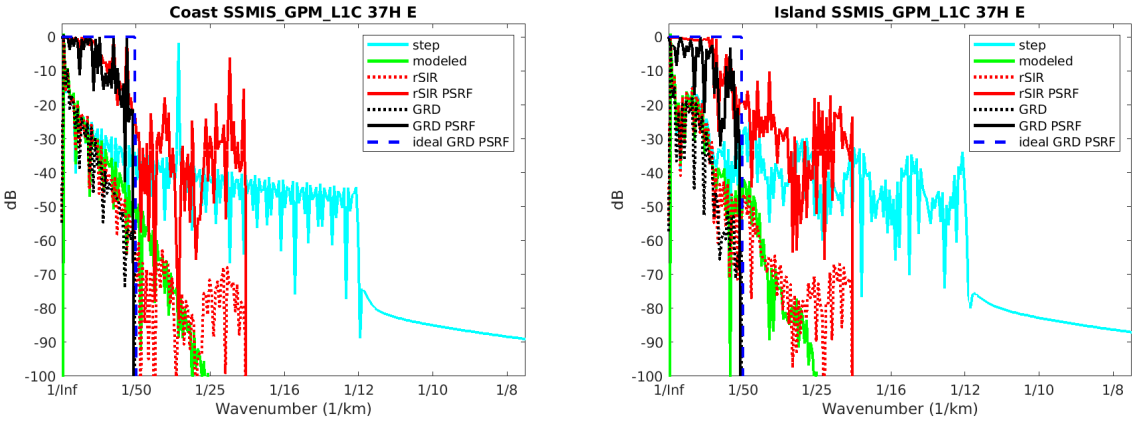

Figure 119: Wavenumber spectra of the T_B slices, the model, and the PSRF. (left) Coast-crossing case. (right) Island-crossing case.

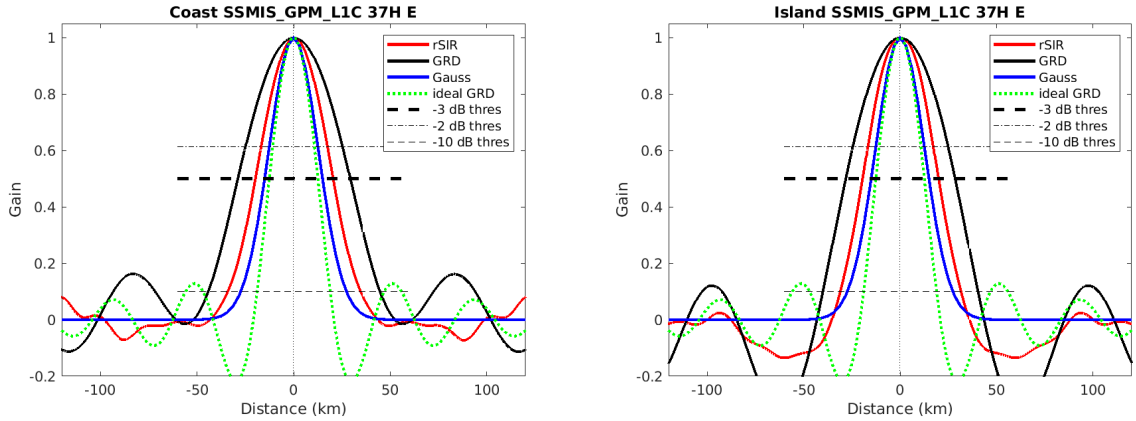

Figure 120: Derived single-pass rSIR and GRD PSRFs from the (left) coast-crossing and (right) island-crossing cases.

Table 43: Resolution estimates for SSMIS_GPM_L1C channel 37H LTOD E

	-3 dB Thres		-2 dB Thres		-10 dB Thres	
Algorithm	Coast	Island	Coast	Island	Coast	Island
Gauss	30.0	30.0	24.4	24.4	54.8	54.8
rSIR	40.3	39.3	33.4	33.1	68.7	62.7
ideal GRD	36.2	36.2	30.3	30.3	54.5	54.5
GRD	58.2	56.7	49.0	48.2	88.9	80.4

8.8 Channel 37H M Figures

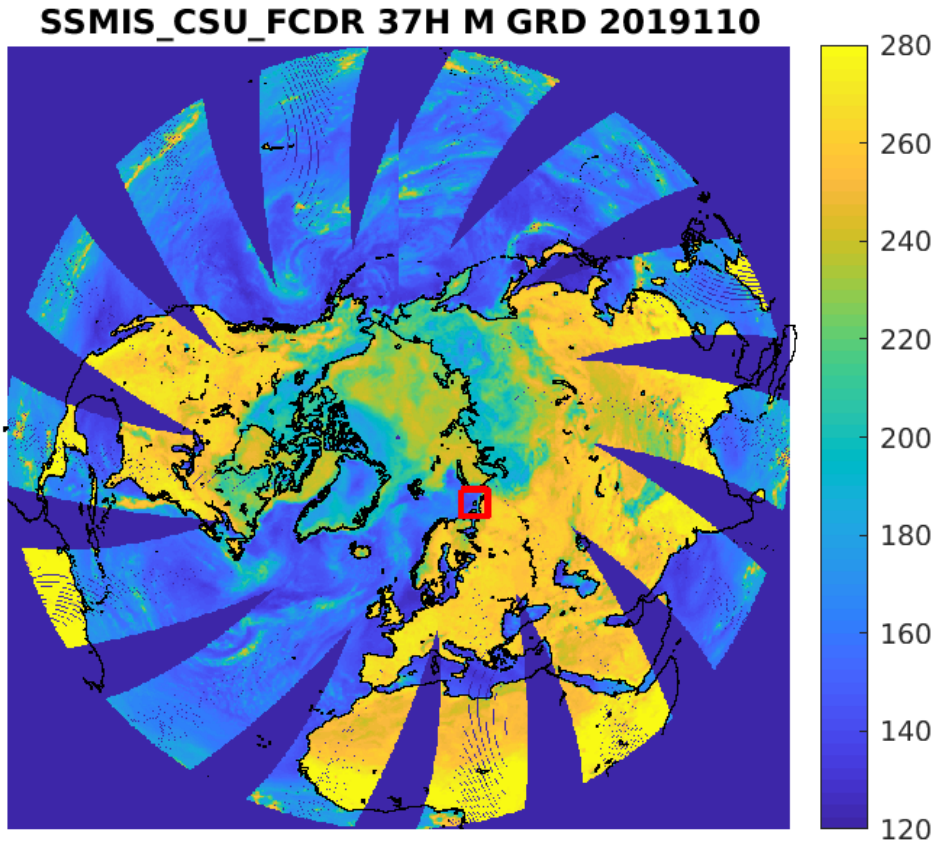

Figure 121: rSIR Northern Hemisphere view.

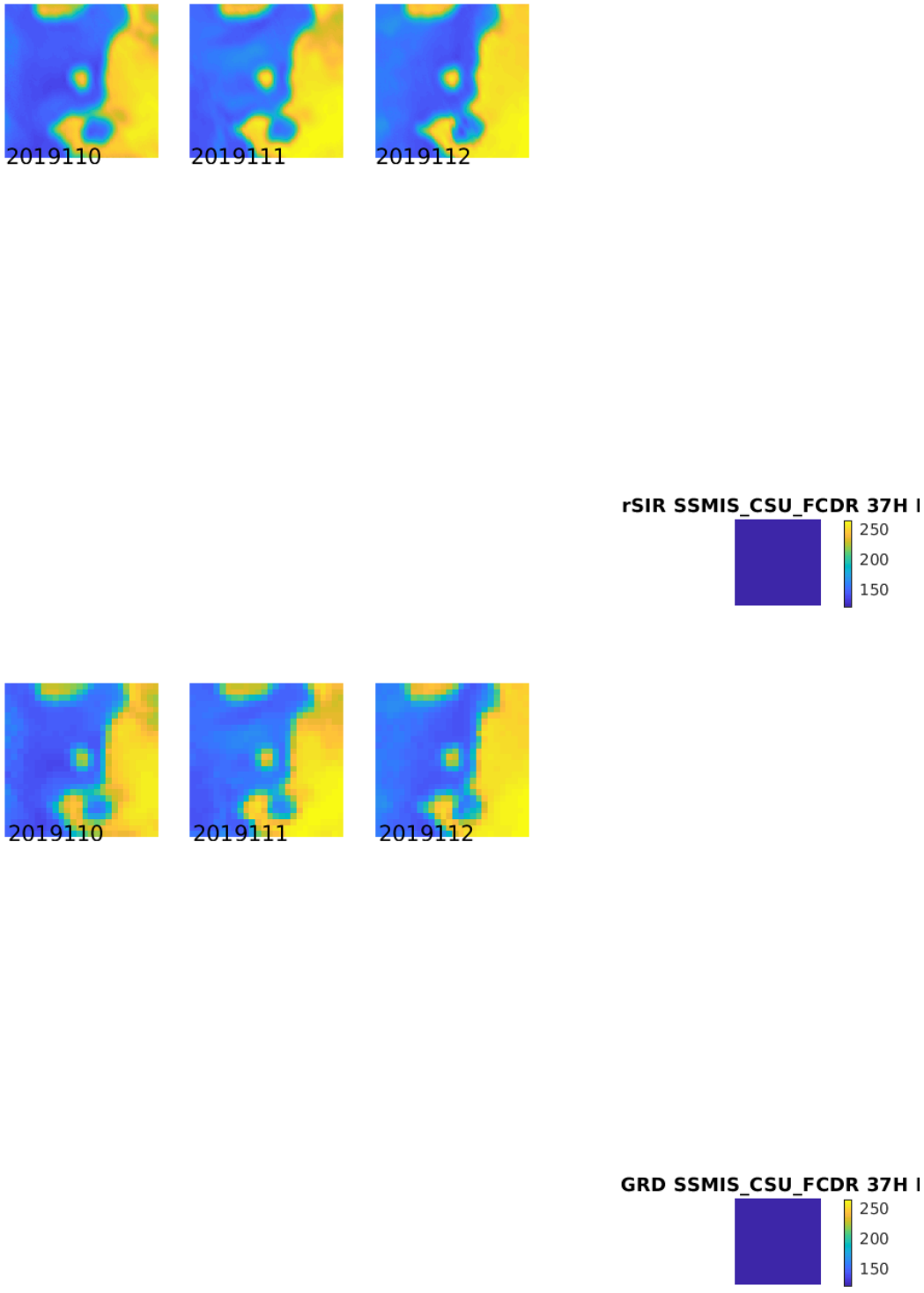

Figure 122: Time series of (top) rSIR and (bottom) GRD T_B images over the study area. Image dates are labeled on the image.

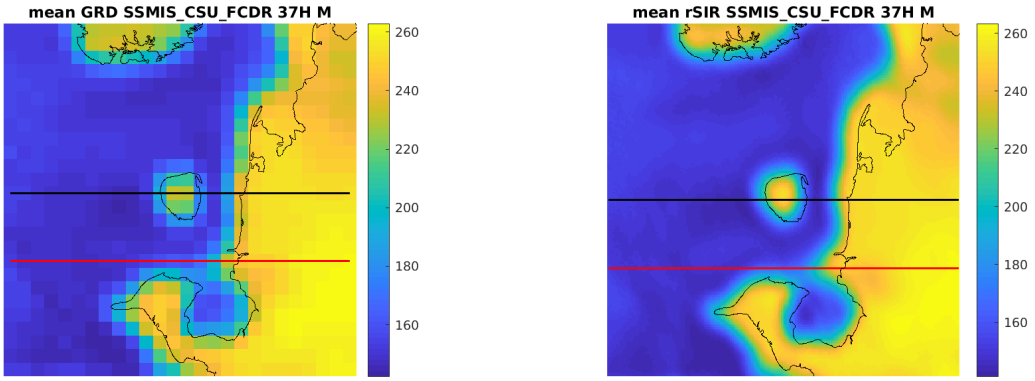

Figure 123: Average of daily T_B images over the study area. (left) 25-km GRD. (right) 3.125-km rSIR. The thick horizontal lines show the data transect locations where data is extracted from the image for analysis.

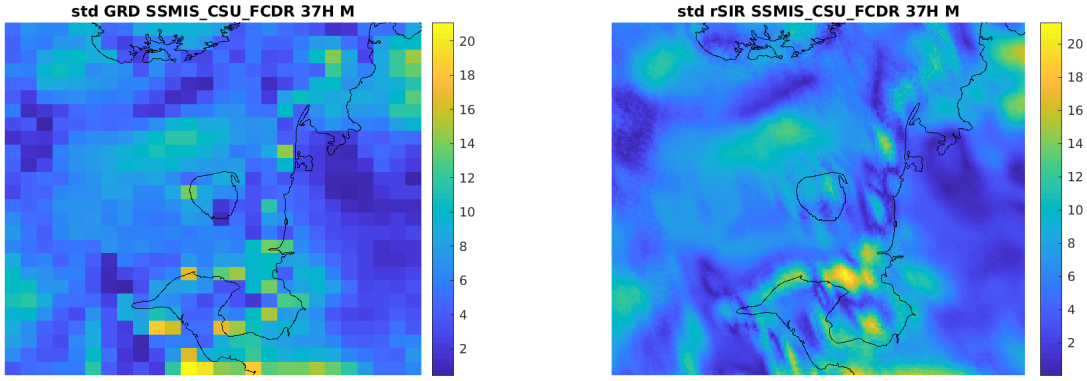

Figure 124: Standard deviation of daily T_B images over the study area. (left) 25-km GRD. (right) 3.125-km rSIR.

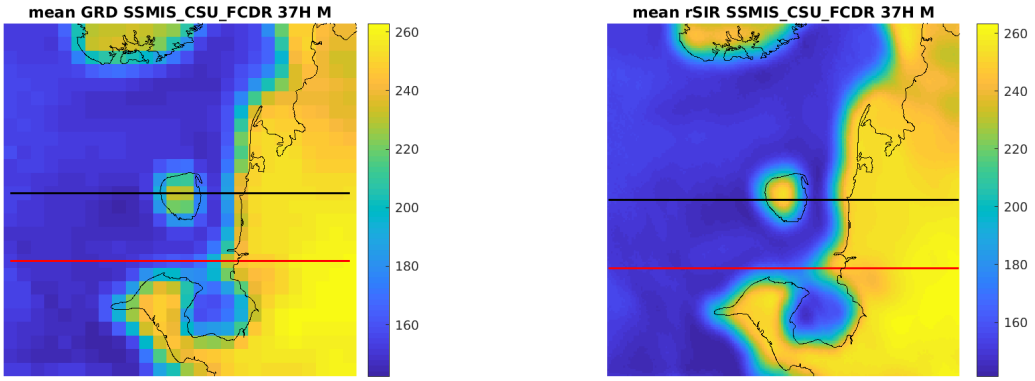

Figure 125: [Repeated] Average of daily T_B images over the study area. (left) 25-km GRD. (right) 3.125-km rSIR. The thick horizontal lines show the data transect locations where data is extracted from the image for analysis.

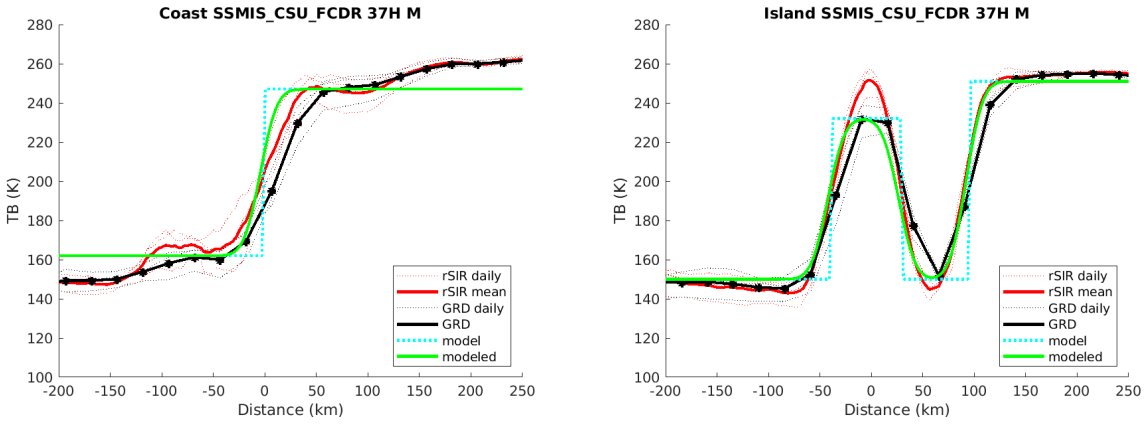

Figure 126: Plots of T_B along the two analysis case transect lines for the (left) coast-crossing and (right) island-crossing cases.

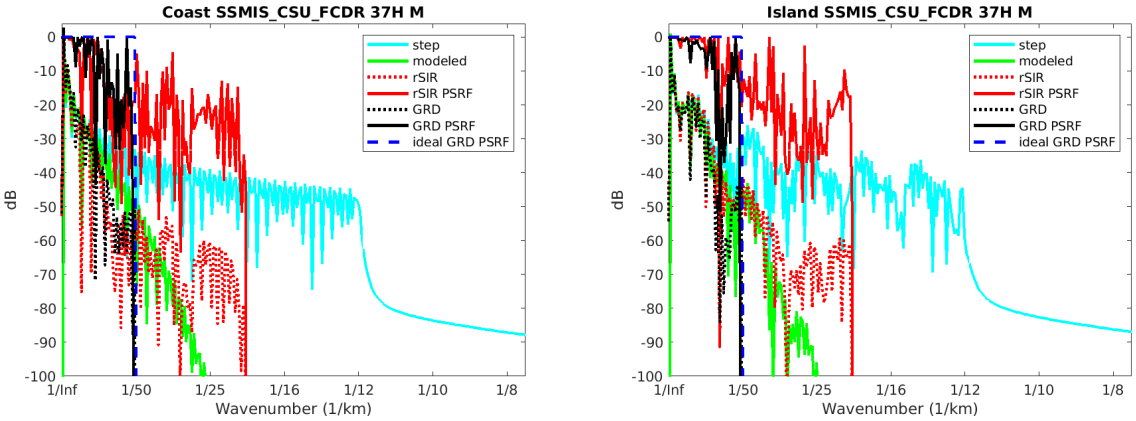

Figure 127: Wavenumber spectra of the T_B slices, the model, and the PSRF. (left) Coast-crossing case. (right) Island-crossing case.

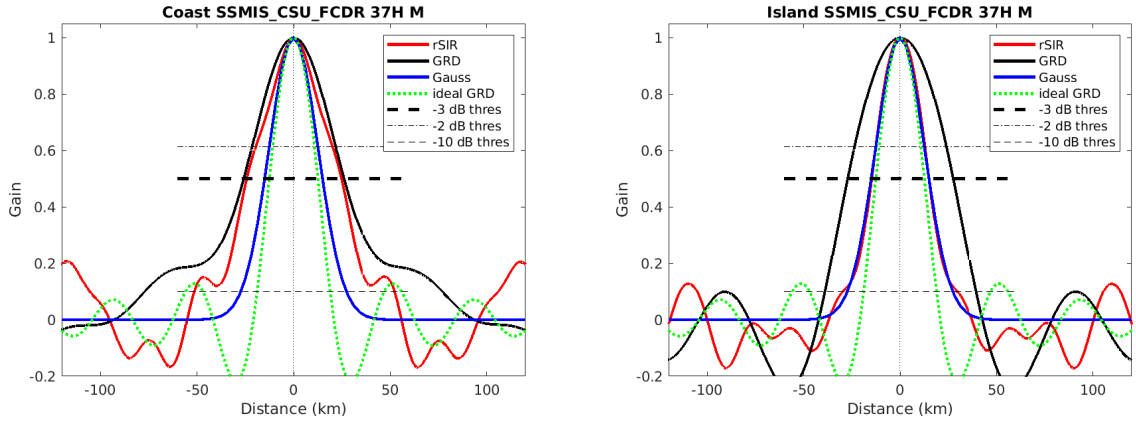

Figure 128: Derived single-pass rSIR and GRD PSRFs from the (left) coast-crossing and (right) island-crossing cases.

Table 44: Resolution estimates for SSMIS_CSU_FCDR channel 37H LTOD M

	-3 dB Thres		-2 dB Thres		-10 dB Thres	
Algorithm	Coast	Island	Coast	Island	Coast	Island
Gauss	30.0	30.0	24.4	24.4	54.8	54.8
rSIR	49.0	29.8	38.0	24.9	103.6	59.6
ideal GRD	36.2	36.2	30.3	30.3	54.5	54.5
GRD	51.9	54.7	42.0	46.5	154.0	78.2

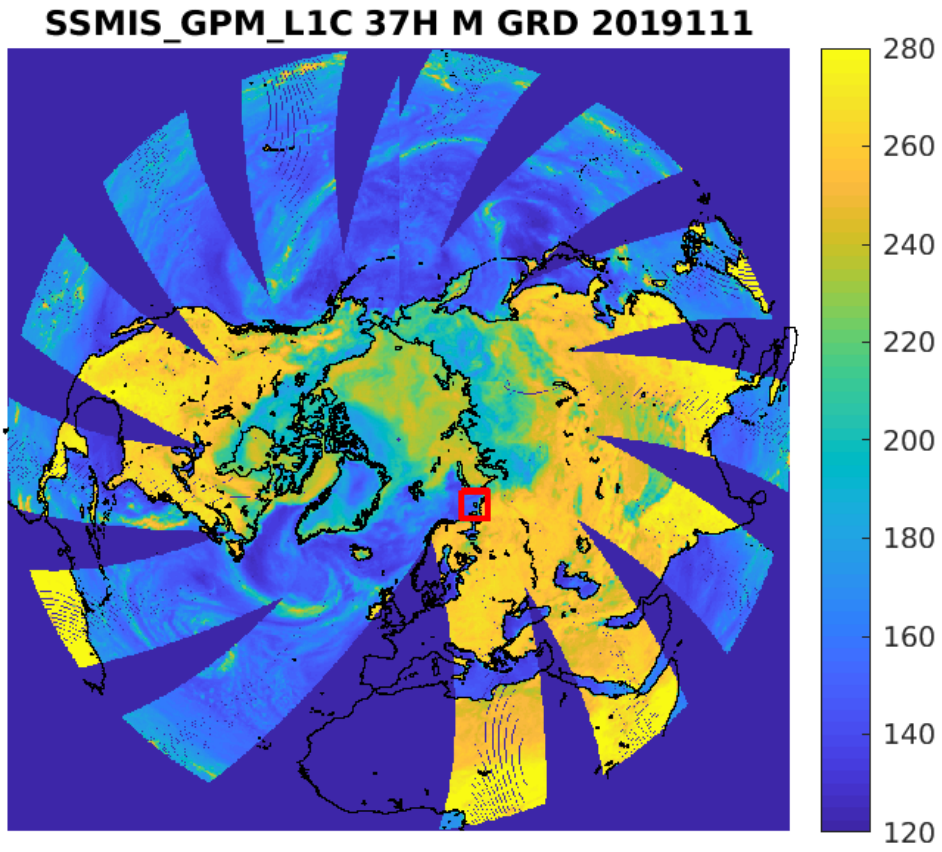

Figure 129: rSIR Northern Hemisphere view.

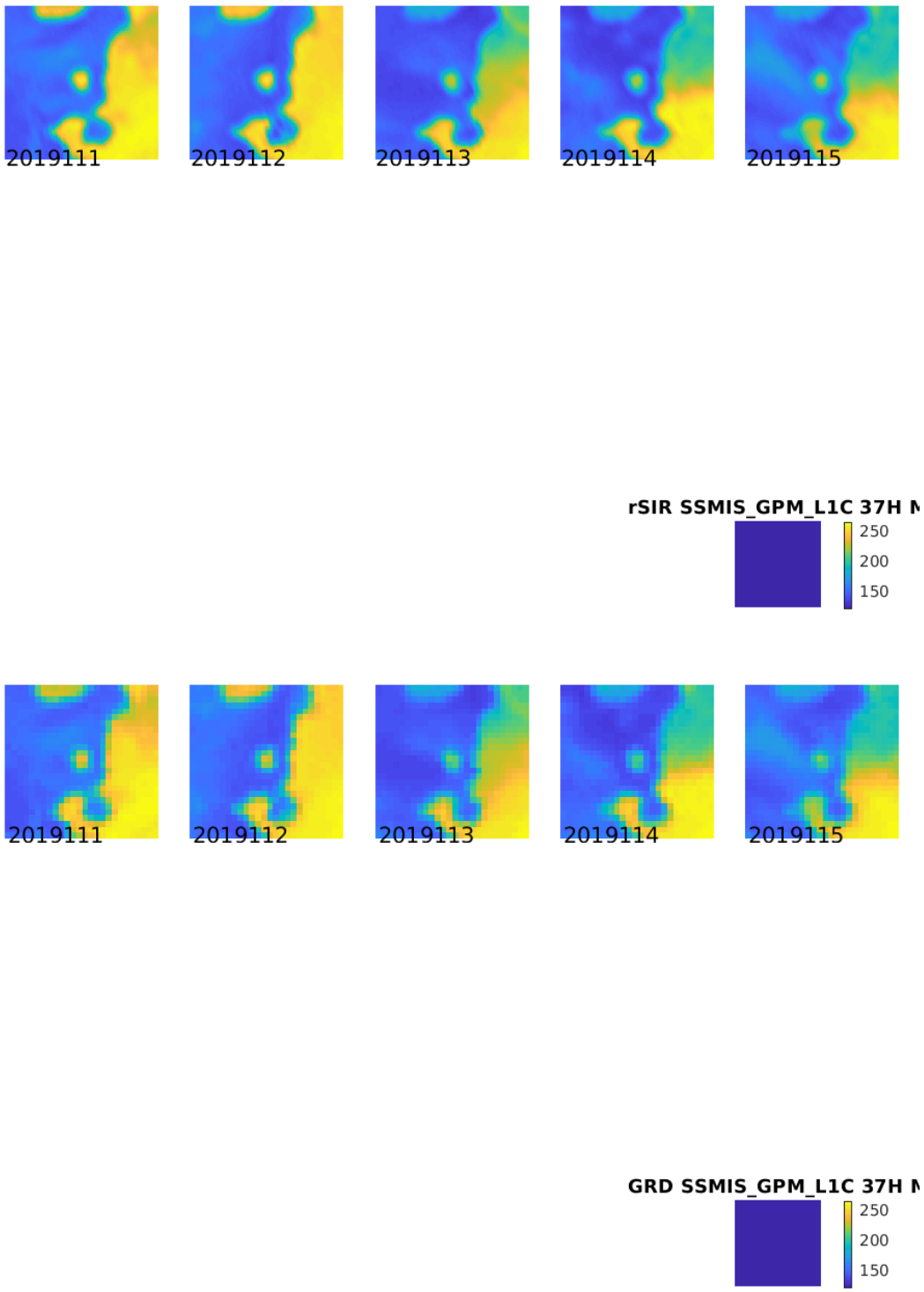

Figure 130: Time series of (top) rSIR and (bottom) GRD T_B images over the study area. Image dates are labeled on the image.

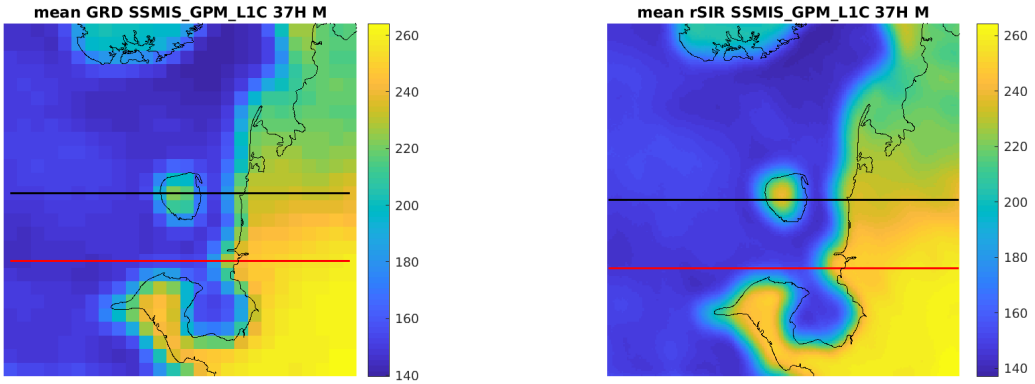

Figure 131: Average of daily T_B images over the study area. (left) 25-km GRD. (right) 3.125-km rSIR. The thick horizontal lines show the data transect locations where data is extracted from the image for analysis.

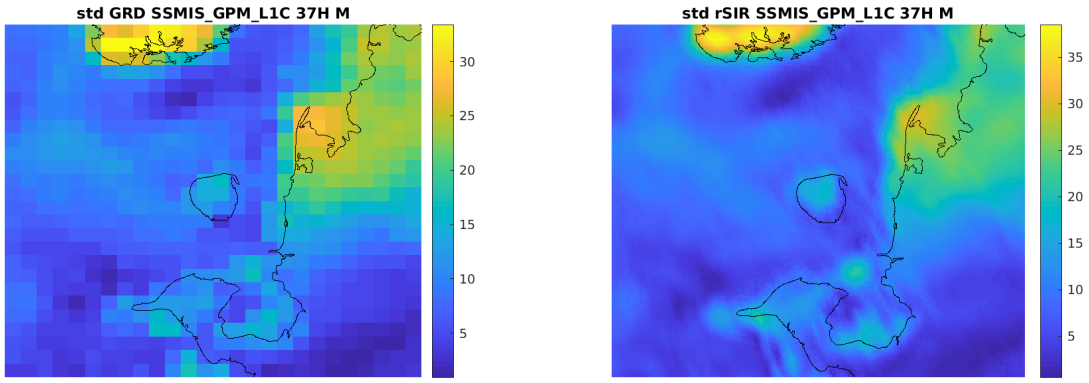

Figure 132: Standard deviation of daily T_B images over the study area. (left) 25-km GRD. (right) 3.125-km rSIR.

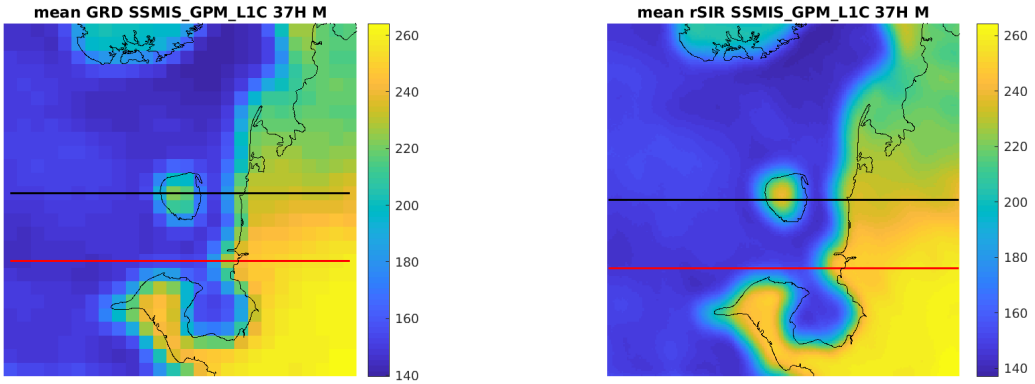

Figure 133: [Repeated] Average of daily T_B images over the study area. (left) 25-km GRD. (right) 3.125-km rSIR. The thick horizontal lines show the data transect locations where data is extracted from the image for analysis.

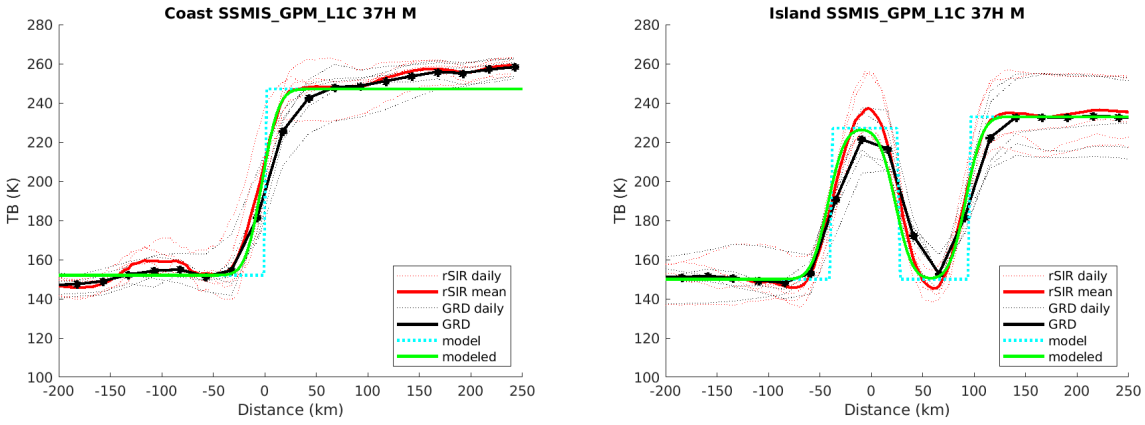

Figure 134: Plots of T_B along the two analysis case transect lines for the (left) coast-crossing and (right) island-crossing cases.

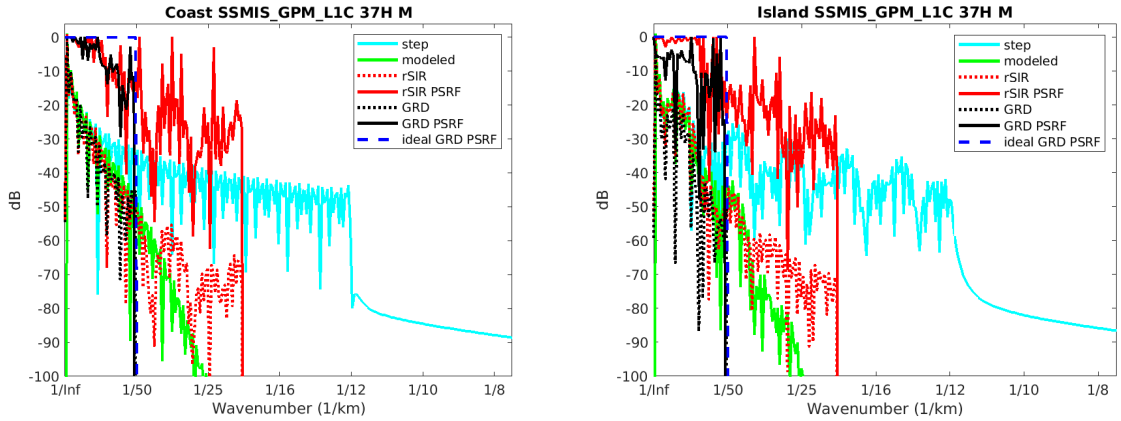

Figure 135: Wavenumber spectra of the T_B slices, the model, and the PSRF. (left) Coast-crossing case. (right) Island-crossing case.

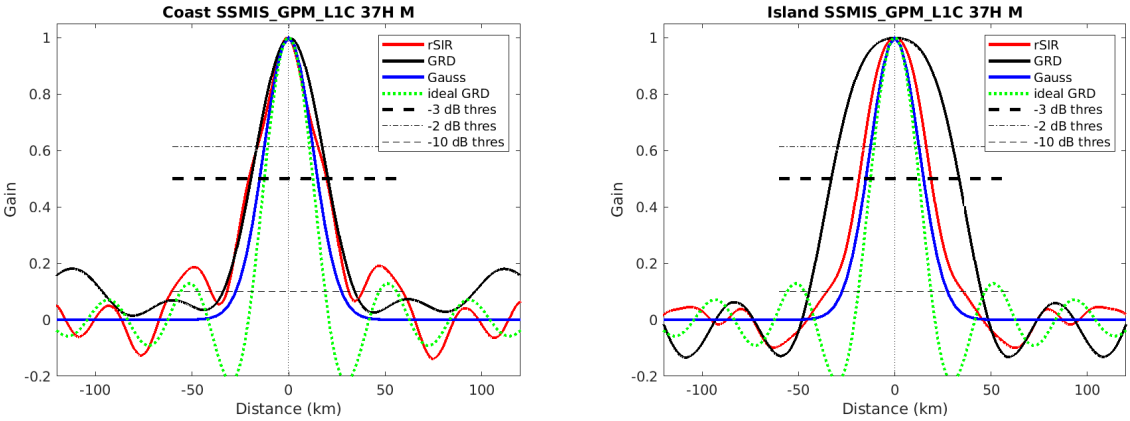

Figure 136: Derived single-pass rSIR and GRD PSRFs from the (left) coast-crossing and (right) island-crossing cases.

Table 45: Resolution estimates for SSMIS_GPM_L1C channel 37H LTOD M

	-3 dB Thres		-2 dB Thres		-10 dB Thres	
Algorithm	Coast	Island	Coast	Island	Coast	Island
Gauss	30.0	30.0	24.4	24.4	54.8	54.8
rSIR	40.3	37.6	29.8	31.8	63.0	70.9
ideal GRD	36.2	36.2	30.3	30.3	54.5	54.5
GRD	39.9	66.4	32.9	58.6	68.1	89.3

8.9 Channel 37V E Figures

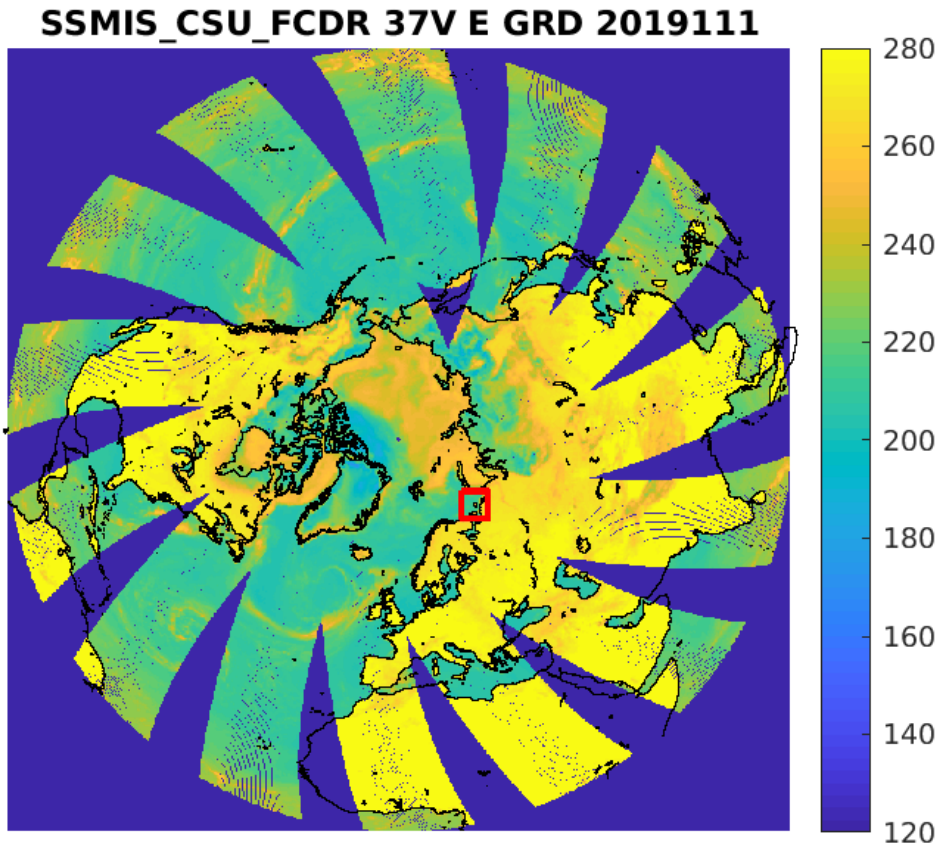

Figure 137: rSIR Northern Hemisphere view.

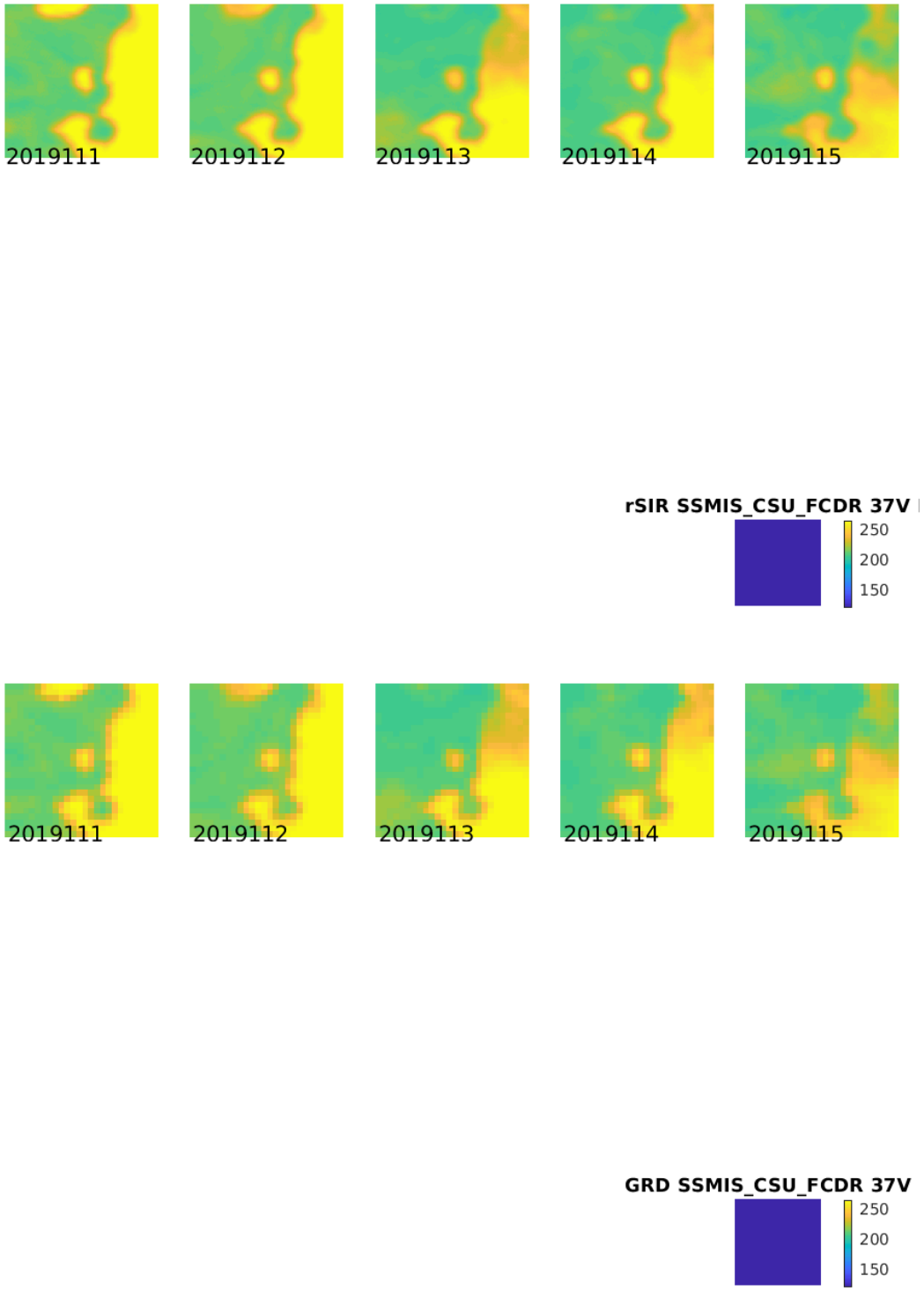

Figure 138: Time series of (top) rSIR and (bottom) GRD T_B images over the study area. Image dates are labeled on the image.

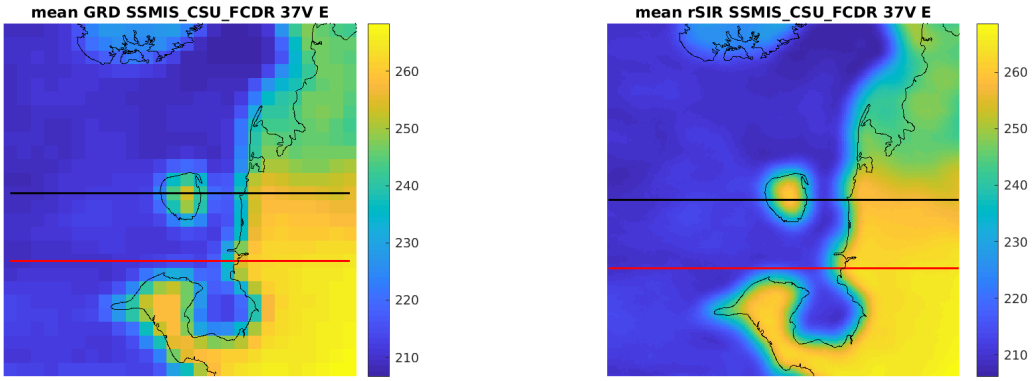

Figure 139: Average of daily T_B images over the study area. (left) 25-km GRD. (right) 3.125-km rSIR. The thick horizontal lines show the data transect locations where data is extracted from the image for analysis.

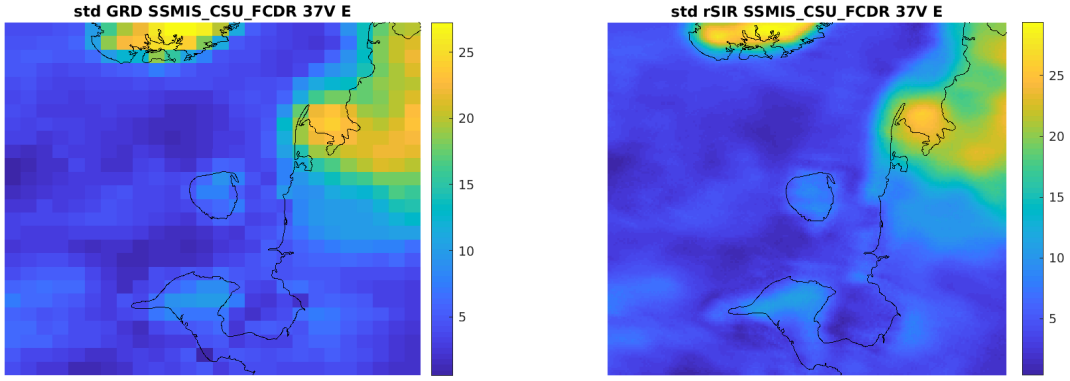

Figure 140: Standard deviation of daily T_B images over the study area. (left) 25-km GRD. (right) 3.125-km rSIR.

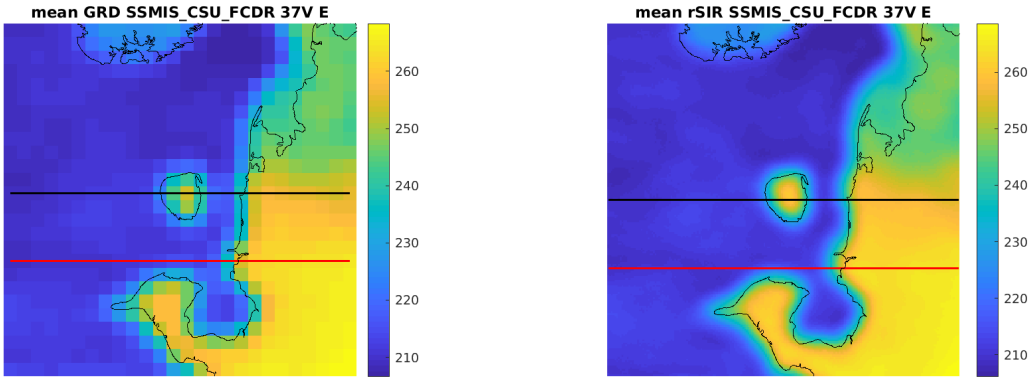

Figure 141: [Repeated] Average of daily T_B images over the study area. (left) 25-km GRD. (right) 3.125-km rSIR. The thick horizontal lines show the data transect locations where data is extracted from the image for analysis.

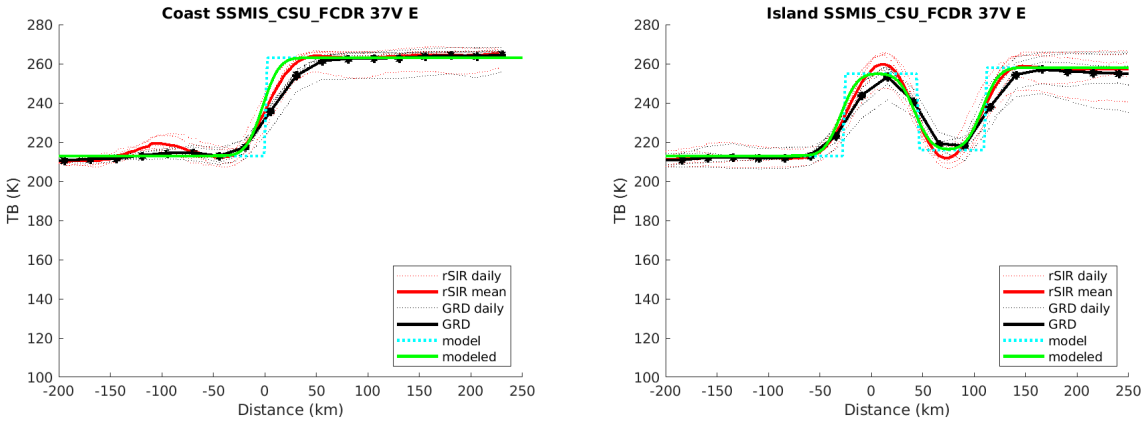

Figure 142: Plots of T_B along the two analysis case transect lines for the (left) coast-crossing and (right) island-crossing cases.

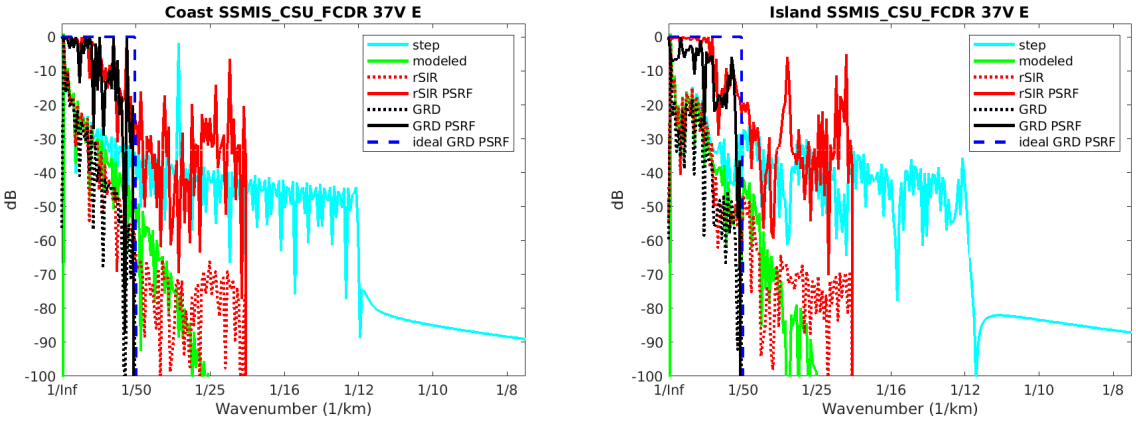

Figure 143: Wavenumber spectra of the T_B slices, the model, and the PSRF. (left) Coast-crossing case. (right) Island-crossing case.

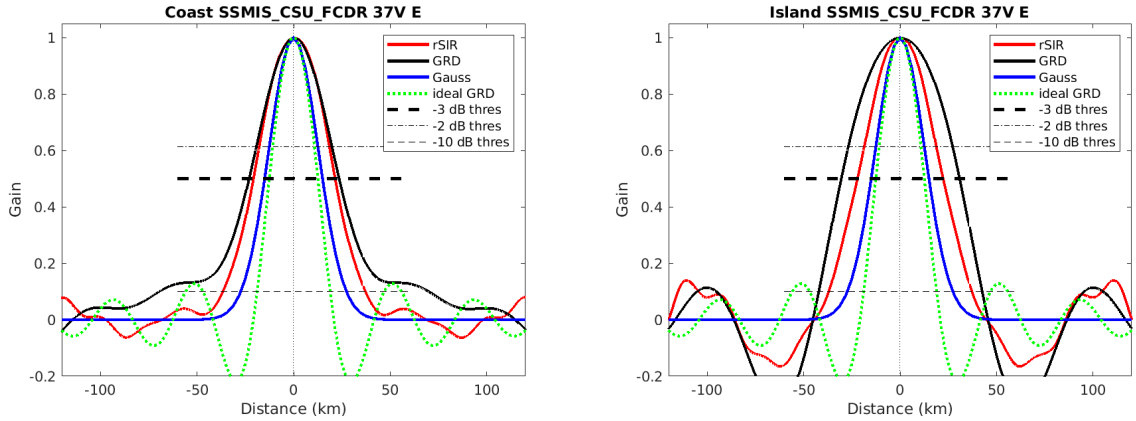

Figure 144: Derived single-pass rSIR and GRD PSRFs from the (left) coast-crossing and (right) island-crossing cases.

Table 46: Resolution estimates for SSMIS_CSU_FCDR channel 37V LTOD E

	-3 dB Thres		-2 dB Thres		-10 dB Thres	
Algorithm	Coast	Island	Coast	Island	Coast	Island
Gauss	30.0	30.0	24.4	24.4	54.8	54.8
rSIR	42.3	44.3	35.4	36.2	73.8	74.1
ideal GRD	36.2	36.2	30.3	30.3	54.5	54.5
GRD	46.7	61.4	38.0	52.9	139.7	84.7

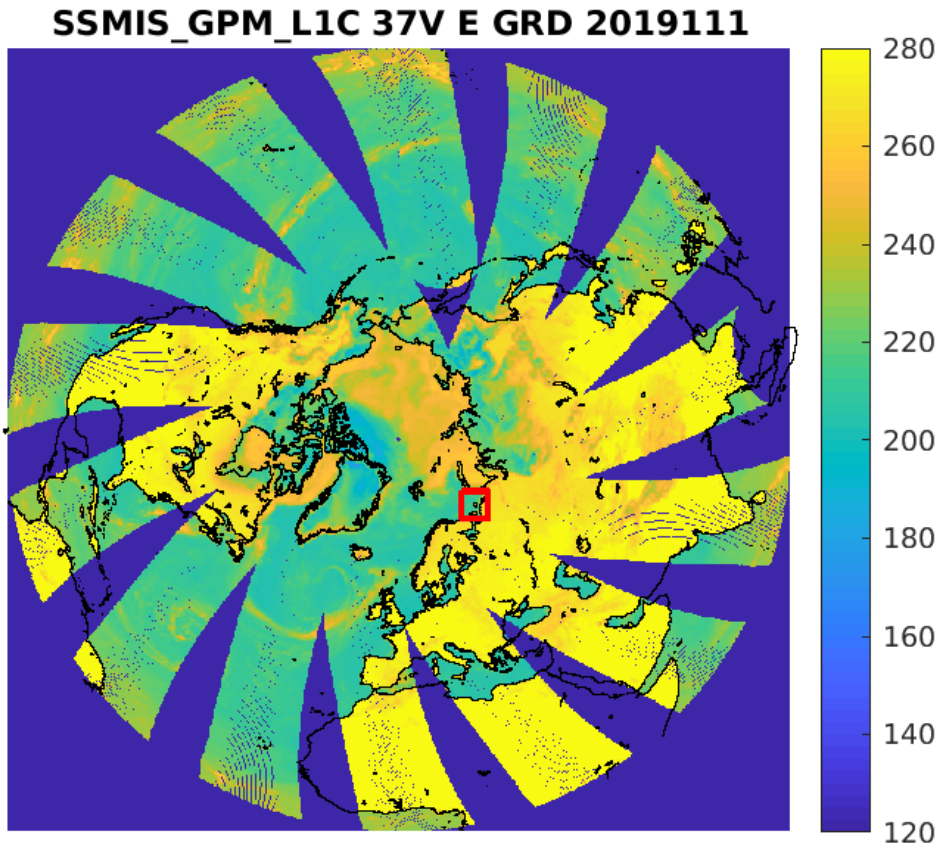

Figure 145: rSIR Northern Hemisphere view.

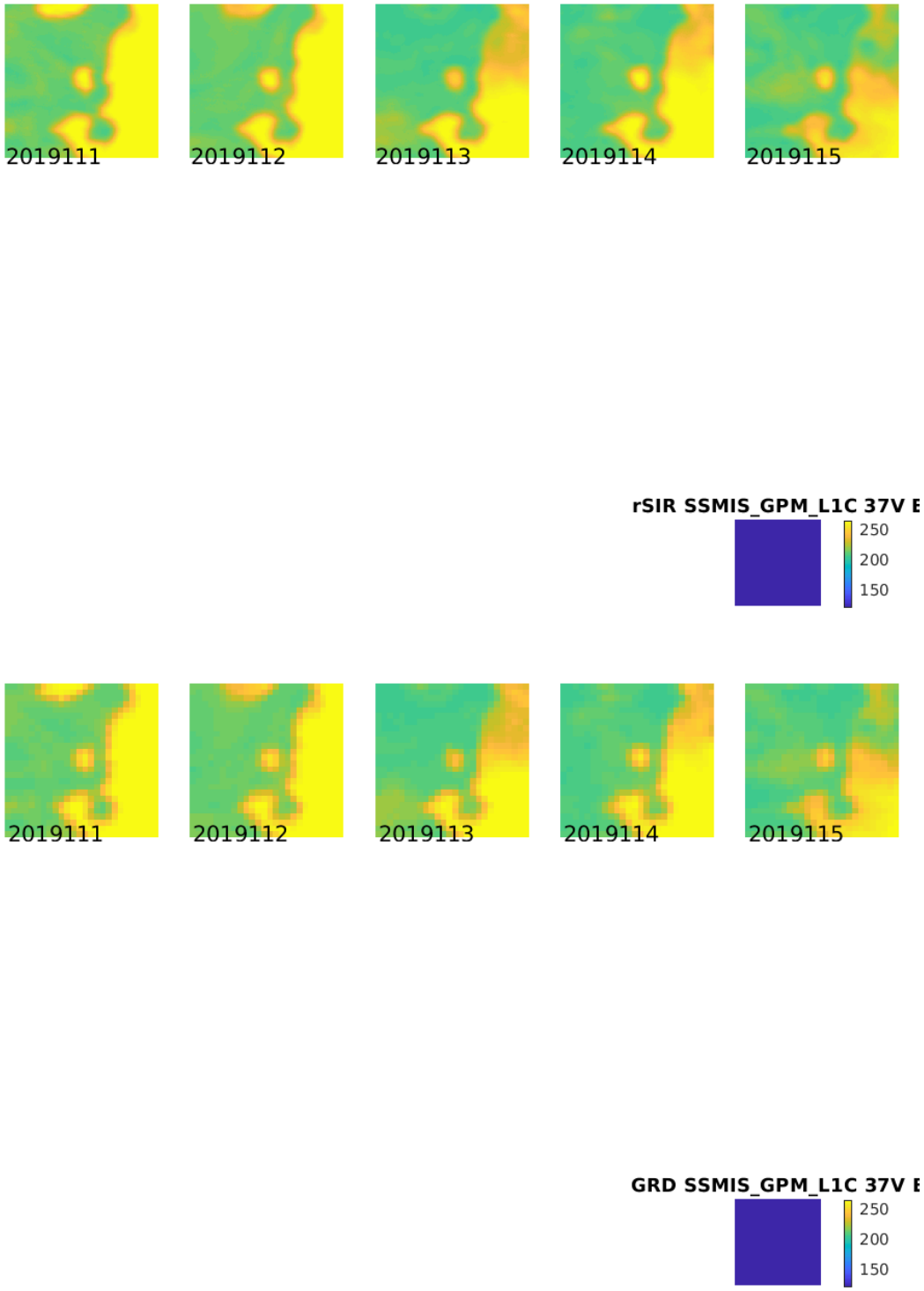

Figure 146: Time series of (top) rSIR and (bottom) GRD T_B images over the study area. Image dates are labeled on the image.

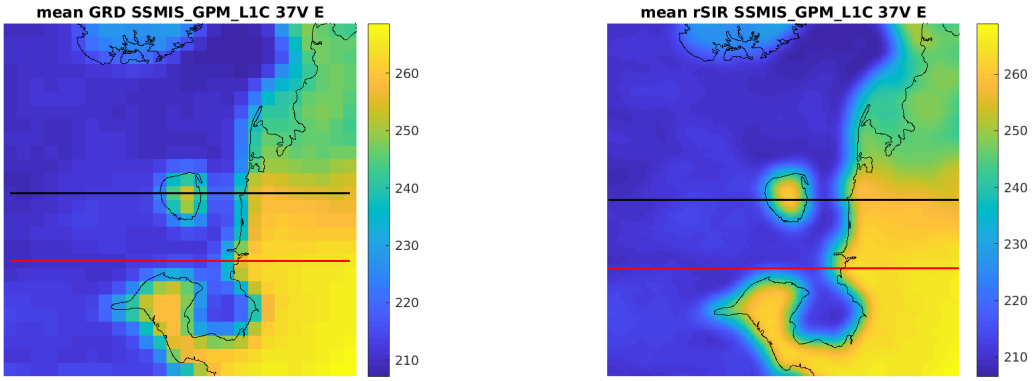

Figure 147: Average of daily T_B images over the study area. (left) 25-km GRD. (right) 3.125-km rSIR. The thick horizontal lines show the data transect locations where data is extracted from the image for analysis.

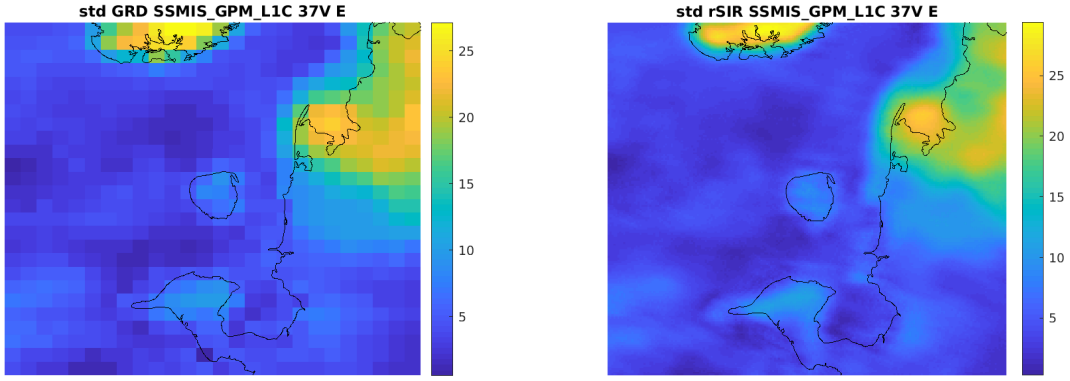

Figure 148: Standard deviation of daily T_B images over the study area. (left) 25-km GRD. (right) 3.125-km rSIR.

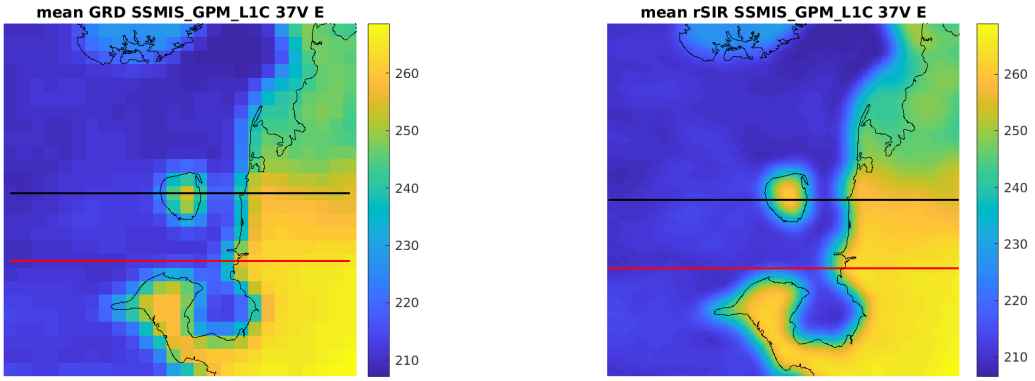

Figure 149: [Repeated] Average of daily T_B images over the study area. (left) 25-km GRD. (right) 3.125-km rSIR. The thick horizontal lines show the data transect locations where data is extracted from the image for analysis.

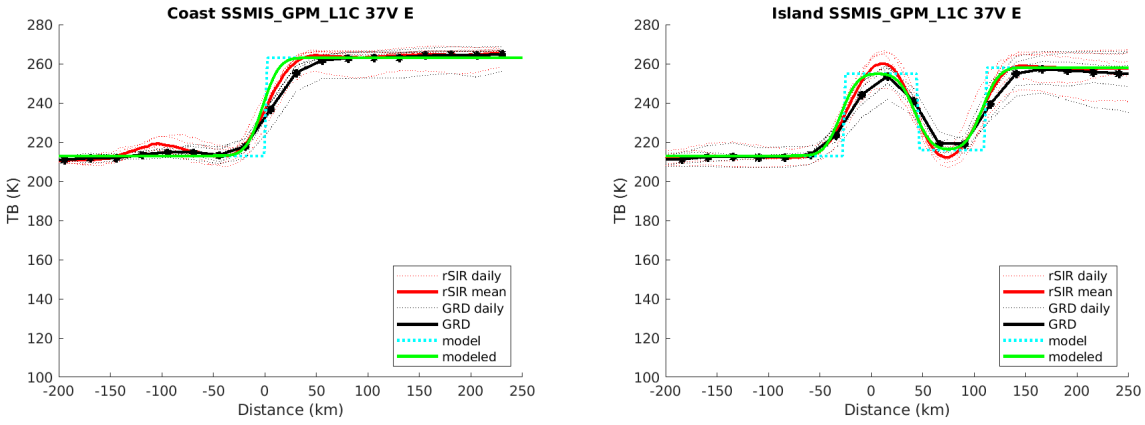

Figure 150: Plots of T_B along the two analysis case transect lines for the (left) coast-crossing and (right) island-crossing cases.

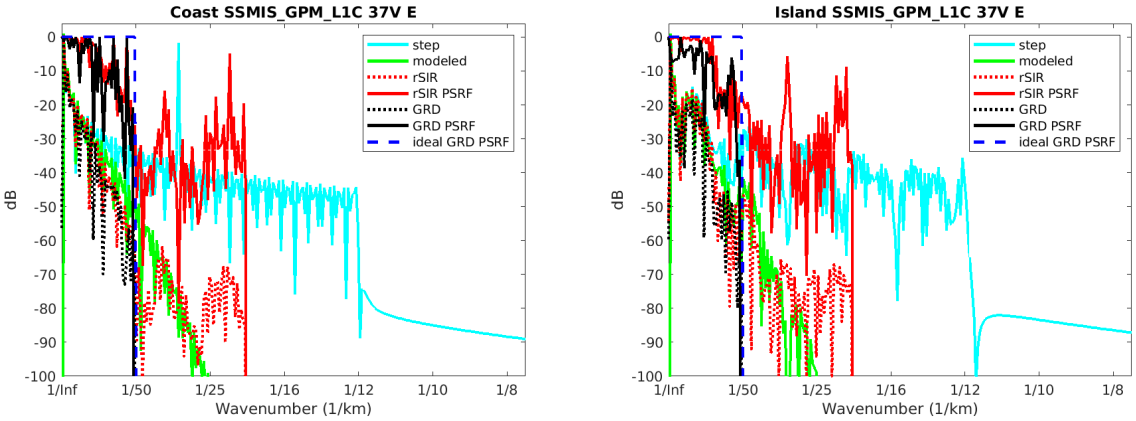

Figure 151: Wavenumber spectra of the T_B slices, the model, and the PSRF. (left) Coast-crossing case. (right) Island-crossing case.

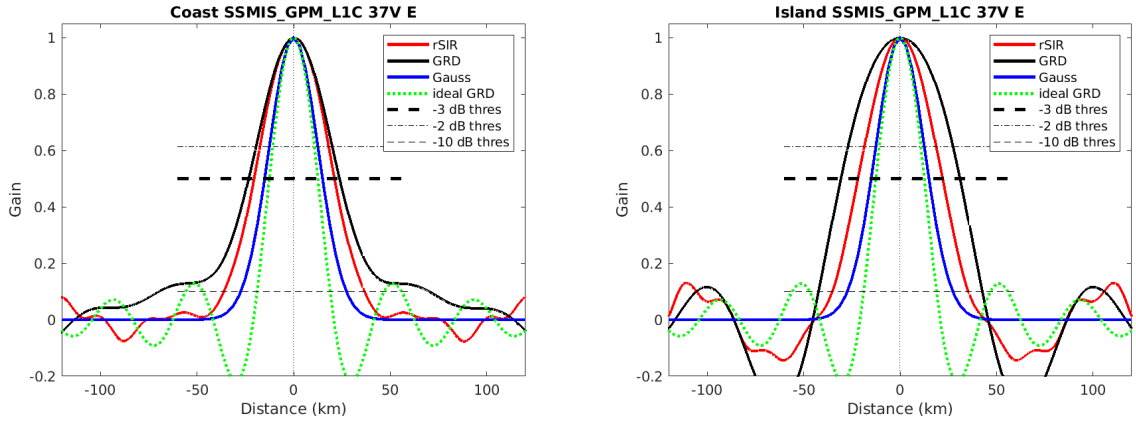

Figure 152: Derived single-pass rSIR and GRD PSRFs from the (left) coast-crossing and (right) island-crossing cases.

Table 47: Resolution estimates for SSMIS_GPM_L1C channel 37V LTOD E

	-3 dB Thres		-2 dB Thres		-10 dB Thres	
Algorithm	Coast	Island	Coast	Island	Coast	Island
Gauss	30.0	30.0	24.4	24.4	54.8	54.8
rSIR	41.7	43.8	34.7	36.1	72.9	70.5
ideal GRD	36.2	36.2	30.3	30.3	54.5	54.5
GRD	47.1	61.8	38.3	53.3	140.2	84.9

8.10 Channel 37V M Figures

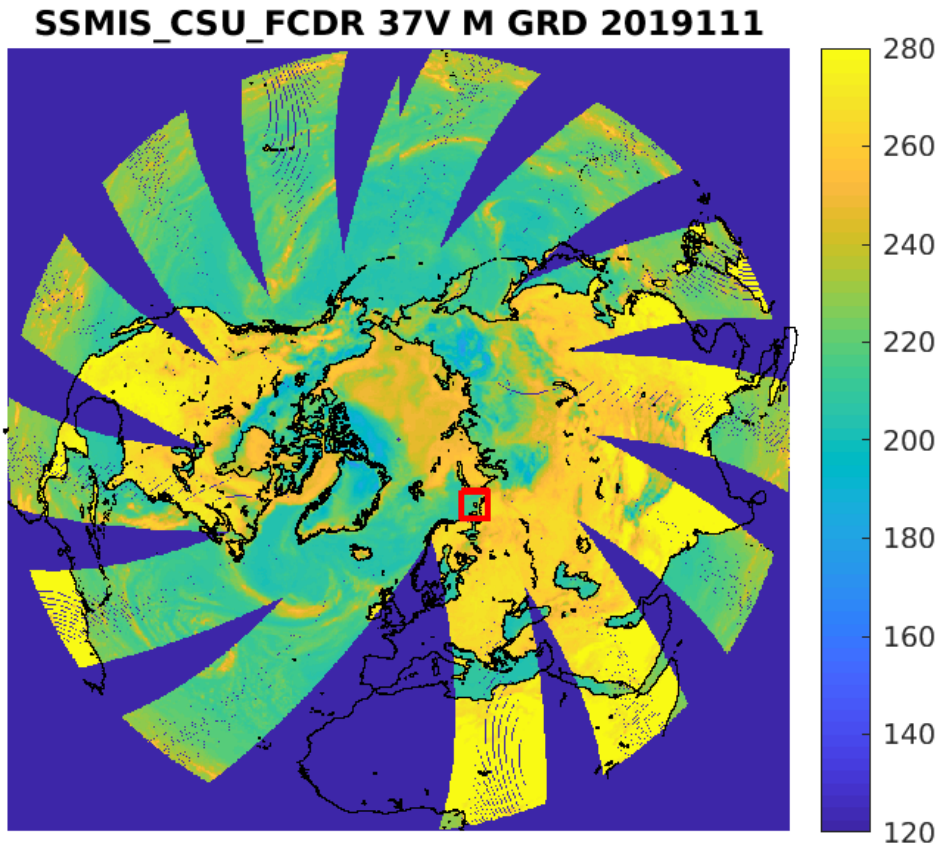

Figure 153: rSIR Northern Hemisphere view.

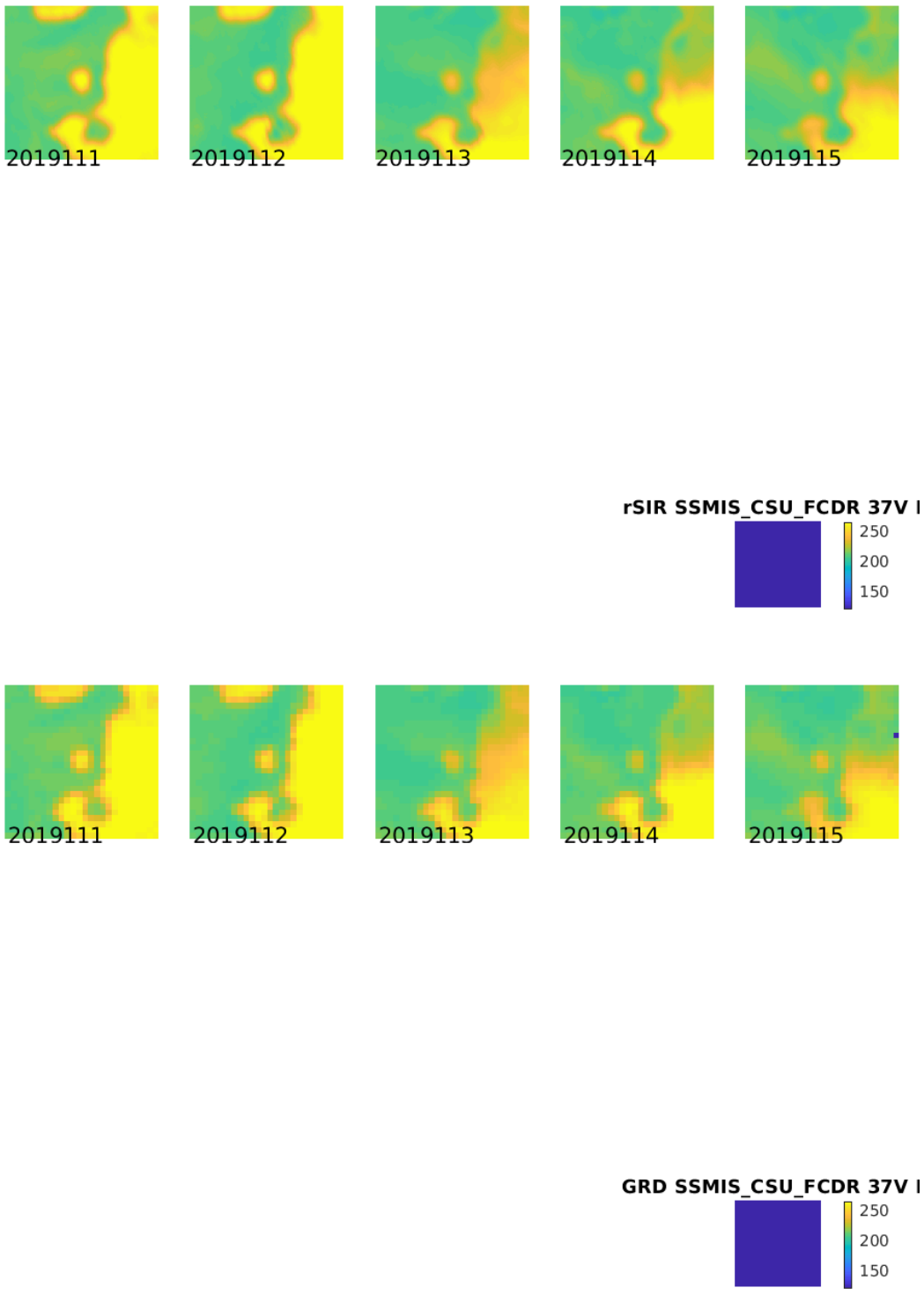

Figure 154: Time series of (top) rSIR and (bottom) GRD T_B images over the study area. Image dates are labeled on the image.

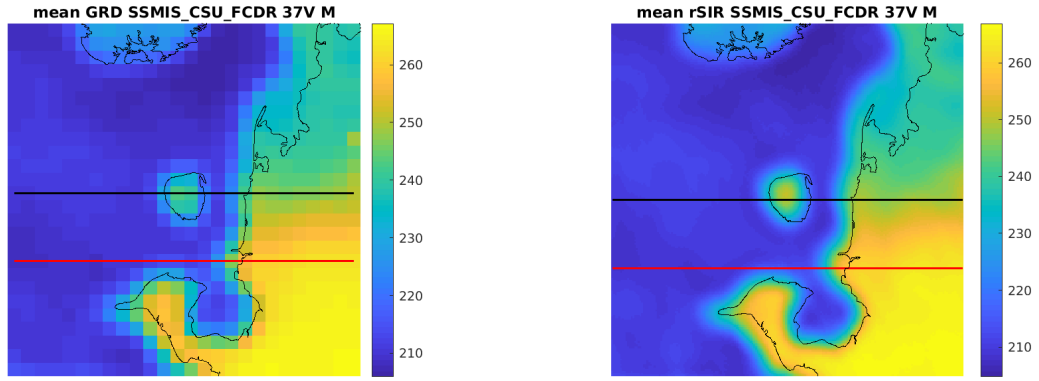

Figure 155: Average of daily T_B images over the study area. (left) 25-km GRD. (right) 3.125-km rSIR. The thick horizontal lines show the data transect locations where data is extracted from the image for analysis.

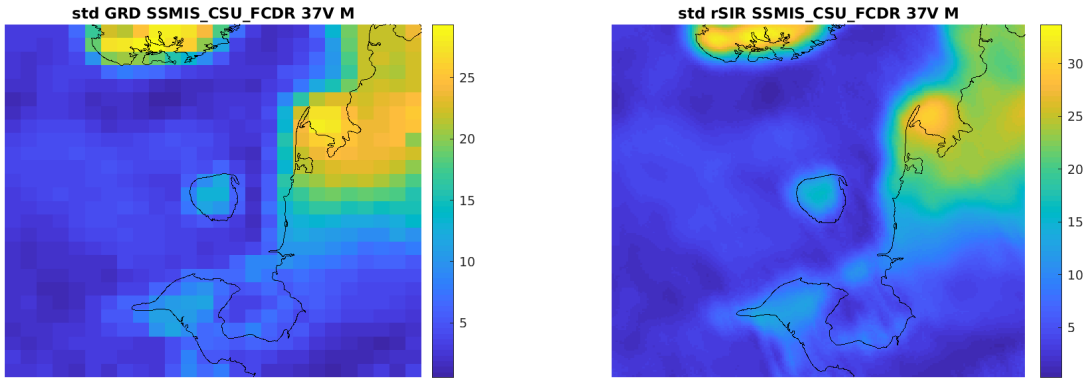

Figure 156: Standard deviation of daily T_B images over the study area. (left) 25-km GRD. (right) 3.125-km rSIR.

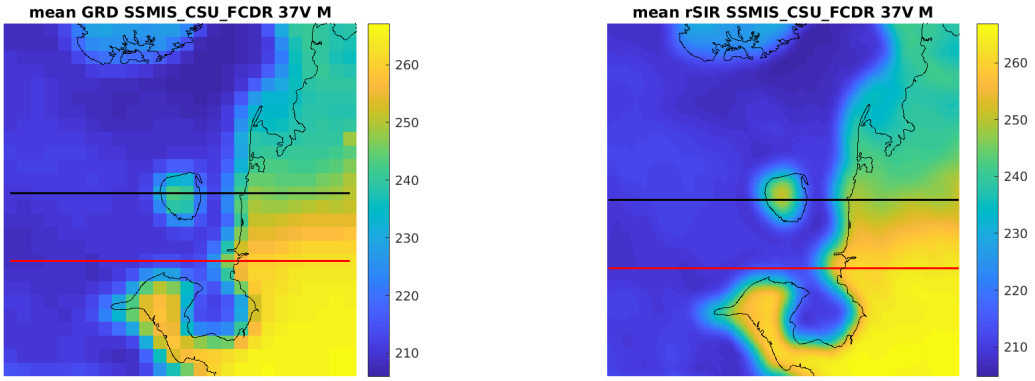

Figure 157: [Repeated] Average of daily T_B images over the study area. (left) 25-km GRD. (right) 3.125-km rSIR. The thick horizontal lines show the data transect locations where data is extracted from the image for analysis.

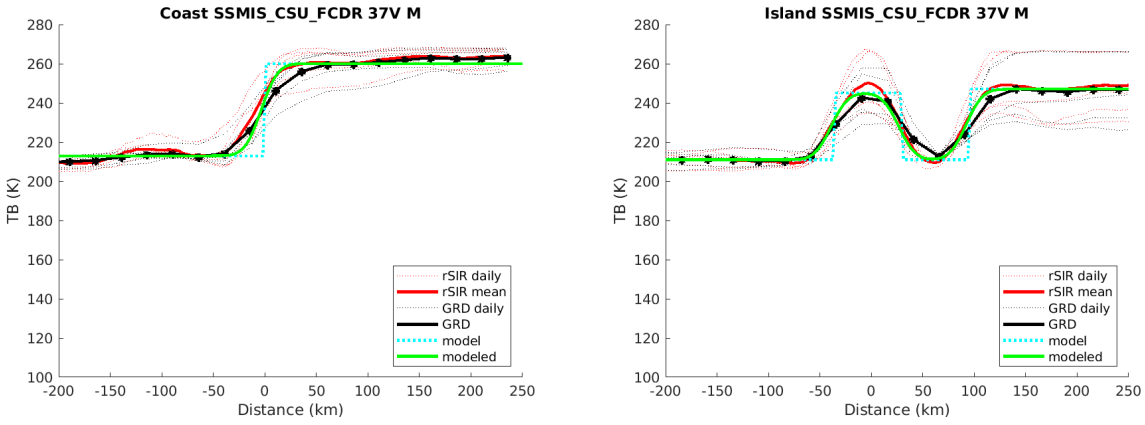

Figure 158: Plots of T_B along the two analysis case transect lines for the (left) coast-crossing and (right) island-crossing cases.

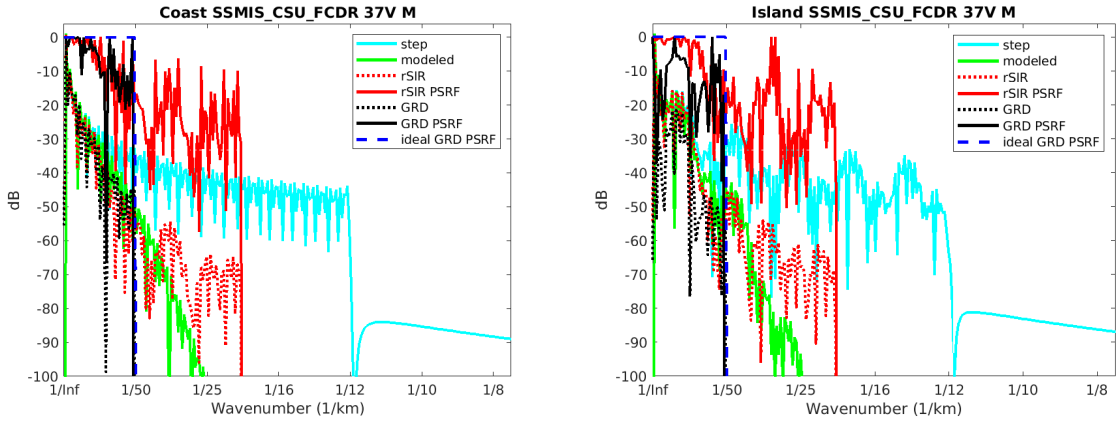

Figure 159: Wavenumber spectra of the T_B slices, the model, and the PSRF. (left) Coast-crossing case. (right) Island-crossing case.

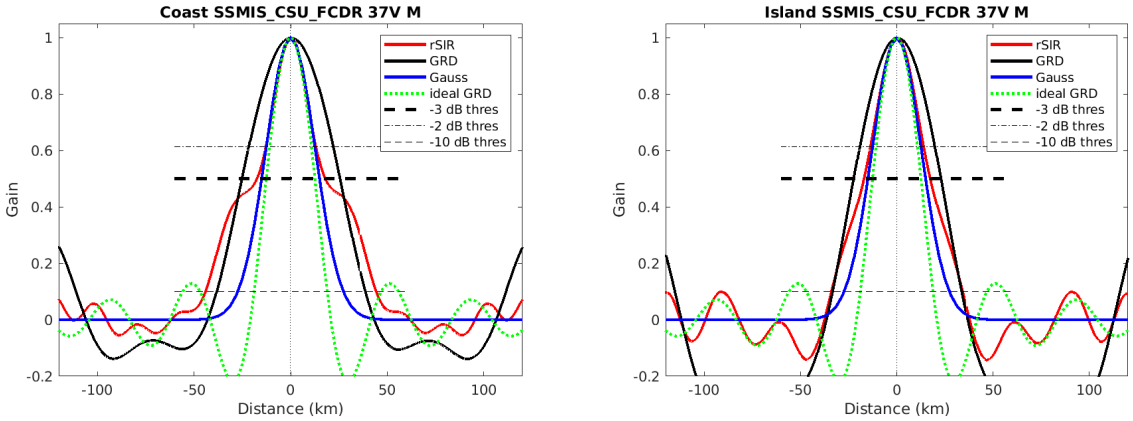

Figure 160: Derived single-pass rSIR and GRD PSRFs from the (left) coast-crossing and (right) island-crossing cases.

Table 48: Resolution estimates for SSMIS_CSU_FCDR channel 37V LTOD M

	-3 dB Thres		-2 dB Thres		-10 dB Thres	
Algorithm	Coast	Island	Coast	Island	Coast	Island
Gauss	30.0	30.0	24.4	24.4	54.8	54.8
rSIR	35.3	34.5	24.8	26.7	88.3	68.2
ideal GRD	36.2	36.2	30.3	30.3	54.5	54.5
GRD	50.7	45.3	42.6	38.0	76.9	67.1

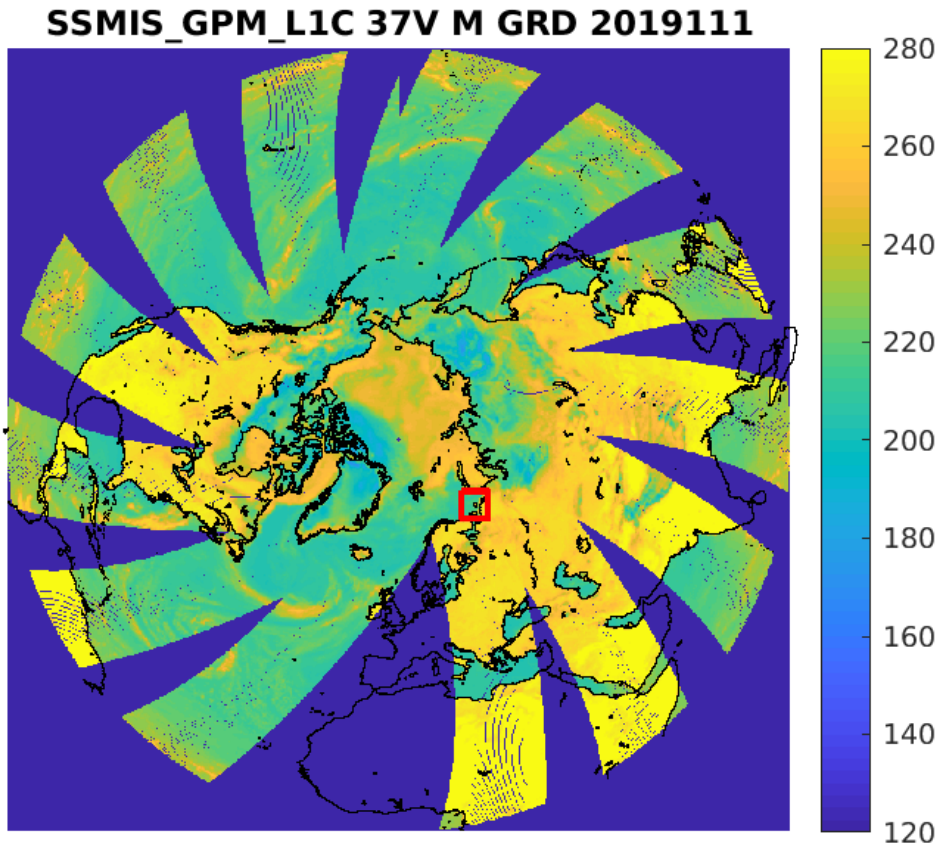

Figure 161: rSIR Northern Hemisphere view.

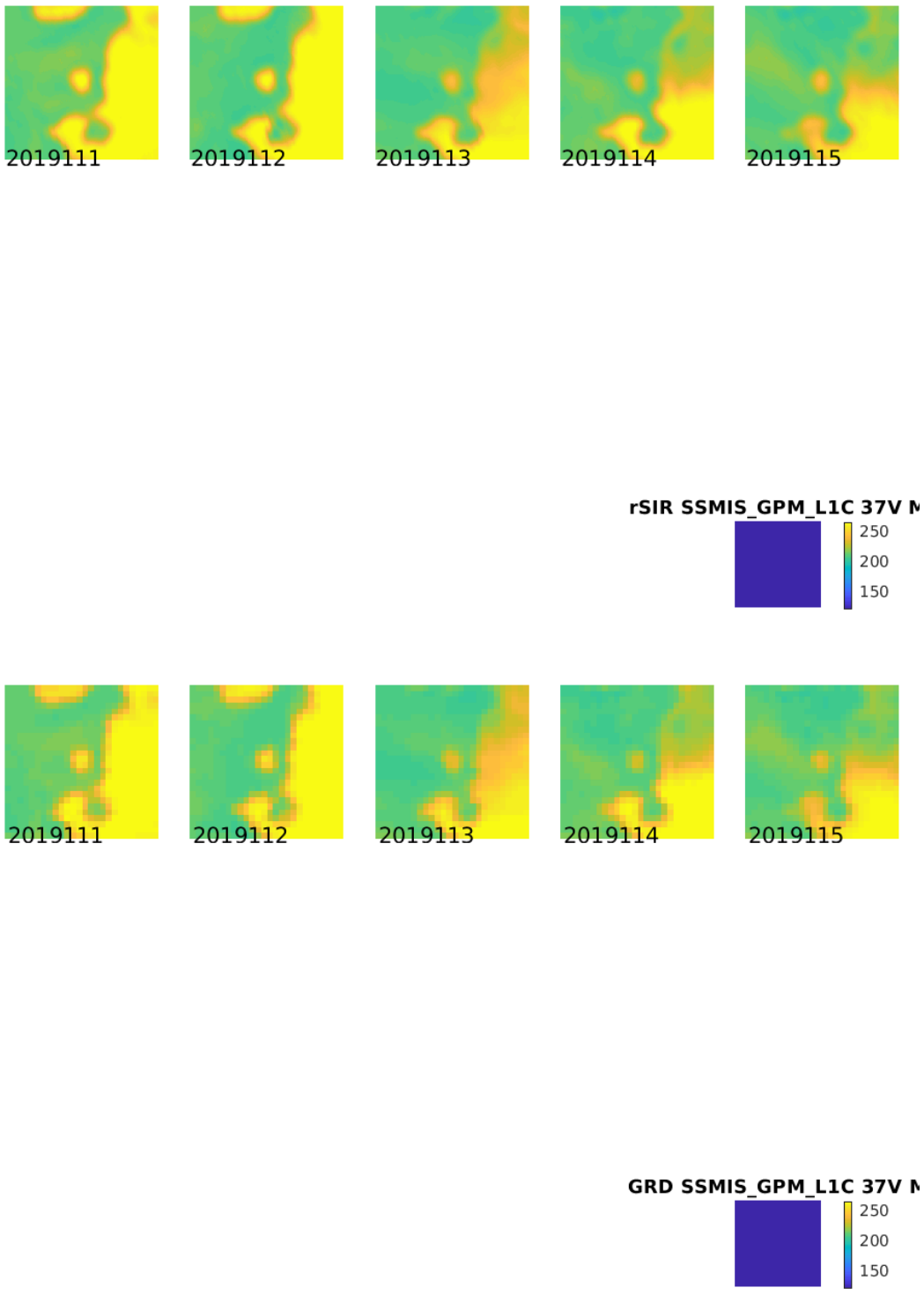

Figure 162: Time series of (top) rSIR and (bottom) GRD T_B images over the study area. Image dates are labeled on the image.

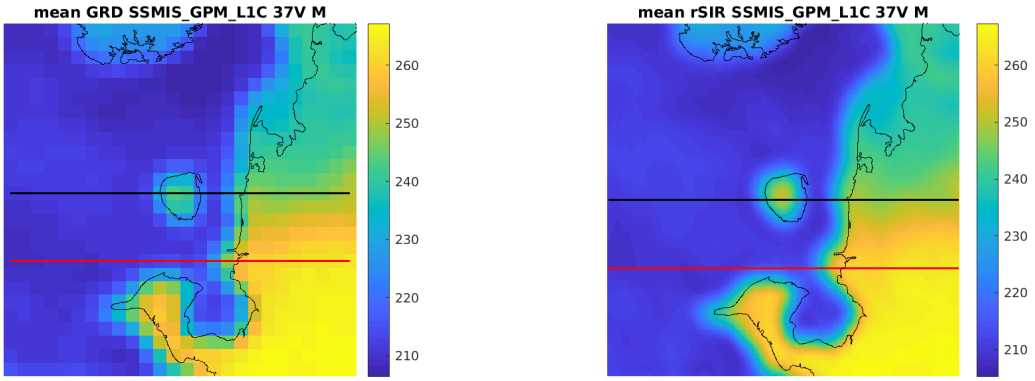

Figure 163: Average of daily T_B images over the study area. (left) 25-km GRD. (right) 3.125-km rSIR. The thick horizontal lines show the data transect locations where data is extracted from the image for analysis.

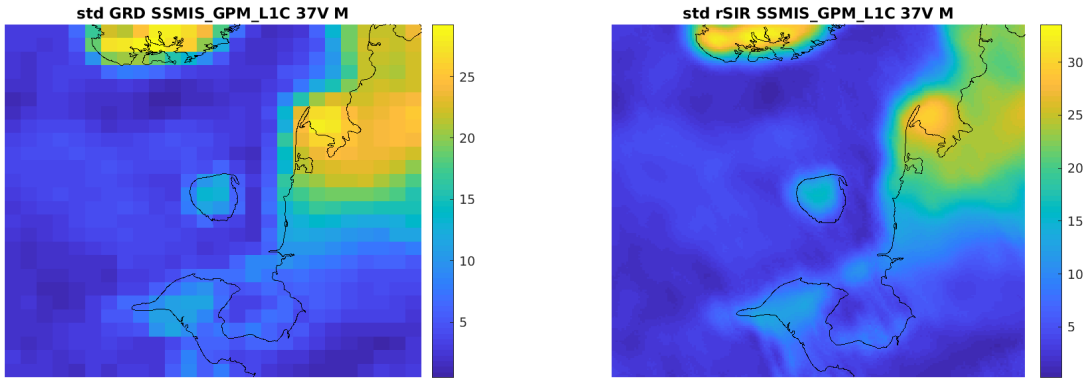

Figure 164: Standard deviation of daily T_B images over the study area. (left) 25-km GRD. (right) 3.125-km rSIR.

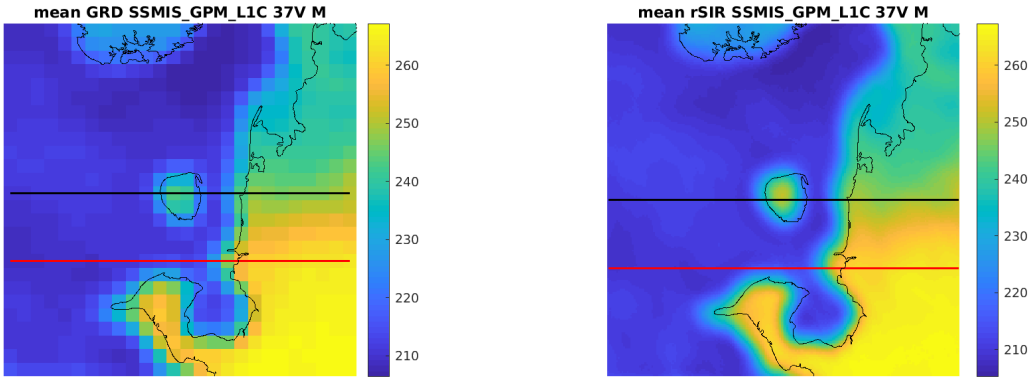

Figure 165: [Repeated] Average of daily T_B images over the study area. (left) 25-km GRD. (right) 3.125-km rSIR. The thick horizontal lines show the data transect locations where data is extracted from the image for analysis.

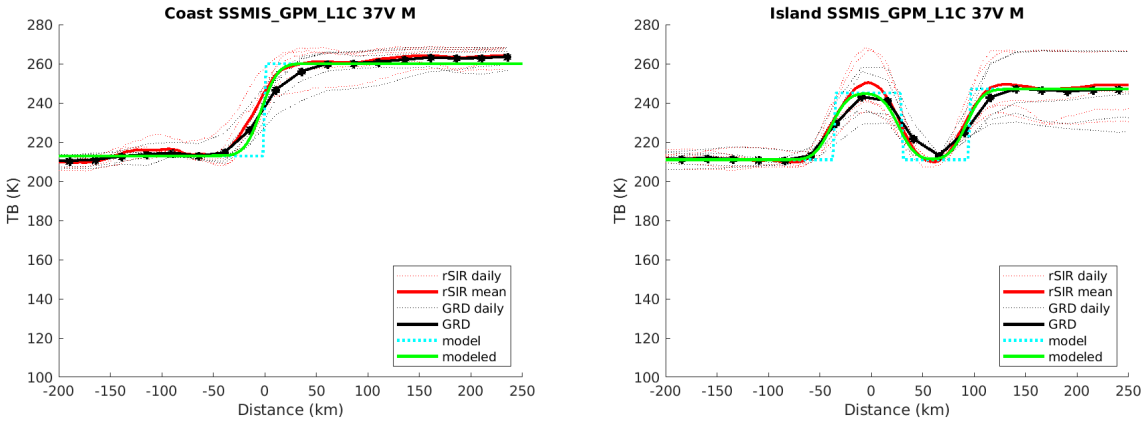

Figure 166: Plots of T_B along the two analysis case transect lines for the (left) coast-crossing and (right) island-crossing cases.

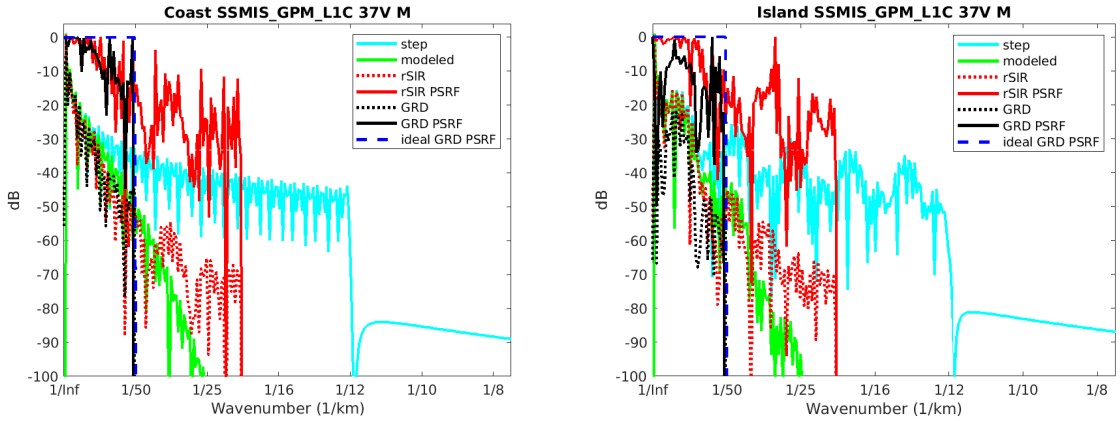

Figure 167: Wavenumber spectra of the T_B slices, the model, and the PSRF. (left) Coast-crossing case. (right) Island-crossing case.

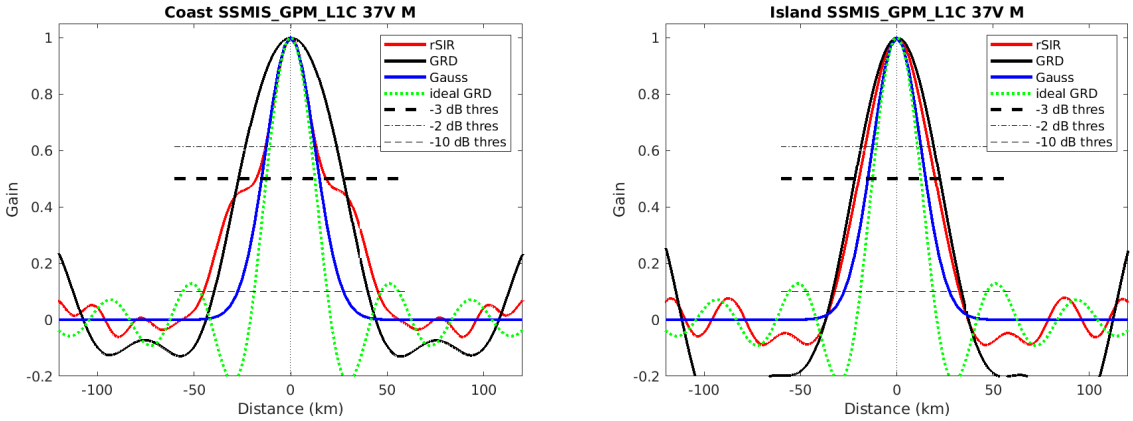

Figure 168: Derived single-pass rSIR and GRD PSRFs from the (left) coast-crossing and (right) island-crossing cases.

Table 49: Resolution estimates for SSMIS_GPM_L1C channel 37V LTOD M

	-3 dB Thres		-2 dB Thres		-10 dB Thres	
Algorithm	Coast	Island	Coast	Island	Coast	Island
Gauss	30.0	30.0	24.4	24.4	54.8	54.8
rSIR	36.1	39.7	25.2	32.2	90.1	64.9
ideal GRD	36.2	36.2	30.3	30.3	54.5	54.5
GRD	54.3	44.1	46.1	36.8	79.5	67.0

8.11 Channel 91H E Figures

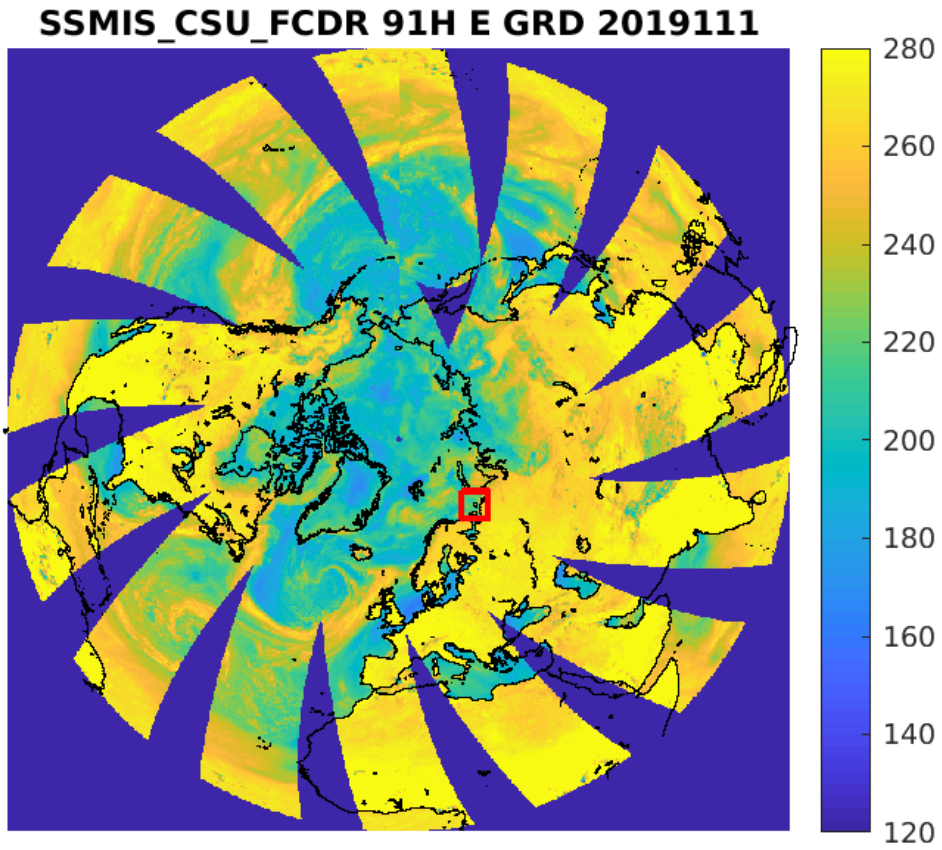

Figure 169: rSIR Northern Hemisphere view.

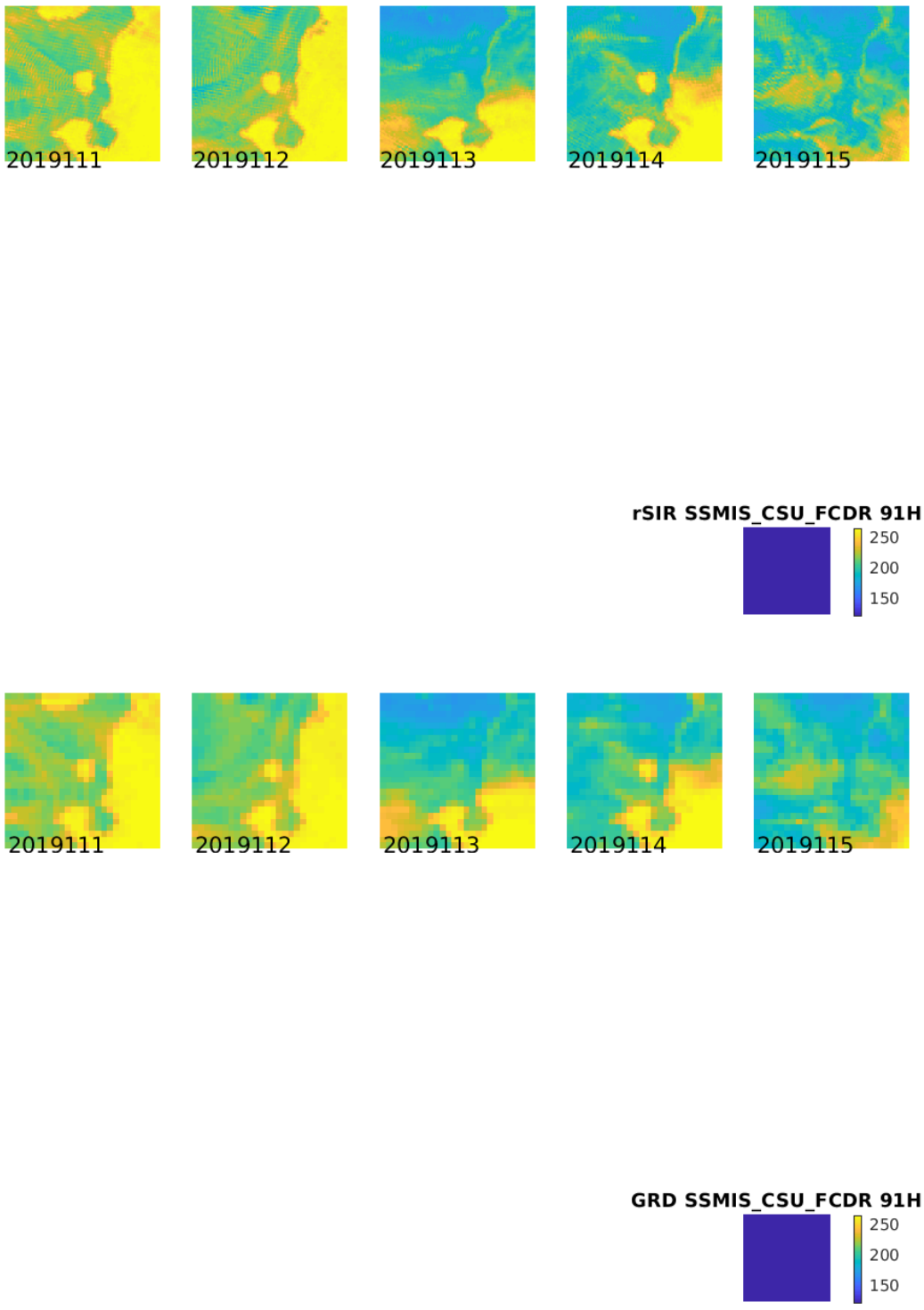

Figure 170: Time series of (top) rSIR and (bottom) GRD T_B images over the study area. Image dates are labeled on the image.

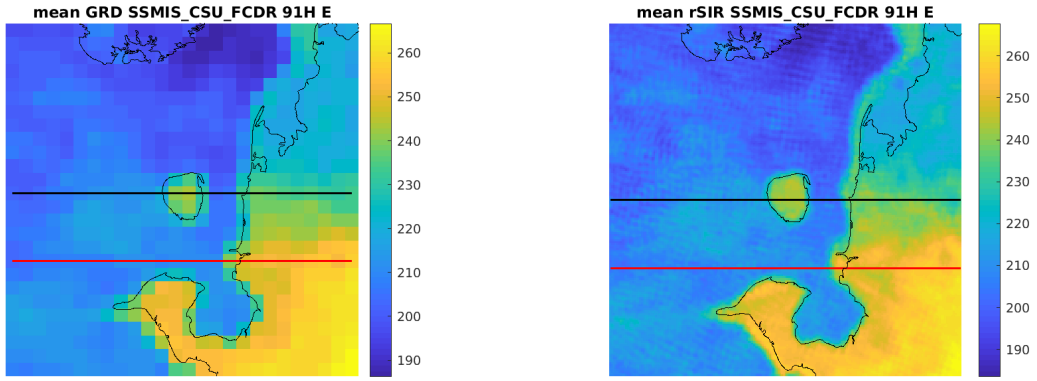

Figure 171: Average of daily T_B images over the study area. (left) 25-km GRD. (right) 3.125-km rSIR. The thick horizontal lines show the data transect locations where data is extracted from the image for analysis.

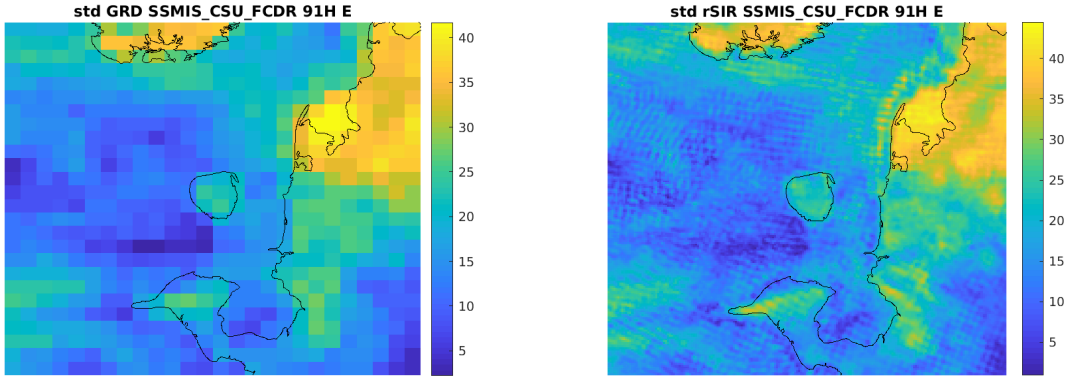

Figure 172: Standard deviation of daily T_B images over the study area. (left) 25-km GRD. (right) 3.125-km rSIR.

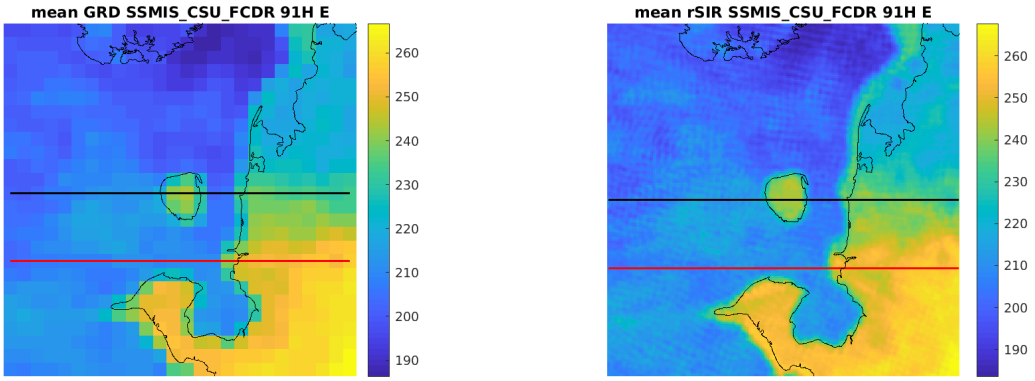

Figure 173: [Repeated] Average of daily T_B images over the study area. (left) 25-km GRD. (right) 3.125-km rSIR. The thick horizontal lines show the data transect locations where data is extracted from the image for analysis.

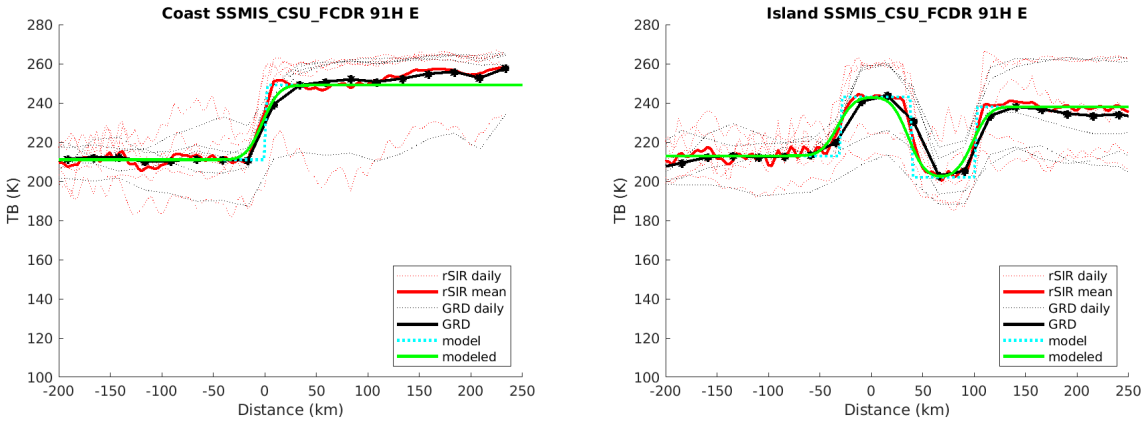

Figure 174: Plots of T_B along the two analysis case transect lines for the (left) coast-crossing and (right) island-crossing cases.

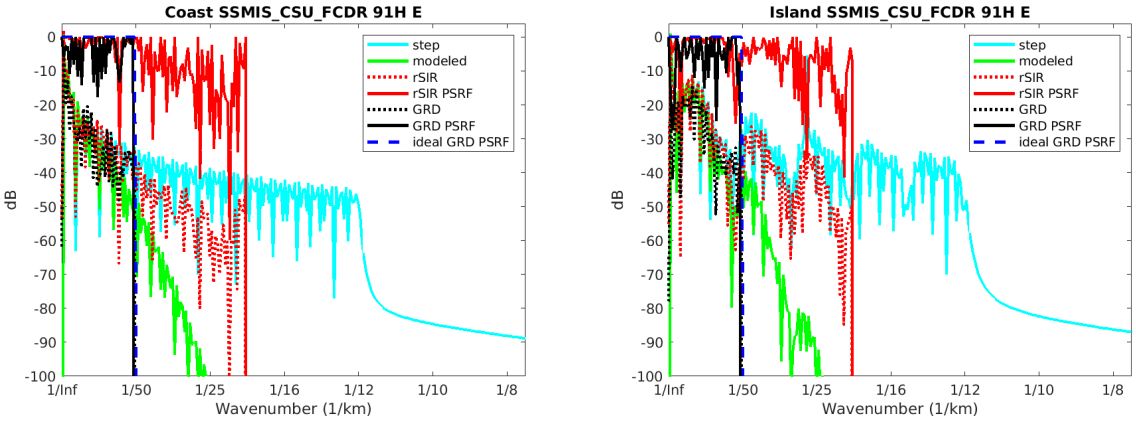

Figure 175: Wavenumber spectra of the T_B slices, the model, and the PSRF. (left) Coast-crossing case. (right) Island-crossing case.

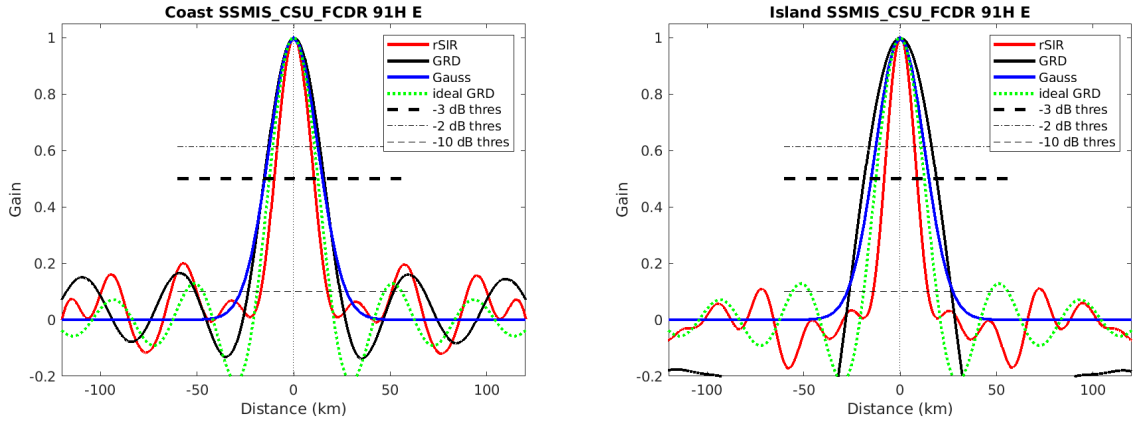

Figure 176: Derived single-pass rSIR and GRD PSRFs from the (left) coast-crossing and (right) island-crossing cases.

Table 50: Resolution estimates for SSMIS_CSU_FCDR channel 91H LTOD E

	-3 dB Thres		-2 dB Thres		-10 dB Thres	
Algorithm	Coast	Island	Coast	Island	Coast	Island
Gauss	30.0	30.0	24.4	24.4	54.8	54.8
rSIR	20.6	17.0	17.0	14.1	34.5	28.5
ideal GRD	36.2	36.2	30.3	30.3	54.5	54.5
GRD	31.0	37.5	25.9	31.7	47.6	52.9

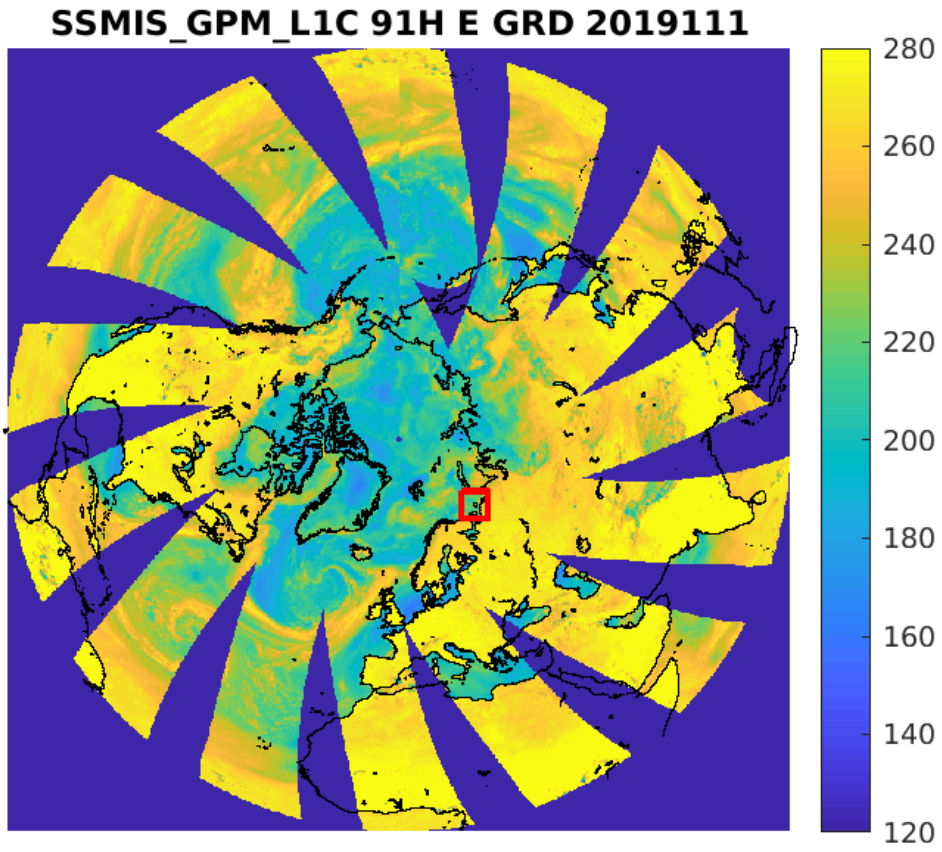

Figure 177: rSIR Northern Hemisphere view.

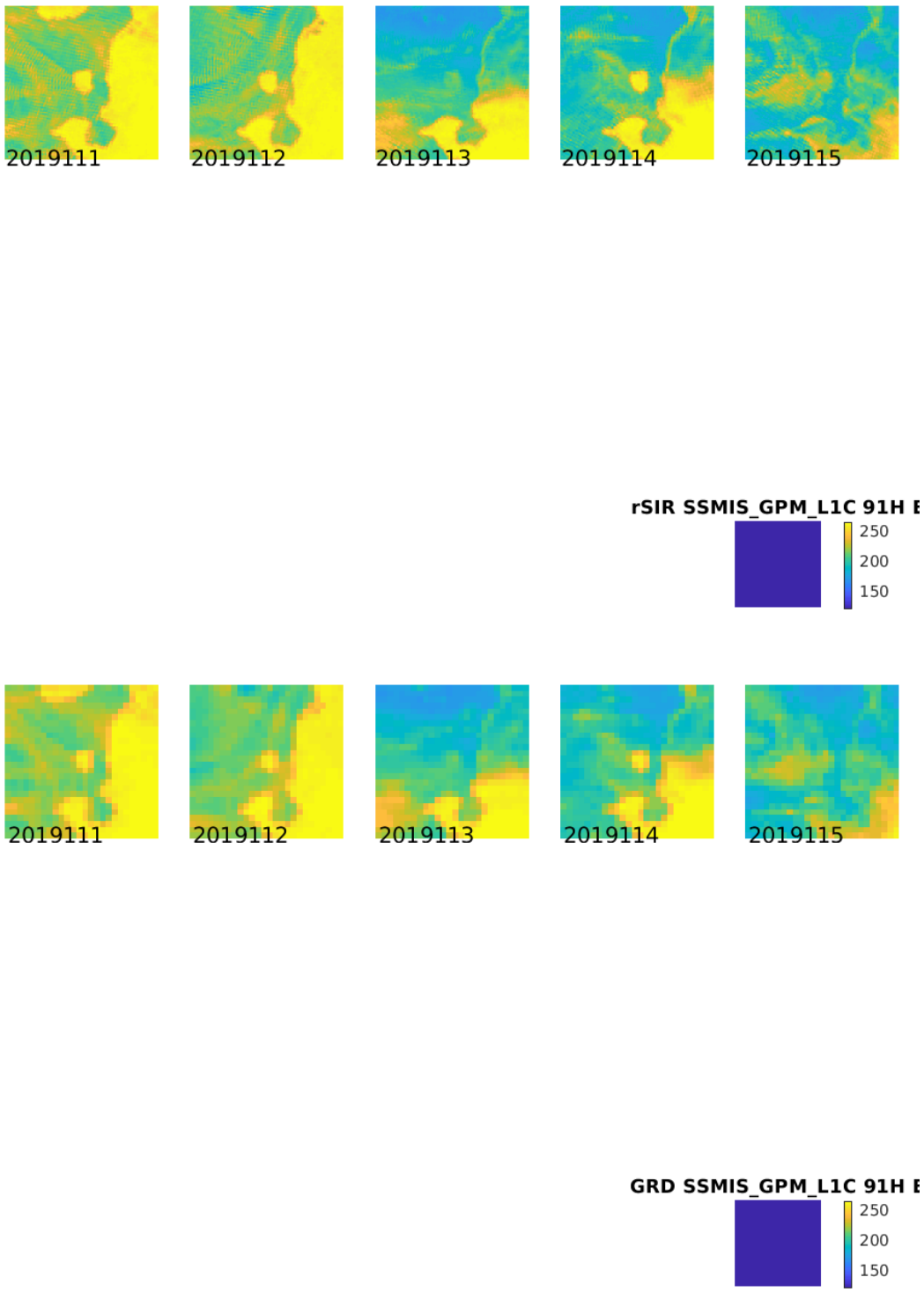

Figure 178: Time series of (top) rSIR and (bottom) GRD T_B images over the study area. Image dates are labeled on the image.

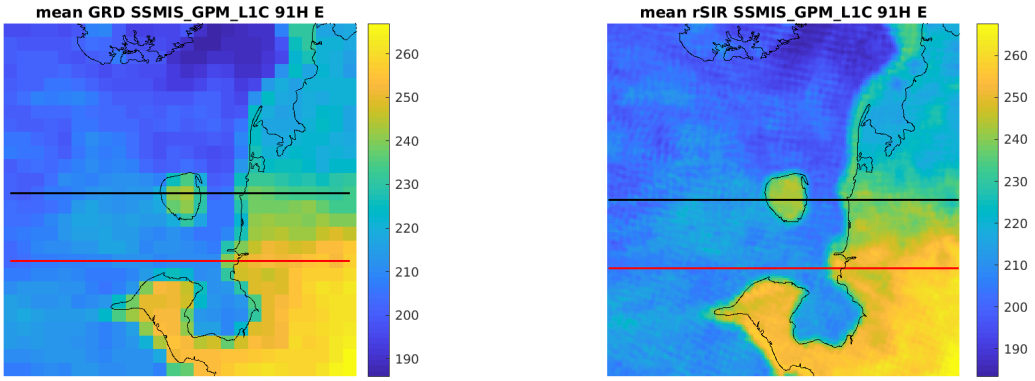

Figure 179: Average of daily T_B images over the study area. (left) 25-km GRD. (right) 3.125-km rSIR. The thick horizontal lines show the data transect locations where data is extracted from the image for analysis.

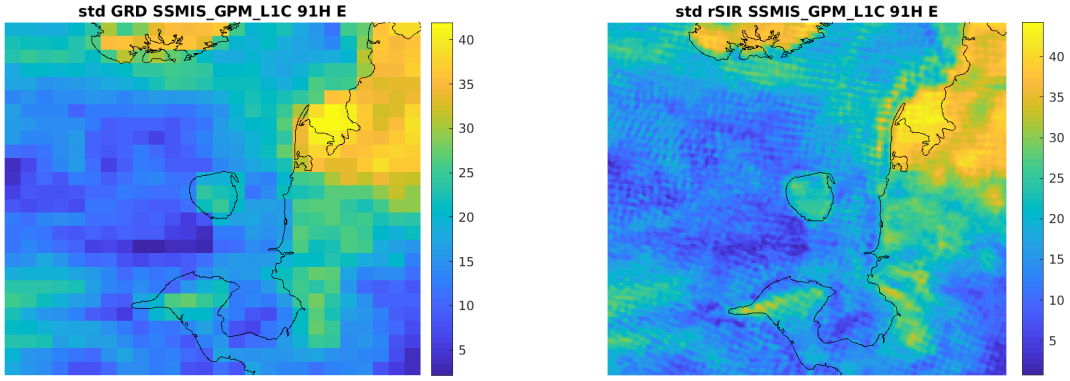

Figure 180: Standard deviation of daily T_B images over the study area. (left) 25-km GRD. (right) 3.125-km rSIR.

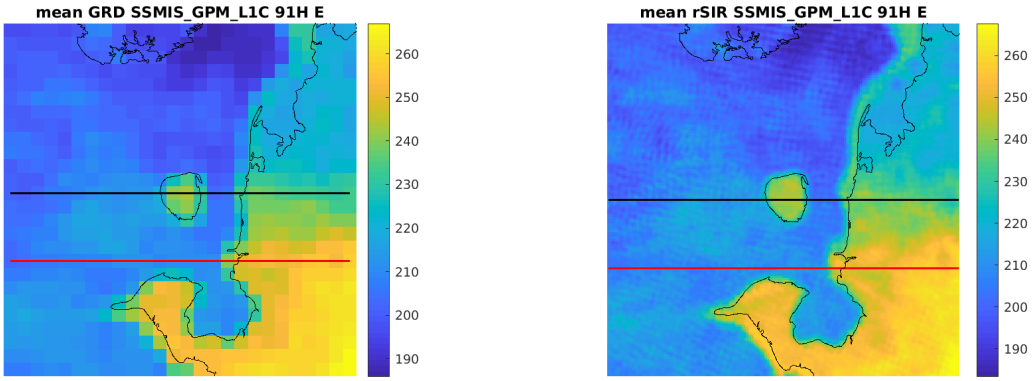

Figure 181: [Repeated] Average of daily T_B images over the study area. (left) 25-km GRD. (right) 3.125-km rSIR. The thick horizontal lines show the data transect locations where data is extracted from the image for analysis.

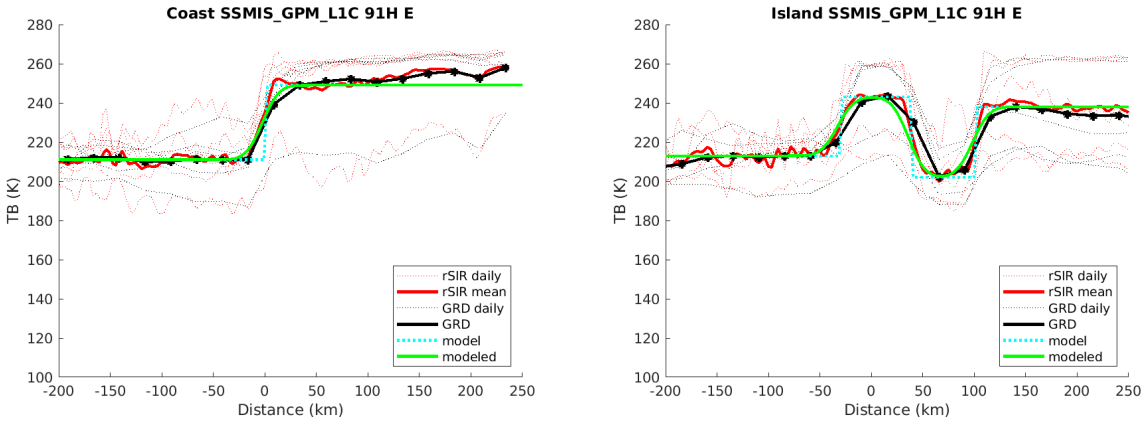

Figure 182: Plots of T_B along the two analysis case transect lines for the (left) coast-crossing and (right) island-crossing cases.

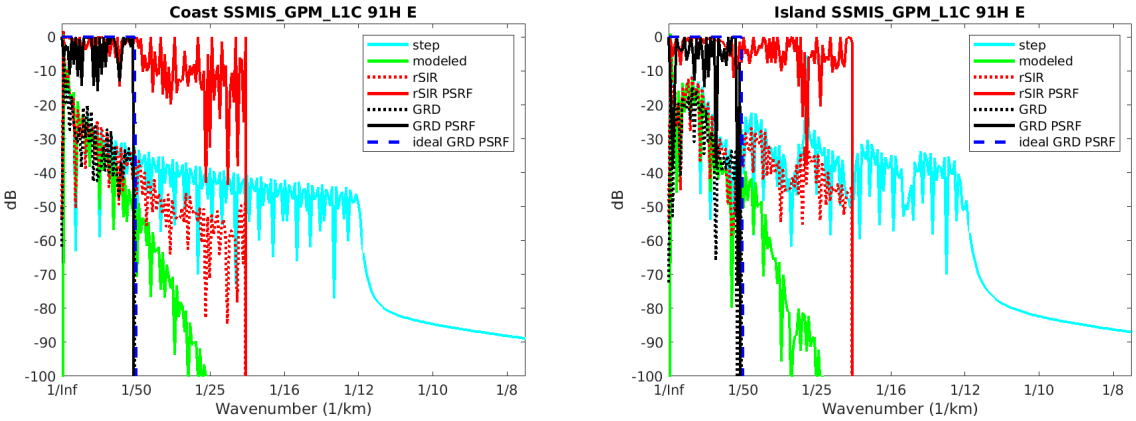

Figure 183: Wavenumber spectra of the T_B slices, the model, and the PSRF. (left) Coast-crossing case. (right) Island-crossing case.

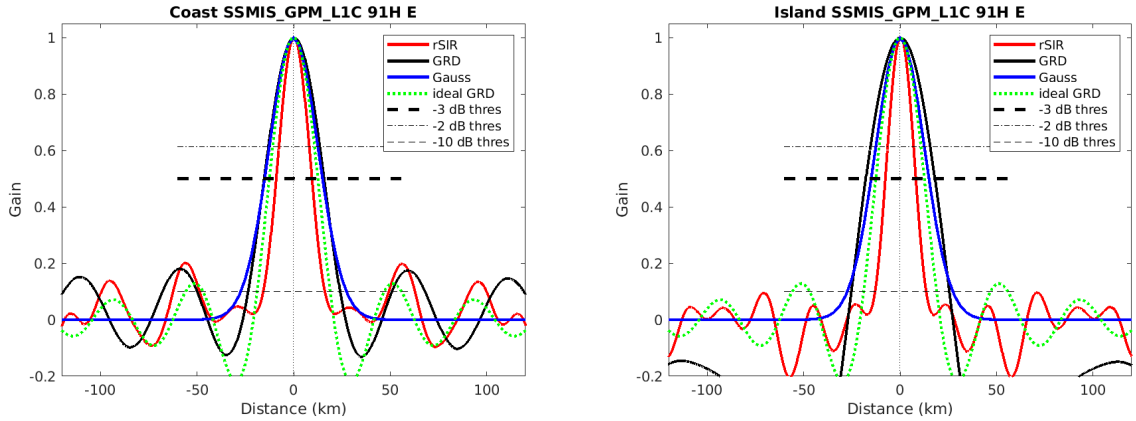

Figure 184: Derived single-pass rSIR and GRD PSRFs from the (left) coast-crossing and (right) island-crossing cases.

Table 51: Resolution estimates for SSMIS_GPM_L1C channel 91H LTOD E

	-3 dB Thres		-2 dB Thres		-10 dB Thres	
Algorithm	Coast	Island	Coast	Island	Coast	Island
Gauss	30.0	30.0	24.4	24.4	54.8	54.8
rSIR	18.5	15.8	15.2	13.0	31.9	26.5
ideal GRD	36.2	36.2	30.3	30.3	54.5	54.5
GRD	31.0	35.8	25.8	30.3	47.6	50.8

8.12 Channel 91H M Figures

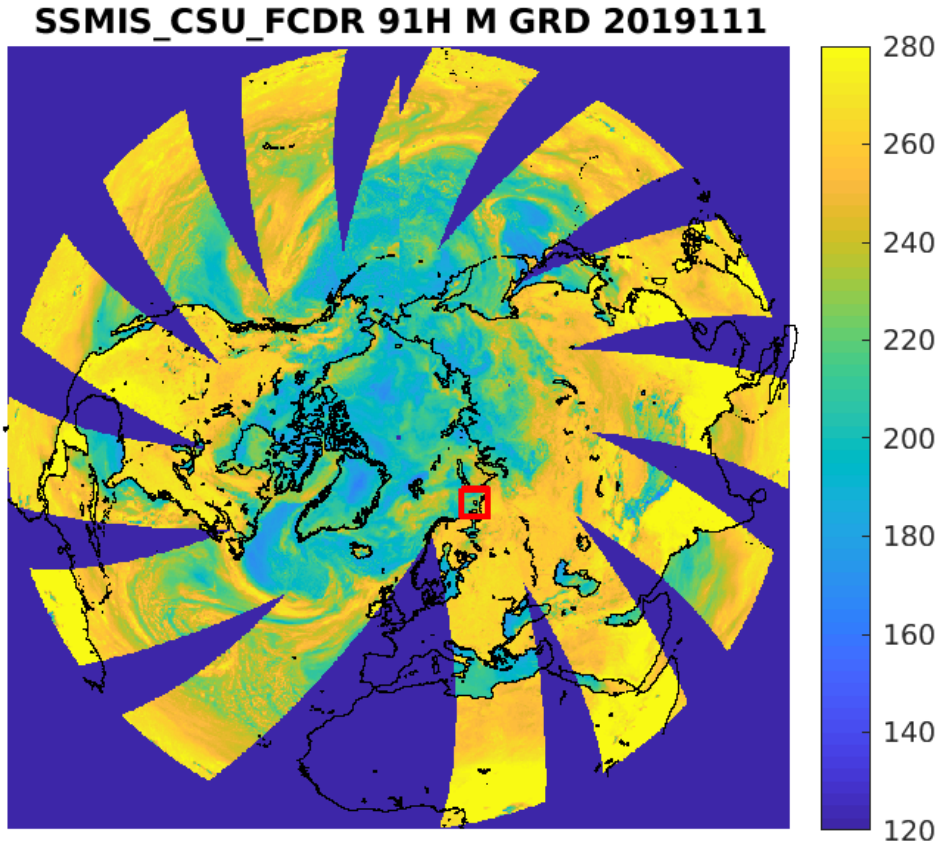

Figure 185: rSIR Northern Hemisphere view.

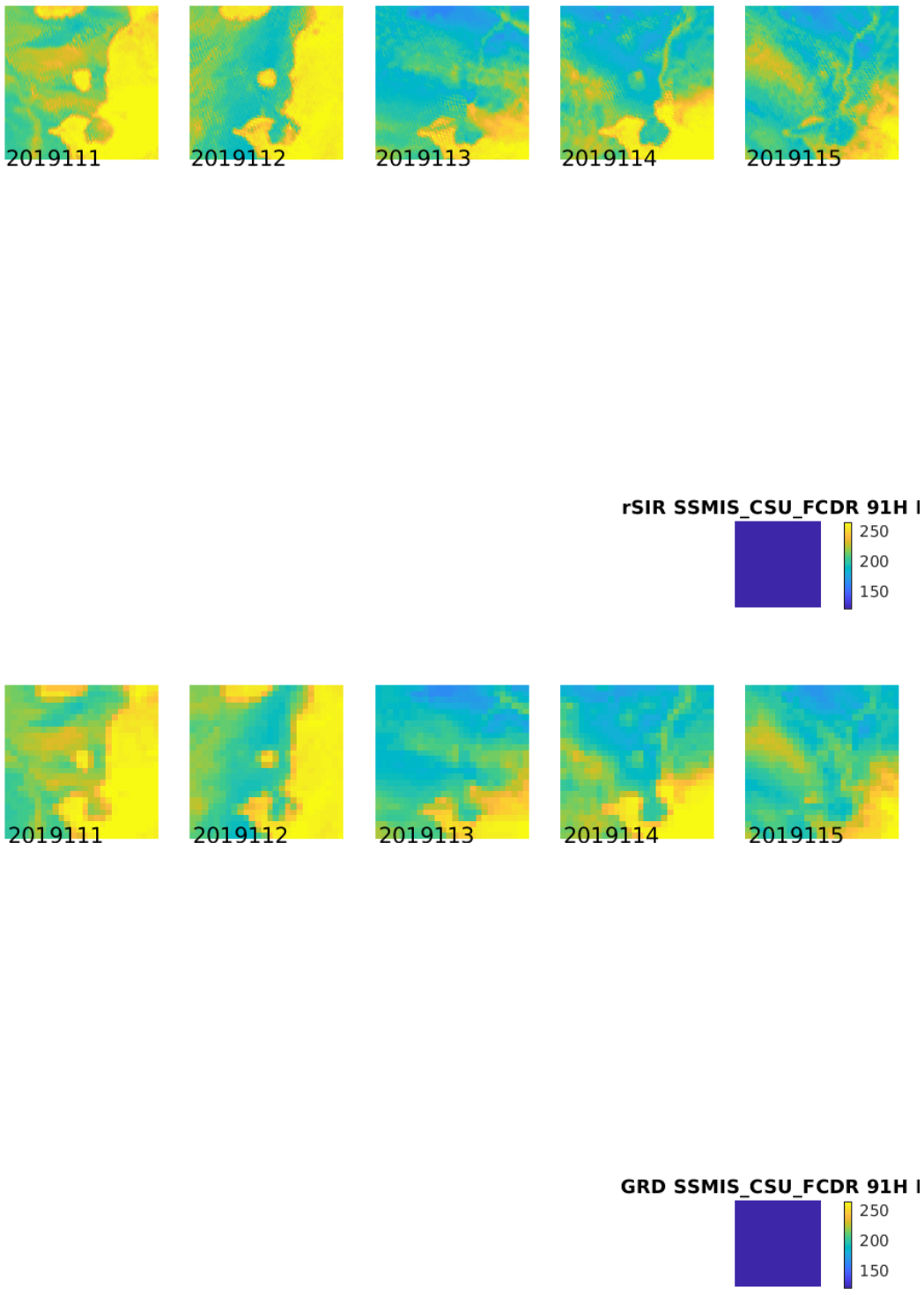

Figure 186: Time series of (top) rSIR and (bottom) GRD T_B images over the study area. Image dates are labeled on the image.

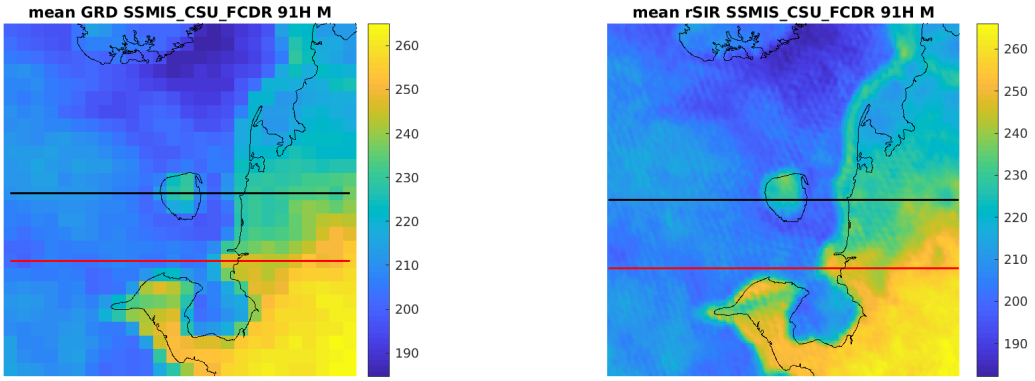

Figure 187: Average of daily T_B images over the study area. (left) 25-km GRD. (right) 3.125-km rSIR. The thick horizontal lines show the data transect locations where data is extracted from the image for analysis.

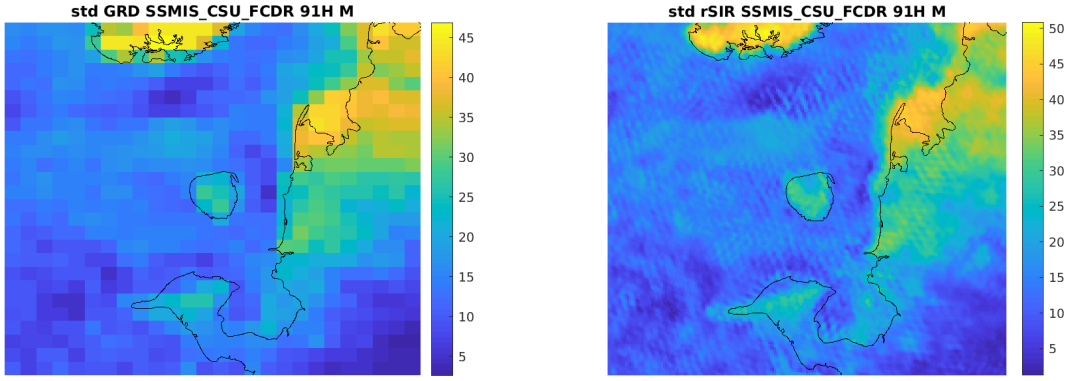

Figure 188: Standard deviation of daily T_B images over the study area. (left) 25-km GRD. (right) 3.125-km rSIR.

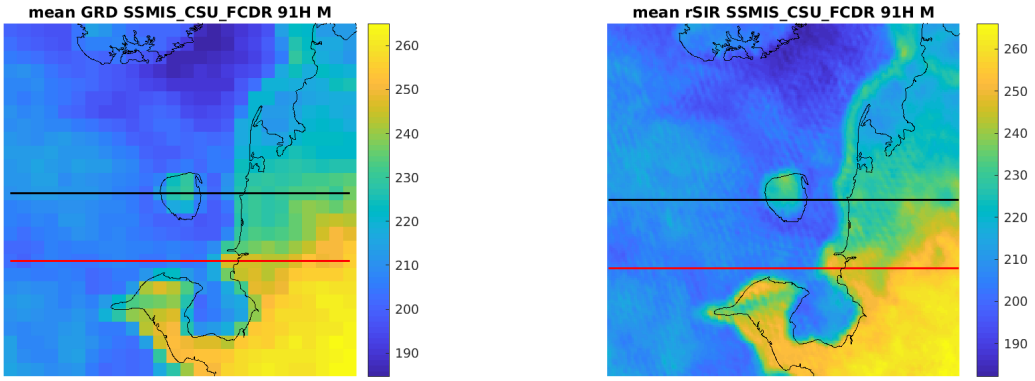

Figure 189: [Repeated] Average of daily T_B images over the study area. (left) 25-km GRD. (right) 3.125-km rSIR. The thick horizontal lines show the data transect locations where data is extracted from the image for analysis.

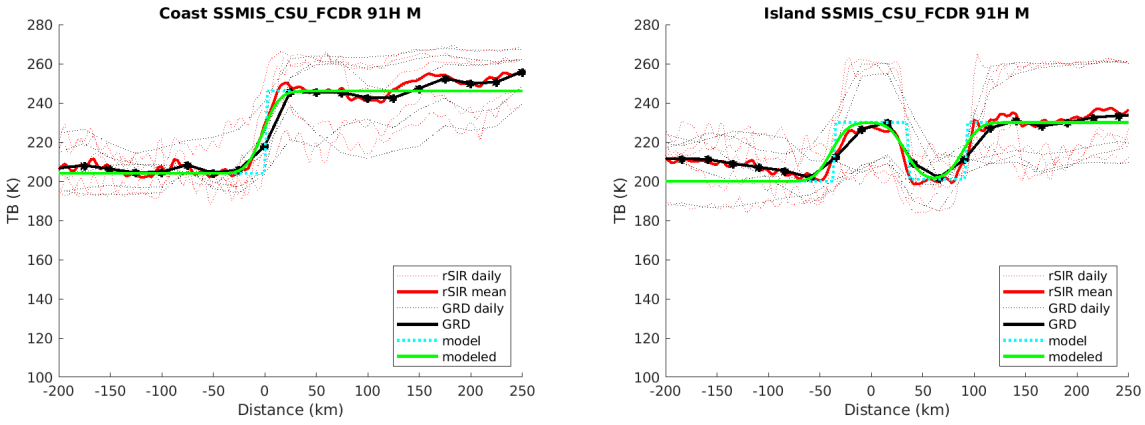

Figure 190: Plots of T_B along the two analysis case transect lines for the (left) coast-crossing and (right) island-crossing cases.

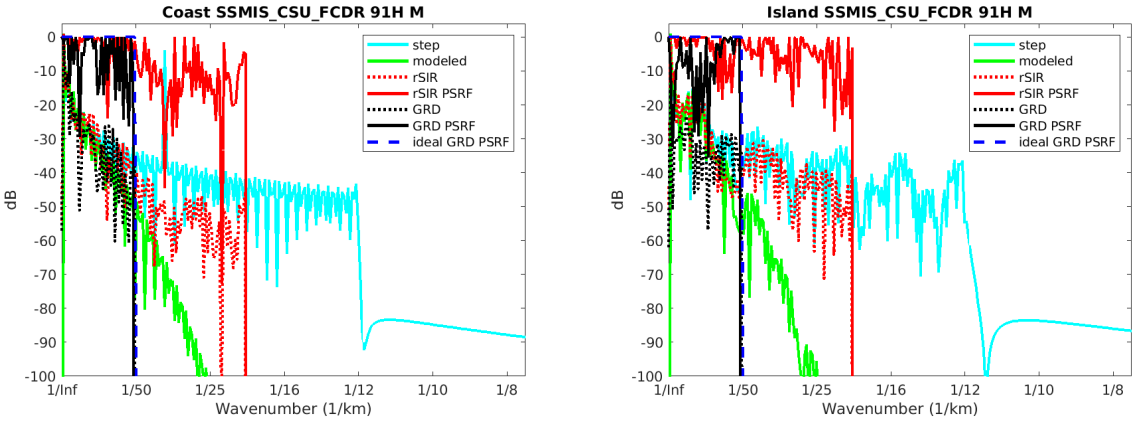

Figure 191: Wavenumber spectra of the T_B slices, the model, and the PSRF. (left) Coast-crossing case. (right) Island-crossing case.

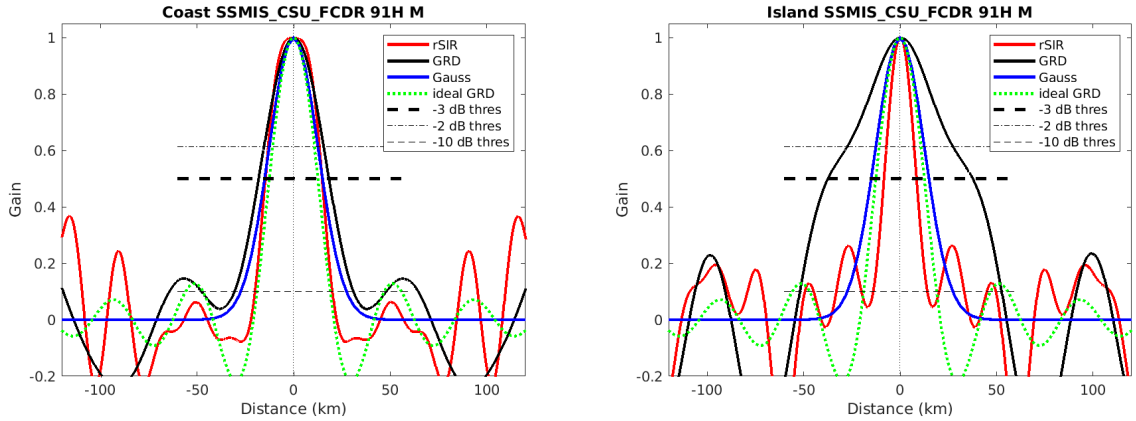

Figure 192: Derived single-pass rSIR and GRD PSRFs from the (left) coast-crossing and (right) island-crossing cases.

Table 52: Resolution estimates for SSMIS_CSU_FCDR channel 91H LTOD M

	-3 dB Thres		-2 dB Thres		-10 dB Thres	
Algorithm	Coast	Island	Coast	Island	Coast	Island
Gauss	30.0	30.0	24.4	24.4	54.8	54.8
rSIR	29.4	16.9	26.1	14.0	40.0	28.2
ideal GRD	36.2	36.2	30.3	30.3	54.5	54.5
GRD	36.4	22.5	30.0	19.0	61.6	31.8

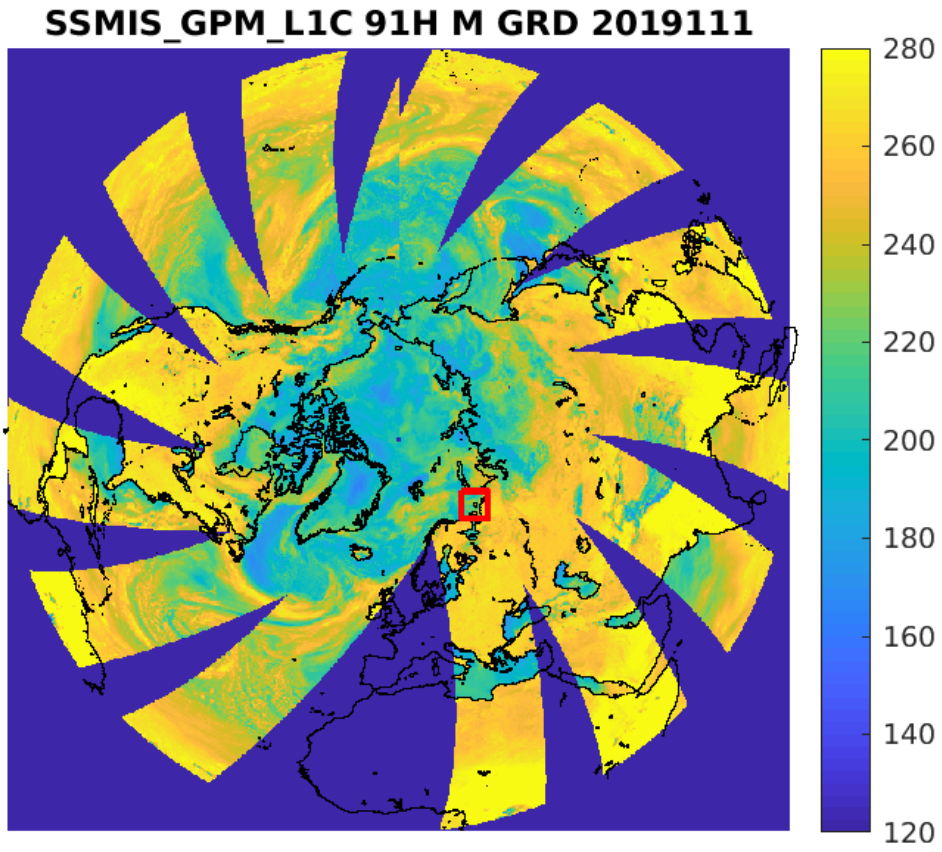

Figure 193: rSIR Northern Hemisphere view.

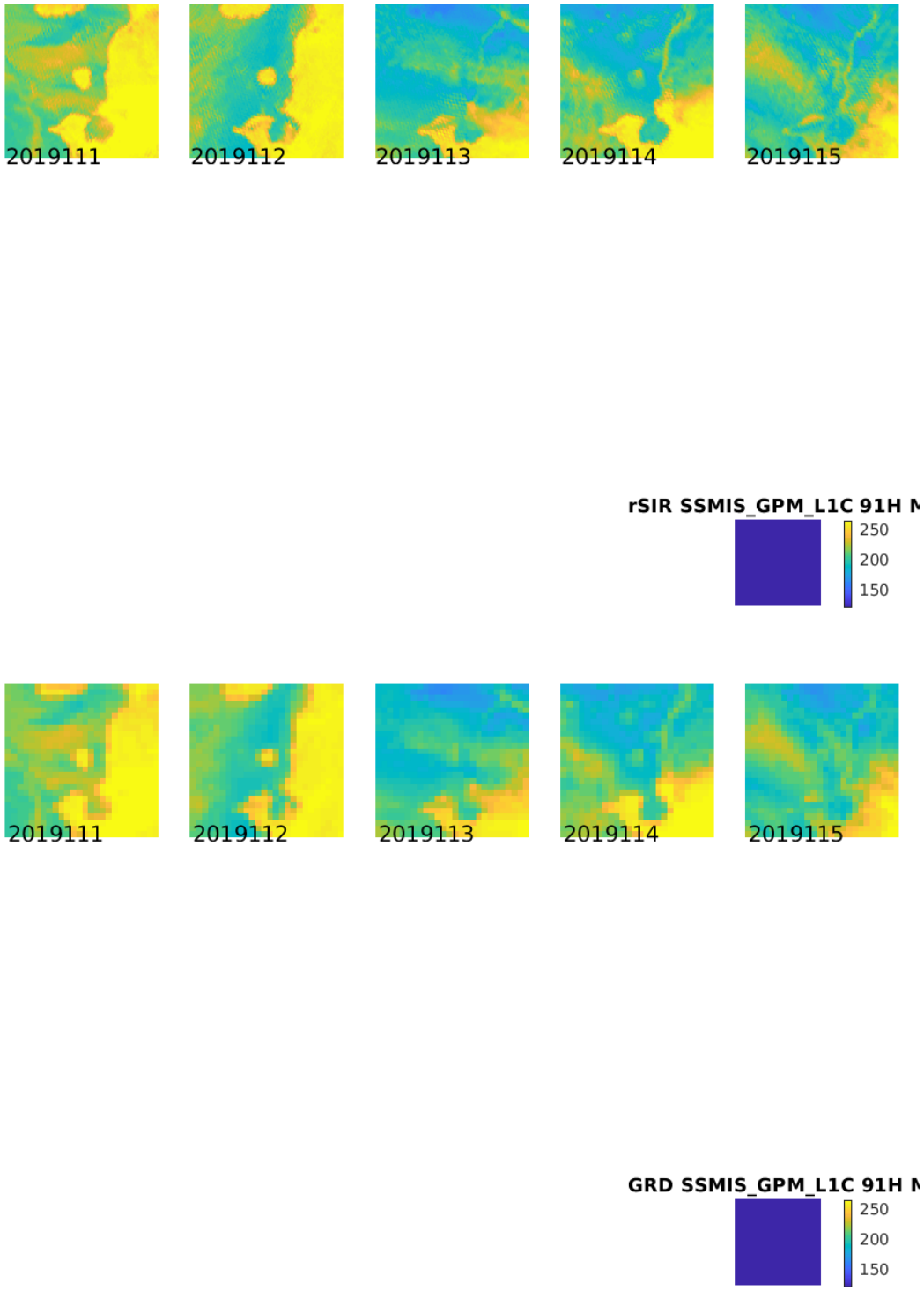

Figure 194: Time series of (top) rSIR and (bottom) GRD T_B images over the study area. Image dates are labeled on the image.

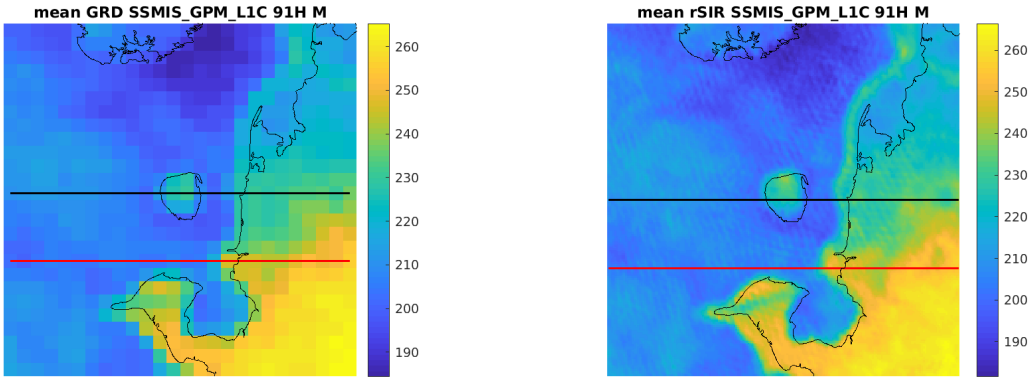

Figure 195: Average of daily T_B images over the study area. (left) 25-km GRD. (right) 3.125-km rSIR. The thick horizontal lines show the data transect locations where data is extracted from the image for analysis.

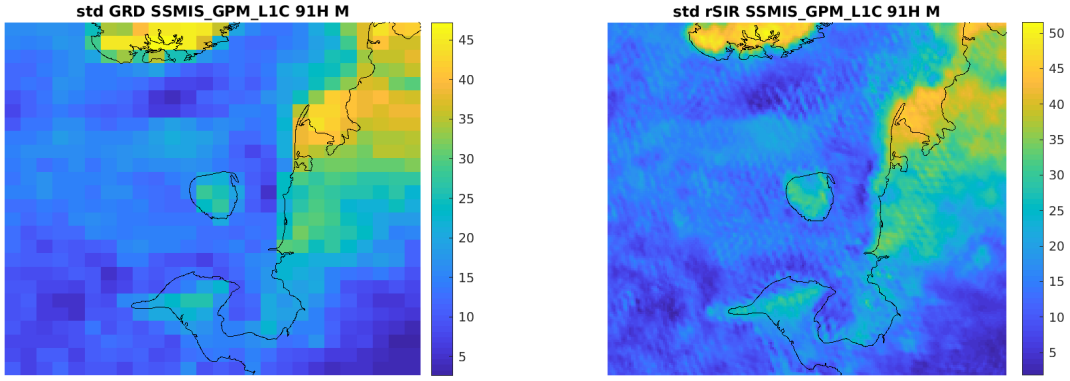

Figure 196: Standard deviation of daily T_B images over the study area. (left) 25-km GRD. (right) 3.125-km rSIR.

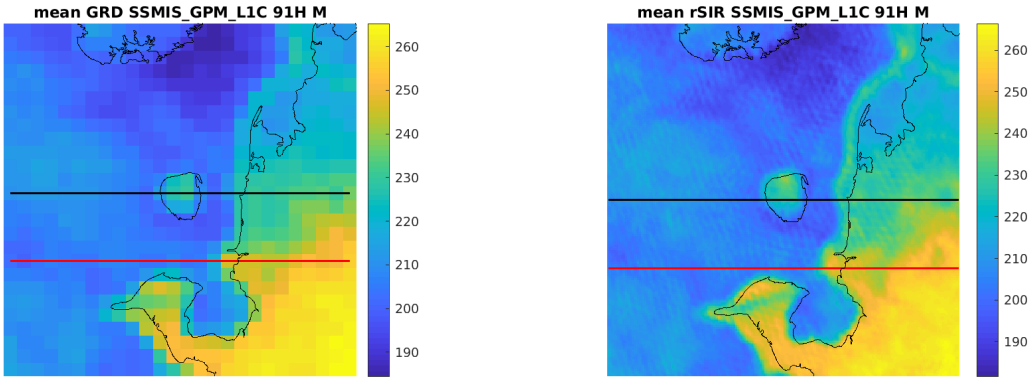

Figure 197: [Repeated] Average of daily T_B images over the study area. (left) 25-km GRD. (right) 3.125-km rSIR. The thick horizontal lines show the data transect locations where data is extracted from the image for analysis.

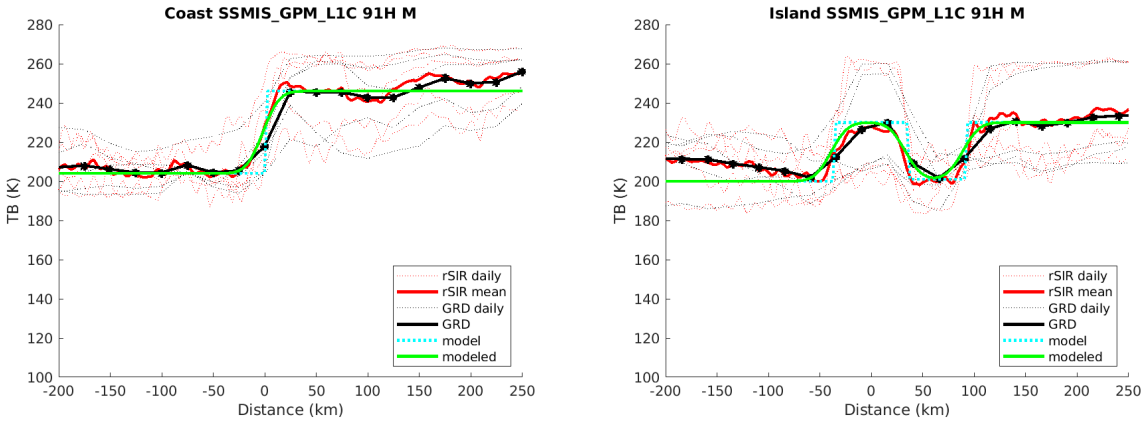

Figure 198: Plots of T_B along the two analysis case transect lines for the (left) coast-crossing and (right) island-crossing cases.

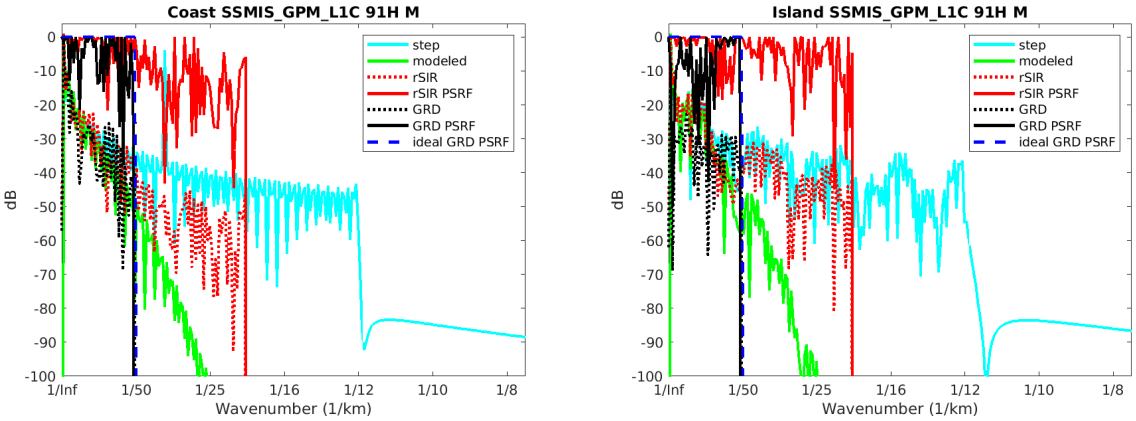

Figure 199: Wavenumber spectra of the T_B slices, the model, and the PSRF. (left) Coast-crossing case. (right) Island-crossing case.

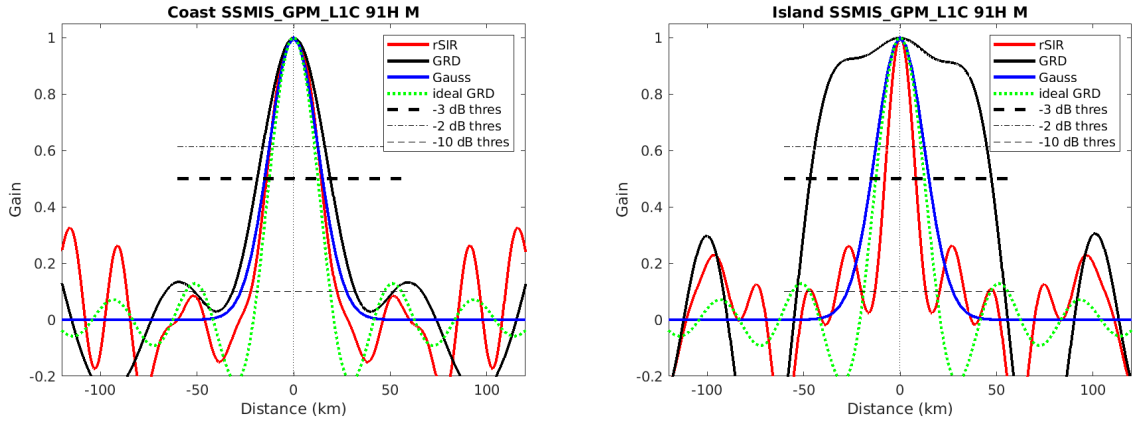

Figure 200: Derived single-pass rSIR and GRD PSRFs from the (left) coast-crossing and (right) island-crossing cases.

Table 53: Resolution estimates for SSMIS_GPM_L1C channel 91H LTOD M

	-3 dB Thres		-2 dB Thres		-10 dB Thres	
Algorithm	Coast	Island	Coast	Island	Coast	Island
Gauss	30.0	30.0	24.4	24.4	54.8	54.8
rSIR	28.4	16.1	24.3	13.3	44.6	26.5
ideal GRD	36.2	36.2	30.3	30.3	54.5	54.5
GRD	37.8	22.3	31.2	18.9	63.5	31.5

8.13 Channel 91V E Figures

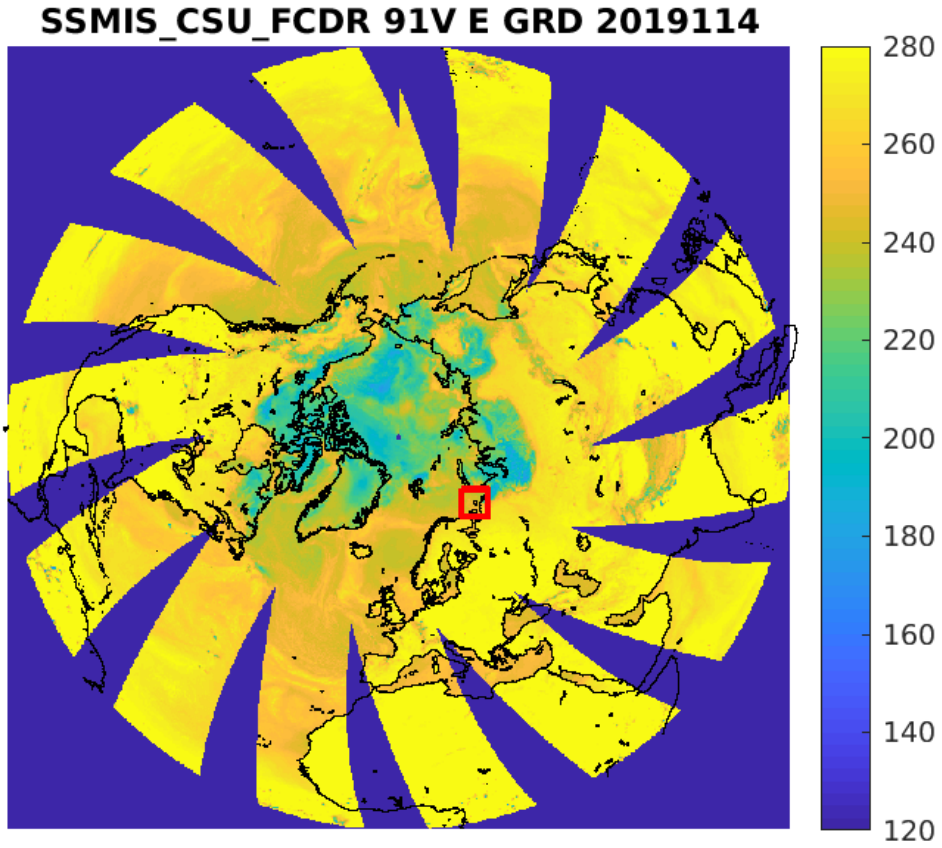

Figure 201: rSIR Northern Hemisphere view.

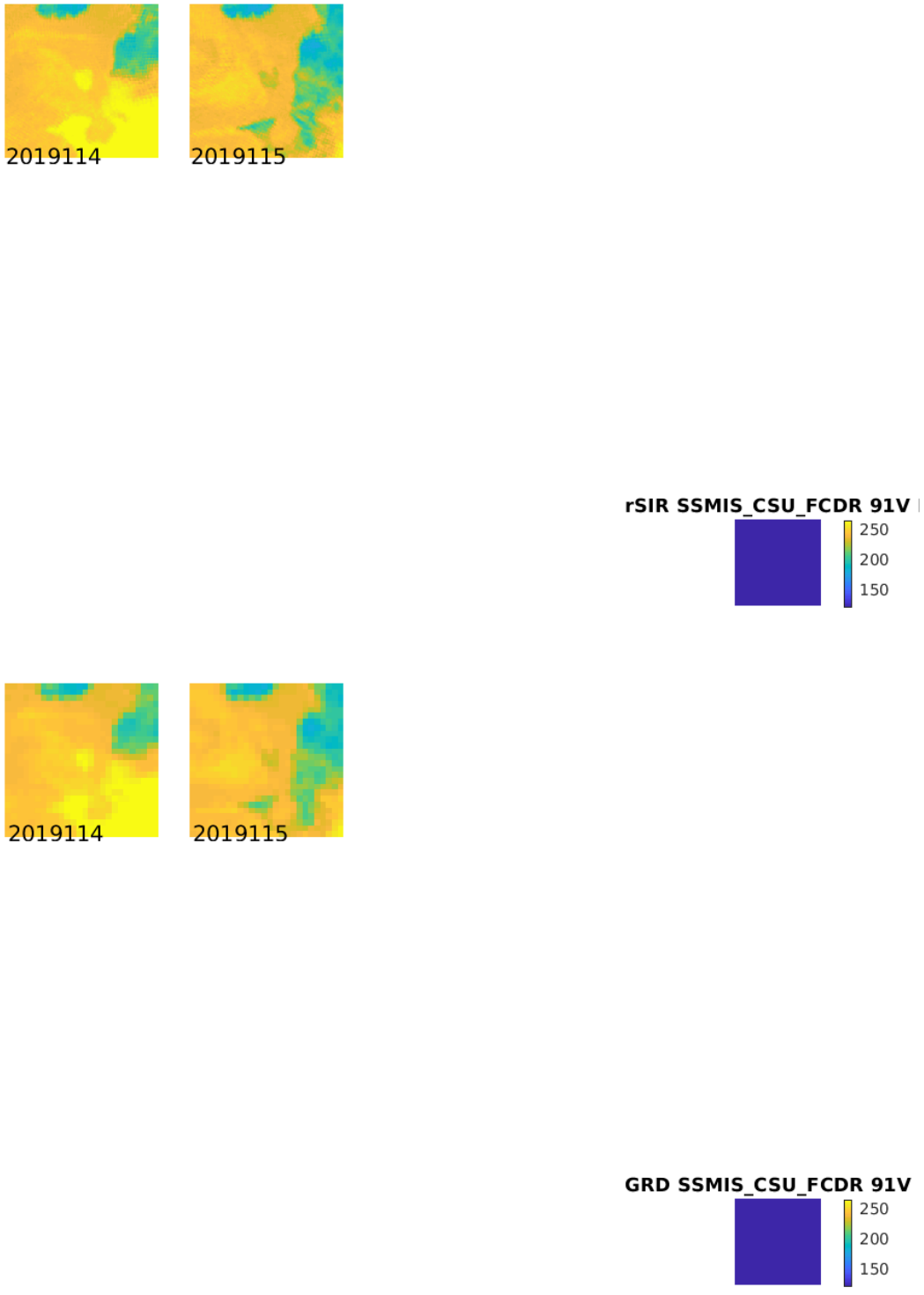

Figure 202: Time series of (top) rSIR and (bottom) GRD T_B images over the study area. Image dates are labeled on the image.

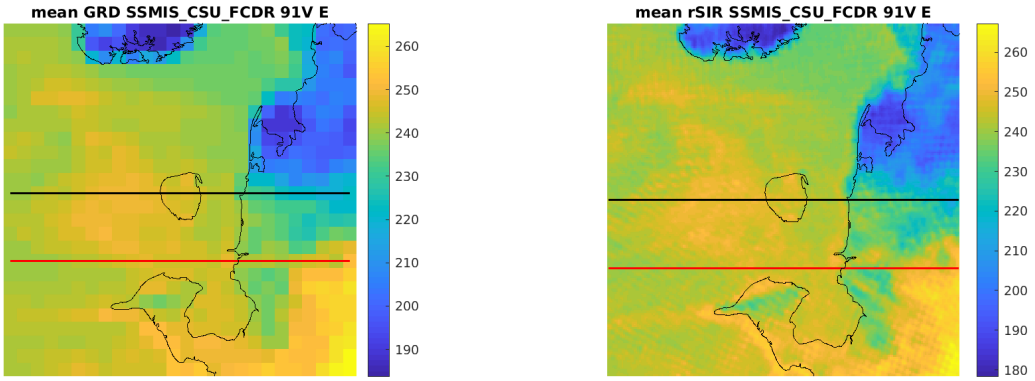

Figure 203: Average of daily T_B images over the study area. (left) 25-km GRD. (right) 3.125-km rSIR. The thick horizontal lines show the data transect locations where data is extracted from the image for analysis.

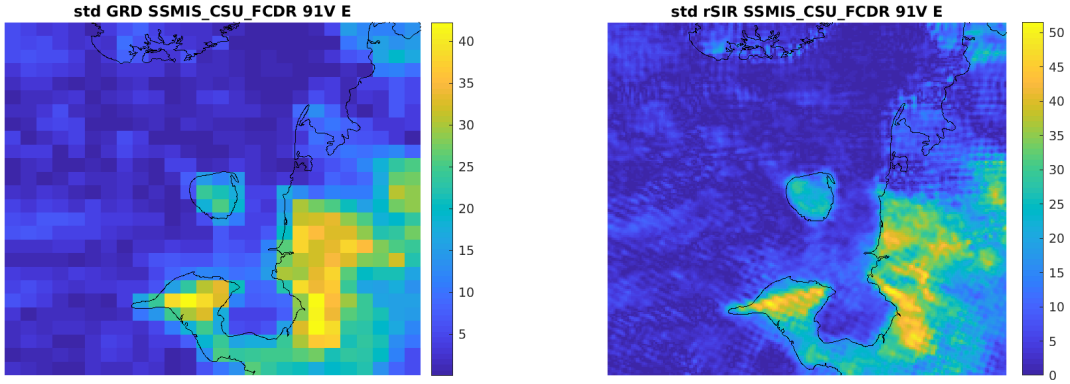

Figure 204: Standard deviation of daily T_B images over the study area. (left) 25-km GRD. (right) 3.125-km rSIR.

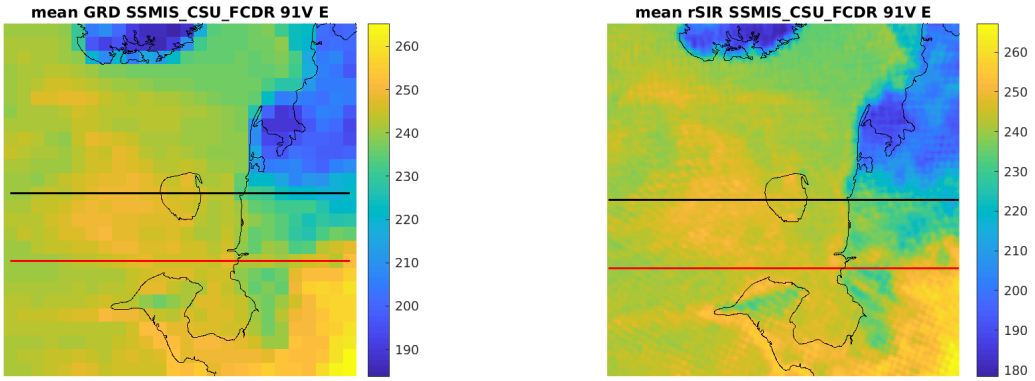

Figure 205: [Repeated] Average of daily T_B images over the study area. (left) 25-km GRD. (right) 3.125-km rSIR. The thick horizontal lines show the data transect locations where data is extracted from the image for analysis.

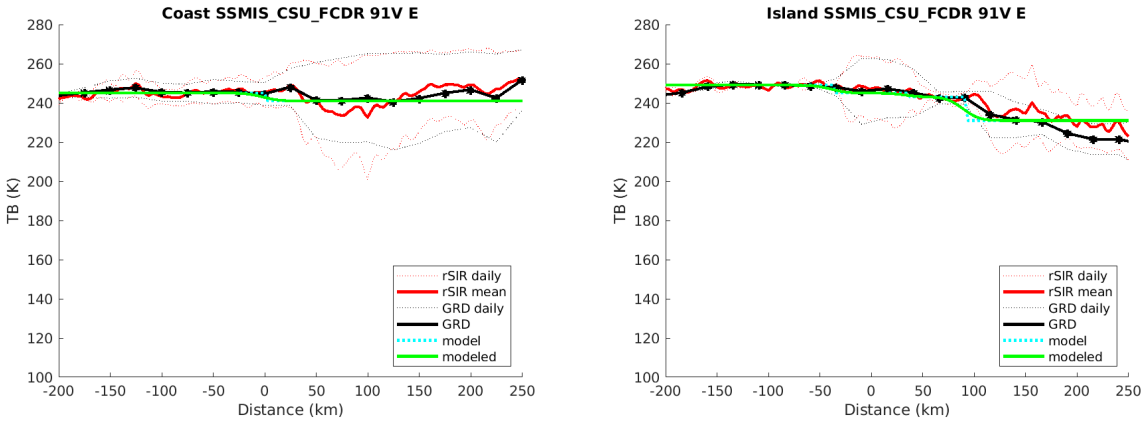

Figure 206: Plots of T_B along the two analysis case transect lines for the (left) coast-crossing and (right) island-crossing cases.

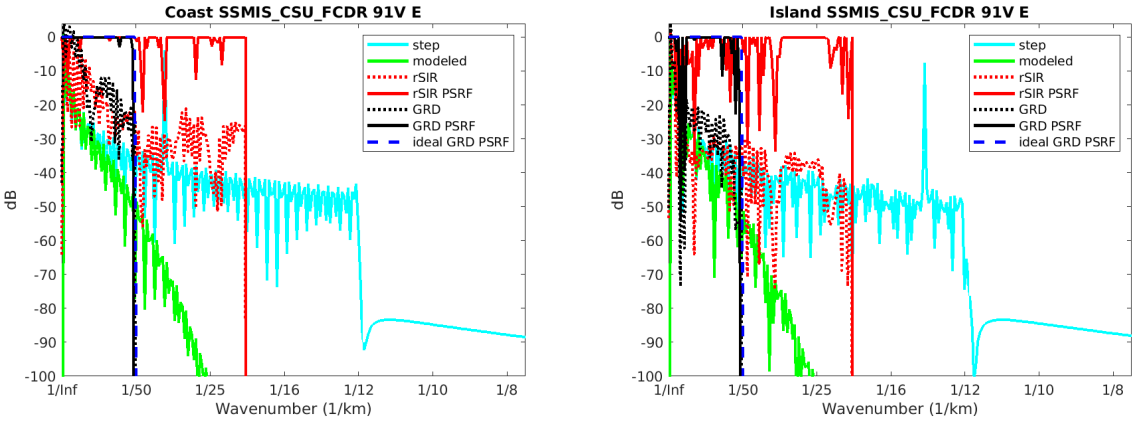

Figure 207: Wavenumber spectra of the T_B slices, the model, and the PSRF. (left) Coast-crossing case. (right) Island-crossing case.

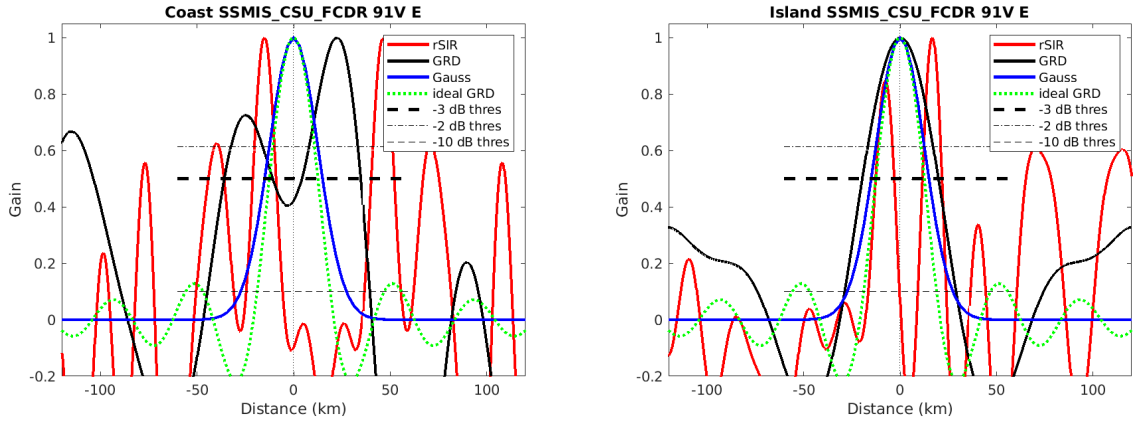

Figure 208: Derived single-pass rSIR and GRD PSRFs from the (left) coast-crossing and (right) island-crossing cases.

Table 54: Resolution estimates for SSMIS_CSU_FCDR channel 91V LTOD E

	-3 dB Thres		-2 dB Thres		-10 dB Thres	
Algorithm	Coast	Island	Coast	Island	Coast	Island
Gauss	30.0	30.0	24.4	24.4	54.8	54.8
rSIR	NaN	NaN	NaN	NaN	NaN	NaN
ideal GRD	36.2	36.2	30.3	30.3	54.5	54.5
GRD	NaN	NaN	NaN	NaN	NaN	NaN

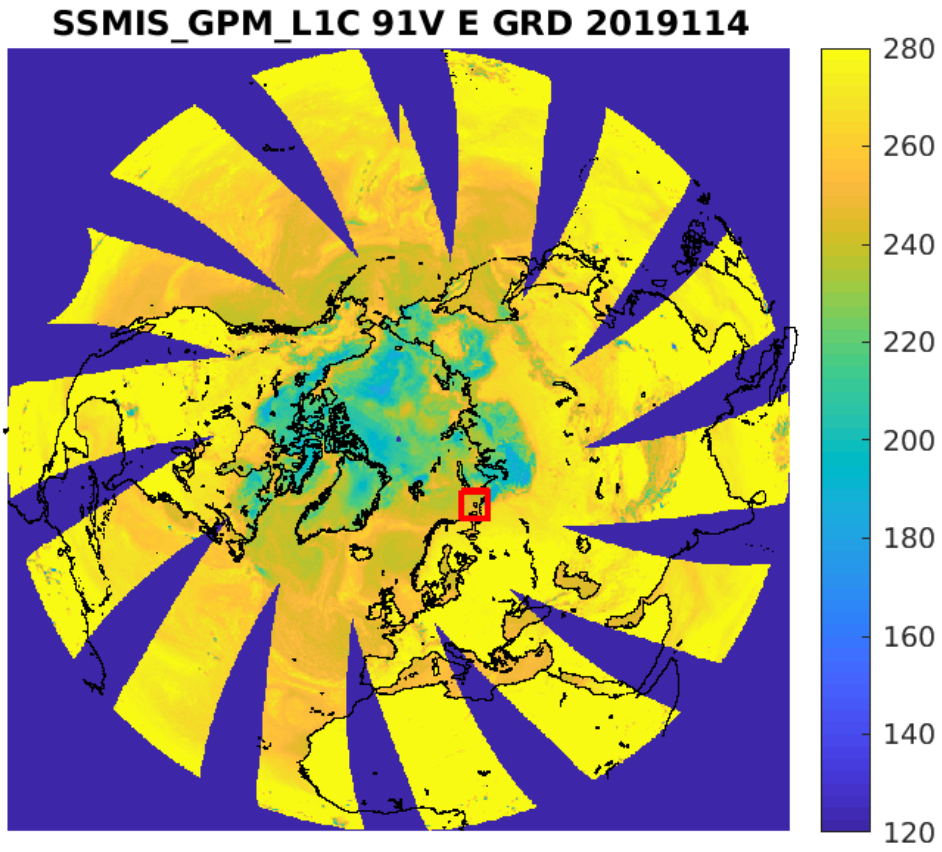

Figure 209: rSIR Northern Hemisphere view.

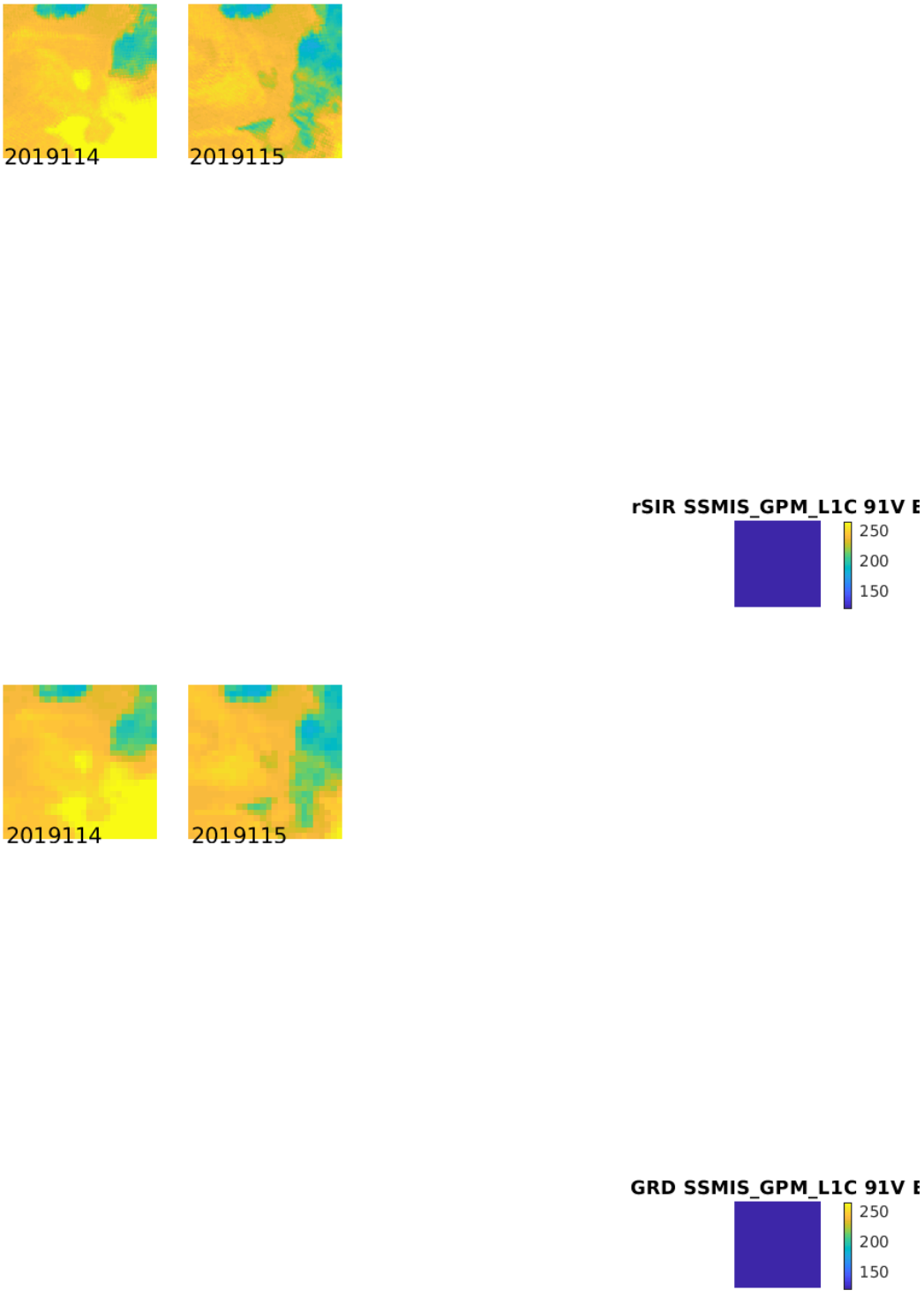

Figure 210: Time series of (top) rSIR and (bottom) GRD T_B images over the study area. Image dates are labeled on the image.

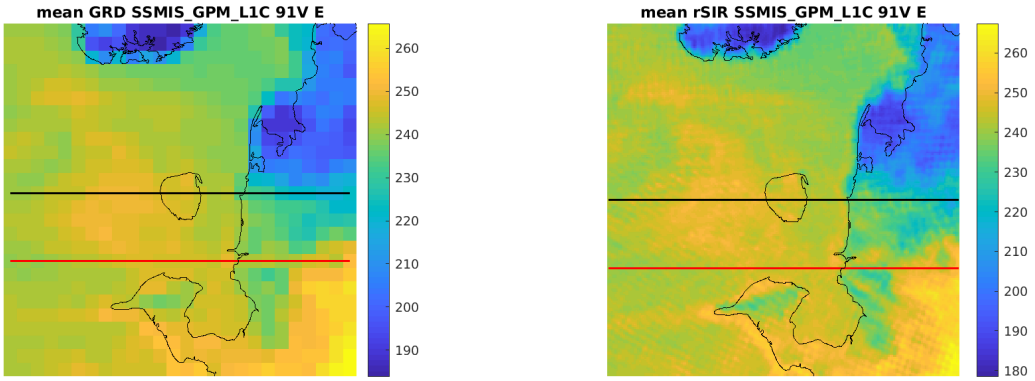

Figure 211: Average of daily T_B images over the study area. (left) 25-km GRD. (right) 3.125-km rSIR. The thick horizontal lines show the data transect locations where data is extracted from the image for analysis.

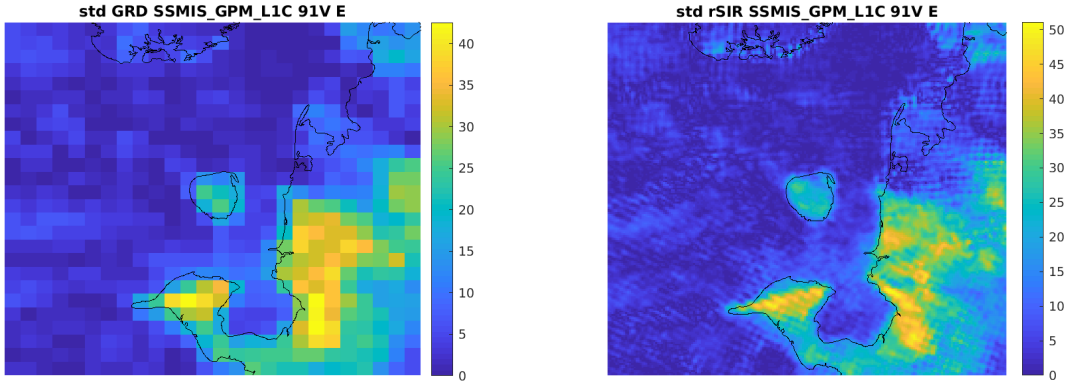

Figure 212: Standard deviation of daily T_B images over the study area. (left) 25-km GRD. (right) 3.125-km rSIR.

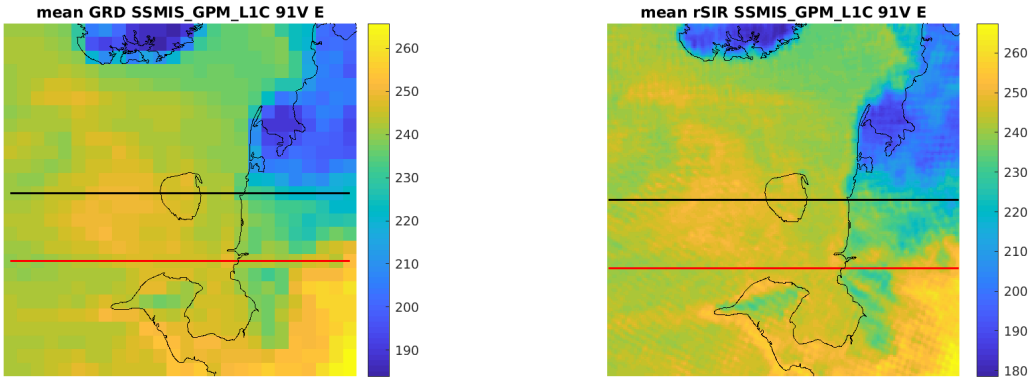

Figure 213: [Repeated] Average of daily T_B images over the study area. (left) 25-km GRD. (right) 3.125-km rSIR. The thick horizontal lines show the data transect locations where data is extracted from the image for analysis.

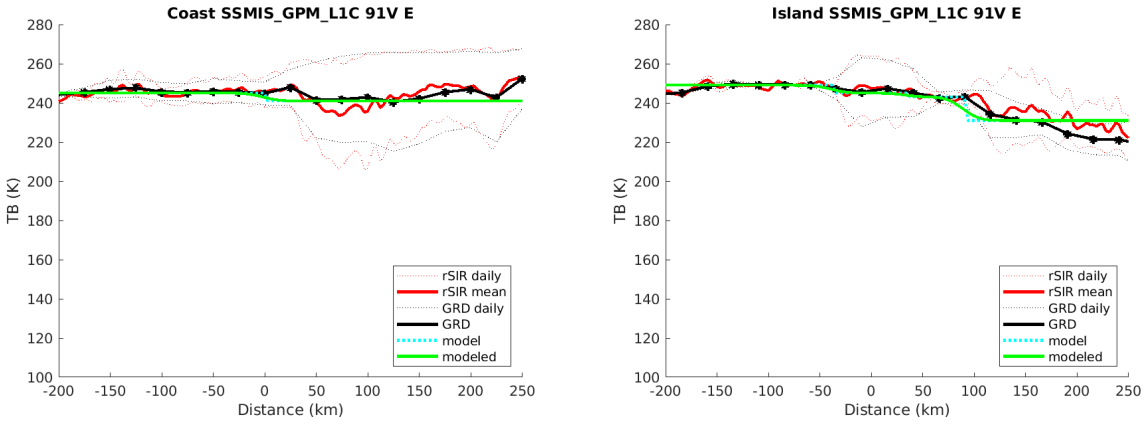

Figure 214: Plots of T_B along the two analysis case transect lines for the (left) coast-crossing and (right) island-crossing cases.

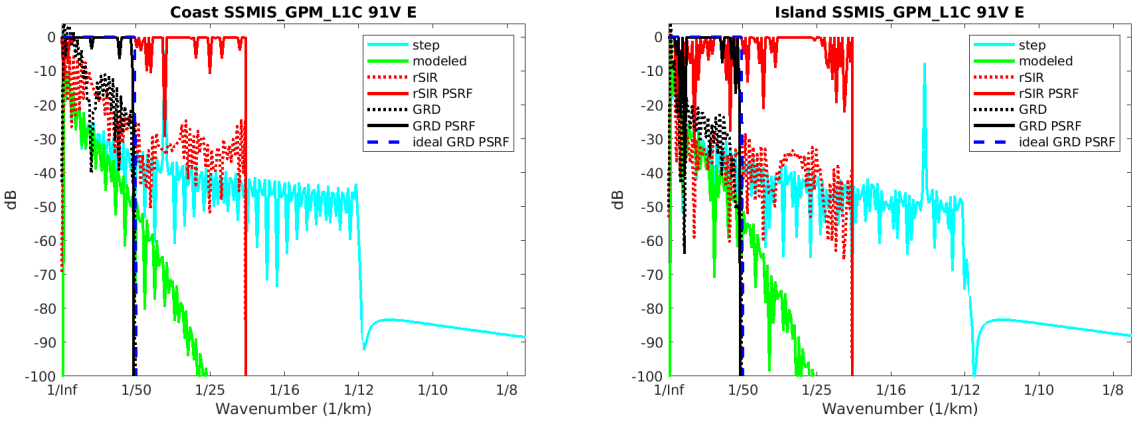

Figure 215: Wavenumber spectra of the T_B slices, the model, and the PSRF. (left) Coast-crossing case. (right) Island-crossing case.

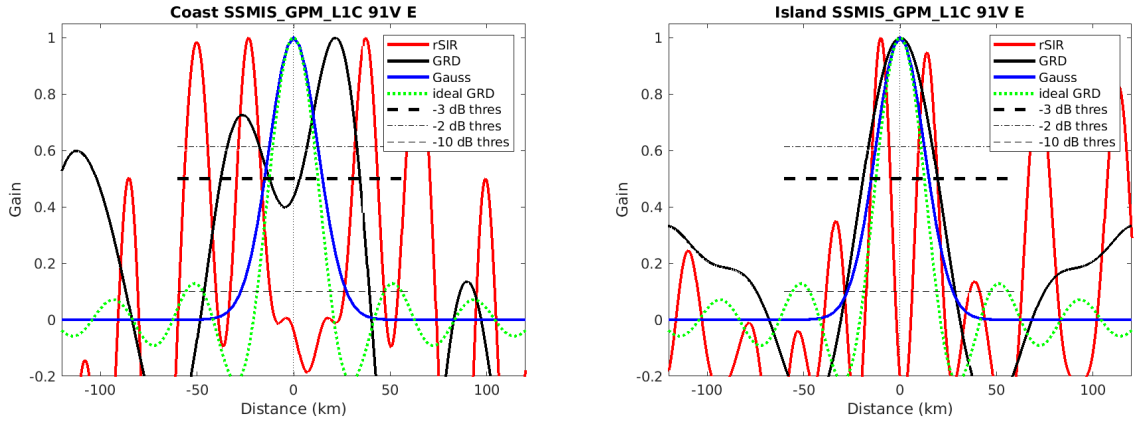

Figure 216: Derived single-pass rSIR and GRD PSRFs from the (left) coast-crossing and (right) island-crossing cases.

Table 55: Resolution estimates for SSMIS_GPM_L1C channel 91V LTOD E

	-3 dB Thres		-2 dB Thres		-10 dB Thres	
Algorithm	Coast	Island	Coast	Island	Coast	Island
Gauss	30.0	30.0	24.4	24.4	54.8	54.8
rSIR	NaN	NaN	NaN	NaN	NaN	NaN
ideal GRD	36.2	36.2	30.3	30.3	54.5	54.5
GRD	NaN	NaN	NaN	NaN	NaN	NaN

8.14 Channel 91V M Figures

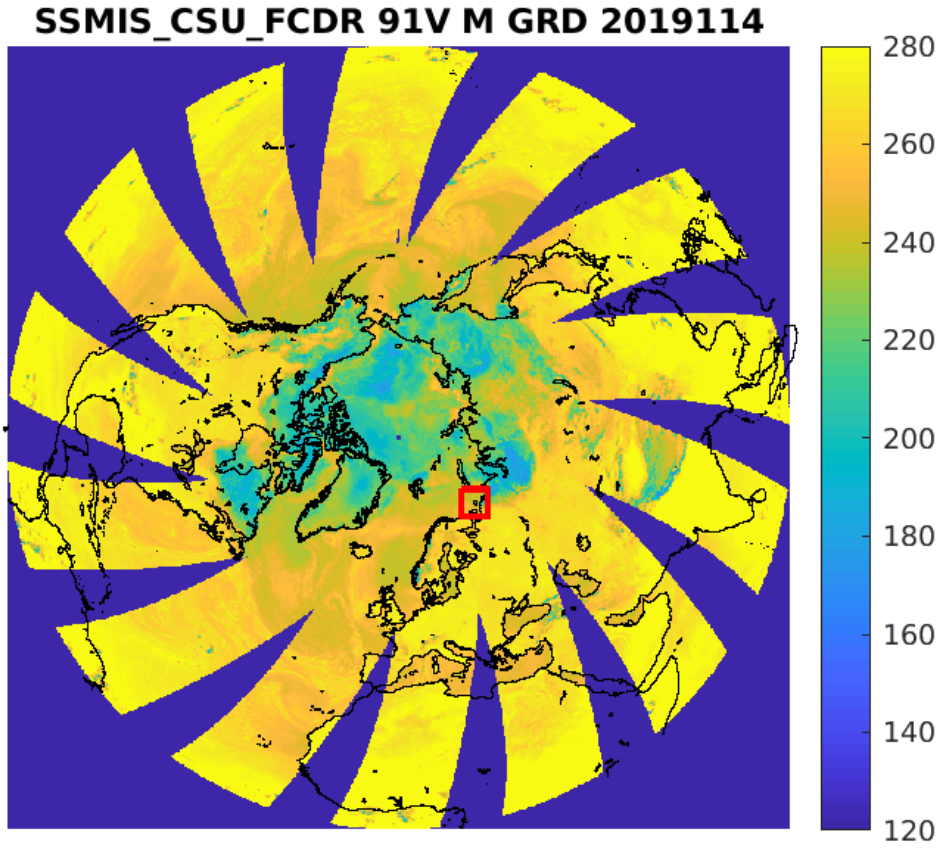

Figure 217: rSIR Northern Hemisphere view.

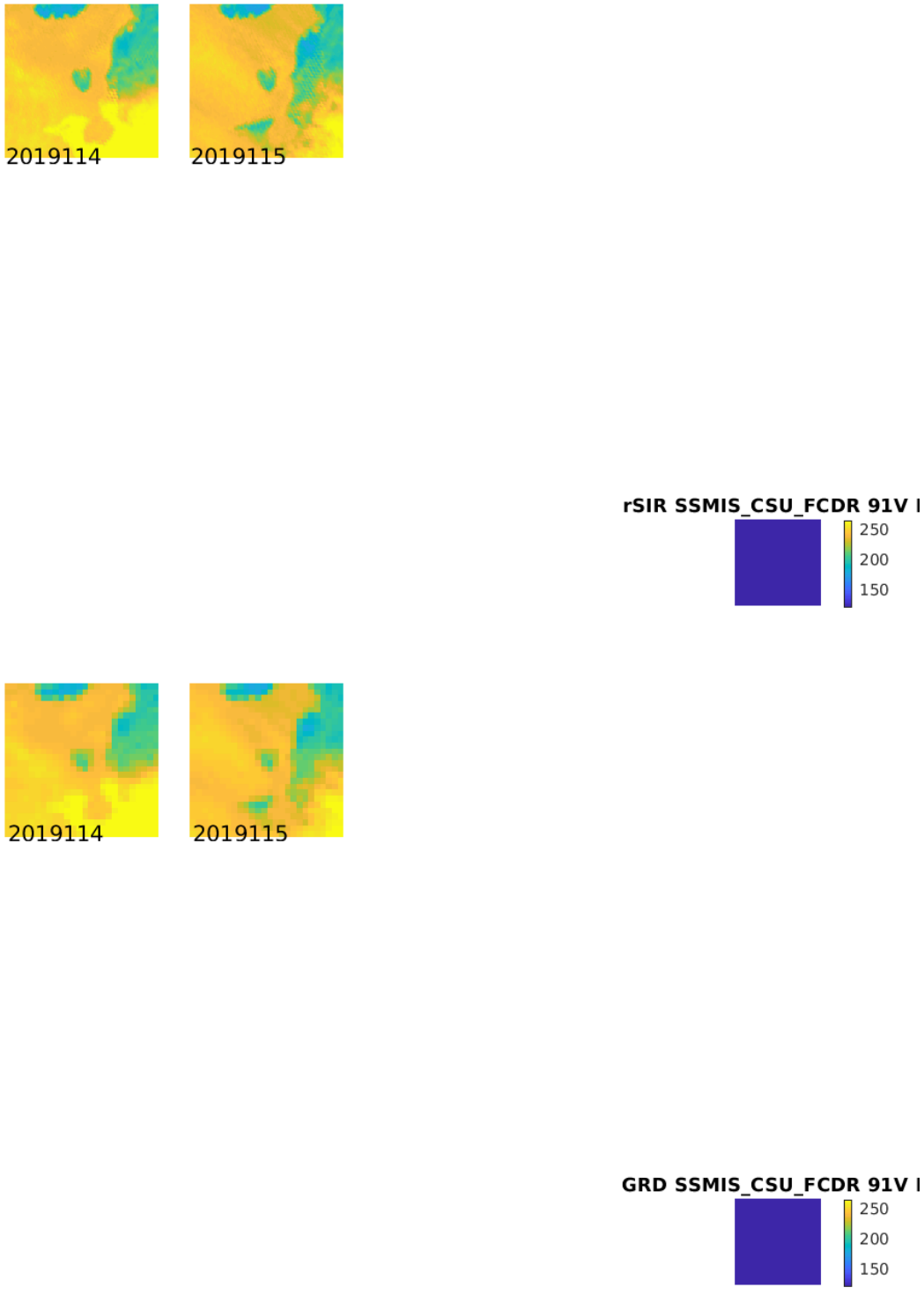

Figure 218: Time series of (top) rSIR and (bottom) GRD T_B images over the study area. Image dates are labeled on the image.

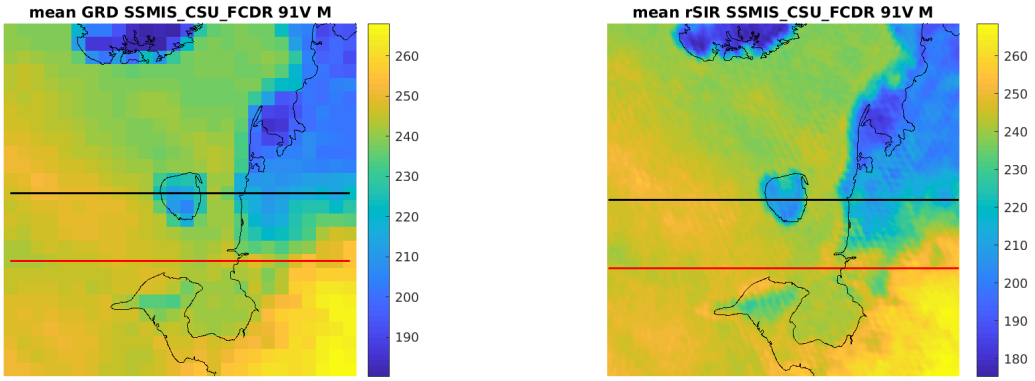

Figure 219: Average of daily T_B images over the study area. (left) 25-km GRD. (right) 3.125-km rSIR. The thick horizontal lines show the data transect locations where data is extracted from the image for analysis.

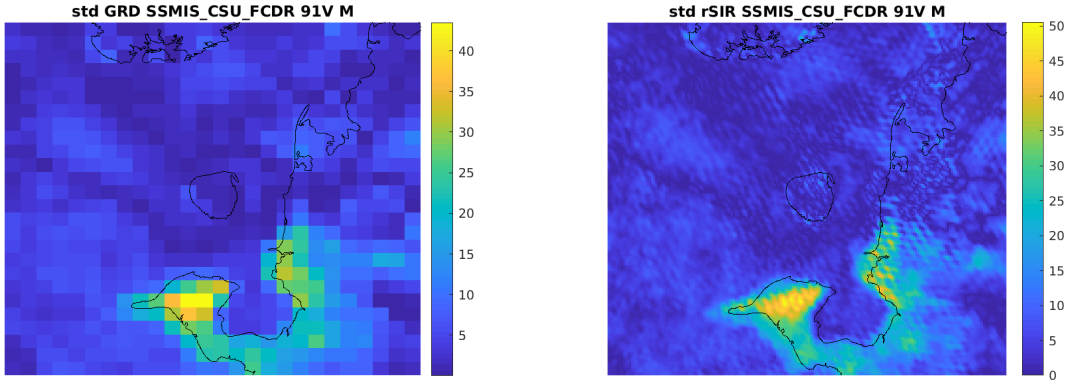

Figure 220: Standard deviation of daily T_B images over the study area. (left) 25-km GRD. (right) 3.125-km rSIR.

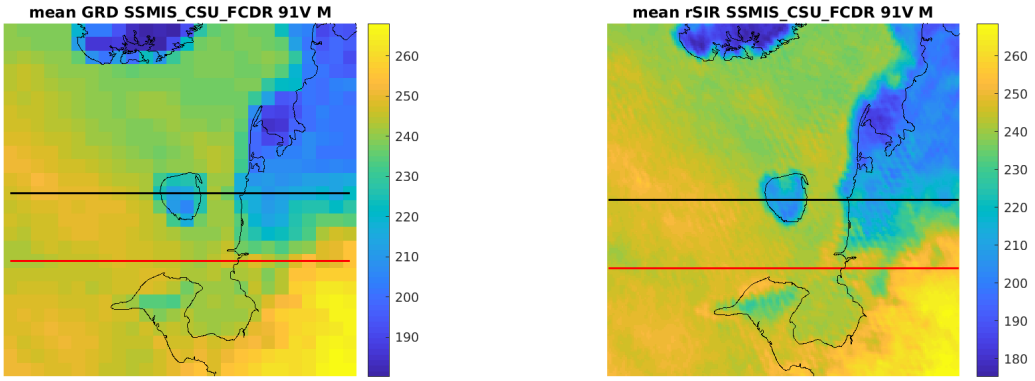

Figure 221: [Repeated] Average of daily T_B images over the study area. (left) 25-km GRD. (right) 3.125-km rSIR. The thick horizontal lines show the data transect locations where data is extracted from the image for analysis.

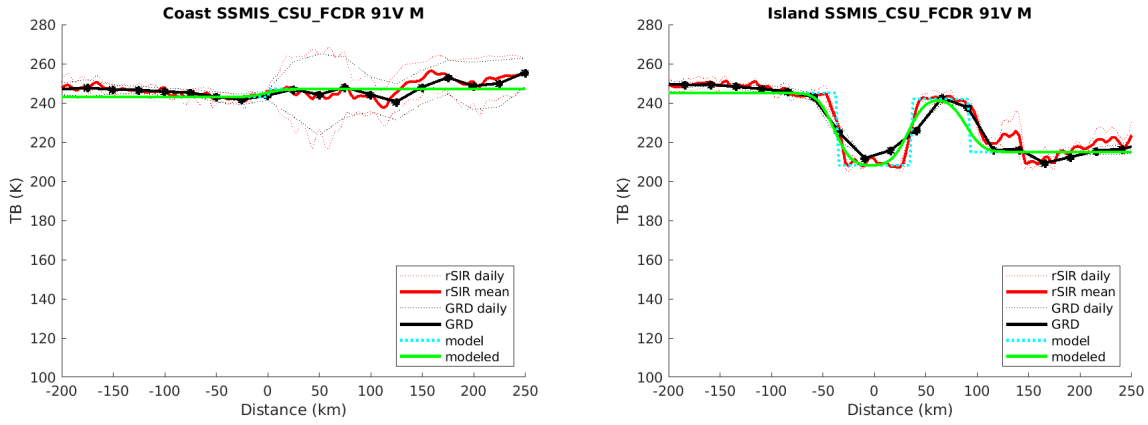

Figure 222: Plots of T_B along the two analysis case transect lines for the (left) coast-crossing and (right) island-crossing cases.

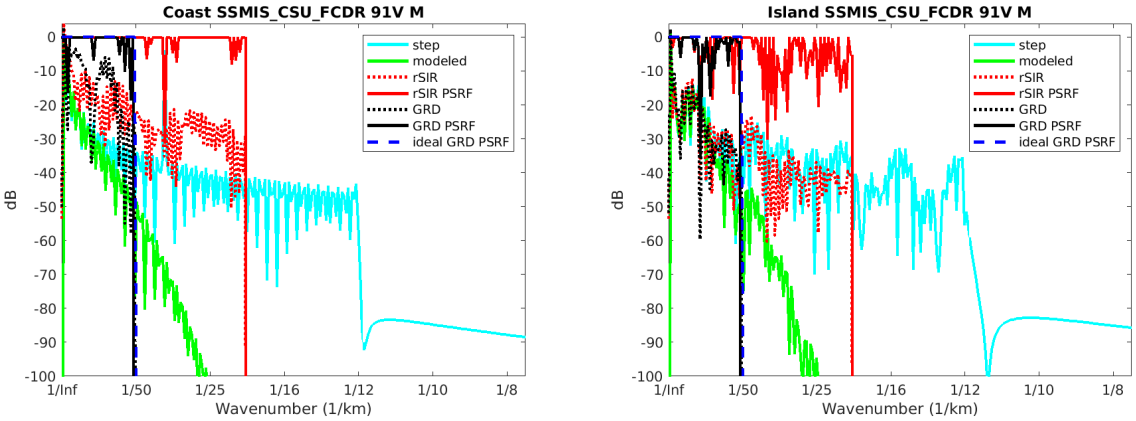

Figure 223: Wavenumber spectra of the T_B slices, the model, and the PSRF. (left) Coast-crossing case. (right) Island-crossing case.

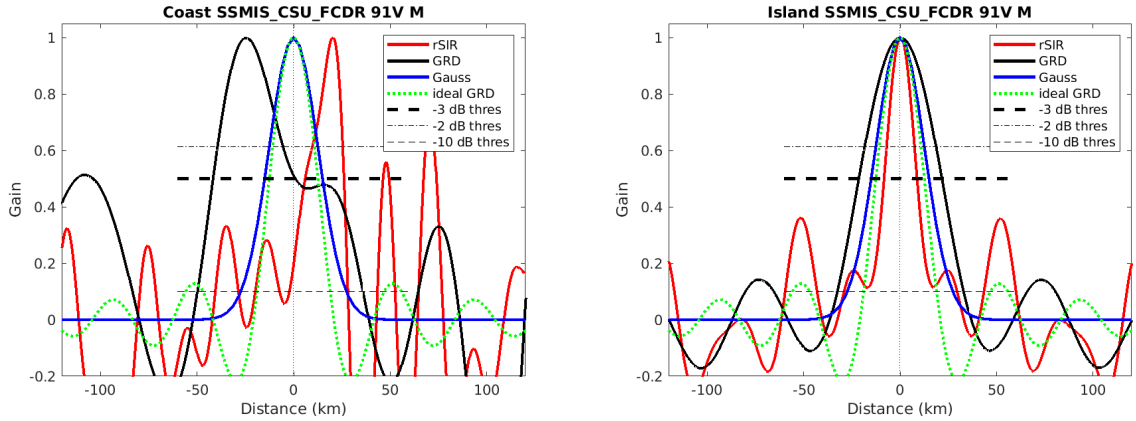

Figure 224: Derived single-pass rSIR and GRD PSRFs from the (left) coast-crossing and (right) island-crossing cases.

Table 56: Resolution estimates for SSMIS_CSU_FCDR channel 91V LTOD M

	-3 dB Thres		-2 dB Thres		-10 dB Thres	
Algorithm	Coast	Island	Coast	Island	Coast	Island
Gauss	30.0	30.0	24.4	24.4	54.8	54.8
rSIR	NaN	17.1	NaN	14.0	NaN	58.6
ideal GRD	36.2	36.2	30.3	30.3	54.5	54.5
GRD	NaN	43.0	NaN	36.0	NaN	65.5

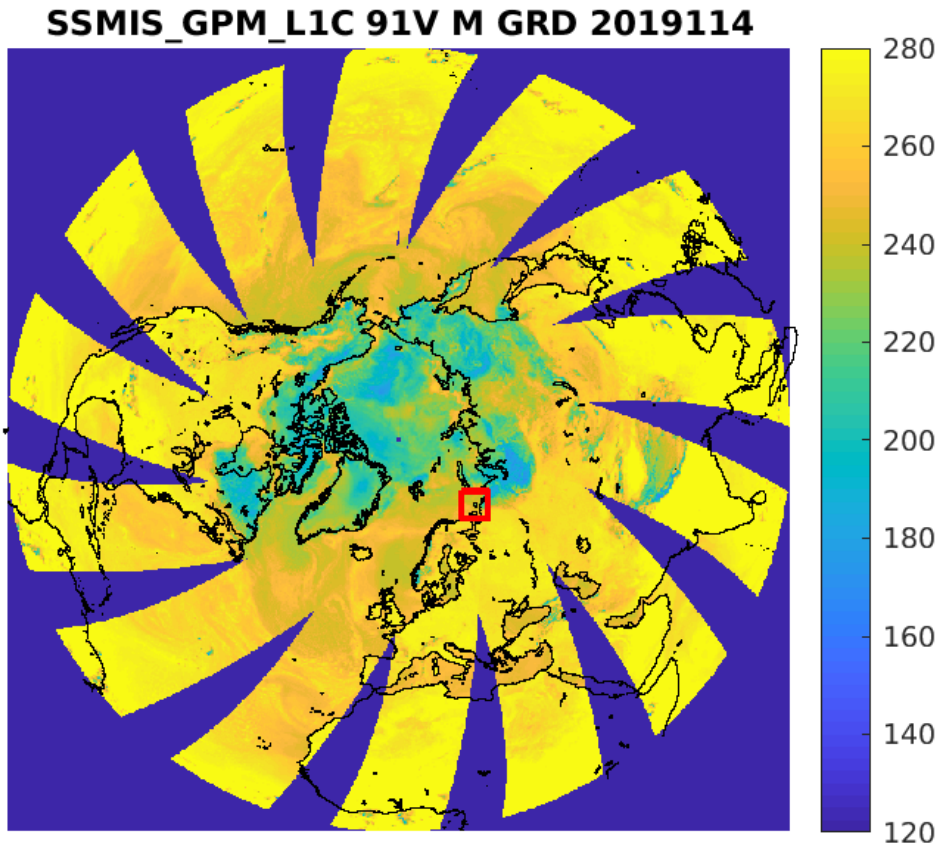

Figure 225: rSIR Northern Hemisphere view.

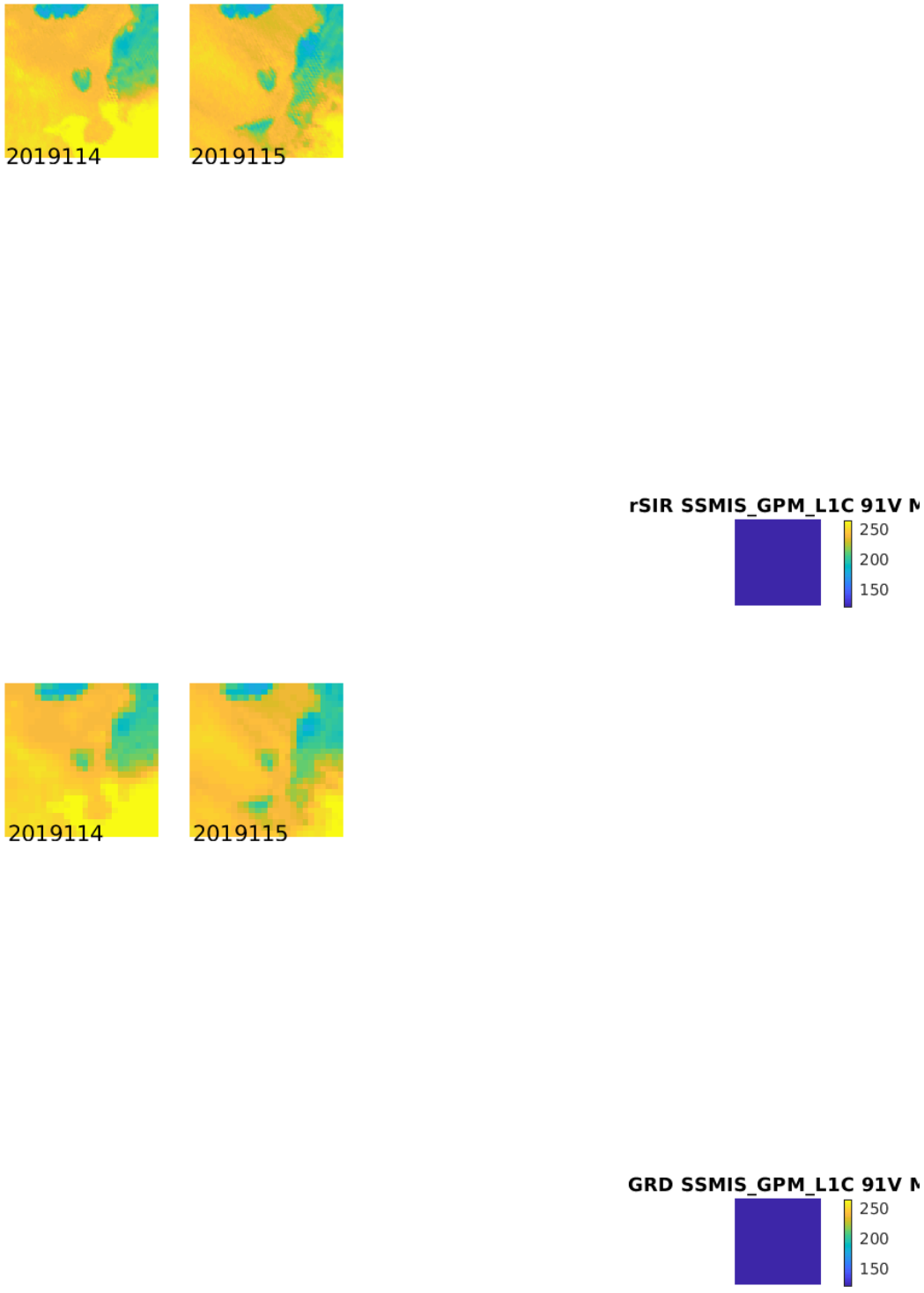

Figure 226: Time series of (top) rSIR and (bottom) GRD T_B images over the study area. Image dates are labeled on the image.

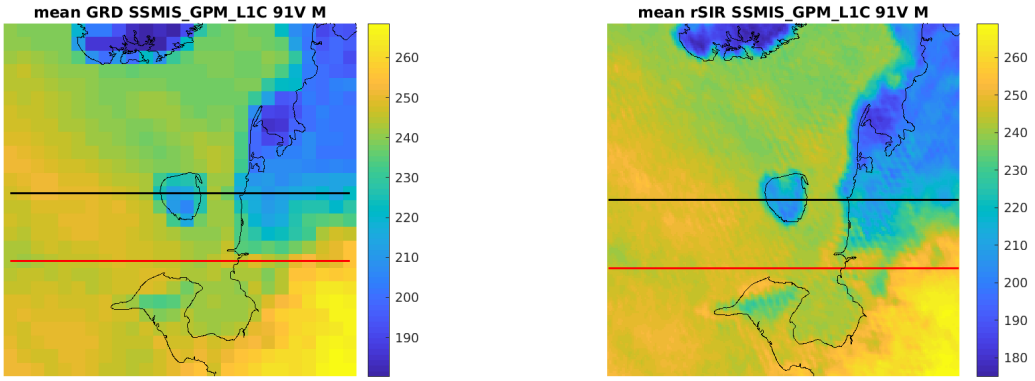

Figure 227: Average of daily T_B images over the study area. (left) 25-km GRD. (right) 3.125-km rSIR. The thick horizontal lines show the data transect locations where data is extracted from the image for analysis.

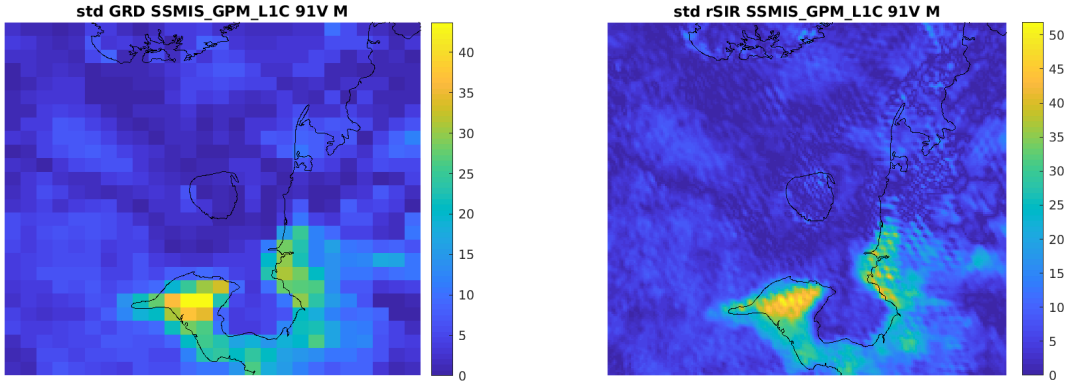

Figure 228: Standard deviation of daily T_B images over the study area. (left) 25-km GRD. (right) 3.125-km rSIR.

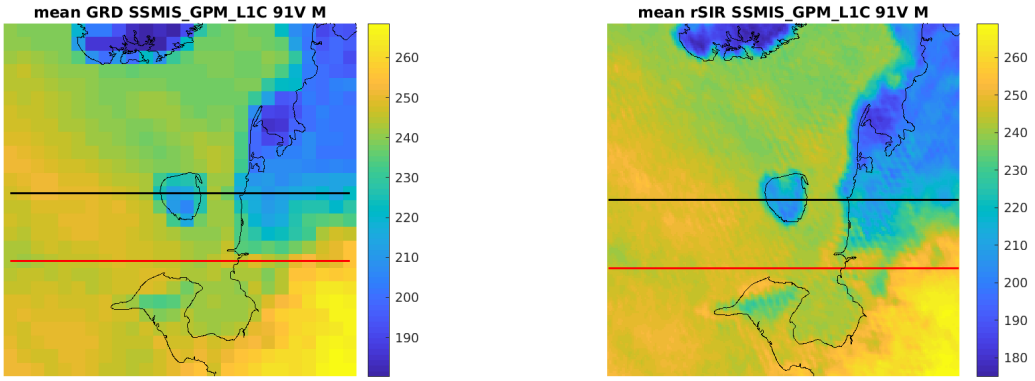

Figure 229: [Repeated] Average of daily T_B images over the study area. (left) 25-km GRD. (right) 3.125-km rSIR. The thick horizontal lines show the data transect locations where data is extracted from the image for analysis.

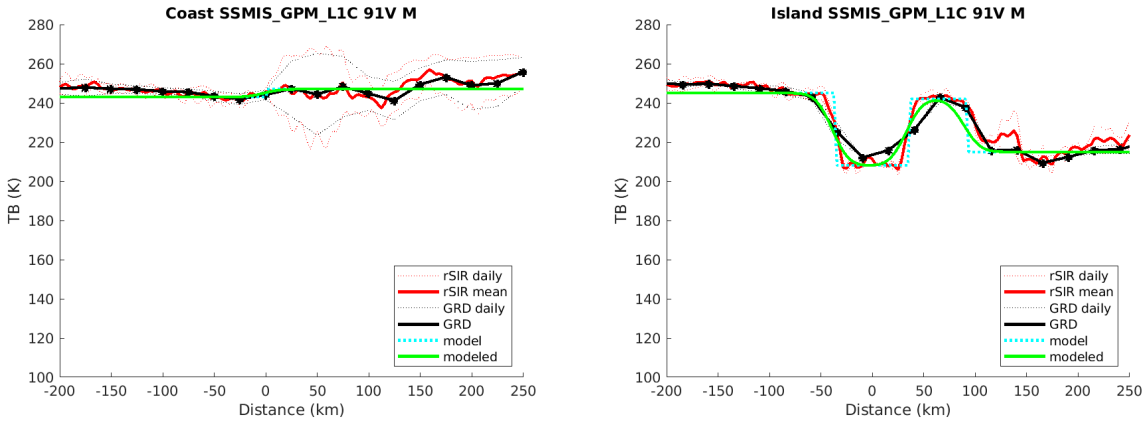

Figure 230: Plots of T_B along the two analysis case transect lines for the (left) coast-crossing and (right) island-crossing cases.

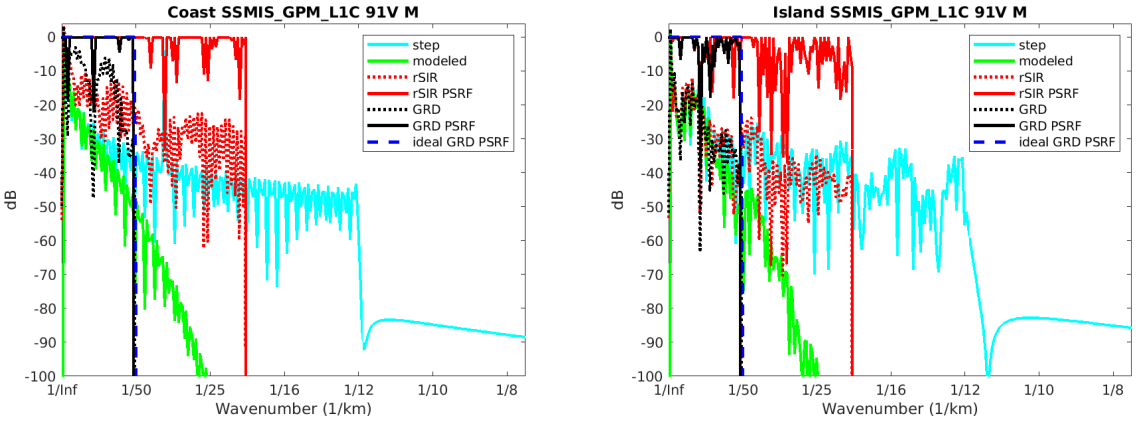

Figure 231: Wavenumber spectra of the T_B slices, the model, and the PSRF. (left) Coast-crossing case. (right) Island-crossing case.

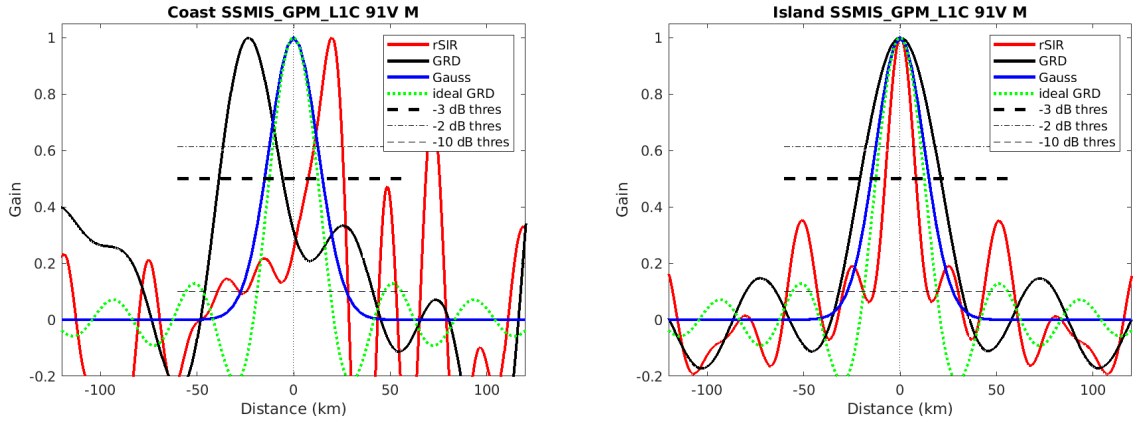

Figure 232: Derived single-pass rSIR and GRD PSRFs from the (left) coast-crossing and (right) island-crossing cases.

Table 57: Resolution estimates for SSMIS_GPM_L1C channel 91V LTOD M

	-3 dB Thres		-2 dB Thres		-10 dB Thres	
Algorithm	Coast	Island	Coast	Island	Coast	Island
Gauss	30.0	30.0	24.4	24.4	54.8	54.8
rSIR	NaN	16.0	NaN	13.2	NaN	27.8
ideal GRD	36.2	36.2	30.3	30.3	54.5	54.5
GRD	NaN	41.8	NaN	34.9	NaN	63.9